INTERPRETATION, ANALYSIS AND DESIGN OF INTER-WELL TRACER TESTS IN NATURALLY FRACTURED RESERVOIRS

A Thesis

by

AYMEN ABDULJALIL JAFAR ALRAMADHAN

Submitted to the Office of Graduate Studies of
Texas A&M University
in partial fulfillment of the requirements for the degree of

MASTER OF SCIENCE

Chair of Committee,	David S. Schechter
Committee Members,	Berna Hascakir
	Yuefeng Sun
Head of Department,	Dan Hill

August 2013

Major Subject: Petroleum Engineering

ABSTRACT

In order to understand the complex fracture network that controls water movement in Sherrod Area of Spraberry Field in West Texas and to better manage the on-going waterflood performance, a field scale inter-well tracer test was implemented. This test presents the largest inter-well tracer test in naturally fractured reservoirs reported in the industry and includes the injection of 13 different tracers and sampling of 110 producers in an area covering 6533 acres.

Sherrod tracer test generated a total of 598 tracer responses from 51 out of the 110 sampled producers. Tracer responses showed a wide range of velocities from 14 ft/day to ultra-high velocities exceeding 10,000 ft/day with same-day tracer breakthrough. Re-injection of produced water has caused the tracers to be re-injected and added an additional challenge to diagnose and distinguish tracer responses affected by water recycling. Historical performance of the field showed simultaneous water breakthrough of a large number of wells covering entire Sherrod area. This research investigate analytical, numerical, and inversion modeling approaches in order to categorize, history match, and connect tracer responses with water-cut responses with the objective to construct multiple fracture realizations based entirely on water-cut and tracers' profiles. In addition, the research highlight best practices in the design of inter-well tracer tests in naturally fractured reservoirs through lessons learned from Sherrod Area.

The large number of tracer responses from Sherrod case presents a case of naturally fractured reservoir characterization entirely based on dynamic data. Results indicates

that tracer responses could be categorized based on statistical analysis of tracer recoveries of all pairs of injectors and producers with each category showing distinguishing behavior in tracers' movement and breakthrough time. In addition, it showed that tracer and water-cut responses in the field are dominantly controlled by the fracture system revealing minimum information about the matrix system. Numerical simulation studies showed limitation in dual porosity formulation/solvers to model tracer velocities exceeding 2200 ft/day. Inversion modeling using Gradzone Analysis showed that east and north-west of Sherrod have significantly lower pore volume compared to south-west.

DEDICATION

This thesis is dedicated with all my heart: To Prophet Mohammad and his family of Ahlulbayt, who taught us that continuous seek of knowledge is an ultimate goal in every Muslim life. To my late grandfather, who created a culture of patience, dedication and determination toward our goals in life. To my mother and father, who taught me my first letters in my early days in life. To my valuable and life-time friends Sunny Wu, Ali Al-Momain, Zuhair Al-Yousif, Hisham Al-Mohmmadi, and Mohammad Kanfar for being as a family to me and for making College Station and the US a home and a wonderful place. To my colleague and officemate Edith Sotelo who has always inspired me by her hard work and dedication. Finally, to my ex-wife, who left me in 12 February 2012 after 8 years of marriage, for teaching me valuable lessons in life.

ACKNOWLEDGEMENTS

I would like to express my sincere appreciation to Dr. David Schechter, my adviser and the chair of my committee, for his academic support, guidance, encouragement, and help during the course of my Master of Science degree.

I would like also to thank my employer and sponsor, Saudi Aramco, for giving me a life time opportunity to be a full-time graduate student at Texas A&M University.

Thanks also go to faculty, friends, and colleagues in the Texas A&M Petroleum Engineering Department for making graduate degree such a great experience. I also want to extend my gratitude to Pioneer Natural Resources, which provided the data needed in this study.

Finally, thanks to my mother and father for their encouragement, patience and love.

TABLE OF CONTENTS

LIST OF FIGURES

LIST OF TABLES

1. INTRODUCTION

1.1 Tracer Tests: Background & Applications

The successful implementation of tracer tests in the areas of petroleum reservoirs and groundwater fields over the years have made those types of tests very reliable tool for reservoir description and characterization. Unlike pressure transient tests which provide a low resolution description of the reservoir by averaging reservoir properties over the bulk drainage volume, tracer tests has the ability to capture small scale features making them suitable for a more detailed and a higher resolution reservoir description. In secondary and enhanced oil recovery projects, the degree of success of economically recovering the remaining oil requires a robust understanding of fluid migration paths and recovery mechanism in the reservoir. Geophysical, geological, petrophysical, and PVT fluid studies are typically used to evaluate the feasibility of implementing a secondary or tertiary recovery project. Information about heterogeneity and dispersion characteristics of the reservoir from dynamic characterization tools such as well tests and inter-well tracer tests can redefine the evaluation results of such projects [(1,2)].

The majority of inter-well tracer tests have the main objective of assessing connectivity and direct communication between injectors and producers [(3)]. Other important objectives of inter-well tracer tests includes: identifying flow anisotropy in the reservoir [(4,5)], evaluating sweep efficiency [(3,4,6,7,8)] ,identifying flow barriers[(3,4)], characterizing areal reservoir heterogeneity[(9)], describing reservoir layering[(10,11,12,13)], estimating fluid velocities, and determining offending injector(s) in case of channeling

[(10,11,12,13)]. Once any or all of these objectives are met, the reservoir engineer will be able to design and implement more efficient sweep improvement strategies.

1.2 Tracer Tests: Classification & Theory

A broad classification of tracers used in waterflood applications can put them into two categories: conservative tracers and partitioning tracers. The basis of such classification is based on the relative interaction of the tracer(s) with water and other phases present in the reservoir. Conservative tracers, also called 'water tracers', move in the reservoir with a velocity equal to the water phase velocity and exhibit no interaction with any other fluids in the reservoir. Such tracers have found successful applications in characterizing fluid flow between wells. On the other hand, partitioning tracers found application in saturation determination due to their solubility in the water phase as well as the hydrocarbon phase present in the reservoir. This solubility of partitioning tracer in oil or gas phases present in the reservoir causes a delay or 'retardation' in tracer propagation when compared to conservative tracer. This chromatographic delay serves as the fundamental basis in estimating hydrocarbon saturation present in the reservoir (Figure 1.1).

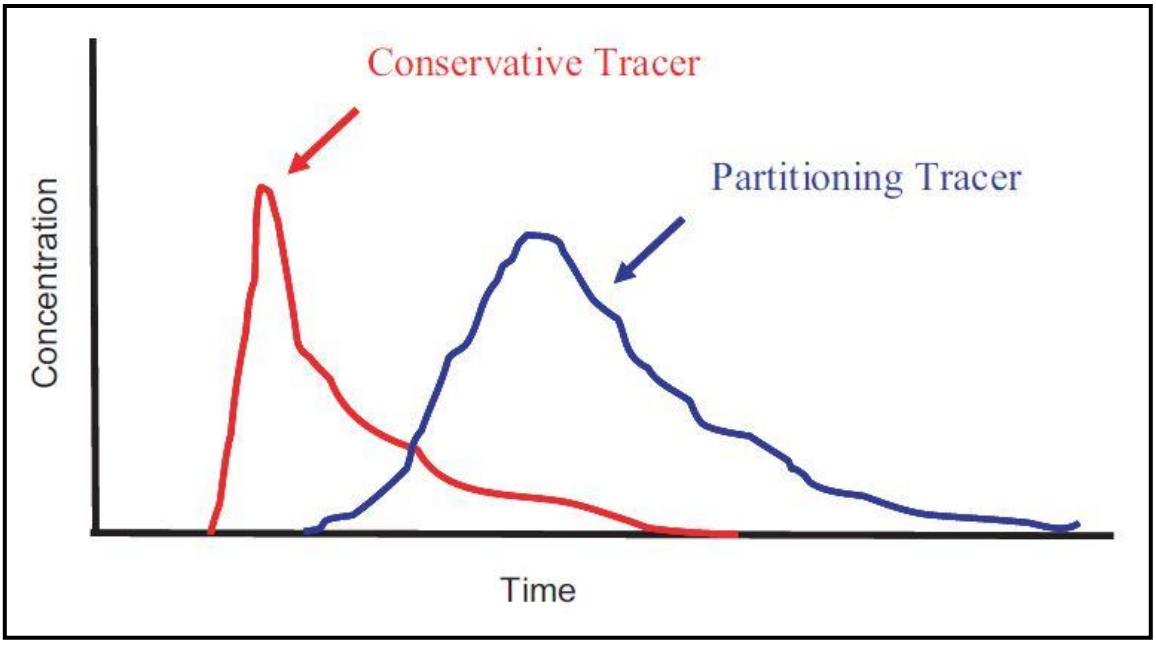

Figure 1.1: Example of partitioning and conservative tracer response

The conservative equation for a waterflood tracer concentration, C(x,t), can be written as :

$$\phi\frac{\partial((S_w+K_oS_o)C)}{\partial t} + u_t \bullet \nabla\big((F_w + K_oF_o)C\big) = m\delta(t) \quad \text{.....(1)}$$

The above conservative equation is the general form for an ideal waterflood tracer. It assumes that tracers are non-adsorbing and it includes the effects of two phase mobility and tracer partitioning in the oil phase. In the ideal tracer flow equation shown above, K_o is the partitioning coefficient which represents the ratio of tracer concentration in the oil phase to tracer concentration in the water phase (K_o=0 for conservative tracers). The total velocity of the two phases is u_t , C is the tracer concentration, S_w and S_o are fluid saturations in the reservoir, ϕ is porosity, and F_w and F_o are water-cut and oil-cut at the

wellbore, respectively. On the right hand side of the equation, $m\delta(t)$ is the source term. In the case of a spike of tracer injected over a very short time interval, the source term become $m\delta(t) = M_T / V_w \, \delta(t)$ where M_T is total mass of tracer produced and V_w is the associated water volume.

Expanding the conservative form and using stream-line time of flight coordinate gives:

$$(S_w + K_o S_o)\frac{\partial C}{\partial t} + (F_w + K_o F_o)\frac{\partial C}{\partial \tau} = \frac{m}{\phi}\delta(t) \quad \text{.....(2)}$$

which shows, in the case of both water and oil phases are flowing, the retardation factor will depend on $(S_w + K_o S_o) / (F_w + K_o F_o)$. This will add a fair complexity to the interpretation and could be avoided by injecting the tracer in near residual oil saturation condition (when $Fw \approx 1$ and $Fo \approx 0$). As mentioned earlier, the retardation of the partitioning tracer provide a critical and direct information of the average oil saturation in the tracer swept area. For test design, several issues must be addresssed like amount of tracer to be injected, injection locations, detectability, etc. Those issues are discussed in detail in later sections [((14))].

1.3 Partitioning Tracers

For an ideal water tracer, the presence of an oil phase in the reservoir will have no impact on the tracer path or its velocity. The path and the velocity of the ideal water tracer will be identical to that of the injected water. Evaluation of the presence of the oil phase in the reservoir requires some sort of interaction between tracer and the oil phase. This is done with the introduction of a non-ideal tracer that can partition between the oil

and water phases. Typically, a set of partitioning tracers with different partitioning coefficients are injected into the reservoir. The difference in residence times between water tracers and partitioning tracers is used to estimate both the residual oil and the power volume swept by the tracer.

In principal, when water containing a pulse of tracer is injected into the reservoir, tracer molecules in the water phase will move with the velocity of water. Similarly, tracer molecules in the oil phase will move with the velocity of oil. In the case when oil saturation is at residual, tracer molecules will only move in the water phase causing the partitioning tracer to lag behind the waterfront. The extent of this delay is directly related to the time the tracer spend in the oil phase compared to the water phase. If this delay could be measured, then knowledge of the equilibrium distribution of tracer molecules between the two phases could be established, and residual oil saturation in the region contacted by water could be estimated.

To illustrate the mathematical formulation of the residual oil saturation estimation, let us suppose we injected, using water, two tracers simultaneously into the reservoir: Tracer A, a partitioning tracer and Tracer B an ideal water tracer. The number of molecules of tracer A in the oil phase at any given time, $N_{A,oil}$, is given by the concentration of tracer A in the oil, $C_{A,oil}$, times the volume of oil phase $V_{o.}$ Similarly, number of tracer A molecules existing in the water phase, $N_{A,water}$, is given by the product of concentration in water, $C_{A,water}$, times the volume of water phase V_w. The ratio of tracer A molecules in oil phase to water phase, $N_{A,oil} / N_{A,water}$, is equal to the ratio of the mean residence time the average tracer molecule spend in the immobile

phase relative to the mobile phase, $t_{A,oil}$ / $t_{A,water}$. This is called the delay factor, β, and can be expressed as follows:

$$\beta = \frac{N_{A,oil}}{N_{A,water}} = \frac{C_{A,oil}\,V_{oil}}{C_{A,water}\,V_{water}} = \frac{t_{A,oil}}{t_{A,water}} \quad \text{.....(3)}$$

The ratio $C_{A,oil}$ / $C_{A,water}$ is the partition coefficient of the tracer. It is a thermodynamic function which can be measured in the laboratory. This coefficient depends on temperature, salinity, concentration, etc. However, when tracer concentration approaches infinite dilution, the partition coefficient becomes independent of tracer concentration. Oil and water volumes in the above equations could be expressed in term of saturations leading to the following expression:

$$\beta = K_d \frac{S_{or}}{1-S_{or}} \quad \text{.....(4)}$$

If t_A is the residence time of the partitioning tracer and t_w is the residence time for the water tracer, then, partitioning tracer t_A is delayed by the factor β relative to the ideal water tracer. This delay is expressed as follows:

$$t_A = t_w(1+\beta) = t_w\left\{1 + K_d \frac{S_{or}}{1-S_{or}}\right\} \quad \text{.....(5)}$$

Since the partitioning coefficient, K_d, is measured in laboratory, and t_A and t_w are obtained from the field test, the above expression can be solved for S_{or} [(15)]:

$$S_{or} = \frac{t_A - t_w}{t_A - t_w + t_w K_d} = \frac{\Delta t}{\Delta t + t_w K_d} \quad \text{.....(6)}$$

Applications of partitioning tracers in residual oil estimation have led to the development of two major field tests: Single Well Partitioning Tracer Test (SWPTT) and Partitioning Inter-well Tracer Tests (PITT) [(2)].

The Single Well Partitioning Tracer Test (SWPTT) is used primarily to measure in-situ oil saturation as the first step in enhanced oil recovery project initiation. Other applications include field assessment for bypassed oil or to measure effectiveness of EOR agents in single well pilot. The test is usually done when one phase is immobile and the other phase can flow to the wellbore. The immobile phase could be either residual oil or irreducible water depending on which stage in the life of the field the test was implemented.

This test with the objective to determine oil saturation involves two major steps: injection of water carrying a chemical tracer into the formation, and back production of water carrying a different tracer formed by the chemical reaction of the original tracer with formation water. In the first part of the test, the injected water is divided into two parts: early part which carries a small concentration of alkyl ester into the formation, and a late part which pushes the early injected volume away from the wellbore. Typically, a material balance tracer is used to tag the entire injected volume to distinguish it from the reservoir water being displaced. After injection is complete, the well will be shut in for a period of time to allow reaction of the ester with formation water to form a new in-situ tracer. Hydrolysis at reservoir temperature will break the ester into its basic components of alcohol and organic acid. The organic acid will be consumed entirely by the natural base components of the reservoir, and the alcohol will be the tracer that will create the elution curve and will allow residual oil saturation estimation when the well is put back on production.

The Partitioning Inter-well Tracer Tests (PITT), in addition to the objectives of SWPTT, it allows assessment of heterogeneity, fluid migration paths, and swept volumes and saturations in a wide area of the field. This is usually done by injecting both water and partitioning tracers in the same injector and observing the separation in the elution curves at the producing wells[((2))].

1.4 Tracer Tests: Analysis & Interpretation

The successful implementation of tracer tests in both petroleum fields and groundwater fields has led to a simultaneous development in interpretation techniques in both areas. The main drive for development of interpretation techniques in oil and gas fields was production optimization. For the groundwater fields, the main drive was to assess, design, and efficiently implement aquifer remediation actions for removal of contaminants from soil and fresh water.

When a pulse of injected tracer reaches the production well, the produced concentration will be a distributed tracer response curve. This is due to water movement in a distribution of flow paths and different flow rates within each path. A typical tracer response curve will show at least four distinctive landmarks as shown in Figure 1.2: breakthrough time, maximum concentration produced, variance of response, and mean of the distribution.

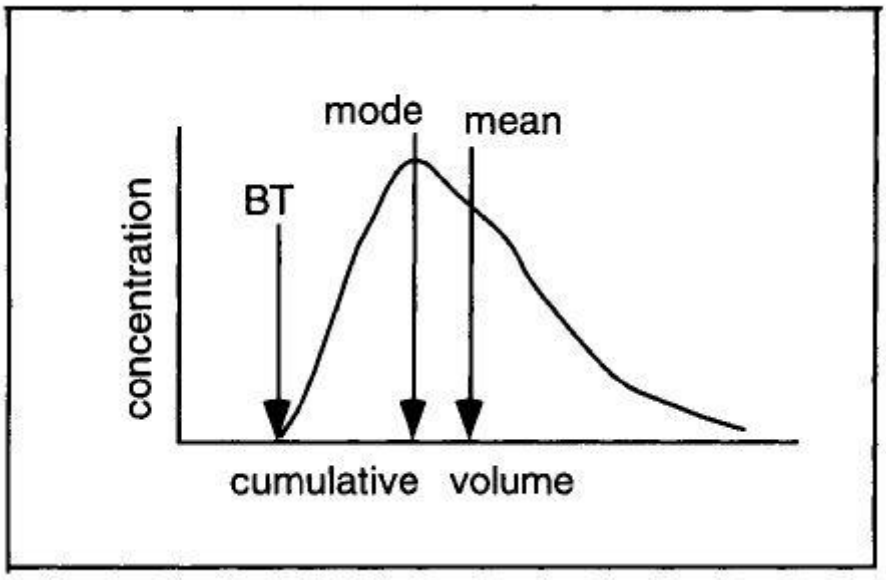

Figure 1.2: Example of a typical tracer response

The first response in the tracer elution curve, the breakthrough time, is usually not very well defined due to its dependency on sensitivity of measurements in the field and sampling frequency. Sweep efficiency is typically described in term of this landmark when it is plotted as a function of cumulative water injection rate. In a one dimensional homogenous system, breakthrough is a measure of the swept pore volume by injected water. In two or three dimensional heterogeneous system, breakthrough is interpreted differently. It represents a measure of the swept volume by only the highest conductive path between injector and producer which is a function of heterogeneity and pattern geometry. A nearly instantaneous tracer breakthrough is an indication of fracturing [((4))]. An early breakthrough with a sharp response is an indication of water channeling

through a high permeability thin stringer [(3,4,16)]. A late breakthrough is an indication of poor communication or low transmissibility path between injector and producer [(3,4)].

The second and the third landmarks in the tracer elution curve are the peak concentration produced and its width. The peak concentration produced represents the mode of the distribution while its width is dependent on local variation in flow velocity and/or on longitudinal dispersion [(14, 15)].

The forth landmark is the mean of the distribution which represents the mean volume injected. This for the case when produced tracer concentration is plotted against cumulative volume injected. By definition, total swept pore volume is the sum of all paths followed by injected water between an injector and a given producer. Due to variability in properties of these paths, total swept volume is better measured by the mean of the distribution [(15)]

Multiple peaks in a response can be extremely informative for reservoir description. However, it does not have a unique interpretation. In Abbaszadah work [(11,17)], he showed that multiple peaks have strong correlation with the minimum number of layers to match the tracer response. Also, if multiple peaks are observed to be close in location to each other, it is an indication of substantial interference between layers contributing to tracer flow. The observed location of each peak is assumed to correspond to the location of that peak from the individual layer response. This assumption showed to be valid by matching tracer responses with multiple peaks from synthetic and actual field inter-well tracer test done on Ranger Field.

Datta-Gupta et. al. [(14)] showed that multiple peaks in a tracer response does not necessarily mean that the reservoir is composed of multiple non-communicating layers. The motive of finding a different way to interpret multiple peaks was the fact that the sum of the calculated thicknesses by Abbaszadeh approach did not sum to the total net pay. In fact, it is not uncommon to see reported sum of thicknesses that are less than 25% of net pay. Based on these observations, Datta-Gupta et. al. proposed that the reported ratios of sum of thicknesses to net pay should be thought of as a measure of sweep efficiency caused by a combination of low vertical sweep efficiency and a less than 100% areal sweep efficiency. Hence, the data should be analyzed in a more general way in term of correlated and uncorrelated heterogeneity. Following this approach, it was shown that Ranger field tracer data could be matched without the use of homogeneous non-communicating layers. The proposed reservoir model has areal variation in permeability as well as vertical communication between layers. The source of the multiple peaks for this case was the multiple continuous high permeability channels running through the reservoir. In conclusion of Data-Gupta et. al. proposed approach, it was shown that the results are consistent with Abbaszadeh analysis in the fact that the small computed net thicknesses in the earlier approach were actually a reflection of the permeability architecture in the field.

Analysis of tracer response data in both petroleum and groundwater applications could be classified into four main approaches: Analytical approaches, stochastic approaches, inversion modeling approaches, and direct history matching approaches.

1.4.1 Analytical Tracer Interpretation Techniques

Analytical methods have a wide range of applications from determining number of layers and their corresponding conductivity and porosity-thickness products to characterizing heterogeneity, estimating saturations, average sweep volumes, and dynamics of fluid flow.

From the petroleum industry side, Cooke [(18)] initiated and patented his approach of estimating fluid saturations in the reservoir by comparing breakthrough times of two types of tracers used in Partitioning Inter-well Tracer Test. Taking advantage of the poor quantitative definition of breakthrough time in Cooke's approach, Tang[(19)] proposed an improvement in the method by utilizing landmarks in tracers' elution curves rather than breakthrough time. Comparison of production time of landmarks in elution curves such as peaks and valleys between water and partitioning tracer could be used to estimate reservoir oil saturation over the whole elution curve. One advantage of this improved method is its ability to provide a range of average oil saturations reflecting the variability of in-situ oil saturation encountered in the path of tracer migration from injectors to producers.

'Methods of Moments' with its roots from the chemical engineering side of the industry is very similar to Cooke's approach. It's used in the chemical process industry to analyze flow behavior in chemical reactors by injecting a pulse of tracer at the inlet of the system and then monitoring the response at the output. The tracer elution curve at the outlet is used to characterize flow in the reactor. Method of Moments (MOM) is also very commonly used in groundwater field applications to assess non-aqueous phase

liquid saturation. This method provides a direct and simple analysis of field tracer data by relying on average arrival time and mass balance. The theory of this method and its application in Sherrod Area in Spraberry field is discussed in detail in chapter 3.

Deans [(20)] dedicated his work to explain and model the differences observed in Single Well Partitioning Tracer Test (SWPTT) preformed on carbonate reservoirs compared to sandstone reservoirs. Consistent anomalies in tracer response in carbonate reservoirs include: poor tracer recovery, extreme dilution of tracer, long tails on tracer elution profile, abnormal low recovery of material balance tracer and high reactive tracers concentration at the very early back production of the well. Dean linked these anomalies to the complex pore geometry existing in carbonate reservoir and built analytical models that successfully matched several tracer tests. His analytical model was based on combining theory of tracer movement with Backley-Leverette for two-phase flow in a two-pore space type system.

Abbaszadeh[(11,17)] used exact expressions for homogenous single-layer pattern breakthrough curves derived from streamtube functions and hyper elliptic integrals and proposed a non-linear optimization techniques that will perform de-convolution of the tracer elution curve to estimate important properties such as permeability and porosity-thickness product for individual contributing layers. In Abbaszadeh work, he showed that pattern breakthrough curves (water-cut versus pore volume injected) for different repeated flooding patterns could be normalized into one single curve by using a dimensionless correlating parameter. Taking advantage of this normalization procedure, it is claimed that his inversion algorithm is applicable on any repeating pattern.

Important assumptions in his work include: piston-like displacement, mobility ratio of one, patterns are balanced, negligible molecular diffusion and transverse dispersion, no cross flow between layers, and every layer is homogeneous covering whole field area. In his approach, concentration of peaks are proportional to layers' flow capacitance (permeability x thickness x width) while layer pore volume scale breakthrough time. Applying his approach on a field example, he showed that the number of peaks observed in a tracer response correlates very well with the minimum number of layers required to capture the tracer profile. Also, he showed that when permeability-thickness product from pressure transient test is used in de-convolution of tracer test data, it provides a high resolution picture of the heterogeneity and layering in the reservoir.

1.4.2 Stochastic Tracer Interpretation Techniques

James et al [(21,22)] developed a stochastic approach that treats hydraulic conductivity and non-aqueous phase liquids (NAPL) in groundwater reservoirs as spatially correlated random fields. This method utilizes co-krigging algorithm and a non-linear Gauss-Newton search technique to minimize the difference between observed and simulated tracer data in a least-square sense. One limitation of this approach is the requirement of a prior knowledge and a cross-covariance model which could be difficult to determine.

1.4.3 Inversion Modeling and Direct History Matching Approaches

Tremendous increase in computational speed and efficiency of reservoir simulators has reduced the time and effort required to design and perform a complete numerical

analysis of the tracer data. Several commercial and non-commercial simulators have the capability of simulating radioactive, chemical and water tracers with different gridding schemes.

The classical approach of history matching where reservoir parameters and saturations are manually adjusted to fit the simulated response to observed data have shown limitations for fields with large number of wells. The main limitation of direct history matching approach is the time required to obtain a reasonable and acceptable full field match. This limitation was the main drive for researchers to investigate inversion modeling and assisted history matching techniques.

Classical inversion modeling techniques dedicated toward improving the tracer profile match by automated history matching and finite-difference simulators did not show wide applications. The main reason behind their limited applications is the computational intensity required for fine scale full field models which make those approaches hardly feasible. For example, gradient-based inversion methods, with its compatibility with finite difference simulators, rely on computation of sensitivity coefficients to perform optimization. In many cases, computation of sensitivities requires excessive computational time compared to solving the fluid flow equations which severely limit their applications. On the other hand, gradient-free optimization techniques such as genetic algorithm and simulated annealing showed very slow convergence due to random perturbation algorithm within them and this prevented them from being widely used.

Vasco et. al. [(23)] showed that streamline simulation is a very efficient computation approach to solve the inverse problem. Such computational efficiency is a result of the possibility to derive analytical equation for sensitivities along streamlines. Yoon et. al.[(24)] showed that streamline-based inversion method worked successfully in matching PITT data and estimating non-aqueous phase liquids saturation for a synthetic and a field case. Also, Illiasov et. al. [(25)] applied this method on Ranger field to match PITT test results and estimate oil saturation.

1.5 Inter-well Tracer Tests Design

Major design aspects of inter-well tracer tests include: selection of tracers types, strategic injection locations, volumes of tracers to inject, sampling producers and sampling frequencies. Inter-well tracers tests are becoming more popular in understanding water movement in naturally fractured reservoirs and in the evaluation of enhance oil recovery projects candidates. However, there is lack of comprehensive discussion in the literature on how optimize efficiency and design of these tests.

1.5.1 Selection of Tracers Types

Careful selection of the tracer type is a critical step in the success of any inter-well tracer test project. An ideal water test tracer must meet several requirements: it must accurately track the path and the velocity of the water, its identification and measurement in produced water must be easily done in small quantities, it must be compatible with the reservoir to ensure no delay, loss or change in chemical form by

bacterial activity, adsorption, reversible or irreversible ion exchange or other chemical interactions with reservoir rock surface [(15)]. In addition, the selected tracers must be environmentally friendly and economically feasible for field applications [(1)]. Thus, tracers selected for the project must undergo detailed laboratory analysis to evaluate tracer ability to meet the above requirements.

1.5.2 Strategic Tracer Injection Locations

Strategic injection locations usually include injectors nearby areas of high producing water cut or in areas where water movement is very difficult to understand due to presence of complex fracture networks or suspected conductive or non-conductive faults. For projects where multiple or large number of injectors exist, it is very important to avoid ambiguity in the analysis of the results by avoiding using the same tracer in adjacent injectors.

1.5.3 Volume of Tracer to Inject

Methodology of injected tracer volume design has not been addressed in many of the field cases reported in the literature. In most cases, the amount of tracer injected is determined by analogy from previous tests with similar reservoir types or testing conditions [(1)]. Brigham and Smith [(26)], assuming unit mobility and non-communicating layers developed a mathematical model to determine the minimum tracer volume to inject in a developed five spot pattern. Mclntyre et. al. [(16)] based on the work of Abbaszadeh and Brigham which includes effects of tracer dispersion, diffusion, dilution

and partitioning, developed dimensionless tracer elution curves and used those to determine the minimum amount of tracer required for a given test. Apparently, those models are not used in field application and experience plays the major role in determining the volume of tracer to inject.

1.5.4 Sampling Schedules

Design of sampling schedules for producers is very important to optimize cost of analysis and to capture tracer breakthrough time and main landmarks of elution curve. Wagner [(4)] proposed that the design of sampling schedules should be based on expected breakthrough time, distance between injectors and producers, and well rates involved. He also highlighted the importance of early sampling within few days of tracer injection to avoid missing fracture or channeling response. Field examples in the literature shows sampling frequency ranging from daily to every 60 days [(3,8,9,16)]. Heisler [(27)] proposed a variable interval sampling frequency with high frequency during early stages until breakthrough occur, then sampling frequency gradually decrease until enough data is taken.

1.6 Research Objectives

- Evaluate inter-well tracer tests as a tool to characterize heterogeneity, connectivity, and sweep efficiency in naturally fractured reservoirs.
- Purpose a work flow to analyze tracers' response in naturally fractured reservoirs using integrated approach.
- Evaluate capabilities of different commercial and non-commercial reservoir simulators in handling tracer flow in naturally fractured reservoirs.
- Propose guidelines to optimize design of tracer tests to reduce cost and maximize information obtained.

2. BACKGROUND OF SPRABERRY FIELD

2.1 Naturally Fractured Reservoirs

It has been estimated that 30% of world oil production comes from naturally fractured reservoirs. According to Nelson [(28)], fractures could be defined as "naturally occurring macroscopic planar discontinuities in rock due to deformation or physical digenesis". Fractured reservoirs could be categorized to four types, as shown in Table 2.1:

Reservoir Type	Definition	Examples
Type I	Fractures provide both flow and storage. No matrix contribution	Amal, Libya ; PC Fields, Kansas
Type II	Fractures provide permeability. Matrix provide storage	Spraberry Trend Area, Texas ; Agha Jari, Iran
Type III	Both fracture and matrix contribute to flow and storage	Kirkuk, Iraq; Ghawar, Saudi Arabia
Type IV	Fractures only create anisotropy without any contribution to flow or storage.	Beaver Creek, Alaska ; Pineview, Utah

Table 2.1: Types of Fractured Reservoirs

Storage system of any reservoir can usually be divided into two parts: Primary porosity and secondary porosity. Primary porosity is controlled by deposition processes

and lithification. Typical primary porosities are the void space systems in sandstones and oolitic limestones. Secondary porosity is created during post-lithification processes such as fracturing, dolomitizataion, recrystallization, jointing, and solution. Typical secondary porosities are fractures, fissures, vugs and joints.

Complexity of naturally fractured reservoirs makes them very challenging projects to develop for both geologists and engineers. Poor knowledge of these reservoirs has resulted in millions of barrels of oil left unrecovered. Research in reservoir engineering, geo-mechanics, and geology was directed toward naturally fractured reservoirs in order to understand depletion mechanism and improve recovery [((29,30))].

2.2 Background of Spraberry Trend Area

The Spraberry Trend Area in West Texas was considered to be the largest oil field in the world at the time of its discovery in 1949 with 8-10 billion barrels of original oil in place [((31))]. Spraberry is composed of naturally fractured, low permeability siltstone which make it problematic for both primary production and waterflooding [((32))]. Based on primary recovery, its original recovery factor was projected to be less than 10% [((33, 34))] . This low anticipated recovery was the main drive to initiate waterflooding projects in several areas of Spraberry in late 1950s. Unexpectedly, waterflooding projects in Spraberry showed very limited success where areas subjected to more than 40 years of waterflooding showed less than 15% oil recovery [((32))]. Reasons for the low waterflood recovery are still poorly understood. Several hypotheses were developed to explain the wide-scale poor performance waterflooding. Those include: low matrix permeability and

extensive fracturing, incorrect well pattern alignment, fracture mineralization, lack of pattern confinement and injection well density, low effective permeability to oil, and stress-sensitive fracture conductivity [(35,36)].

2.3 Geology of Spraberry Field

The Spraberry formation consists of basin plane deposits and submarine fans with a complex stratigraphy comprised of sandstone, siltstone, shale, and limestone interbedding. Deposition of Spraberry formation dates back to Permian age in Midland Basin, a geological province of the Permian Basin. Well logs and core analysis showed the reservoir to be composed of both low porosity and low permeability matrix. Matrix permeabilities were in the order of 0.05 md or less with matrix porosities of 6-14%. Effective permeability from dynamic measures such as pressure transient tests or advanced declined analysis showed values in the range of 1-200 md. Such higher permeability values are believed to be the result of fracture contribution. Spraberry formation is subdivided into three main intervals: Lower Spraberry, Middle Spraberry, and Upper Spraberry. Their average depth intervals are about 7,200, 7,400 and 8,000 feet, respectively. These intervals were further subdivided to different units as shown in Figure 2.1. Only two units of Upper Spraberry, 1U and 5U sands, where identified as reservoir rocks capable of contributing significantly to production.

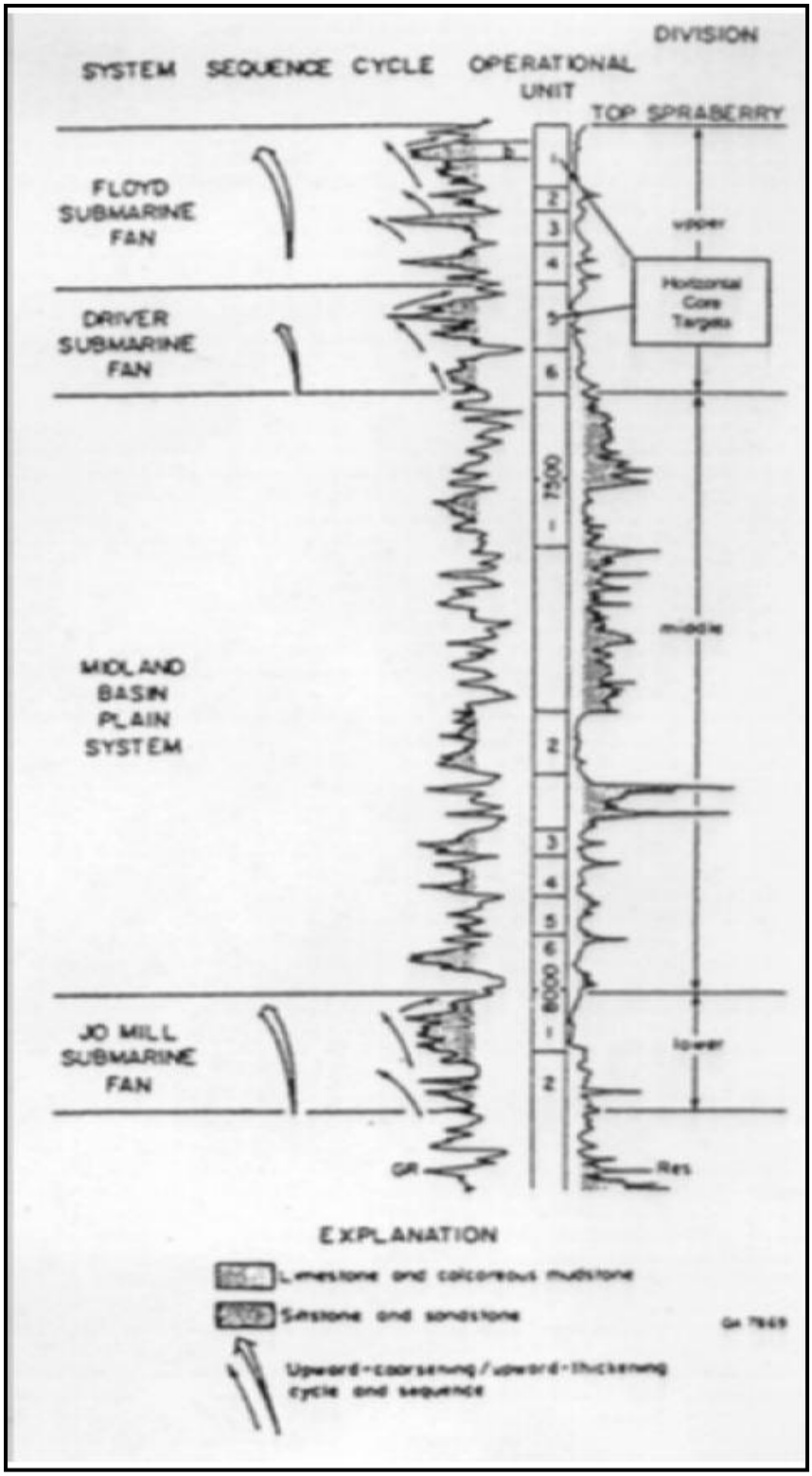

Figure 2.1: Division of Spraberry Formation in the central trend area.

2.4 Spraberry Field Fracture System

Although Spraberry field was discovered 64 years ago in 1949 and it has a long production history, the nature of the fracture system in this field is still not completely understood. Difficulties in constructing a fracture model starts from the inability to directly sample the fractures to scaling their effect and modeling their implications. Moreover, integration of dynamic data is even more challenging in fractured reservoirs when compared to conventional ones. This is due to the fact that fractures act as 'highways' that can dominate reservoir performance.

In an attempt to improve the understanding of Spraberry fracture network characteristics and its interaction with the supporting matrix framework, several dynamic tests and static studies were made. Those include outcrop studies, fracture logs, horizontal and vertical cores, interference tests, buildup tests, fall-off tests, step rate tests, inter-well tracers, salt tracers, production tests, profile logging, and discrete fracture modeling.

The abundance of dynamic data and geological static data and the different information that could be inferred from them highlight the need to integrate all of these data together to build a representative fracture model. Such data integration is critical to maximize recovery and to fully understand production profiles and the nature of the Spraberry fracture system.

In an attempt to build a composite fracture model by integration of all of the dynamic and static data together, Baker et. al. [(34)], proposed that Spraberry Trend Area could be described as a heterogeneous triple component system: First component is the long and

well-connected fractures, second is the shorter and partially-connected fractures, and third component is the low permeability matrix. A schematic of the triple component fracture system is shown in Figure 2.2

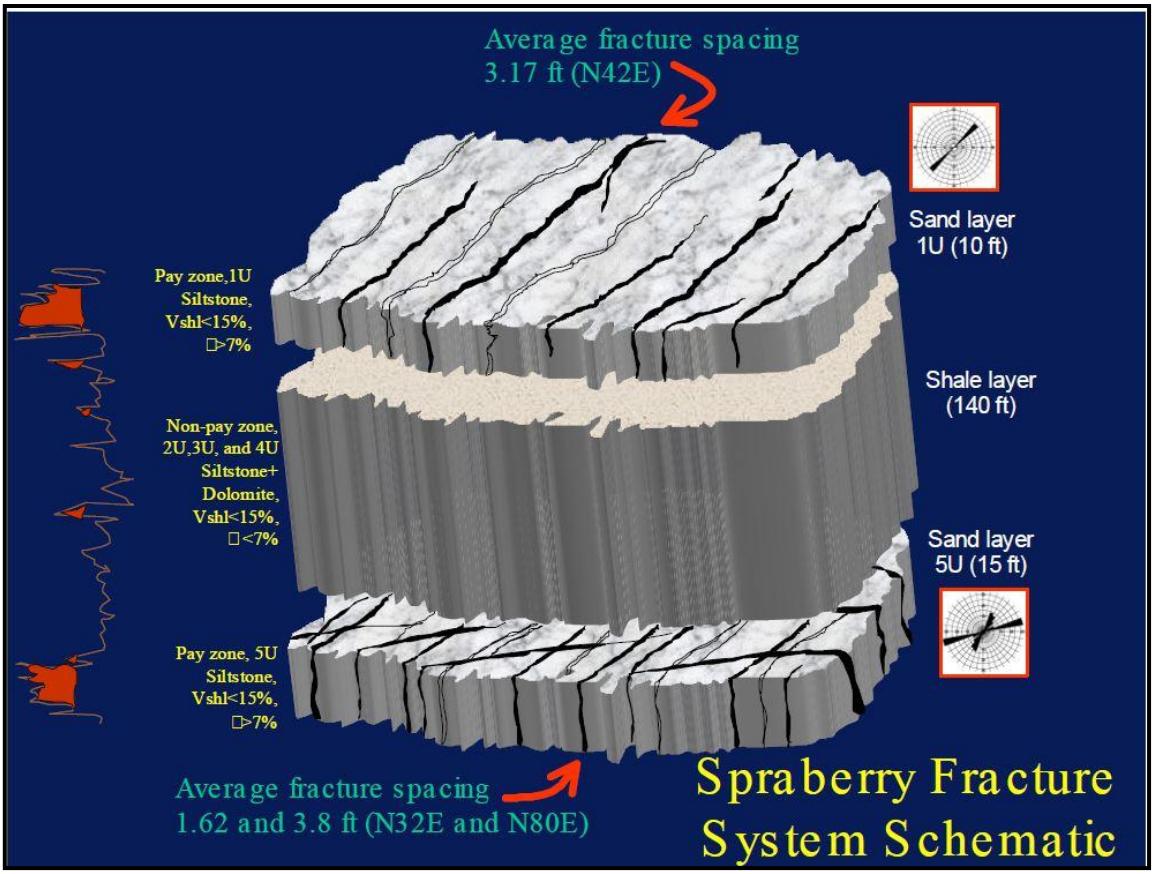

Figure 2.2: Schematic diagram of Spraberry fracture system.

The first component of Spraberry Trend Area are the stress sensitive, well connected fracture clusters that extends greater than 1000 feet in length and have unknown fracture

spacing. This system of very long fractures controls fluid flow in the reservoir and dictate which areas receive the injected fluids first. It was also observed that for any short term transport test with less than 1 month, this component completely dominate the response. Although these long fractures are important in early stages of reservoir development, their flow contribution is only less than 5% during the entire well's productive life.

The second component of Spraberry Trend Area is the secondary, short and partially connected fracture network. These fracture clusters have inter-fracture spacing of 2 to 4 feet range.

The long term production response of Spraberry field is controlled by fracture sets from both components and their cross-flow with matrix. With continuous water injection, water will distribute initially along the long fractures but with time water will invade more of the partially connected fracture system. Production profiles and waterflooding performance are strongly controlled by imbibition rate, average fracture spacing and matrix permeability [((34))].

2.5 Vertical and Horizontal Cores

Both vertical and horizontal cores were taken from different areas in Spraberry field to better understand the complex fracture system. Vertical core data showed vertical fractures with NE-SW and East-West orientation. It also indicated that fracture heights in the range of one to four feet and they usually do not extend through shale barriers existing between Upper Spraberry productive sand units 1U and 5U. Lateral cores were

also taken from each of Spraberry productive sand units. The first lateral core was a 400 feet horizontal core taken from the two main pay sections in O'Daniel Unit, Well# 28 in Midland County, Texas. It showed a clear distinction of three fracture sets trending NNE, NE, and ENE. Each fracture set has its own distinct pattern and characteristics in term of mineralization, spacing, distribution of strikes, surface characteristics, and correlation to lithology. Hence, it is very likely that each of these fracture set has originated from a separate stress event. Summary of characteristics of each fracture set is shown in Table 2.2 [(37,38)].

For the first set of fractures trending NE, the entire sampled population with a total of 46 observed fractures is contained within the 1U sand unit and none of them extend to shale layers. The fracture spacing for this set have a wide range from 0.73 to 5.75 foot with an average spacing of 3.17 foot. The distribution of spacing in Figure 2.3 shows a fair number of both widely and closely spaced fractures. It also shows that this fracture set has more evenly distributed fracture spacing compared to the other two sets, or compared to what is typical of regional fractures. In term of mineralization, only the NE fracture set shows obvious mineralization. The barite mineralization varies in extent from completely filling fractures with less than a millimeter wide aperture to a complete absence along hairline cracks in the intact rock. Majority of NE fractures contain some mineralization with 75% average percentage of filling. Presence of rosettes, local crystal faces and patches of barite indicate that these partially mineralized fractures offer open permeability and porosity pathways at reservoir depth. The total range of strikes for NE set is from 20-45 degrees with an average of 32 degree.

For the second set of fractures trending NNE, the entire sampled population of 28 fractures exist within the 5U sand and, similar to NE fracture set, none of them extend to shale layers. The fracture spacing for this set has a narrower range from 0.05 to 4.50 foot with significantly smaller average spacing of 1.62 foot. The distribution of spacing in Figure 2.3 shows a log-normal pattern typical of regional fractures. Typical regional fractures have large population of closely spaced fractures and fewer widely spaced fractures. In term of mineralization, none of NNE fracture set shows mineralization even in intervals where they occur in conjunction with mineralized NE fractures. NNE fractures appear as hairline cracks in intact core surfaces and this suggest significant conductivity under in situ conditions. The total range of strikes for NNE set is from 35-50 degrees with an average of 43 degree.

For the third set of fractures trending ENE, the 28 observed fractures are not confined to either the 1U sand unit or the 5U sand unit. In fact, this is the only fracture set observed to be present in the black shale facies overlying both the 1U and 5U sand units. However, this fracture set is not present in any core taken from black shale facies below either reservoir. The fracture spacing for this set has a range from 0.04 to 13.00 foot with an average spacing of 3.79 foot. The distribution of spacing in Figure 2.3 shows irregular scatter and the widest range among other sets. It also shows that majority of samples have fracture spacing of 5 foot and below. The ENE fracture set appears to be very similar to the NNE in term of hairline size cracks with no mineralization. However, surfaces of ENE fractures tend to be planar and smooth compared to anastomosed or

enechelon NNE fractures. The total range of strikes for NE set is from 50-85 degrees with an average of 70 degree.

Fracture Set	Minimum Spacing, ft	Average Spacing, ft	Maximum Spacing, ft	Average Strike, deg	Total Range of Strikes, deg
NE	0.05	1.62	4.50	32	20-45
NNE	0.73	3.17	5.75	43	35-50
ENE	0.04	3.79	13.00	70	50-85

Table 2.2: Fracture properties by set.

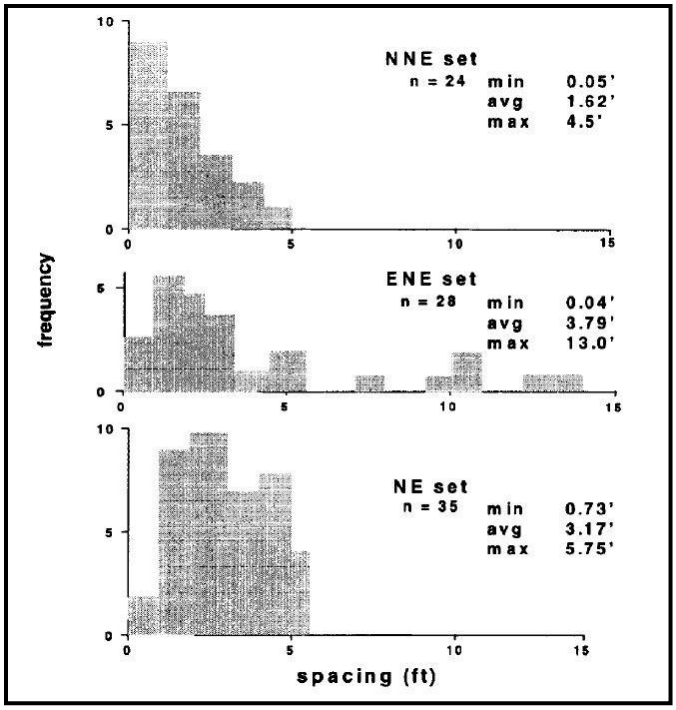

Figure 2.3: Distribution of spacing for the three fracture sets in Spraberry Field.

Recent horizontal cores acquired in 2012 through wells 3049 and 1019 Giddings Area of Spraberry showed another three fracture sets trending NE-SW, NW-SE, and E-W. Out of 53 fractures observed in well # 3049 horizontal cores, 50 were oriented NE-SW, 2 were oriented NW-SE, and only a single fracture oriented E-W. NE-SW fracture set are expected to dominate reservoir flow as original width of these fractures have been retained by an average of 44% as open void space despite the common calcite mineralization. There average spacing is less than three feet. The NW-SE and E-W fracture sets are not well developed but they are expected to offer permeability enhancement over matrix in the direction normal to NE-SW fractures.

When horizontal core samples from wells 3049 and 1019 were compared, significant but subtle differences in fracture populations were indicated. Both horizontal cores showed the closely spaced NE-SW fracture set to be dominant (Figure 2.4). In addition, both cores captured the widely spaced and rare E-W fracture set. On the other hand, comparing NE-SW fracture set from each core shows differences in fracture population indicating that they have different mechanical origin. The NE-SW fractures in well 3049 are extension fractures with more uniform dips, average 33% remnant porosity, and consistent confinement in the sandy/silty facies while the NE-SW fractures in well 1019 are normal shear fractures with steep but inclined dips, average 44% remnant porosity, and noticeable but limited presence in shaly intervals. Moreover, the E-W fracture set is mineralized in well 3049 core while in well 1019 it is not. The rare, irregular NW-SE fracture set observed in well 3049 core does not exist in well 1019 core [((39))].

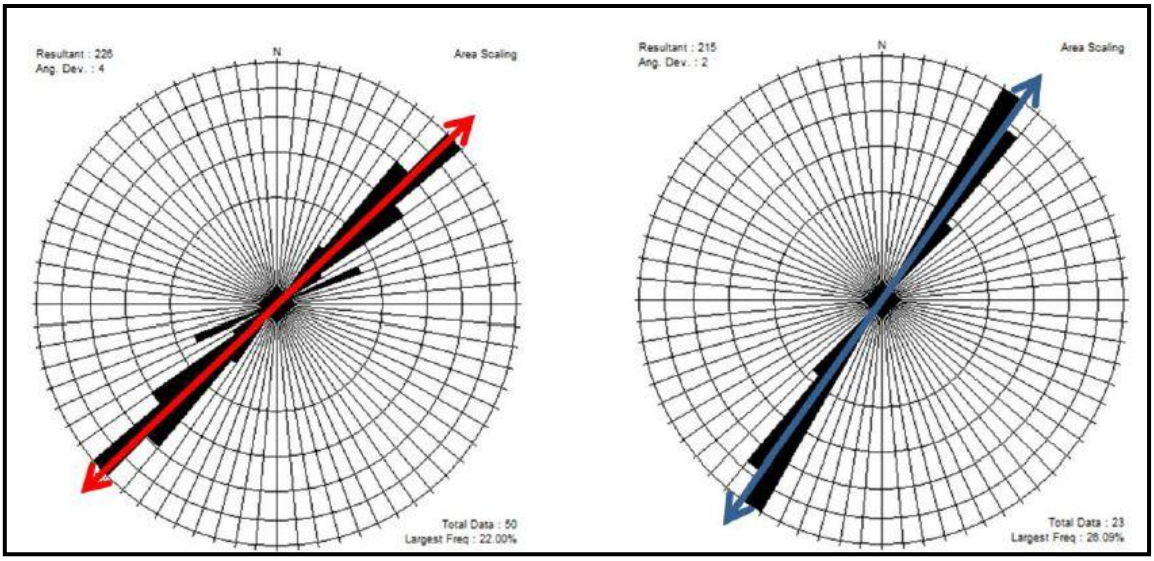

Figure 2.4: NE-SW fracture sets observed on Well 3049 (left) and Well 1019 (right).

2.6 Outcrops and Well Studies

Geological data from a deviated well in The Humble Unit Midkiff in Figure 2.5 confirmed that fractures are contained within the productive sand units and none exist at the shale. This is due to the ductility of shales compared to brittle sands. Shale content in many reservoir control fracture intensity as increased shale content in sands causes the rock be more ductile.

Outcrop studies on analogous reservoir provided information about fractures length, orientation, and their stress sensitivity. In addition, it showed large variation in fractures' characteristics. Outcrops showed that most fractures are short and less than 30 foot in length. Fracture maps, fracture images, and average fracture lengths for these outcrops are shown in Figures 2.6 and 2.7 [(34)].

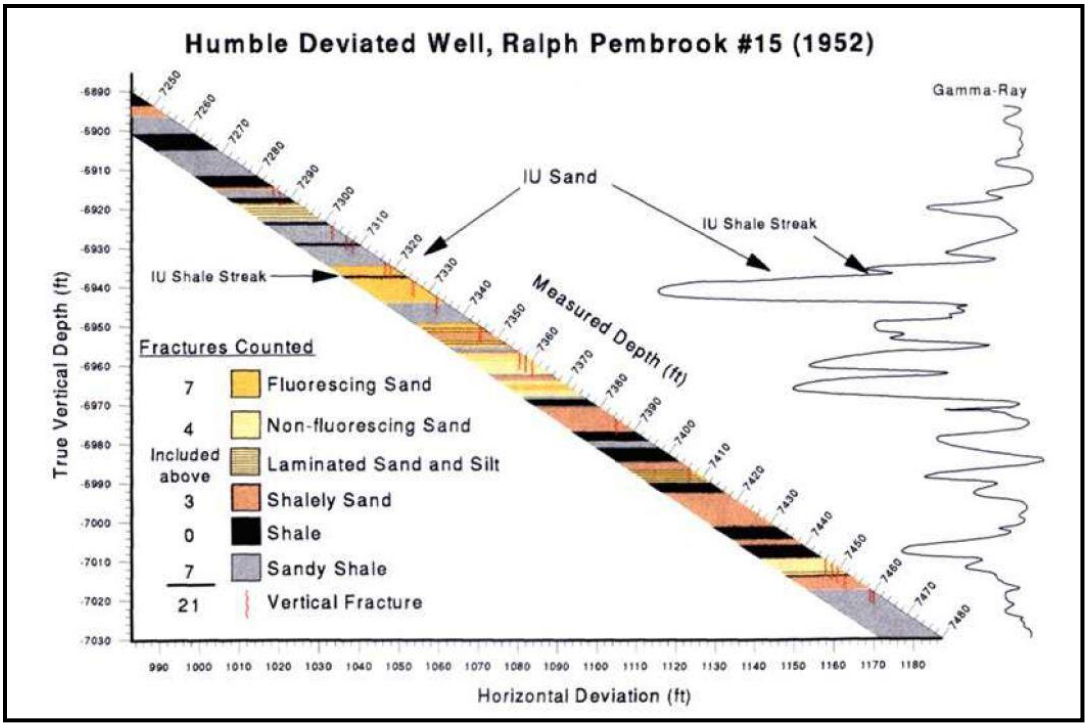

Figure 2.5: Humble deviated well showing fracture behavior and pattern.

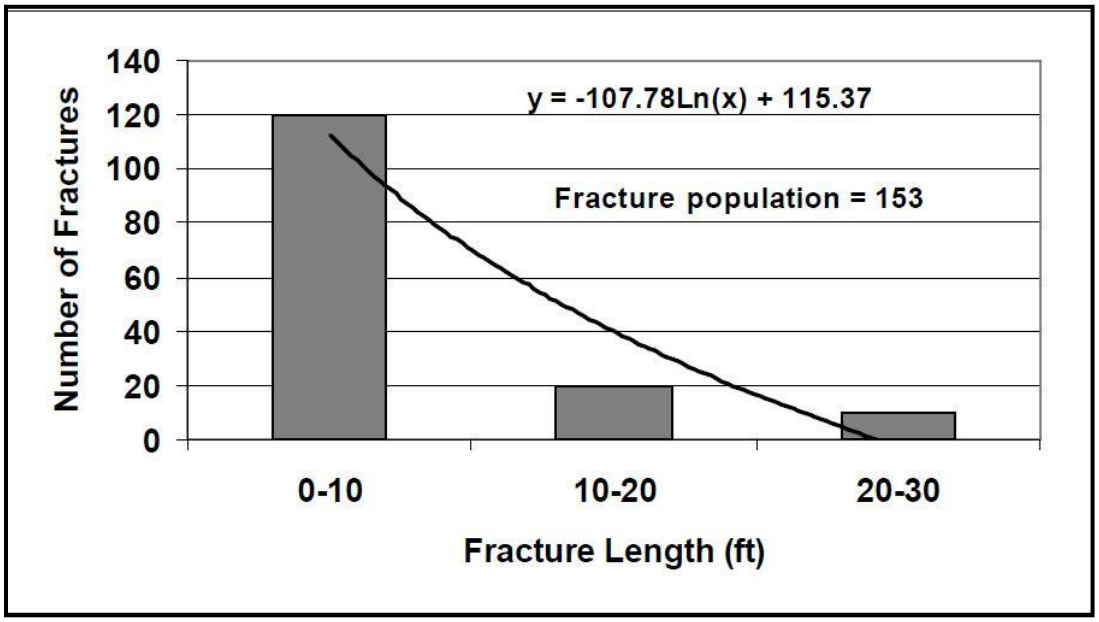

Figure 2.6: Fracture length frequency of Delaware outcrop data, West Texas

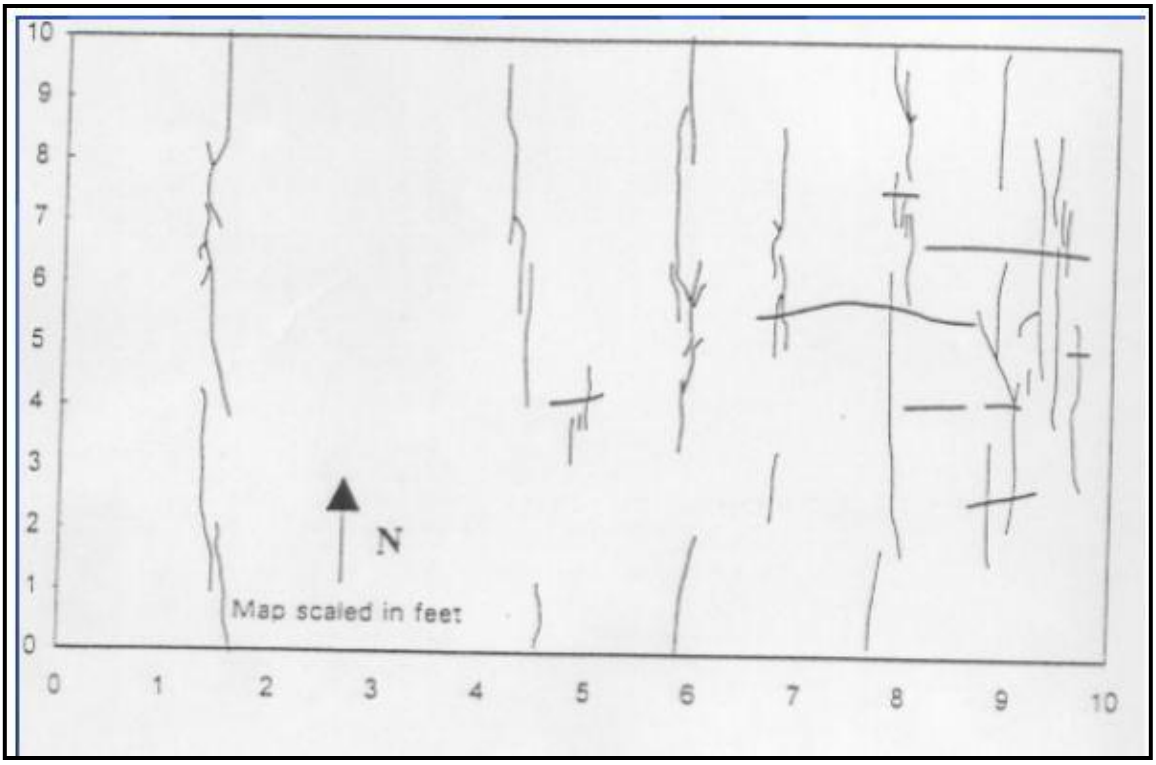

Figure 2.7: Fracture map of the Delaware outcrop data, West Texas.

2.7 Tracer Tests & Water Breakthrough Data

Since the start of waterflood projects in Spraberry field in 1951, numerous injection and production data is available for many Spraberry Units. Breakthrough behavior of injected water indicate N-E fracture trend with N50^{o}E average in Humble Water Flood and N42^{o}E average in Atlantic Water Flood. Gas injection test in Pembrook Area showed N48^{o}E.

Inter-well tracer test preformed in late 2000 in O'Daniel Unit using 6 tracers injected through 6 injectors also confirmed the NE-SW communication paths along with an East-West trend. Salt-water tracers were also used in O'Daniel Unit and confirmed the NE-

SW trend and showed a very weak communication in the north-west direction. Radioactive gas tracer in Pembrook Area showed a fracture orientation of N53^{o}E [(34)].

2.8 Pressure Tests and Advanced Decline Analysis

Early pressure build up tests prior to 1960 showed high effective permeability values in the range of 2-200 md. At that time, reservoir pressure was near original [(40)]. Later in the 1960s in Midkiff Unit, multi-well interference tests were run at a variable water injection rate. Test results showed that fractures are stress sensitive with strong trends in NE-SW, East-West, and NNE-SW directions. A key observation from this multi-well test is that tests with higher injection rates consistently showed higher values of permeability. Baker et. al.[(34)] analyzed ten single-well pressure falloff and buildup tests using both single porosity and dual porosity models. All of these wells were stimulated and hydraulically fractured and the tests confirmed the linear flow and the negative skins. Analysis of these tests confirmed the stress sensitive nature of fractures where buildup tests showed low permeability values (<1 md) and falloff tests showed much higher permeability vlues (>1 md) [(40)]. The higher permeability values measured for falloff tests is believed to be a result of the higher reservoir pressure around injectors. Mini-frac and step rate tests showed that hydraulic fracturing occurs at low pressures close to hydrostatic pressure gradient.

Advance decline analysis showed effective permeability to oil in range of 0.4 to 0.9 md. This enhancement to the measured core permeability of less than 0.05md is believed to be because of the presence of the short and partially continuous fracture set mentioned

earlier. Decline analysis also showed that the effective average fracture spacing to be of 3.1 feet [(41,42)]. The value of average effective fracture spacing agrees well with spacing obtained from horizontal cores described earlier.

2.9 Production Logging and Temperature Logs

Available production logging tests (PLTs) for three injectors in O'Daniel Unit show that injected water is uniformly distributed within 1U and 5U sands [(37)]. A sample PLT for one of the injectors is shown in Figure 2.8 below. Although core samples show that fractures do not cross shale boundaries, temperature logs gives indication that this is likely to happen in some areas. The temperature log in Figure 2.8 shows low temperature above 5U sand unit confirming the presence of cooler injected water. As this well was not hydraulically fractured, it is very likely that the injected water is flowing through fractures crossing shale boundaries [(34)].

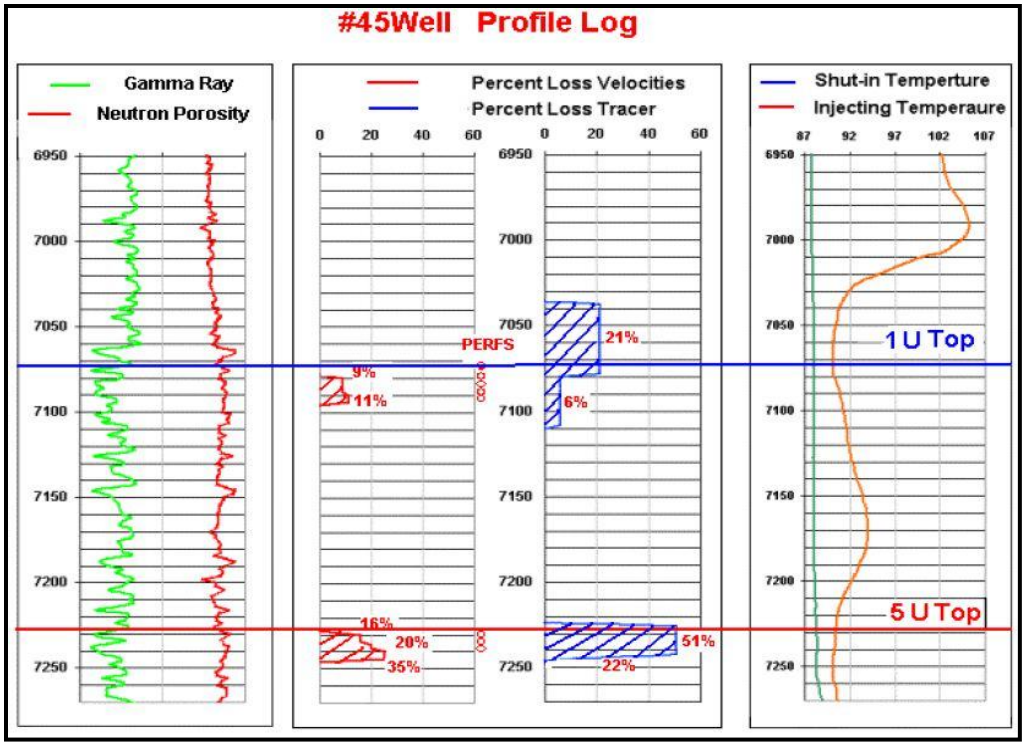

Figure 2.8: Injection Profile Log on Well 45 in O'Danial Area, Spraberry.

2.10 Initial Water Saturation

A careful evaluation of initial water saturation is made based on cores from 46 wells acquired before 1954. A plot of initial water saturation versus air permeability is presented in Figure 2.9. The figure shows no core with initial water saturation below 20%. In addition, the low permeability region exhibit more scatter in saturation data compared to the high permeability region. An approximation of the average water saturation could be presented by the following equation:

$$S_{wi} = 0.20 + 0.12\, e^{-0.60\,(K - 0.1)}$$

Where k is the air permeability in milidarcies and S_{wi} is the initial water saturation.

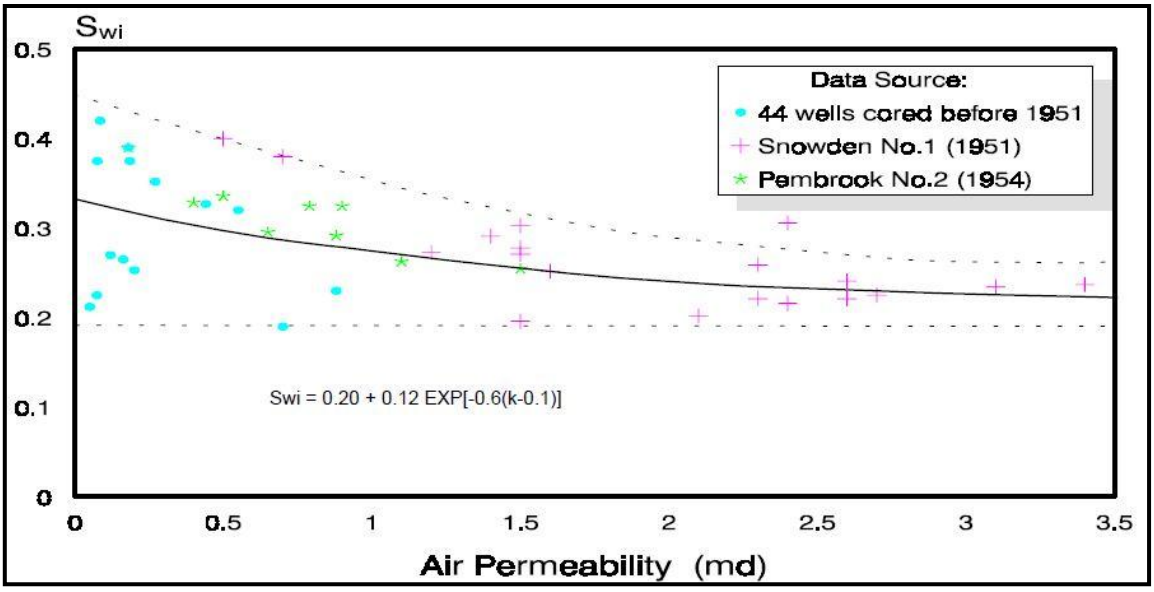

Figure 2.9: Initial water saturation in Spraberry sandstone.

Using the above correlation for initial water saturation determination and laboratory measurements of cores' permeability, an evaluation of macroscopic displacement efficiency (E_{dm}) of Spraberry cores subjected to waterflooding is made and summarized in Table 2.3

Year	Core Permeability, md	S_{wi}, %	E_{dm}, % of OOIP	Well Cored
1963	0.4-1.3	32-40	10-16	Tippett #5
1974	0.3-0.5	35-45	20	Parish #7
1987	0.3-1.0	35-55	17-21	Judkins A#5
1990	0.6-1.2	31-52	15-26	Pembrook #9407
1995	0.2-1.6	20-50	12-28	E.T.O'Daniel #37

Table 2.3: Estimated macroscopic displacement efficiency in Spraberry cores.

2.11 Rock Wettability by Imbibition Experiments

The interaction between reservoir rock, crude oil, and formation water is very important to be understood and evaluated. Thus, water and oil imbibition experiments using Spraberry reservoir rock, Spraberry oil and synthetic reservoir brine were made. Based on spontaneous water and oil imbibition tests done on cores taken from Spraberry Shackelford 1-38A, wettability of Spraberry field was found to be weakly water-wet with mixed wetting behavior. The Amott wettability index to water for these cores was found to be in the range of 0.5 to 0.7. The macroscopic displacement efficiency during spontaneous water imbibition ranges from 40% to 70% based on core permeability.

The effect of core cleaning and aging on wettability and displacement efficiency was investigated. Some cores were cleaned with chloroform to establish a wetting condition similar to reservoir condition before running imbibition tests. On the other hand, 10 core plugs were assumed to be clean and were not treated with chloroform. Oil recovery curves for some of the cleaned cores and the un-cleaned core plugs are presented in Figures 2.10 and 2.11, respectively. Final oil recovery due to imbibition varies from 15-70% for cleaned cores and 10-40% for un-cleaned cores. Rock properties and imbibition results for cleaned and un-cleaned cores are summarized in Tables 2.4 and 2.5.

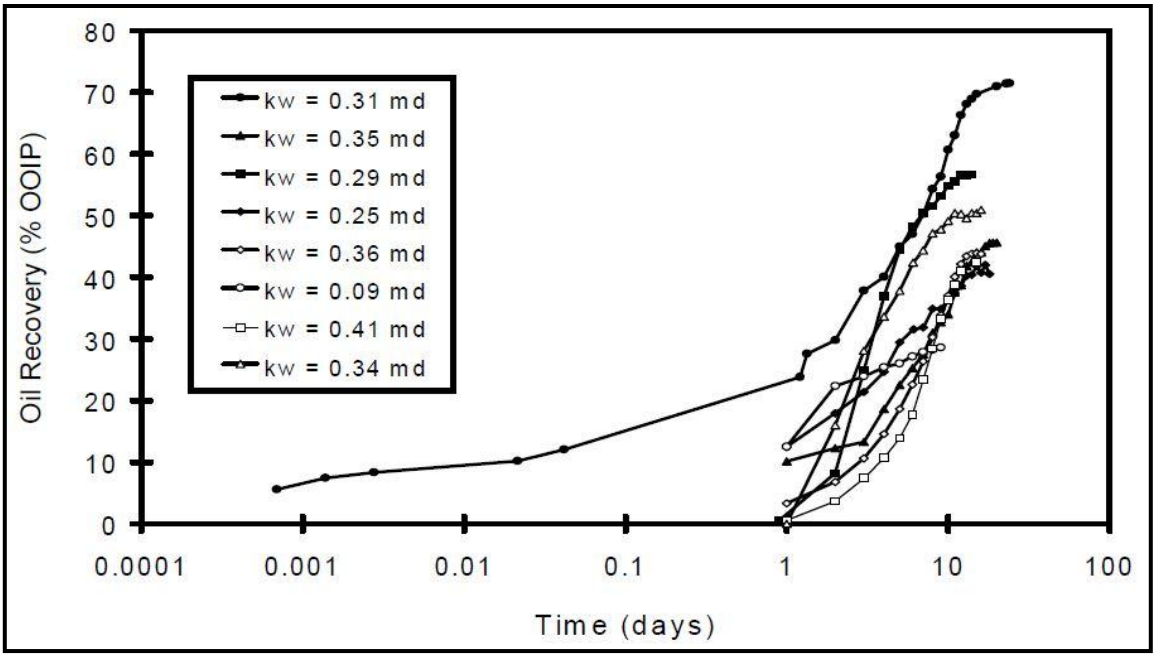

Figure 2.10: Oil recovery from cleaned Spraberry cores during water imbibition.

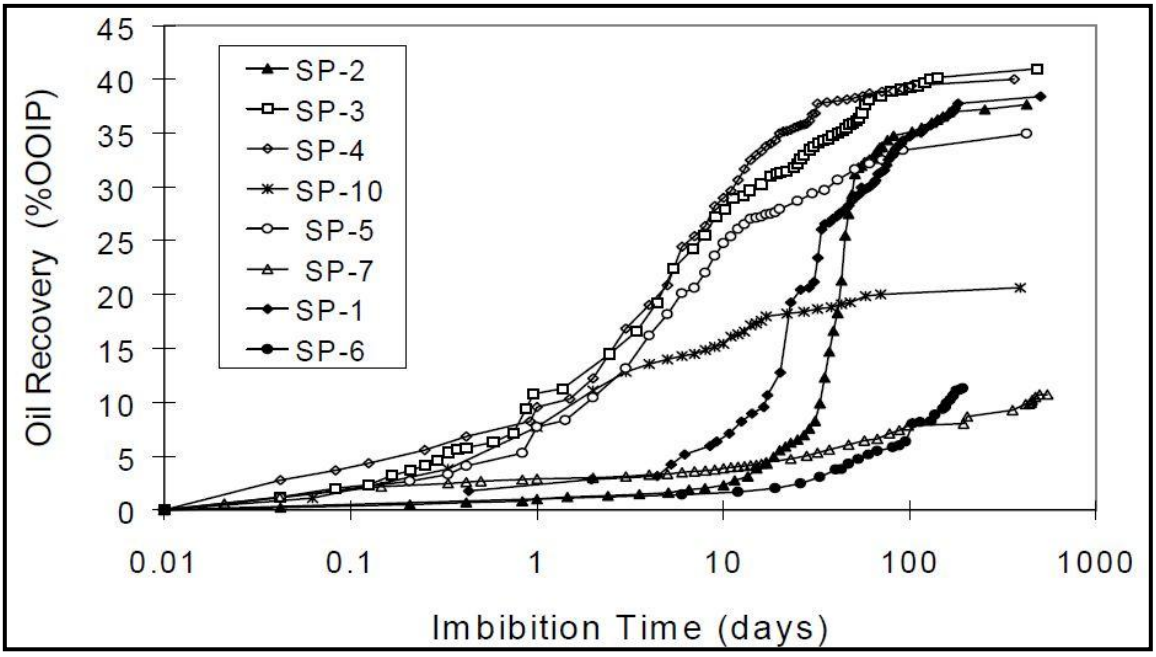

Figure 2.11: Oil recovery from untreated Spraberry cores during brine imbibition

Test No.	Before Cleaning			After Cleaning			t_{oil}	R_{im}	I_w
	φ (%)	k_w (md)	S_{wi} (%)	φ (%)	k_w (md)	S_{wi} (%)	(days)	(OOIP)	-
SP-11	10.0	0.11	-	13.2	0.31	38	6	0.71	0.76
SP-21	10.8	0.10	-	14.4	0.35	36	15	0.45	0.64
SP-22	5.0	0.03	-	10.1	0.25	42	49	0.42	0.49
SP-24	4.1	0.03	-	11.6	0.36	38	1	0.79	0.75
SP-27	6.8	0.04	-	10.6	0.29	39	30	0.57	0.66
SP-28	2.9	0.02	-	7.8	0.09	53	90	0.29	0.35
SP-33	11.8	0.21	13.9	13.9	0.41	35	60	0.47	0.55
SP-1	10.0	0.28	21.3	12.0	0.34	37	21	0.50	0.55

Table 2.4: Rock properties for cores used in Figure 2.10

Test No.	φ (%)	k_a (md)	k_w (md)	k_o (md)	S_{wi} (%)	ρ_w (g/cc)	ρ_o (g/cc)	μ_w (cp)	μ_o (cp)	R_{im} (%)
SP-1	10.0	0.43	0.28	0.09	13.9	1.09	0.86	1.16	38	41
SP-2	10.0	0.45	0.22	0.10	18.4	1.09	0.87	1.18	38	38
SP-3	9.8	0.44	0.23	0.14	21.3	1.08	0.87	1.17	41	22
SP-4	10.0	0.49	0.14	0.06	14.3	1.08	0.87	1.17	40	27
SP-5	10.7	0.49	0.27	0.09	15.3	1.08	0.87	1.18	35	40
SP-6	9.8	0.43	0.22	0.06	17.2	1.08	0.87	1.18	>11	25
SP-7	10.4	0.34	0.20	0.08	22.0	1.08	0.75	1.18	>10	-
SP-10	12.8	0.36	0.15	0.05	26.5	1.08	0.87	1.18	21	24

Table 2.5: Rock and fluid properties for cores used in Figure 2.11

Figures 2.10 and 2.11 showed that cleaning cores with chloroform caused significant improvement to rate of water imbibition and hence, to the final oil recovery. Table 2.4 shows that chloroform cleaning caused porosity and permeability to increase, hence increasing cores' water saturation. This suggests that chloroform cleaning will change the wettability of the rock causing cores to be more water wet. This is supported by the improvement in average Amott wettability index to water (I_w) from 0.5 to 0.6 after waterflooding the core. A plot of final oil recovery versus core permeability to brine is shown in Figure 2.12

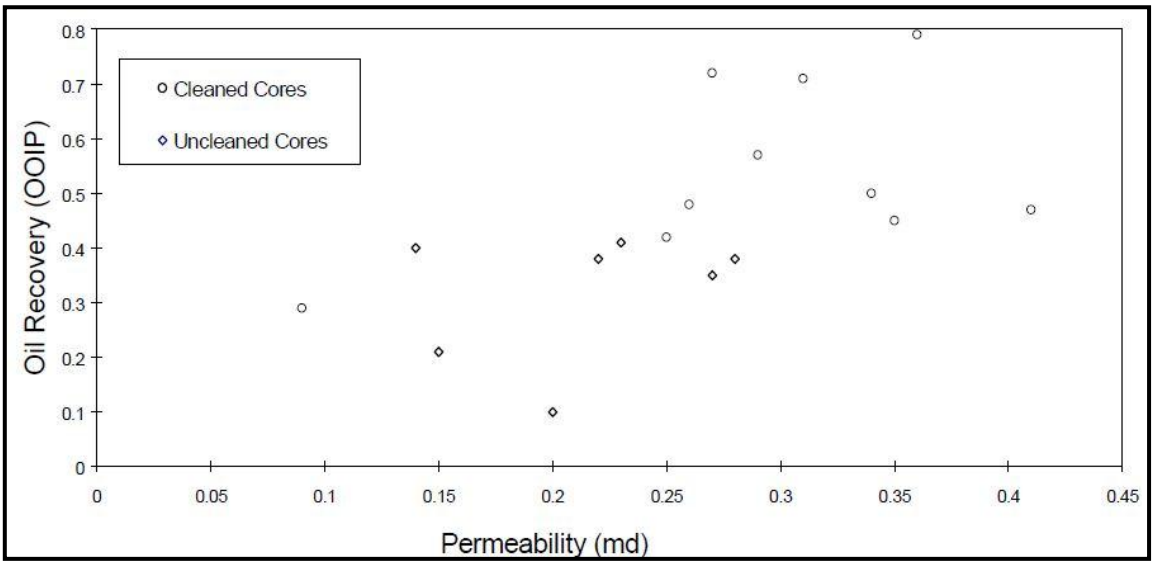

Figure 2.12: Effect of core permeability to water on final oil recovery

2.12 Water-oil Capillary Pressure Determination

Estimation of water-oil capillary pressure in Upper Spraberry productive sand units 1U and 5U was made by the utilization of Leverett J-function on previously measured mercury injection capillary pressure data. Capillary pressure measurements by mercury injection were done on 9 cores from Spraberry Shackelford # 1-38A and 5 cores from Spraberry Judkins A#5. Figures 2.13 and 2.14 show capillary pressure curves for the 9 Shackelford cores and the 5 Judkins cores after conversion to Leverett J-function, respectively. Since the 7 complete curves shown in Figures 2.13 and 2.14 appear to be similar, the average J-function of the seven cores could be used to estimate the water-oil capillary pressure of the system. The average J-function curve is shown in Figure 2.15. Water-oil capillary pressure curve for a 0.5 md and 10% porosity Spraberry core is shown in Figure 2.16 and was estimated by assuming water-oil interfacial tension of 42 mN/m and a contact angle of 45 degrees. Imbibition capillary pressure for the 0.5md Spraberry core is also shown in Figure 2.16 and was estimated by subtracting a pressure of 15 psia from the estimated drainage capillary pressure in order for the curve to intersect water saturation axis at a point corresponding to Amott wettability index to water of 0.55 as determined by imbibition tests. Other capillary pressure measurements on different areas of Spraberry field were made using static equilibrium methods, centrifuge method, and mercury injection [(43)]. Drainage and imbibition capillary pressure curves from those measurements are shown in Figures 2.17 and 2.18. It is seen from Figures 2.17 and 2.18 that capillary pressure curves using centrifuge method is significantly higher than that obtained from static equilibrium method. In addition, those

figures show that static capillary pressure curve from static equilibrium is close to the mercury injection data when a contact angel of 50 degrees is assumed.

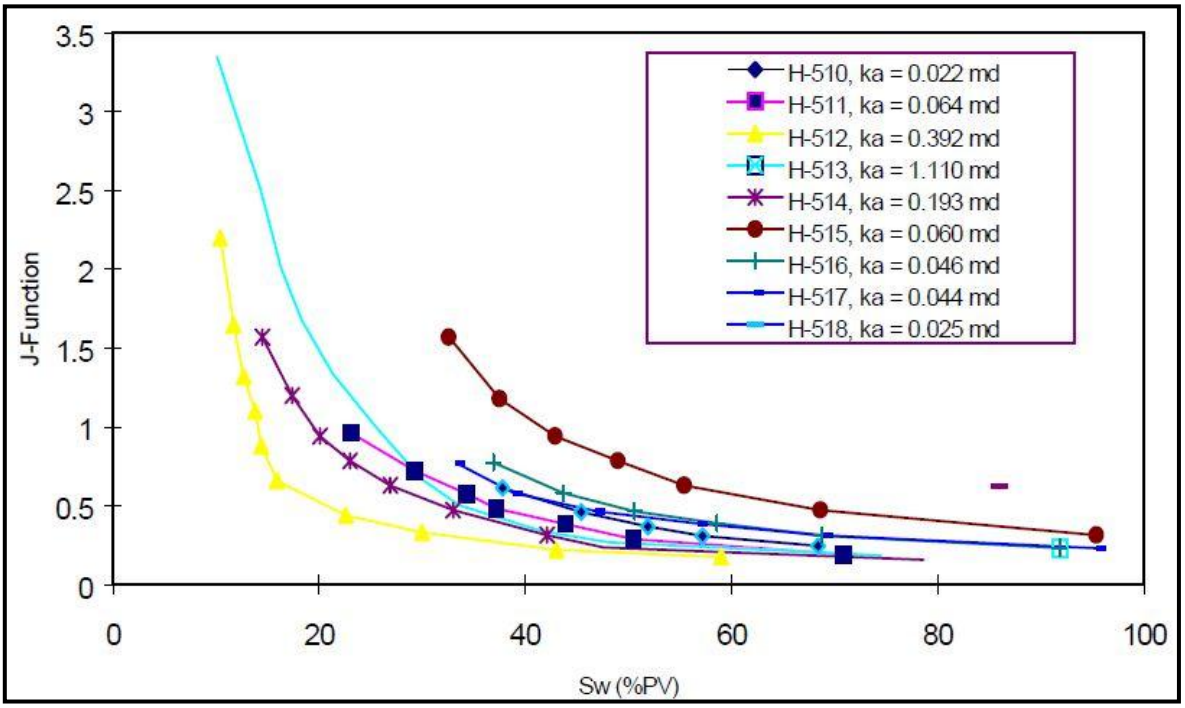

Figure 2.13: Capillary pressure curves converted to J-function for 9 Shackelford, Spraberry cores

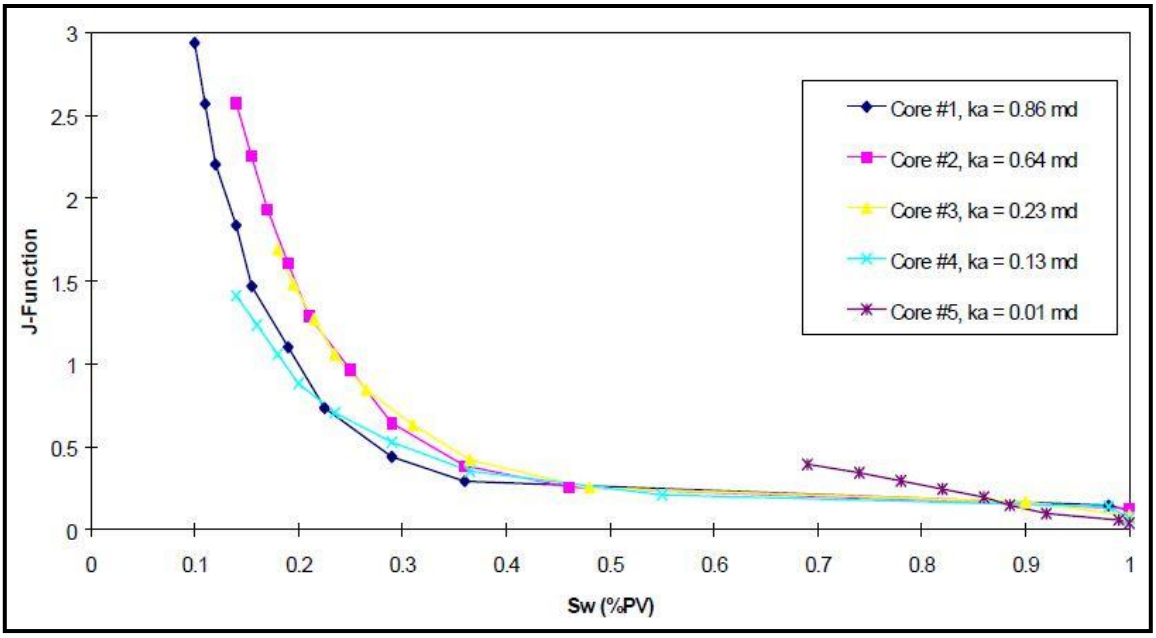

Figure 2.14: Capillary pressure curves converted to J-function for 5 Judkins, Spraberry cores

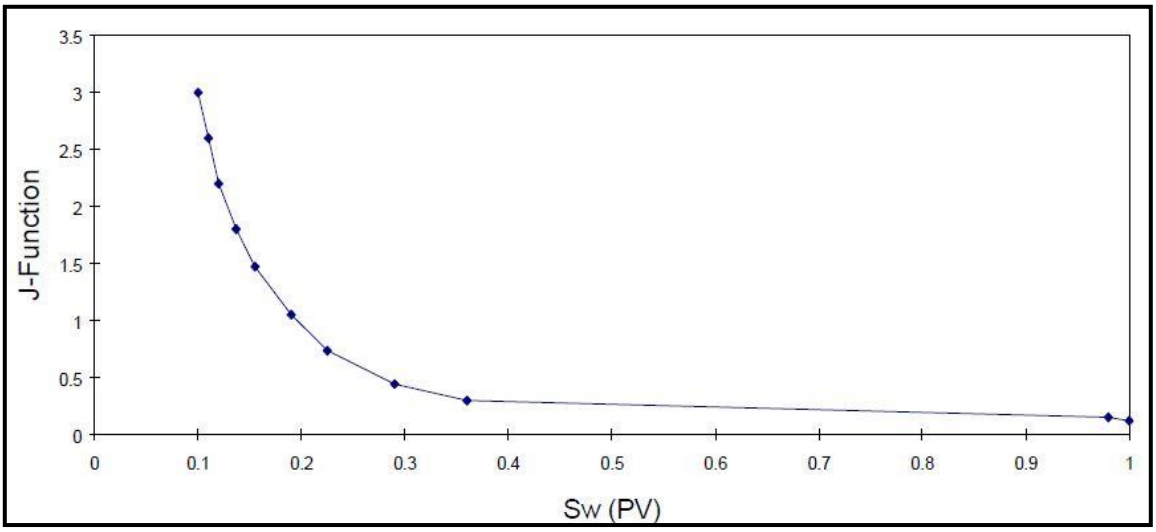

Figure 2.15: J-function calculated from mercury injection capillary pressure data

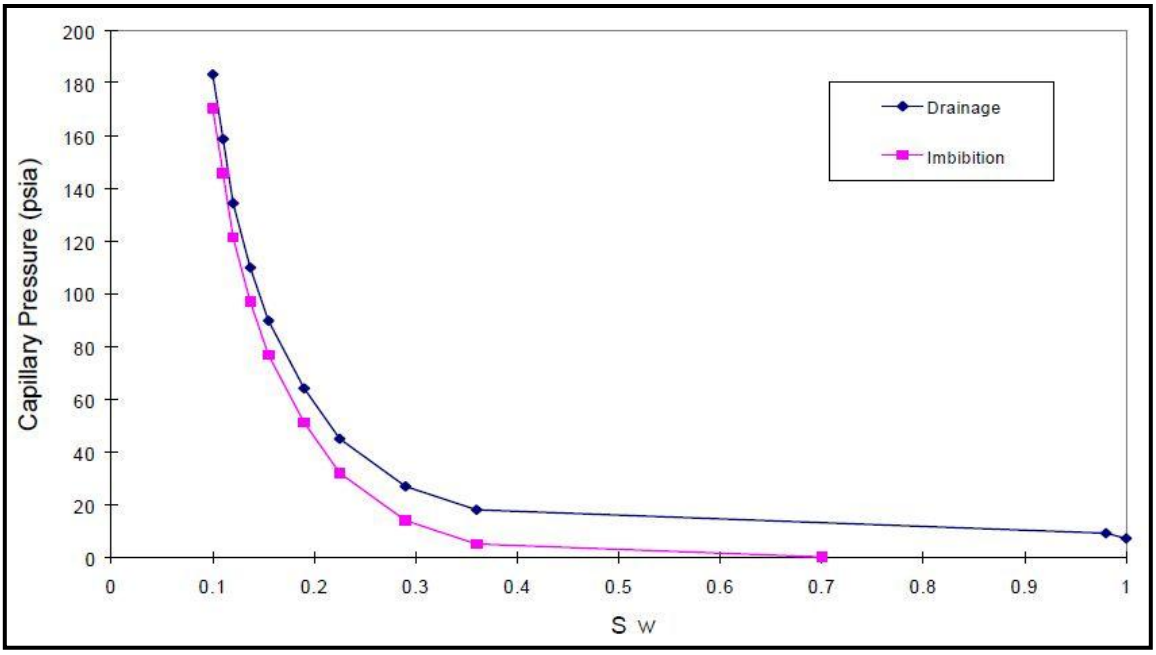

Figure 2.16: Estimated water-oil capillary pressure in Spraberry sand.

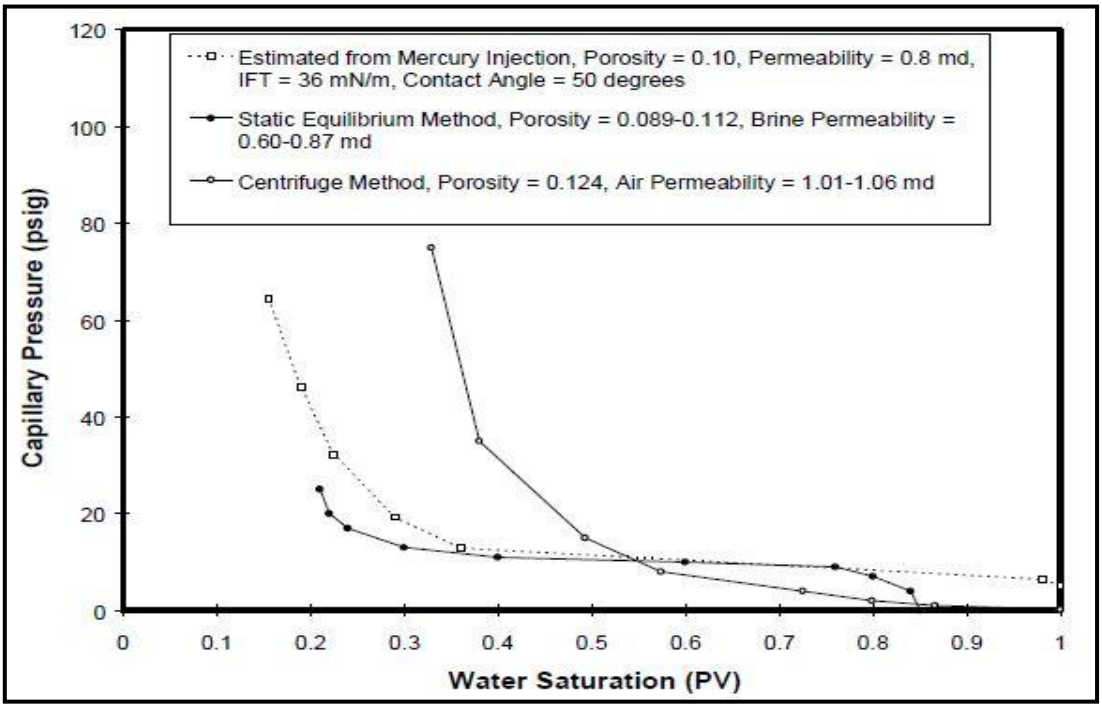

Figure 2.17: Drainage capillary pressure curves for Spraberry cores

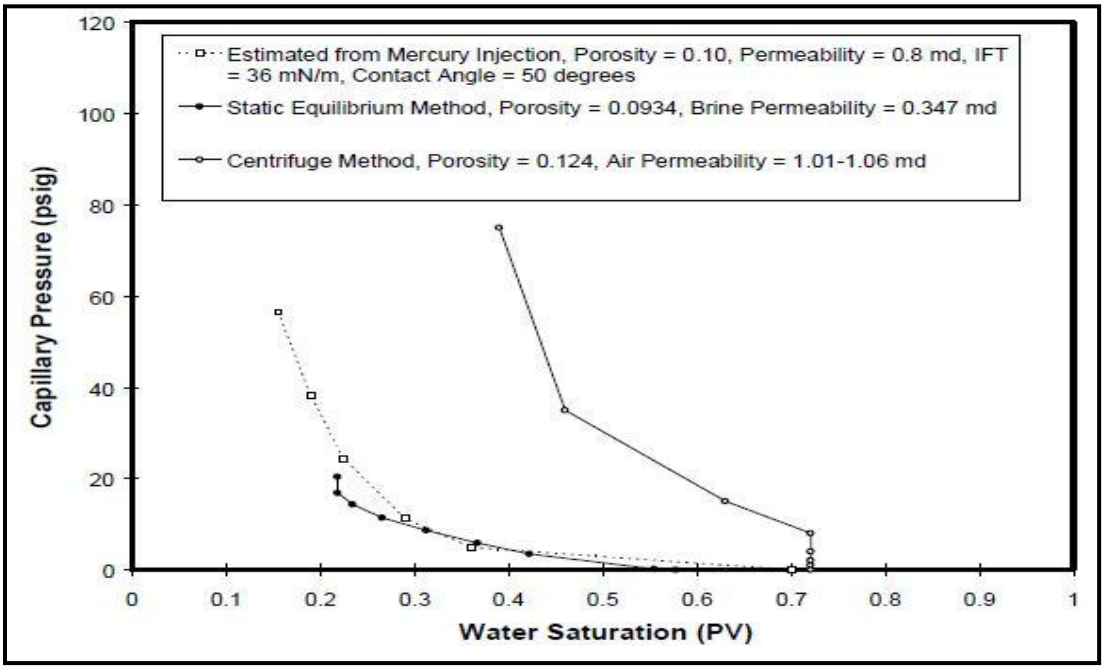

Figure 2.18: Imbibition capillary pressure curves for Spraberry cores

3. INTER-WELL TRACER TEST IN SHERROD AREA OF SPRABERRY FIELD

3.1 Sherrod Production History & Tracer Project Description

Sherrod Area of Spraberry Field was first put on production in July 1951. The field oil production was dry for about 22 years until the first water breakthrough occurred in January 1973. Early water production data shows complex water-cut behavior indicating the presence of a complex fracture system. Example of such water-cut behavior is shown in Figure 3.1. Water injection in the field started in January 1983 after around 32 years of primary depletion with one power water injector. Additional injector was introduced in 1990 and three more were introduced in late 2001 / early 2002. Field performance plots from July 1951 until March 2012 are shown in Figures 3.2 through 3.4. Well by well production and injection histories are shown in Appendix A. It must be noted that production history prior to January 1970 must be handled with precaution as different wells shows exactly the same monthly average allocated rates.

In 2010, a decision was made to develop a large area of Spraberry using 11 inverted 9-spot patterns. In order to effectively manage the pattern water flood area as well as the area outside the pattern, 13 non-reactive water tracers were injected through 13 injectors and 110 producers were water sampled. Objectives of Sherrod inter-well tracer test are to understand complex water movement in the reservoir, to assess injector-producer connectivity, and to understand sweep and fracture system heterogeneity. The tracer test lasted for 114 days from start of tracer injection in April 25, 2011 until last water sample were analyzed in August 17, 2011. Tracer breakthrough was observed from the same day

of tracer injection, and a total of 598 tracer elution curve were detected from 51 out of the 110 sampled wells. Tracer test design is discussed in more detail in next section.

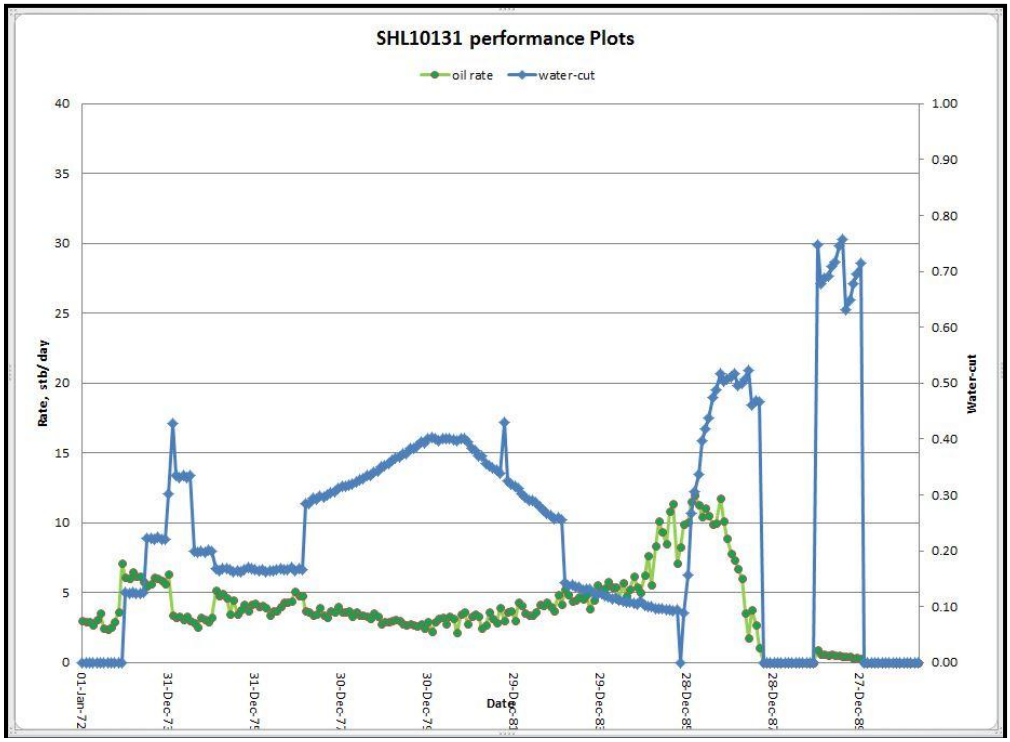

Figure 3.1: Example of early complex water-cut behavior

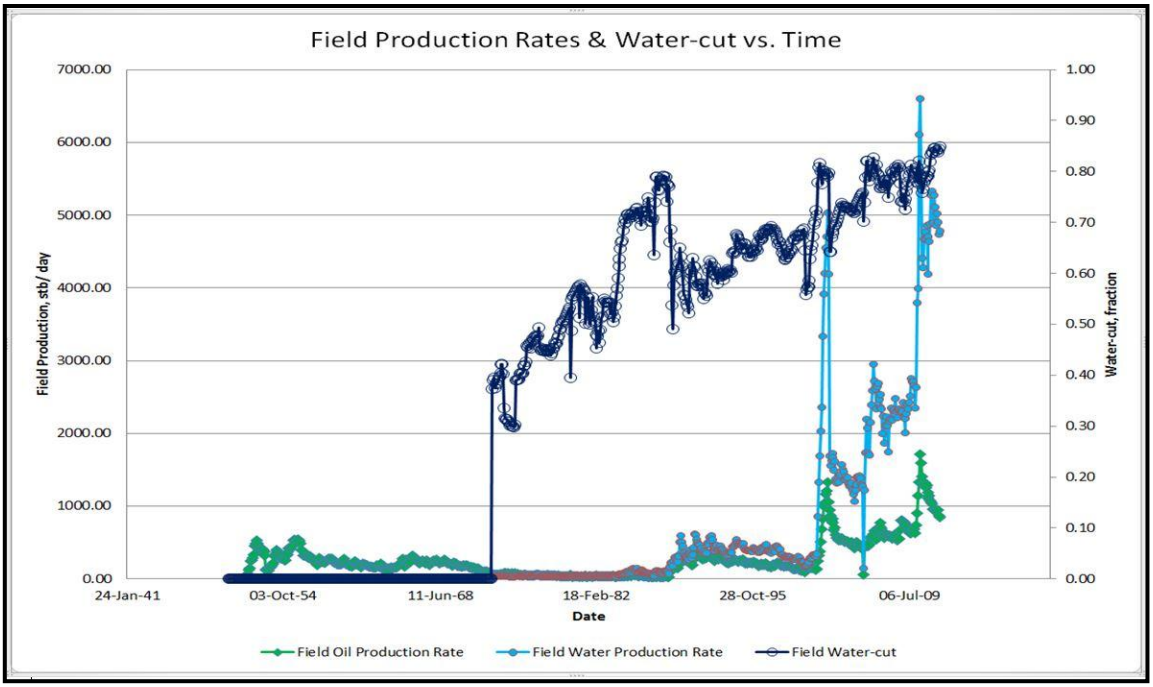

Figure 3.2: Field oil and water production rates and field water-cut with time.

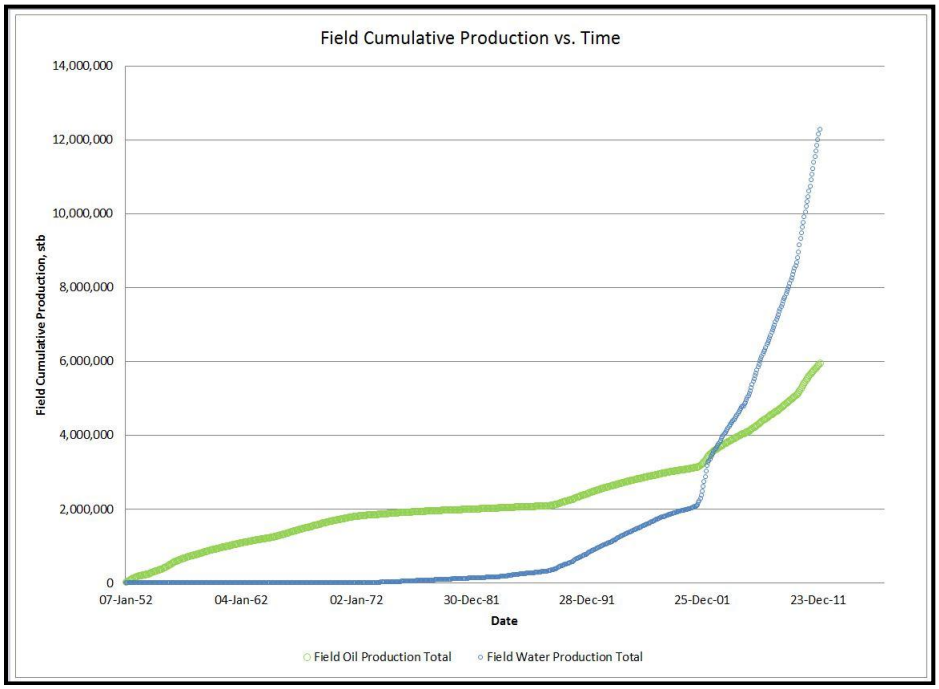

Figure 3.3: Field oil and water cumulative production

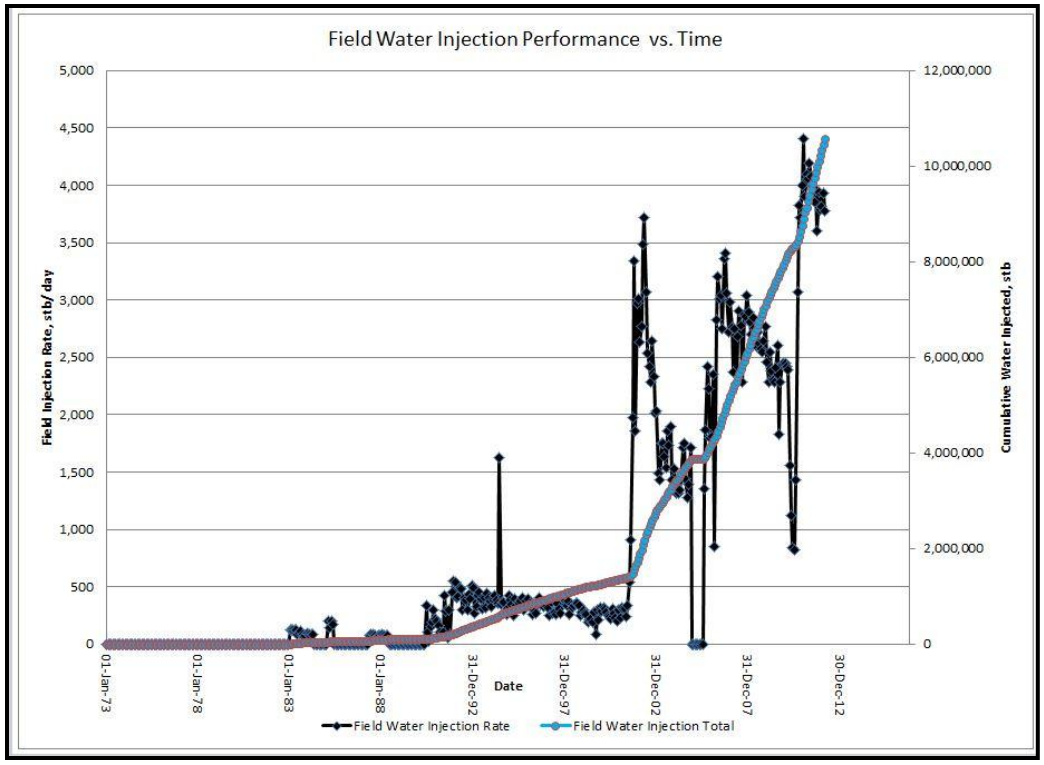

Figure 3.4: Field water injection performance versus time

3.2 Tracer Injection Design

In Sherrod inter-well tracer test, a decision was made to use non-reactive water tracers over chemical and radioactive tracers to tag 13 out of the 15 active water injectors. Injection and water sampling locations are shown in Figure 3.5 below. Tracer volumes used, injection durations and injection rates used for mixing tracer with water are shown in Table 3.1 below.

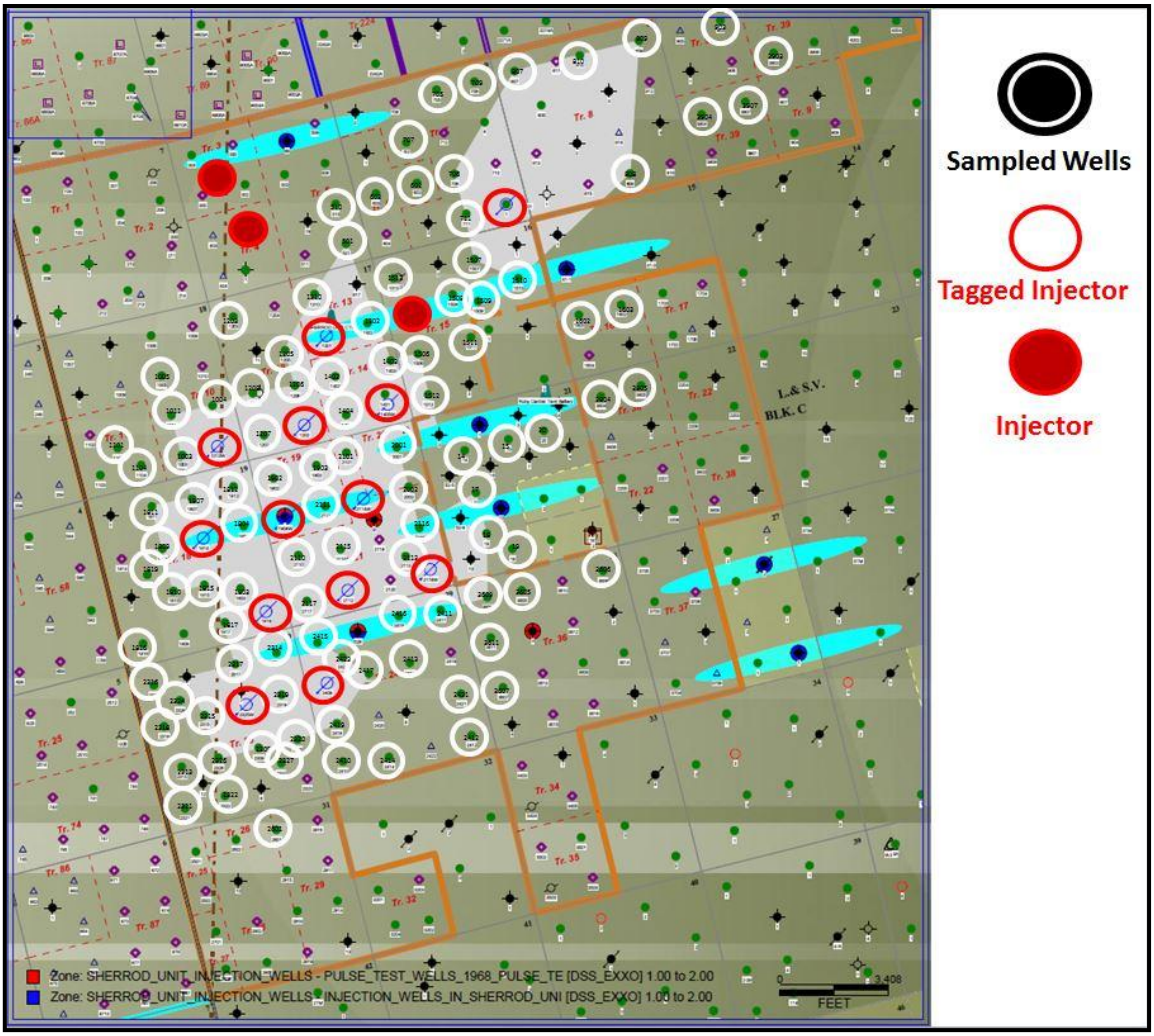

Figure 3.5: Tracer sampling & injection locations

Injection Well ID	Tracer Type	Tracer Amount (L)	Tracer Amount (g)	Date of Injection	Start Time	End Time	Injection Time (hours)	Well Injection Rate (BPD)	Tracer Slug Volume (ml)	Injected Tracer Concentration (W/V) , ppt
Sherrod U 1814W	IWT 1900	200	20000	25-Apr-11	12:00 PM	4:00 PM	4	365	9871892	2,025,954,161
Sherrod U 1202W	IWT 2400	118	11800	25-Apr-11	5:00 PM	8:00 PM	3	321	6497474	1,816,090,446
Sherrod U 1818W	IWT 1100	212	21200	26-Apr-11	7:00 AM	11:30 AM	4.5	260	7962763	2,662,392,606
Sherrod U 2112W	IWT 1700	193	19300	26-Apr-11	12:00 PM	4:30 PM	4.5	345	10477666	1,842,013,354
Sherrod U 2409W	IWT 1200	231	23100	26-Apr-11	5:00 PM	10:00 PM	5	355	11989635	1,926,664,089
Sherrod U 1301W	IWT 1500	88	8800	27-Apr-11	6:00 AM	9:00 AM	3	390	7838763	1,122,626,180
Sherrod U 1904W	IWT 2200	159	15900	27-Apr-11	9:30 AM	2:30 PM	5	275	9267802	1,715,617,129
Sherrod U 1405W	IWT 1500	92	9200	27-Apr-11	3:00 PM	6:00 PM	3	310	6252863	1,471,326,133
Sherrod U 2114W	IWT 2500	128	12800	27-Apr-11	6:30 PM	11:00 PM	4.5	340	10263613	1,247,124,246
Sherrod U 2325W	IWT 1000	273	27300	28-Apr-11	6:00 AM	10:30 AM	4.5	190	5937019	4,598,267,439
Sherrod U 2118W	IWT 1600	148	14800	28-Apr-11	11:00 AM	2:30 PM	3.5	330	7799394	1,897,583,386
Sherrod U 1012W	IWT 2100	154	15400	28-Apr-11	3:00 PM	6:30 PM	3.5	325	7689464	2,002,740,492
Sherrod U 701W	IWT 2000	168	16800	28-Apr-11	7:00 PM	10:00 PM	3	145	3049694	5,508,749,854

Table 3.1: Tracer injection concentrations & schedules

3.3 Effect of Water Recycling on Tracer Test Results

In Sherrod Area, the produced water from all wells flow through surface pipelines to Sherrod Battery Injection Unit where water is being re-injected. The re-injection of produced water has also caused the tracers to be re-injected and to impact the results of the tracer test. Measurement of tracers' concentration at Sherrod Battery Unit before re-injecting the produced water was made and reported as part of the test. Tracer data was provided in two versions: First version in Appendix B shows tracer response data as measured without applying any correction. Second version in Appendix C shows tracer response data after applying corrections for water recycling. Basis for correcting tracer data is unexplained.

3.4 Pressure Data

Available pressure data are extremely limited covering one point in time for a few number of wells. Due to the singularity nature of pressure data, they were not used in the history match process. A summary of available pressure data are summarized in Table 3.2. Pressure measurement reports are shown in Appendix D.

Well	Pressure Data	Date
1012w	Gradient Data	07/2010
1202	Gradient Data	07/2010
1405	Gradient Data	07/2010
1814	10 days P_{bh} monitoring	07/2010
1818w	34 days P_{bh} monitoring	07/2010
1904	07 days P_{bh} monitoring	07/2010
2112	10 days P_{bh} monitoring	07/2010
2325w	26 days P_{bh} monitoring	07/2010
2409w	31 days P_{bh} monitoring	07/2010

Table 3.2: Summary of available pressure data in Sherrod Area

3.5 PVT Data

Five oil samples are available from five different areas in Spraberry Field: Fasken #1-8, Midkiff A#23, RW Clark #1, Shackleford #1, and SHER M7. Solution gas-oil ratio, oil formation volume factor, and viscosity are shown in Figures 3.6 through 3.8. Compositional Analysis for Fasken, Midkiff, and Shackleford samples is shown in Figure 3.9. Separator tests results were provided in Table 3.3 to correct PVT properties from lab condition to actual separator condition.

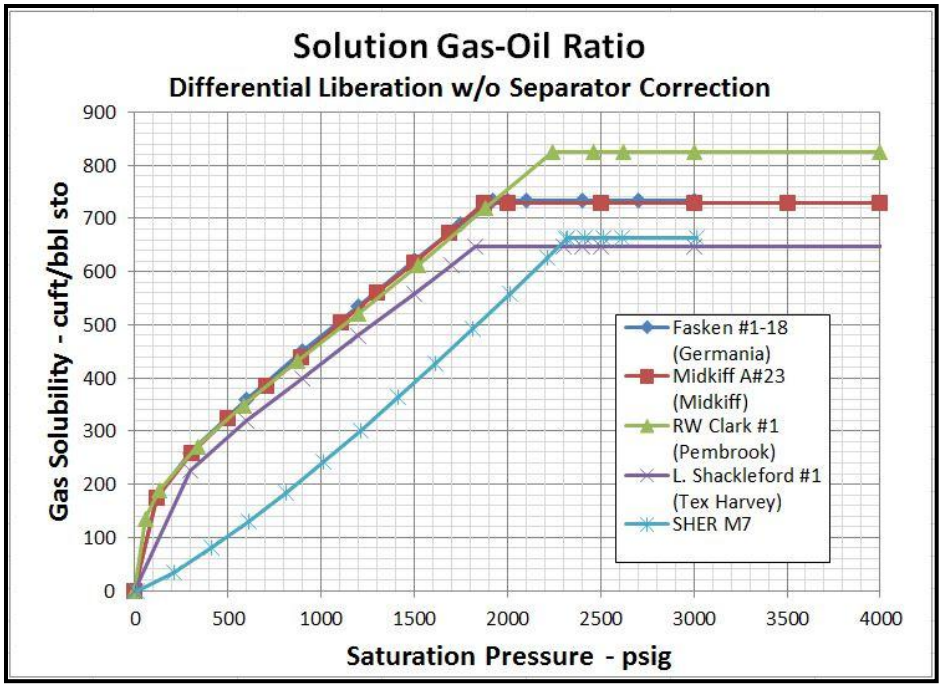

Figure 3.6: Solution gas-oil ratio versus pressure

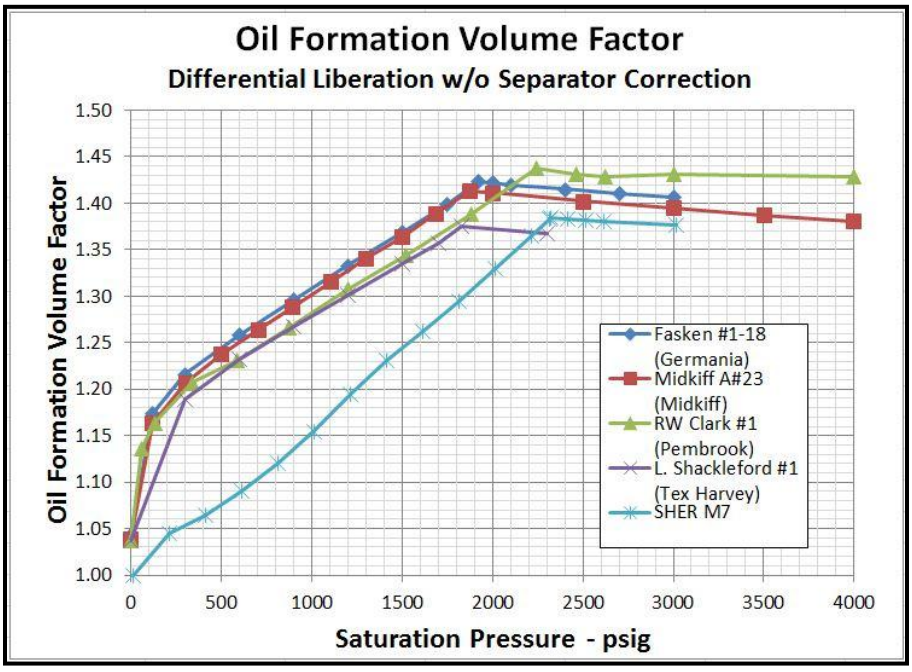

Figure 3.7: Oil formation volume factor versus pressure

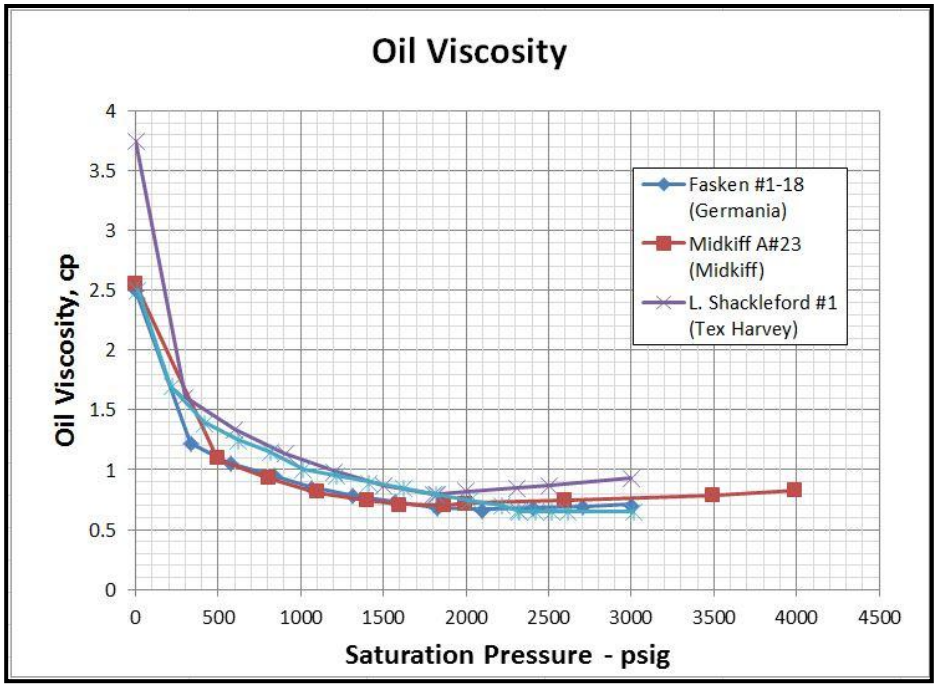

Figure 3.8: Oil viscosity versus pressure

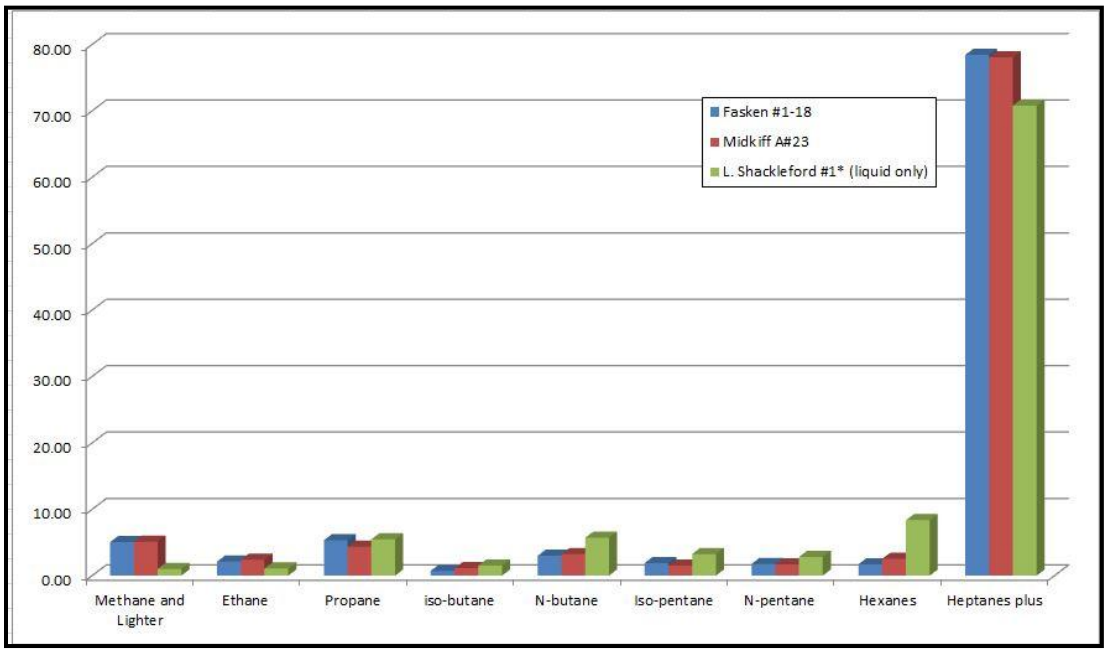

Figure 3.9: Fluid compositional analysis for three Spraberry PVT samples

Spraberry PVT Separator Corrections														
Well No.	Sampling	Differential Expansion PVT Test Results						Multi-Stage Separation (Flash) Results			*1st Stage*		Ratios	
	Date	Pb,psig	Rs scf/stb	Bob rb/stb	API	Viscosity cp	PVTCo@Psat ,1/psi	Rs scf/stb	Bo rb/stb	API	Pres, psig	Temp °F	Rsflash/Rsdiff	Boflash/Bodiff
L. Shackleford #1	15-Sep-51	1825	648	1.367	37.8	0.800	11.37E-06	562	1.2963	36.00	120	75	0.867	0.948
								579	1.3042	36.00	80	76	0.894	0.954
								596	1.3250	36.00	40	76	0.920	0.969
								607	1.3360	36.00	30	75	0.937	0.977
								695	1.4096	36.00	0	75	1.073	1.031
Fasken #1-18	11-Jun-51	1920	735	1.423	37.7	0.680	11.46E-06	558	1.325	37.00	200	74	0.759	0.931
								641	1.372	37.00	40	76	0.872	0.964
								691	1.404	37.00	20	76	0.940	0.987
								764	1.458	37.00	0	76	1.039	1.025

Table 3.3: Separator Test for two Spraberry fluid samples

3.6 Structural, Petrophysical, and Geological Model

Spraberry Field structure tends to be flat over vast distances. Thus, Sherrod Area is assumed to be a linear reservoir with a top depth of 6930 feet as shown in Sherrod 1012 injection profile. No structural, petro-physical or geological model available for Sherrod Area at the time of study. Thus, the reservoir characterization part will be entirely based on tracer, oil rates and water-cut response of wells.

3.7 Pressure Transient Tests

A falloff test was performed on Sherrod 1202w and this represent the only pressure transient test available in Sherrod Area. The pressure and pressure derivative were matched with a dual porosity model with high horizontal anisotropy. The pressure matches as well as key findings from the tests are shown in Figure 3.10 and Table 3.4 below.

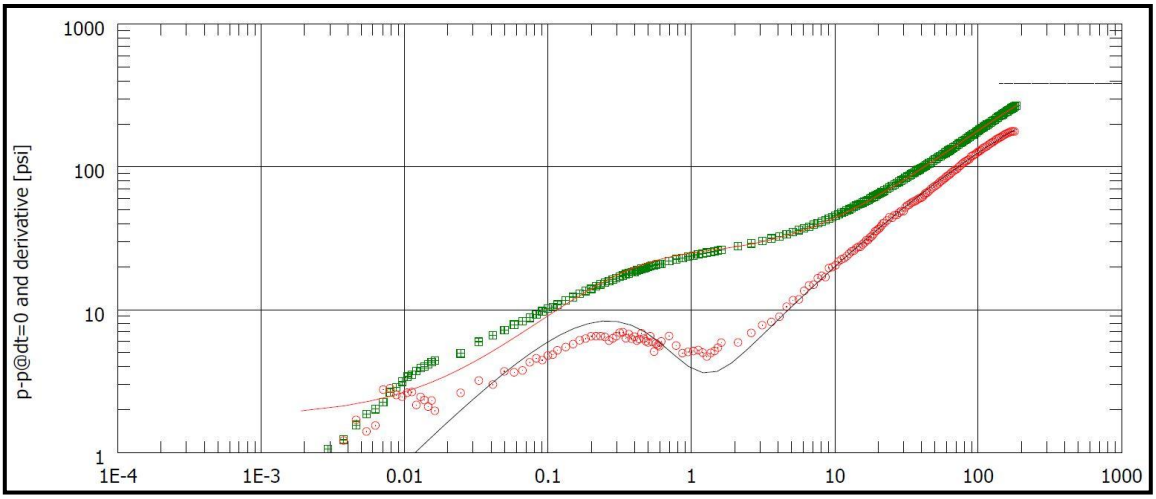

Figure 3.10: Pressure transient test match using PSS dual porosity model

Model Matched	
Well	Vertical, Changing Storage
Reservoir	Two porosity PPS, Horizontal Anisotropy
Boundary	Infinite
Reservoir and Model Parameters	
Pi	2128 psi
k.h, total	41.4 md-ft
k	3.45 md
Total Skin	-7.78
Omega	0.0993
Lambda	7.79e-7
kx / ky	70.4

Table 3.4: Results and model used to match pressure transient test

3.8 PLTs

The two injection profile logs ran on Sherrod 1012W present the only two available profile logs in Sherrod Area. Injection profile logs ran in January 2011 and January 2012 are shown in Figure 3.11. Both profile logs shows almost a uniform distribution of

injected water through perforations at 1U and 5U sand units. First PLT in 2011 showed a uniform distribution of injected water across perforations of the two sand units. This indicates no clear distinction in reservoir properties effecting injectivity. Second PLT in 2012 indicated that sand unit 1U receives 62% of injected water compared to 27% for sand unit 5U. The remaining 10.6% , as indicated by temperature log, flows downward indicating channel flow.

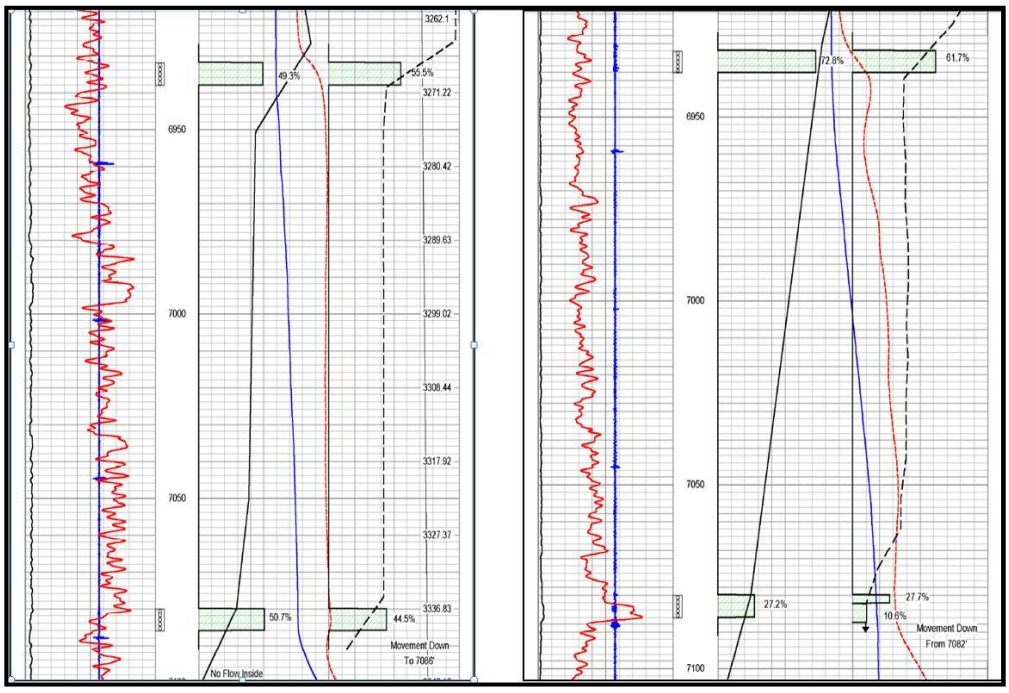

Figure 3.11: ‘Sherrod 1202’ 2011 (on left) and 2012 (on right) injection profiles

4. ANALYTICAL TRACER INTERPRETATION TECHNIQUES

4.1 Analytical Interpretation Techniques

Analytical tracer interpretation techniques are any type of interpretation that does not require building and running numerical simulation models. This includes analyzing tracers responses using Method of Moments (MOM), searching for data patterns in tracer or water-cut responses, analyzing distributions of tracer recovered, tracer velocities, and tracer breakthroughs, assessing layering from multiple tracer peaks, mapping observations, and making links between tracers' responses and wells' or field performance.

4.2 Theory of Method of Moments

The Method of Moments (MOM) originated from the chemical processing industry to analyze non-ideal flow in chemical reactor. In a similar manner to the petroleum industry, a tracer is injected at the inlet of the system either as a pulse (delta function) or as a continuous injection (step function), and the tracer response is monitored at the output as a cumulative function of time. The distribution of the tracer curve produced at the outlet is used to analyze flow through the reactor.

The Method of Moments approach is applicable to tracer flow in porous media as long as the injected water passes a pore volume only once. In this approach, the analysis is done by relating two moments of the tracer response curve: the mean residence time

(first moment), and the variance of tracer response curve (second moment). The first moment of the distribution represents the average injected volume and is given by:

$$\overline{V} = \frac{\int_0^\infty C(V)\, V\, dV}{\int_0^\infty C(V) dV} = \frac{\sum_0^\infty C(V)\, V\, \Delta V}{\sum_0^\infty C(V) \Delta V} \quad \text{.....(5)}$$

the integral is approximated by a summation due to the discrete nature of production data. In order to evaluate the summation to its upper limit of infinity, the complete tracer profile is needed. In almost all of tracer tests, the test is terminated before tracer concentration drops to zero. Thus, there is always a need to extrapolate the tracer elution curve to infinity. Experience shows that majority of tracer elution curves, after a certain time, follow an exponential decline. As proposed by Dean [(44)], the tail of the response curve could be fitted by an exponential equation:

$$C = C_e e^{-\left(\frac{V - V_e}{a}\right)} \quad \text{.....(6)}$$

where "a" is the reciprocal of the slope of the line, C_e is the concentration at which the exponential decline start, and V_e is the corresponding cumulative injection after tracer injection. Integrals of equation 5 can be evaluated over two time periods: pre-exponential decline and post-exponential decline. Substituting the exponential model for the late period gives the following equation:

$$\overline{V} = \frac{\int_0^{V_e} C(V)\, V\, dV + \int_{V_e}^\infty C(V)\, V\, dV}{\int_0^{V_e} C(V)\, dV + \int_{V_e}^\infty C(V)\ dV} = \frac{\sum_0^{V_e} C(V)\, V\, \Delta V + aC_e(a + V_e)}{\sum_0^{V_e} C(V) \Delta V + aC_e} \quad \text{.....(7)}$$

The above equation provides an estimate of the average swept pore volume. It must be highlighted that the water injected will not be completely confined within the planned flood pattern. As a result, the tracer response will not be fully recovered. Another factor effecting tracer recovery is the excessive dilution of tracers travelling long distances

between injectors and producers. The amount of tracer escaping the flood pattern is directly related to the amount of injected water escaping the flood pattern. In another word, if "M" is the total amount of tracer injected, m_{ip} is the total amount of tracer recovered, then fraction "f" gives both the fraction of tracer produced and the fraction of water injected produced.

$$f = \frac{m_{ip}}{M} \quad \text{.....(8)}$$

From this key relation, the fraction of average swept pore volume that can be attributed to a production well "i" can be obtained by combining equations 7 and 8. This is called the net swept pore volume which is given by:

$$\overline{V_{si}} = f\,\overline{V} = \frac{m_{ip}}{M_i}\,\overline{V} \quad \text{.....(9)}$$

$$\overline{V_{si}} = \left(\frac{\sum_0^{V_e} C(V)\Delta V + aC_e}{M_i}\right)_{prod} \left(\frac{\sum_0^{V_e} C(V)\, V\, \Delta V + aC_e(a+V_e)}{\sum_0^{V_e} C(V)\, \Delta V + aC_e}\right)_{inj} \quad \text{.....(10)}$$

Subscripts used in Equation 10 indicate which cumulative volume "V" should be used to evaluate net swept pore volume. Subscript "prod" indicate that the term in parenthesis should be evaluated using cumulative production data while subscript "inj" indicate that the term in parenthesis should be evaluated using cumulative injection data.

4.3 Moment Analysis on Sherrod Area of Spraberry Field

By the end of Sherrod inter-well tracer test, a total of 598 tracer elution curves were detected from 51 out of the 110 sampled wells. Net swept volume calculation using moment analysis requires three basic entries: produced concentration, water production and injection rates during tracer production. This is done for each injector-producer pair

where tracer production is detected. Due to the large number of tracer elution curves produced during the inter-well tracer test, one sample calculation for one injector-producer pair is shown in Table 4.1 below and the rest is documented in Appendix E.

Well	Tracer	Sample Date	qw	dt	V, prod	C	ΔV, prod	C x ΔV, prod	iw	V, inj	ΔV, inj	C x ΔV, inj	C x V,inj x ΔV, inj
			stb/d	days	stb	ppt	stb	tracer mass, g	stb/d	stb	stb	g	g.stb
Sherrod 1208	IWT-2100	29-Apr-11	73	1	73	56	73	0.001	351	351	351	0.003	1
		3-May-11	73	5	365	181,083	292	8.407	344	1,727	1,376	39.611	68,407
		7-May-11	73	9	657	333,130	292	15.446	341	3,091	1,364	72.234	223,276
		11-May-11	73	13	949	209,670	292	9.726	340	4,451	1,360	45.330	201,766
		25-May-11	74	27	1982	119,150	1033	19.568	334	9,127	4,676	88.569	808,373
		8-Jun-11	75	41	3034	108,372	1052	18.127	343	13,929	4,802	82.728	1,152,325
		22-Jun-11	77	55	4109	93,238	1075	15.931	346	18,773	4,844	71.798	1,347,864
		20-Jul-11	80	83	6361	69,227	2252	24.789	344	28,405	9,632	106.000	3,010,939
		4-Aug-11	80	98	7557	57,243	1196	10.880	252	32,185	3,780	34.398	1,107,090
		31-Aug-11	78	125	9665	60,642	2108	20.326	343	41,446	9,261	89.278	3,700,234
		28-Sep-11	91	153	12219	55,024	2553	22.334	406	52,814	11,368	99.438	5,251,707

Table 4.1: Method of Moments sample calculation for ‘Sherrod 1012–Sherrod 1208’

In Table 4.1, “q_w” is water production rate measured in stb/d , “dt” is cumulative time in days after the tracer was injected, “V,prod” is the cumulative water produced in stock tank barrels after the tracer was injected, “C” is the produced tracer concentration in part per trillion, “ΔV,prod” is the volume water produced in one time interval, “i_w” is the

water injection rate in stb/d, "V,inj" is the cumulative water injected after the tracer was introduced, and "ΔV,inj" is the volume of water injected in one time interval.

Extrapolation of tracer elution curve assuming exponential decay is shown in Figure 4.1 below. The value of "a" is obtained from equation 11 below.

$$1/a = \frac{\ln(\frac{C_e}{C})}{t - t_e} \quad \text{.....(11)}$$

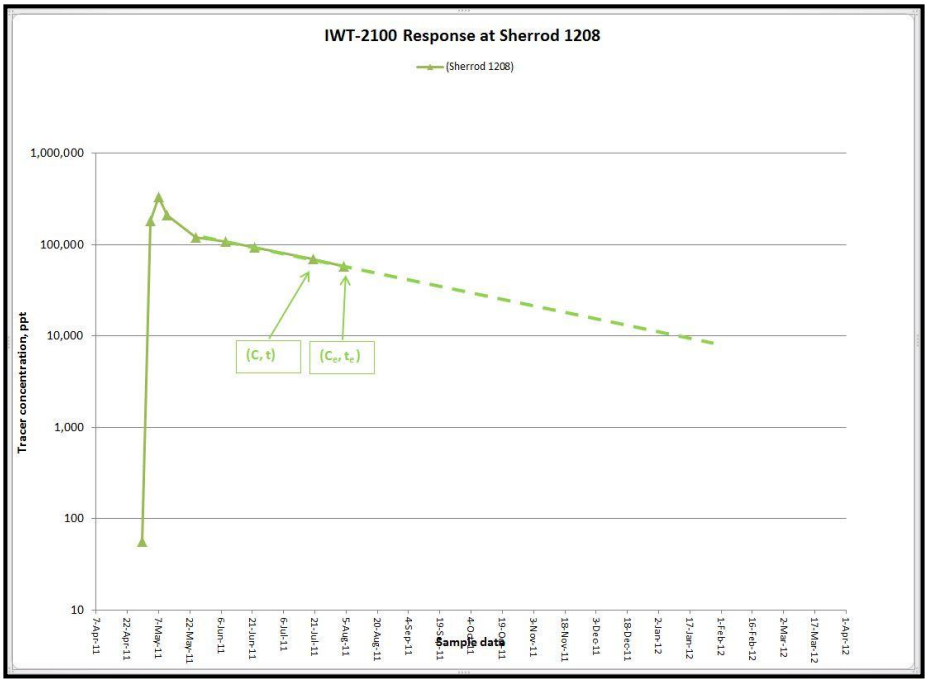

Figure 4.1: Extrapolation of tracer response using exponential decay

The results of all net swept volume calculations are summarized in Table 4.2

	1814	1202	1818	2112	2409	1904	2114	2325	2118	1012	701	1301	1405
	IWT-1900	IWT-2400	IWT-1100	IWT-1700	IWT-1200	IWT-2200	IWT-2500	IWT-1000	IWT-1600	IWT-2100	IWT-2000	IWT-1400	IWT-1300
Ruby 18	17502	17757	18477	18707	18077	20872	14920	7994	13405	14742	10925	21195	19255
Ruby 19	28826	27015	26218	26345	25715	0	25258	11142	22655	22573	0	0	23731
Sherrod 711	22224	24028	24019	25432	24044	0	14253	11691	23344	22141	6570	25544	22864
Sherrod 1003	13833	14181	15274	17928	14747	15033	9811	6834	14680	12957	8257	20467	13139
Sherrod 1004	27868	29902	27240	29652	29064	0	25050	14669	30018	25899	0	29525	27908
Sherrod 1205	18767	19392	19962	20514	19005	21578	14328	9270	18755	17006	11492	14651	18318
Sherrod 1206	31921	28870	30855	38049	34228	0	31153	20359	38068	28947	0	42172	35756
Sherrod 1207	16470	15391	18360	19243	17526	16579	8297	7585	16259	14781	8929	21826	15016
Sherrod 1208	23484	22626	23997	27354	24995	22153	20293	13296	26260	23132	19971	31691	25467
Sherrod 1302	20627	21425	21641	22209	21284	21592	16227	10341	21326	19609	0	18334	20141
Sherrod 1310	0	15510	0	0	21770	0	20808	12857	32354	23641	0	25831	22962
Sherrod 1402	29472	22584	27945	31470	29884	28497	26934	16403	31638	30277	0	37308	31587
Sherrod 1403	40013	29359	35551	47620	40257	30360	37833	21241	41914	38932	24810	51578	40291
Sherrod 1404	18624	16126	19205	18213	18065	16697	12161	8973	18560	14906	9109	22972	15442
Sherrod 1506	23671	24050	23295	24242	24108	0	18661	11515	23851	22415	0	17894	18454
Sherrod 1511	0	0	0	0	0	0	0	17521	0	39072	0	0	34249
Sherrod 1512	16666	16316	16599	15867	15697	18988	14817	8526	17116	12812	8778	21024	12913
Sherrod 1513	0	35499	0	0	41497	0	36151	20231	42274	36134	0	32902	28680
Sherrod 1804	14368	17546	19283	20680	18792	13355	12128	9153	18732	15045	8732	21799	18178
Sherrod 1807	22431	19978	20576	22121	20214	21592	14949	9861	19852	15766	0	26633	20589
Sherrod 1809	14662	16890	20828	22531	19799	17748	8472	8718	19448	16008	9629	23909	18010
Sherrod 1810	30673	20059	18365	23156	21034	10158	20582	8466	25303	26757	5448	17842	24203
Sherrod 1811	0	0	0	0	0	0	0	0	0	20655	0	0	0
Sherrod 1812	22583	28850	26911	32605	29129	19237	24425	16472	31188	28423	0	36408	30546
Sherrod 1815	20899	22111	24726	29511	24920	25118	21001	14317	27023	24781	24014	33349	28234
Sherrod 1817	16131	16022	13416	17690	15182	15997	10764	7383	15185	13381	8954	19544	13922
Sherrod 1819	18395	18990	27109	27383	26174	18885	21804	10425	26144	21658	9561	28529	25551
Sherrod 1902	18789	16533	18741	19983	20046	13814	15748	10622	19810	18774	0	22254	17419
Sherrod 1903	31080	31321	31228	32609	32544	21363	26880	16524	33917	31705	0	0	27539
Sherrod 2001	28211	22582	27083	27351	28367	0	23753	18704	30508	28450	0	39062	29652
Sherrod 2002	19438	25979	13246	6844	25571	16507	16910	3069	26217	24648	0	0	26524
Sherrod 2101	20574	20803	20680	20384	20398	21578	16904	9937	20511	17872	0	24494	16244
Sherrod 2110	31735	30599	24000	35041	32550	23354	32072	19069	35480	34213	0	38489	36809
Sherrod 2111	13315	12308	15540	11717	14075	10973	8611	6659	13759	12282	7756	18291	11303
Sherrod 2113	19031	20045	22066	22697	20673	17578	11880	9358	15418	17105	9392	23422	16698
Sherrod 2115	29309	27005	20815	32710	29078	29010	28843	17866	31688	29574	0	38057	32676
Sherrod 2116	34914	33776	31070	30098	34375	21978	30922	19737	37772	35275	24926	44451	35991
Sherrod 2117	20183	20547	17758	18582	21984	17780	14563	9752	20265	17706	12016	22740	19011
Sherrod 2309	20231	21243	21735	20908	15080	21091	19004	9590	21689	17783	9951	24539	18087
Sherrod 2313	35987	35322	32948	46203	34960	0	28314	17707	39024	36571	0	0	41279
Sherrod 2314	33279	31977	24974	22741	32826	0	37313	15860	35759	35908	0	42223	36874
Sherrod 2315	16243	17097	13681	19785	18282	19280	10570	6689	18203	14283	9429	23620	17032
Sherrod 2317	31701	30344	25332	34635	31986	31560	30616	21288	33449	33733	0	39189	35353
Sherrod 2319	17824	18160	17658	19358	15343	17022	12590	7394	18384	15527	9067	22377	16166
Sherrod 2320	22003	22259	22597	22574	18510	0	17333	10695	22731	19934	0	28836	18788
Sherrod 2324	0	0	30881	0	0	0	0	15820	0	39072	0	0	0
Sherrod 2326	31366	34716	31538	33847	33029	22618	24494	15355	34118	33631	11866	32852	33102
Sherrod 2411	32878	23846	36484	41532	20292	31560	36691	23631	40525	40091	24922	48210	46220
Sherrod 2415	28609	29272	27525	31882	31211	3690	28394	14085	33628	32479	0	38279	33143
Sherrod 2416	32968	29121	31950	32791	31188	0	29725	17595	27123	31332	0	42374	33601
Sherrod 2417	19776	19848	20460	20547	16168	19765	18324	9177	21195	16681	11852	23821	16012
Sherrod 2423	25216	26435	25429	25417	19058	20450	14151	11499	24837	22867	0	29302	23984

Table 4.2: Summary of net swept volumes calculations

To make results of net swept volumes more meaningful, all volumes were normalized by dividing by maximum value. Table 4.3 shows normalized swept volume calculations.

	1814	1202	1818	2112	2409	1904	2114	2325	2118	1012	701	1301	1405
	IWT-1900	IWT-2400	IWT-1100	IWT-1700	IWT-1200	IWT-2200	IWT-2500	IWT-1000	IWT-1600	IWT-2100	IWT-2000	IWT-1400	IWT-1300
Ruby 18	0.3	0.3	0.4	0.4	0.4	0.4	0.3	0.2	0.3	0.3	0.2	0.4	0.4
Ruby 19	0.6	0.5	0.5	0.5	0.5	0.0	0.5	0.2	0.4	0.4	0.0	0.0	0.5
Sherrod 711	0.4	0.5	0.5	0.5	0.5	0.0	0.3	0.2	0.5	0.4	0.1	0.5	0.4
Sherrod 1003	0.3	0.3	0.3	0.3	0.3	0.3	0.2	0.1	0.3	0.3	0.2	0.4	0.3
Sherrod 1004	0.5	0.6	0.5	0.6	0.6	0.0	0.5	0.3	0.6	0.5	0.0	0.6	0.5
Sherrod 1205	0.4	0.4	0.4	0.4	0.4	0.4	0.3	0.2	0.4	0.3	0.2	0.3	0.4
Sherrod 1206	0.6	0.6	0.6	0.7	0.7	0.0	0.6	0.4	0.7	0.6	0.0	0.8	0.7
Sherrod 1207	0.3	0.3	0.4	0.4	0.3	0.3	0.2	0.1	0.3	0.3	0.2	0.4	0.3
Sherrod 1208	0.5	0.4	0.5	0.5	0.5	0.4	0.4	0.3	0.5	0.4	0.4	0.6	0.5
Sherrod 1302	0.4	0.4	0.4	0.4	0.4	0.4	0.3	0.2	0.4	0.4	0.0	0.4	0.4
Sherrod 1310	0.0	0.3	0.0	0.0	0.4	0.0	0.4	0.2	0.6	0.5	0.0	0.5	0.4
Sherrod 1402	0.6	0.4	0.5	0.6	0.6	0.6	0.5	0.3	0.6	0.6	0.0	0.7	0.6
Sherrod 1403	0.8	0.6	0.7	0.9	0.8	0.6	0.7	0.4	0.8	0.8	0.5	1.0	0.8
Sherrod 1404	0.4	0.3	0.4	0.4	0.4	0.3	0.2	0.2	0.4	0.3	0.2	0.4	0.3
Sherrod 1506	0.5	0.5	0.5	0.5	0.5	0.0	0.4	0.2	0.5	0.4	0.0	0.3	0.4
Sherrod 1511	0.0	0.0	0.0	0.0	0.0	0.0	0.0	0.3	0.0	0.8	0.0	0.0	0.7
Sherrod 1512	0.3	0.3	0.3	0.3	0.3	0.4	0.3	0.2	0.3	0.2	0.2	0.4	0.3
Sherrod 1513	0.0	0.7	0.0	0.0	0.8	0.0	0.7	0.4	0.8	0.7	0.0	0.6	0.6
Sherrod 1804	0.3	0.3	0.4	0.4	0.4	0.3	0.2	0.2	0.4	0.3	0.2	0.4	0.4
Sherrod 1807	0.4	0.4	0.4	0.4	0.4	0.4	0.3	0.2	0.4	0.3	0.0	0.5	0.4
Sherrod 1809	0.3	0.3	0.4	0.4	0.4	0.3	0.2	0.2	0.4	0.3	0.2	0.5	0.3
Sherrod 1810	0.6	0.4	0.4	0.4	0.4	0.2	0.4	0.2	0.5	0.5	0.1	0.3	0.5
Sherrod 1811	0.0	0.0	0.0	0.0	0.0	0.0	0.0	0.0	0.0	0.4	0.0	0.0	0.0
Sherrod 1812	0.4	0.6	0.5	0.6	0.6	0.4	0.5	0.3	0.6	0.6	0.0	0.7	0.6
Sherrod 1815	0.4	0.4	0.5	0.6	0.5	0.5	0.4	0.3	0.5	0.5	0.5	0.6	0.5
Sherrod 1817	0.3	0.3	0.3	0.3	0.3	0.3	0.2	0.1	0.3	0.3	0.2	0.4	0.3
Sherrod 1819	0.4	0.4	0.5	0.5	0.5	0.4	0.4	0.2	0.5	0.4	0.2	0.6	0.5
Sherrod 1902	0.4	0.3	0.4	0.4	0.4	0.3	0.3	0.2	0.4	0.4	0.0	0.4	0.3
Sherrod 1903	0.6	0.6	0.6	0.6	0.6	0.4	0.5	0.3	0.7	0.6	0.0	0.0	0.5
Sherrod 2001	0.5	0.4	0.5	0.5	0.5	0.0	0.5	0.4	0.6	0.6	0.0	0.8	0.6
Sherrod 2002	0.4	0.5	0.3	0.1	0.5	0.3	0.3	0.1	0.5	0.5	0.0	0.0	0.5
Sherrod 2101	0.4	0.4	0.4	0.4	0.4	0.4	0.3	0.2	0.4	0.3	0.0	0.5	0.3
Sherrod 2110	0.6	0.6	0.5	0.7	0.6	0.5	0.6	0.4	0.7	0.7	0.0	0.7	0.7
Sherrod 2111	0.3	0.2	0.3	0.2	0.3	0.2	0.2	0.1	0.3	0.2	0.2	0.4	0.2
Sherrod 2113	0.4	0.4	0.4	0.4	0.4	0.3	0.2	0.2	0.3	0.3	0.2	0.5	0.3
Sherrod 2115	0.6	0.5	0.4	0.6	0.6	0.6	0.6	0.3	0.6	0.6	0.0	0.7	0.6
Sherrod 2116	0.7	0.7	0.6	0.6	0.7	0.4	0.6	0.4	0.7	0.7	0.5	0.9	0.7
Sherrod 2117	0.4	0.4	0.3	0.4	0.4	0.3	0.3	0.2	0.4	0.3	0.2	0.4	0.4
Sherrod 2309	0.4	0.4	0.4	0.4	0.3	0.4	0.4	0.2	0.4	0.3	0.2	0.5	0.4
Sherrod 2313	0.7	0.7	0.6	0.9	0.7	0.0	0.5	0.3	0.8	0.7	0.0	0.0	0.8
Sherrod 2314	0.6	0.6	0.5	0.4	0.6	0.0	0.7	0.3	0.7	0.7	0.0	0.8	0.7
Sherrod 2315	0.3	0.3	0.3	0.4	0.4	0.4	0.2	0.1	0.4	0.3	0.2	0.5	0.3
Sherrod 2317	0.6	0.6	0.5	0.7	0.6	0.6	0.6	0.4	0.6	0.7	0.0	0.8	0.7
Sherrod 2319	0.3	0.4	0.3	0.4	0.3	0.3	0.2	0.1	0.4	0.3	0.2	0.4	0.3
Sherrod 2320	0.4	0.4	0.4	0.4	0.4	0.0	0.3	0.2	0.4	0.4	0.0	0.6	0.4
Sherrod 2324	0.0	0.0	0.6	0.0	0.0	0.0	0.0	0.3	0.0	0.8	0.0	0.0	0.0
Sherrod 2326	0.6	0.7	0.6	0.7	0.6	0.4	0.5	0.3	0.7	0.7	0.2	0.6	0.6
Sherrod 2411	0.6	0.5	0.7	0.8	0.4	0.6	0.7	0.5	0.8	0.8	0.5	0.9	0.9
Sherrod 2415	0.6	0.6	0.5	0.6	0.6	0.1	0.6	0.3	0.7	0.6	0.0	0.7	0.6
Sherrod 2416	0.6	0.6	0.6	0.6	0.6	0.0	0.6	0.3	0.5	0.6	0.0	0.8	0.7
Sherrod 2417	0.4	0.4	0.4	0.4	0.3	0.4	0.4	0.2	0.4	0.3	0.2	0.5	0.3
Sherrod 2423	0.5	0.5	0.5	0.5	0.4	0.4	0.3	0.2	0.5	0.4	0.0	0.6	0.5

Table 4.3: Summary of normalized swept volumes

Figure 4.2 shows distribution of average water injection rate of the 13 tagged injectors during tracer test. Figures 4.3 through 4.16 show distribution of normalized net volume swept for field wide and individual injectors. Figure 4.17 shows a cross plot of tracer recovery in percentage versus normalized net swept volumes. Mapping the magnitude and direction of normalized sweep could provide an important link between locations of high or poor swept volumes. Table 4.3 above show magnitudes of normalized net swept volumes for the 13 tagged injector. The five different colors used in the table are used to map these values as shown in Figures 4.18 through 4.30. Results are discussed in more details in next section.

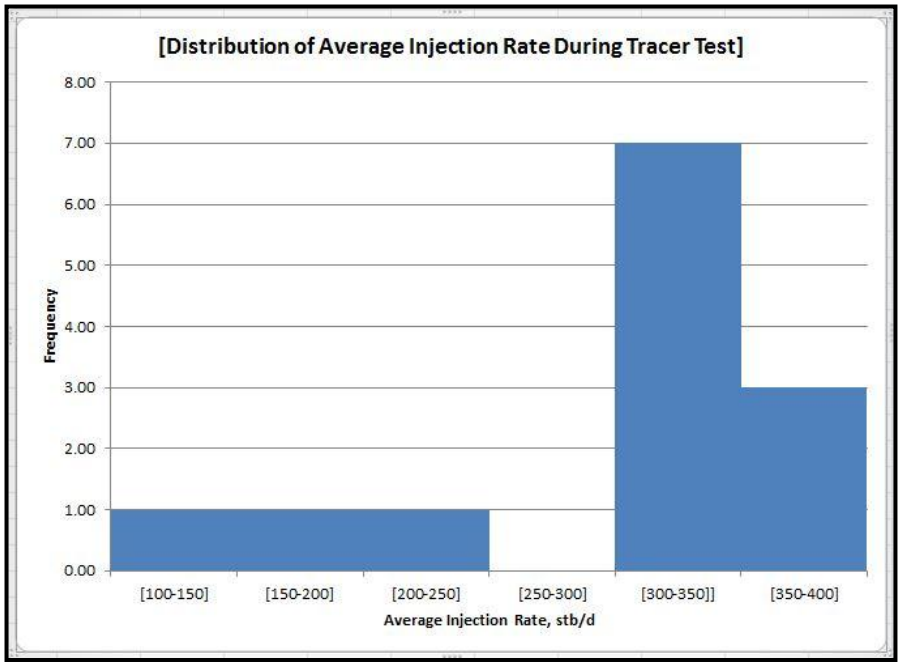

Figure 4.2: Distribution of tagged wells' injection rates in Sherrod Area

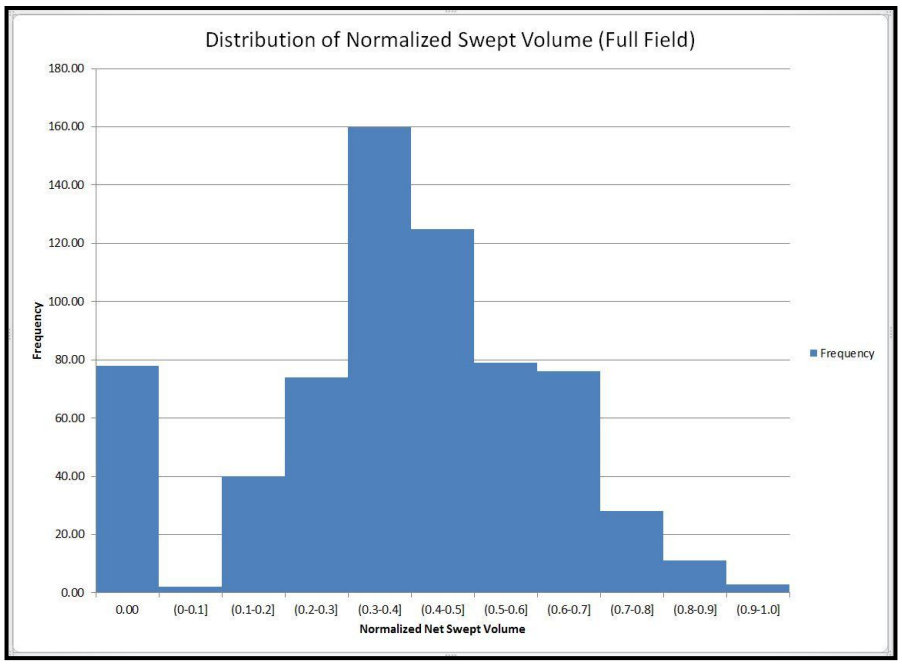

Figure 4.3: Distribution of normalized net swept volumes (full field)

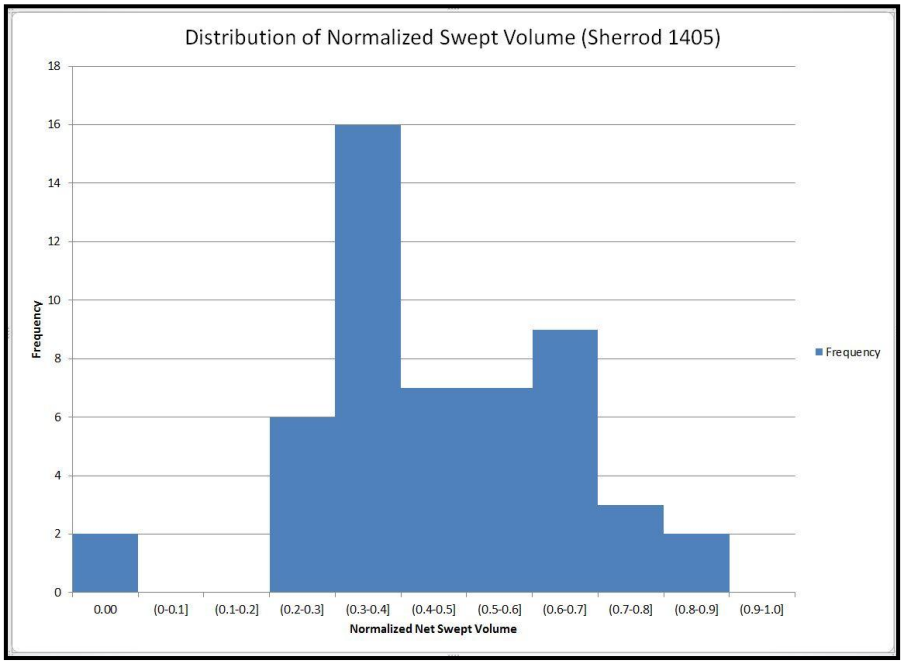

Figure 4.4: Distribution of normalized net swept volumes (Sherrod 1405)

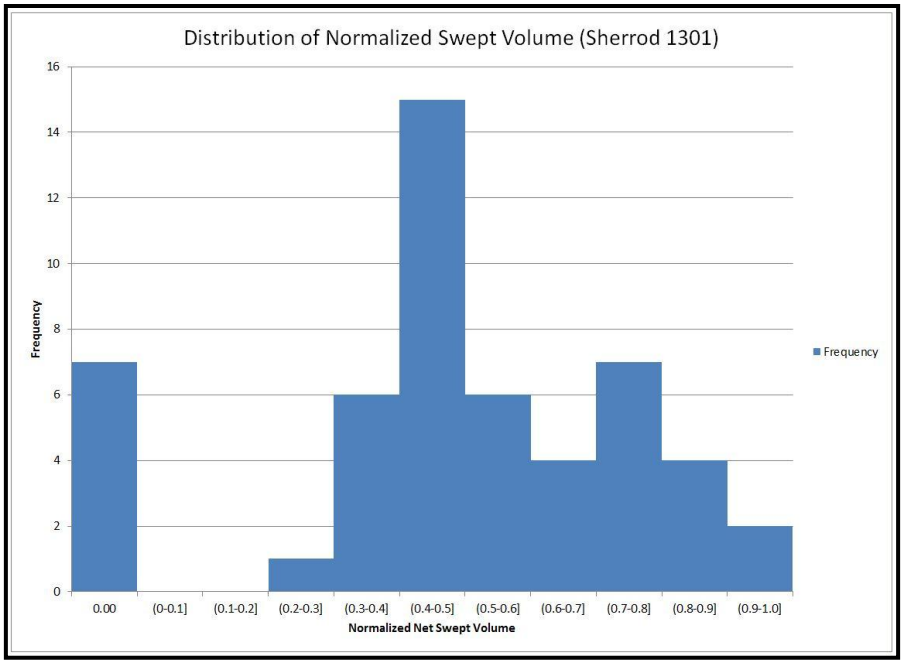

Figure 4.5: Distribution of normalized net swept volumes (Sherrod 1301)

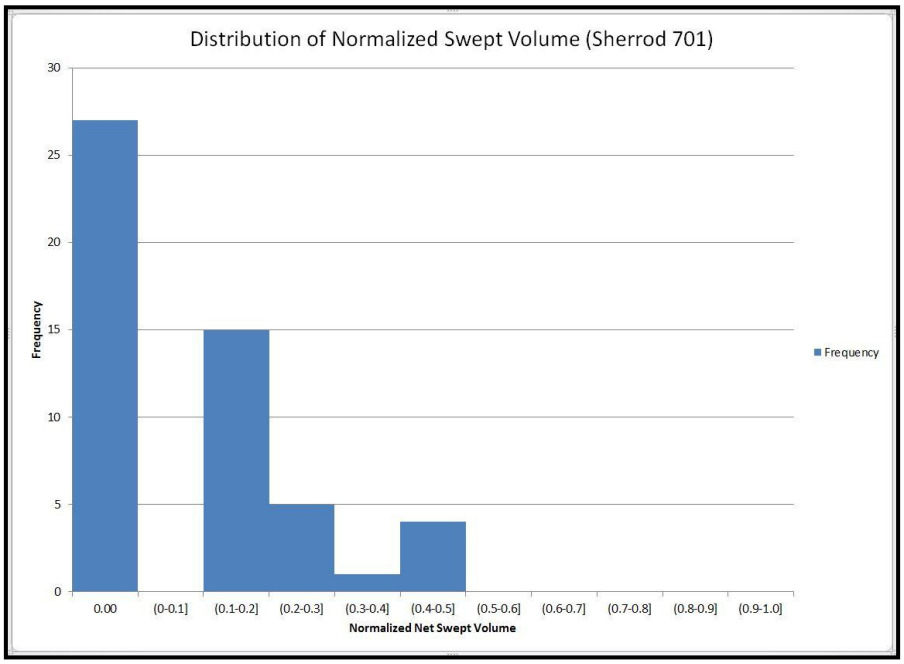

Figure 4.6: Distribution of normalized net swept volumes (Sherrod 701)

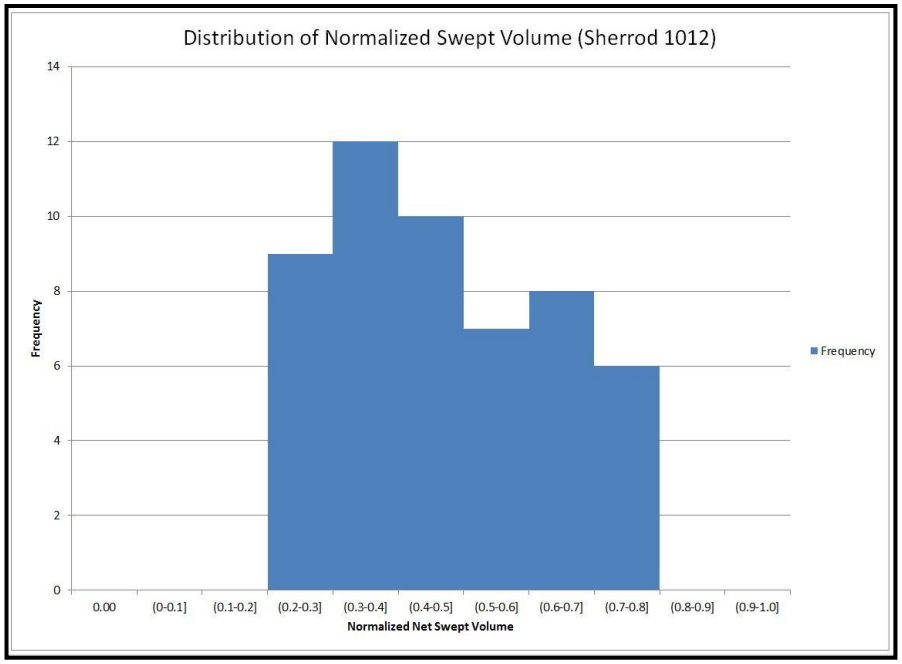

Figure 4.7: Distribution of normalized net swept volumes (Sherrod 1012)

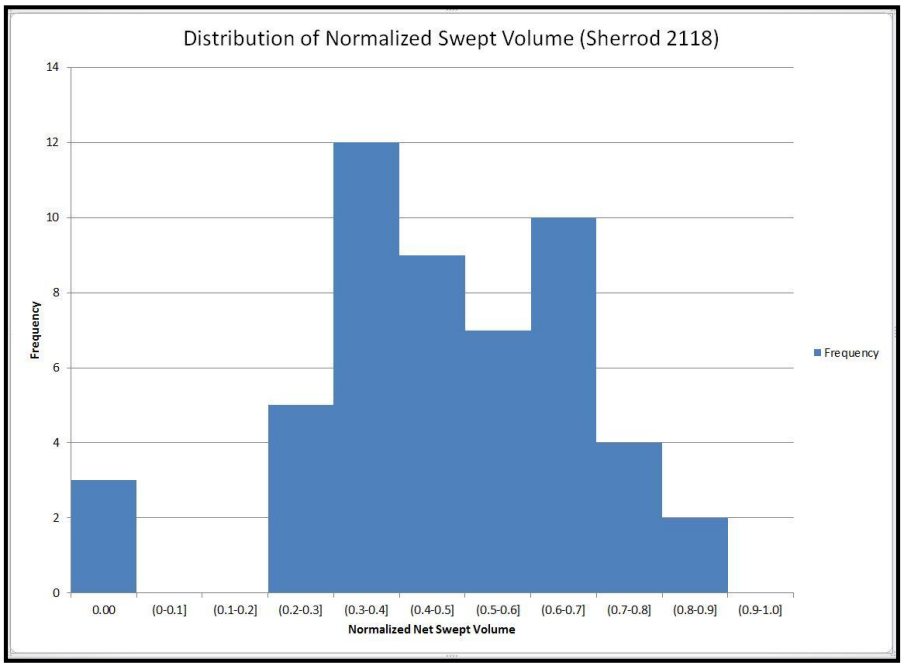

Figure 4.8: Distribution of normalized net swept volumes (Sherrod 2118)

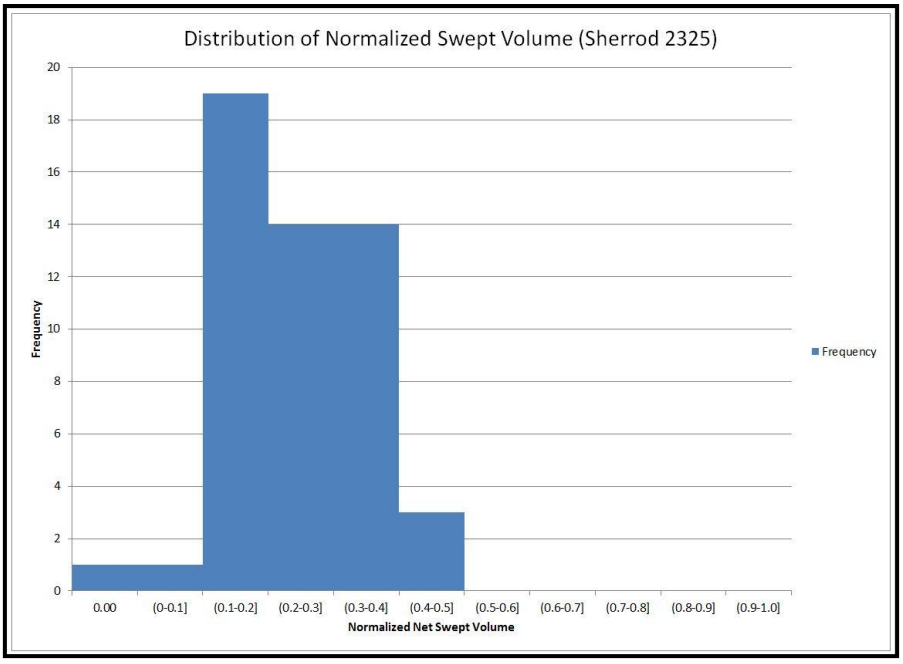

Figure 4.9: Distribution of normalized net swept volumes (Sherrod 2325)

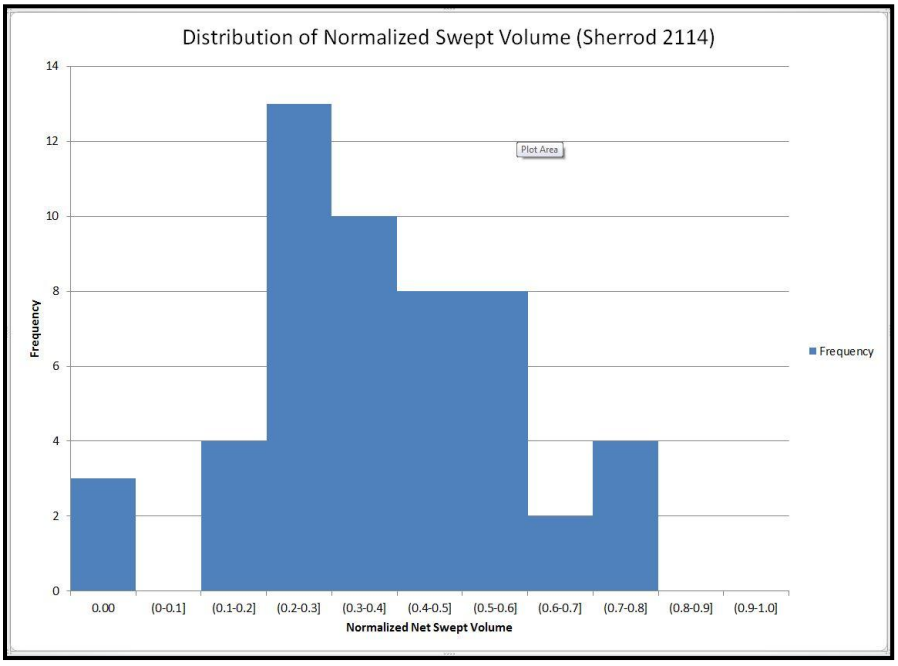

Figure 4.10: Distribution of normalized net swept volumes (Sherrod 2114)

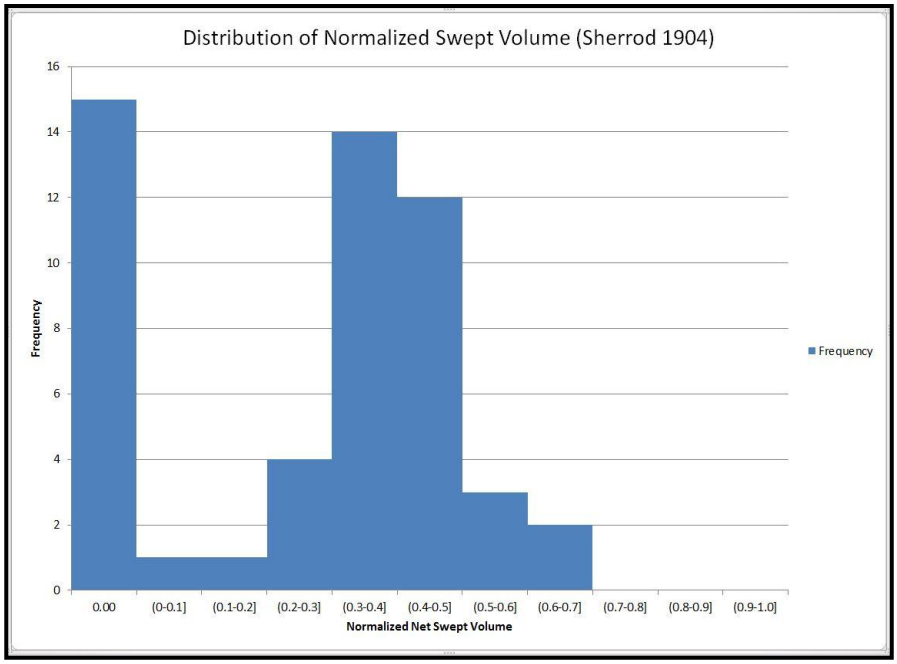

Figure 4.11: Distribution of normalized net swept volumes (Sherrod 1904)

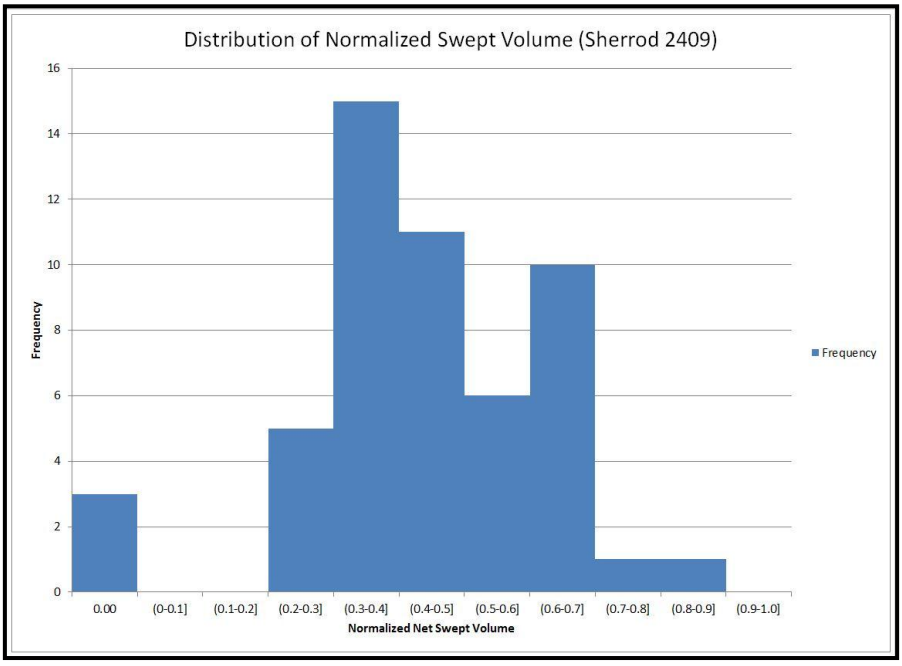

Figure 4.12: Distribution of normalized net swept volumes (Sherrod 2409)

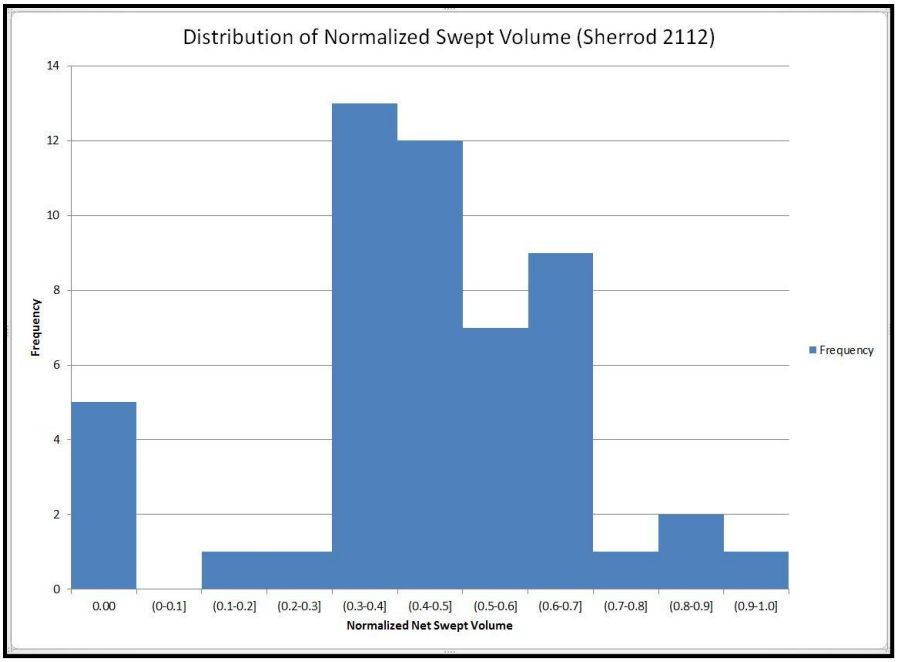

Figure 4.13: Distribution of normalized net swept volumes (Sherrod 2112)

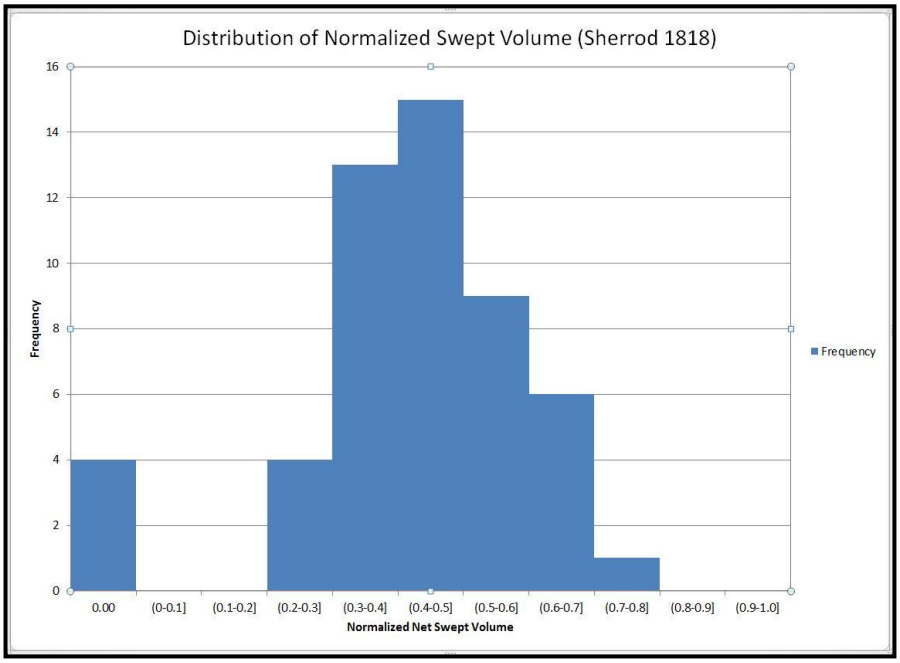

Figure 4.14: Distribution of normalized net swept volumes (Sherrod 1818)

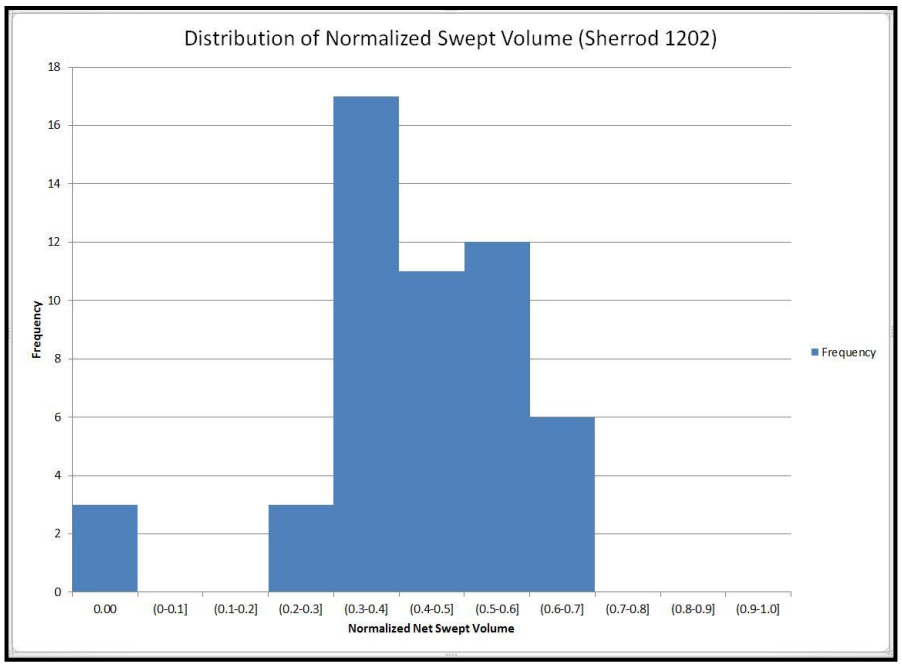

Figure 4.15: Distribution of normalized net swept volumes (Sherrod 1202)

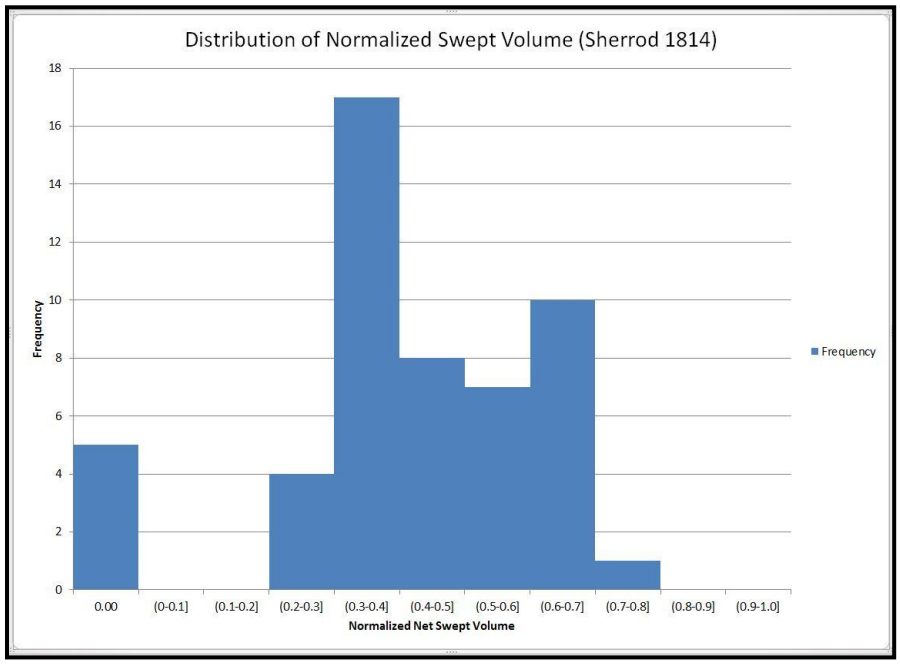

Figure 4.16: Distribution of normalized net swept volumes (Sherrod 1814)

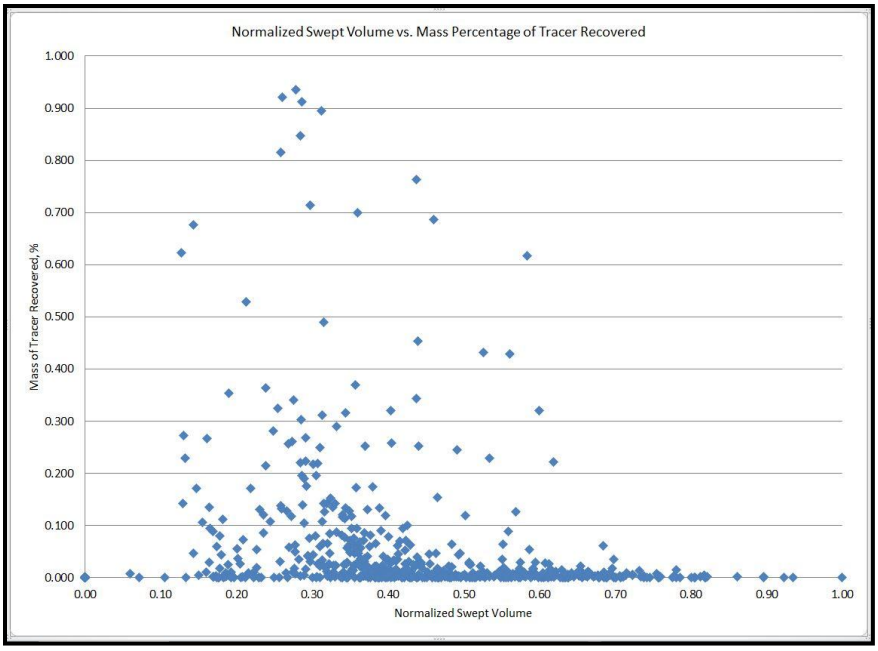

Figure 4.17: Cross plot of tracer recovery (%) versus normalized swept volume.

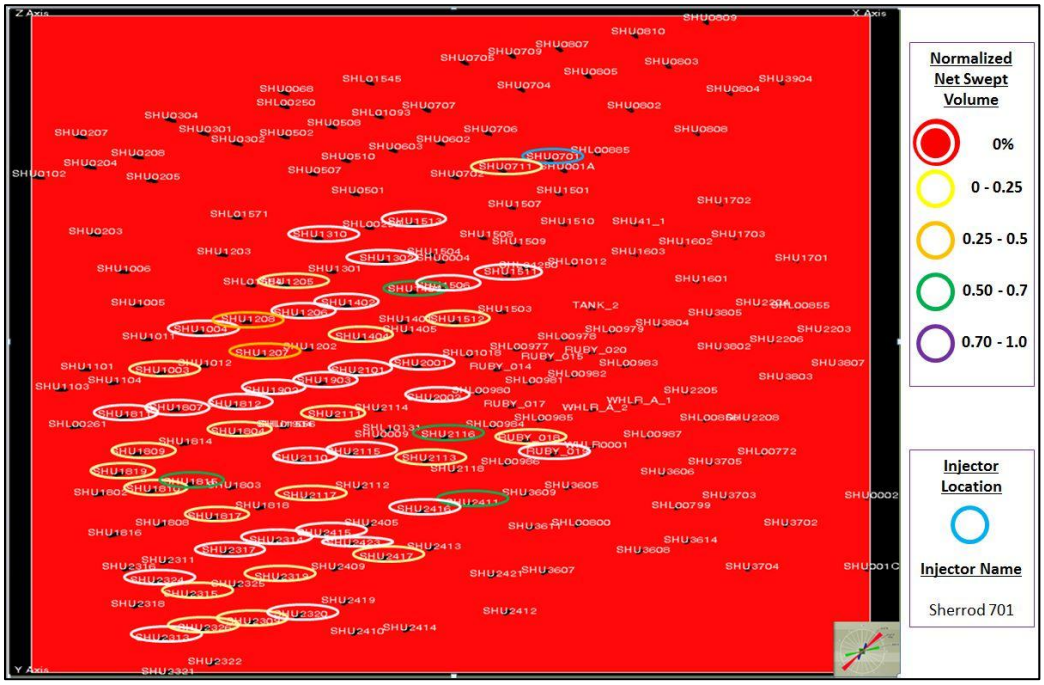

Figure 4.18: Normalized swept volume map for Sherrod 701

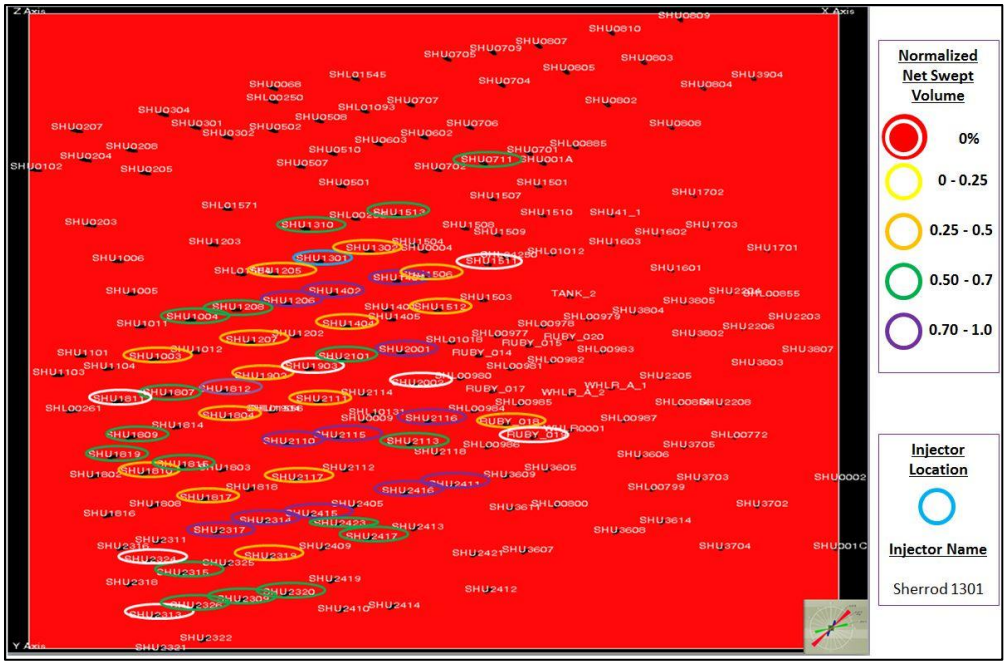

Figure 4.19: Normalized swept volume map for 'Sherrod 1301'

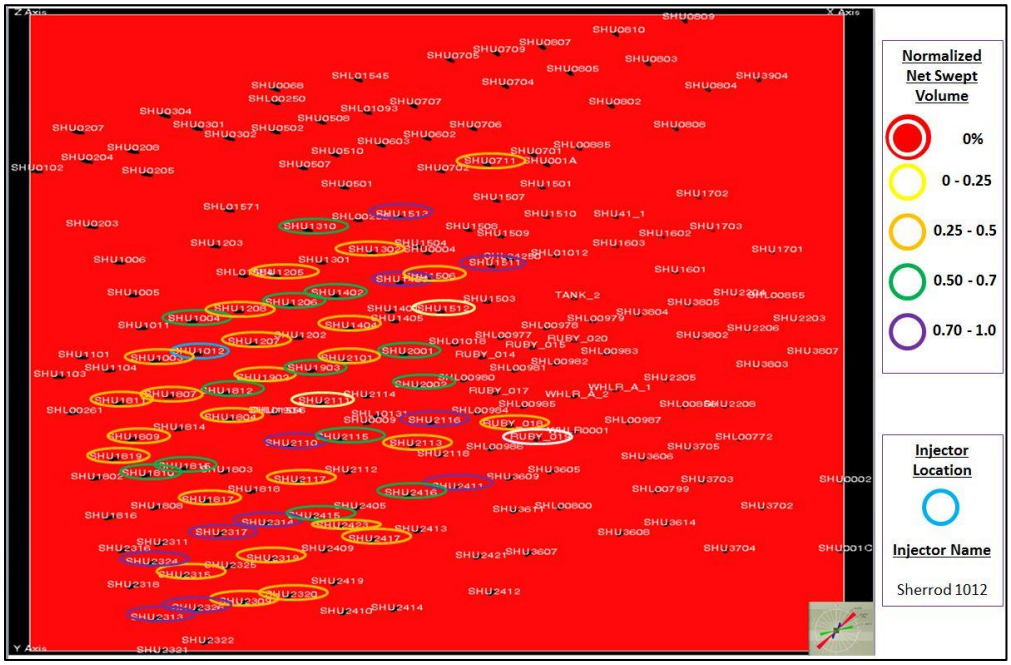

Figure 4.20: Normalized swept volume map for 'Sherrod 1012'

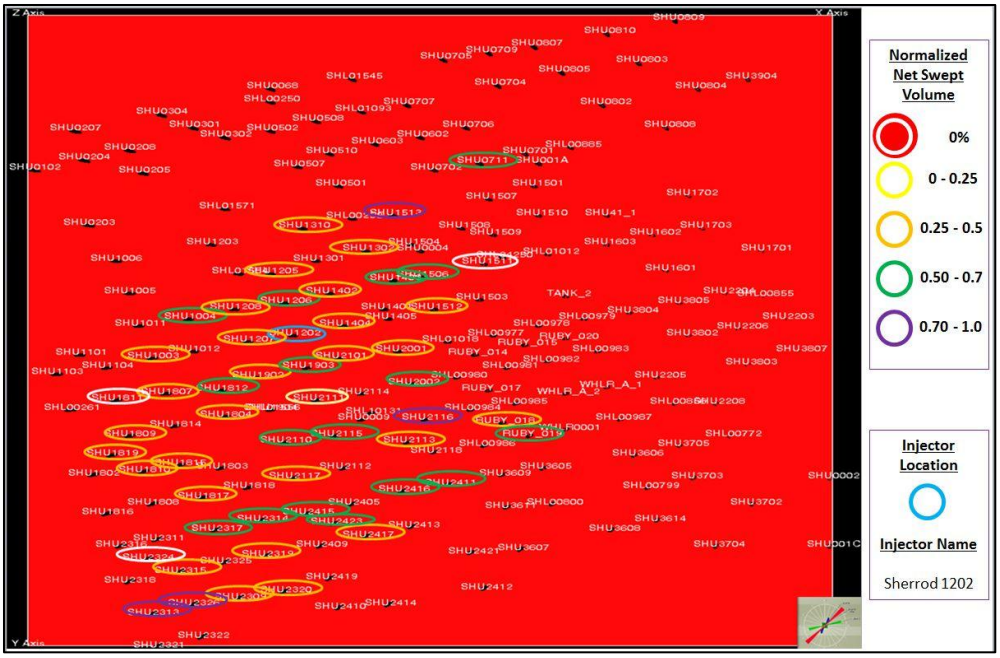

Figure 4.21: Normalized swept volume map for 'Sherrod 1202'

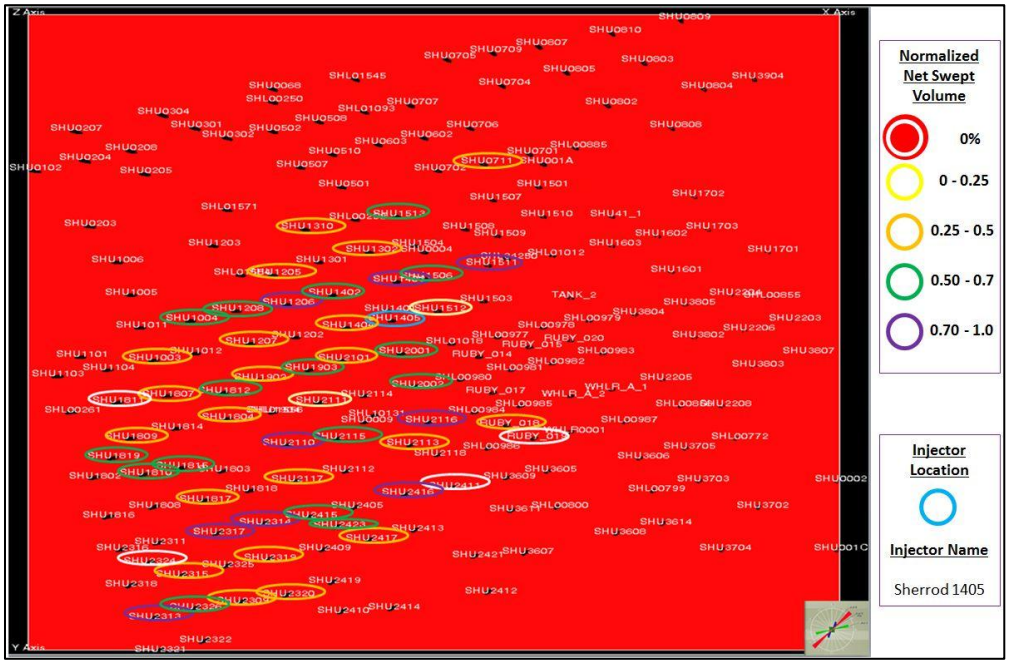

Figure 4.22: Normalized swept volume map for 'Sherrod 1405'

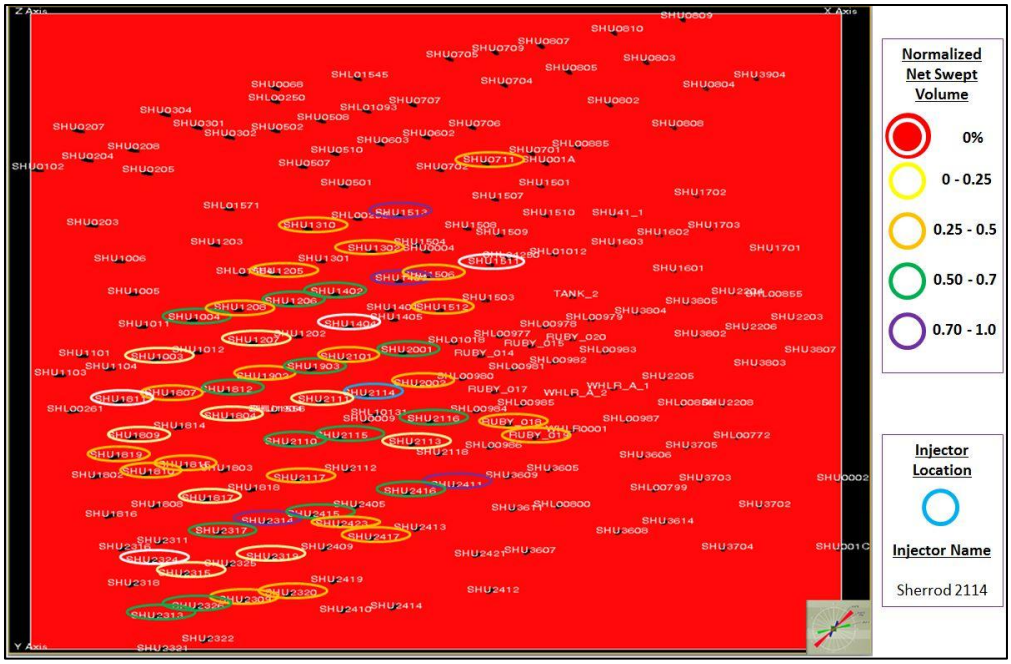

Figure 4.23: Normalized swept volume map for 'Sherrod 2114'

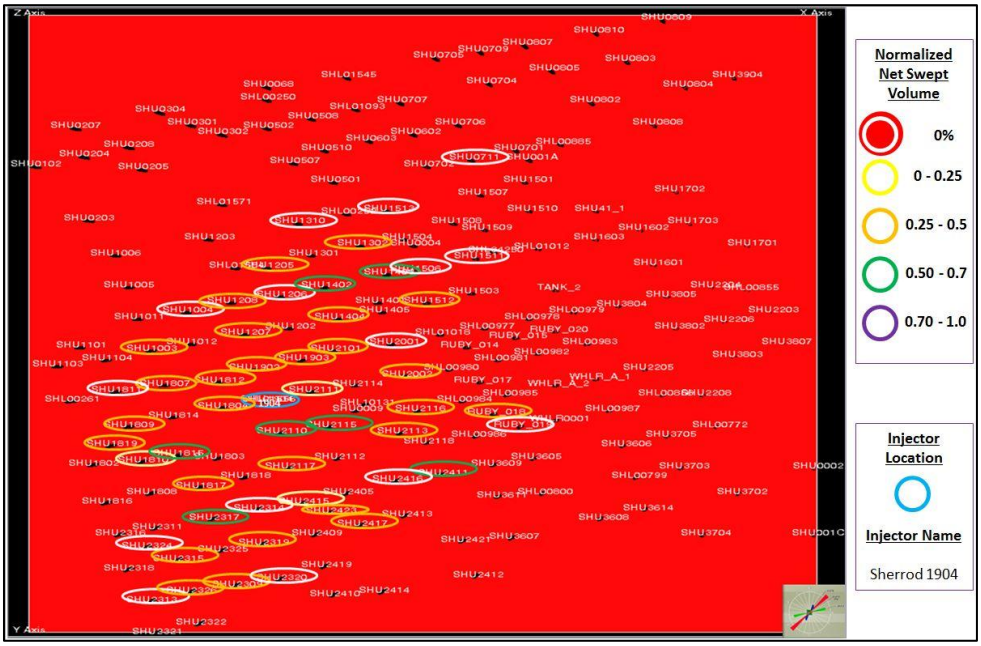

Figure 4.24: Normalized swept volume map for 'Sherrod 1904'

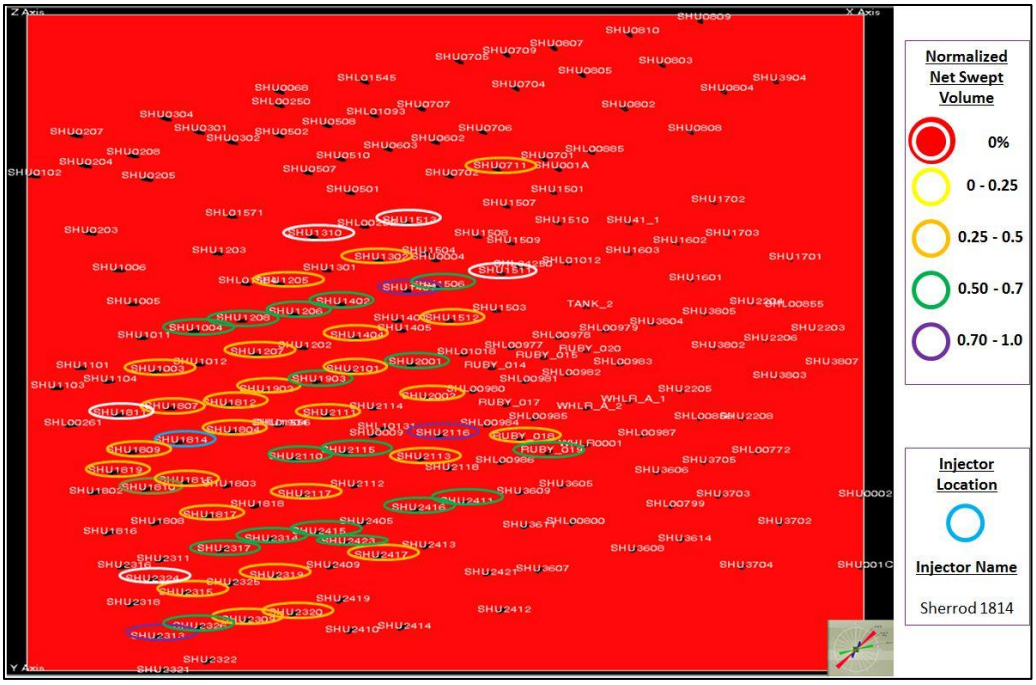

Figure 4.25: Normalized swept volume map for 'Sherrod 1814'

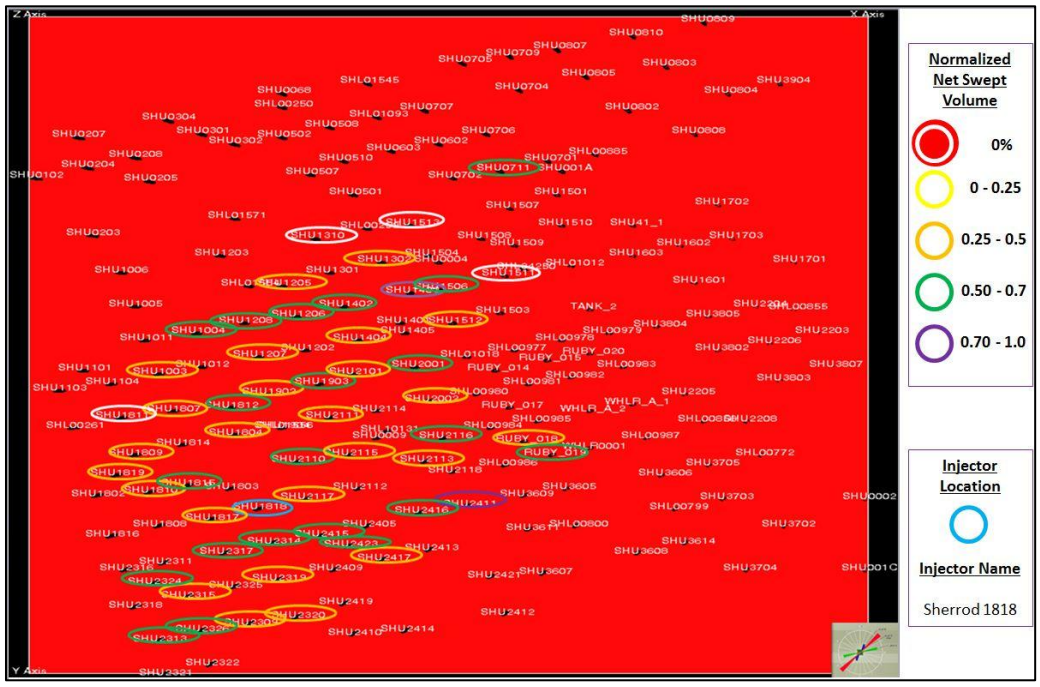

Figure 4.26: Normalized swept volume map for Sherrod '1818'

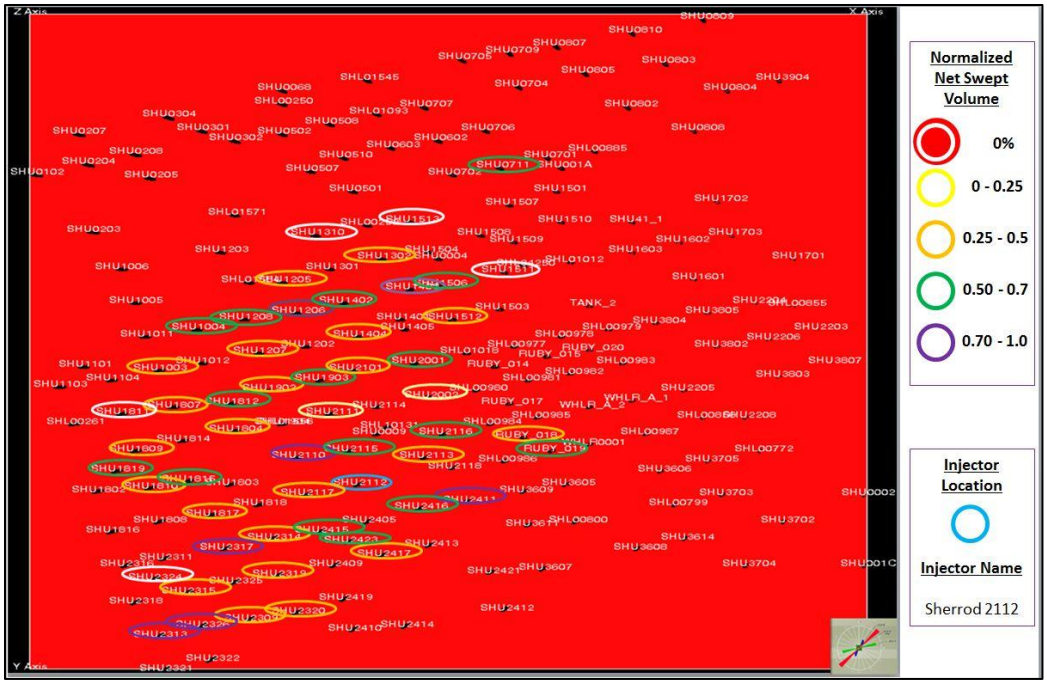

Figure 4.27: Normalized swept volume map for 'Sherrod 2112'

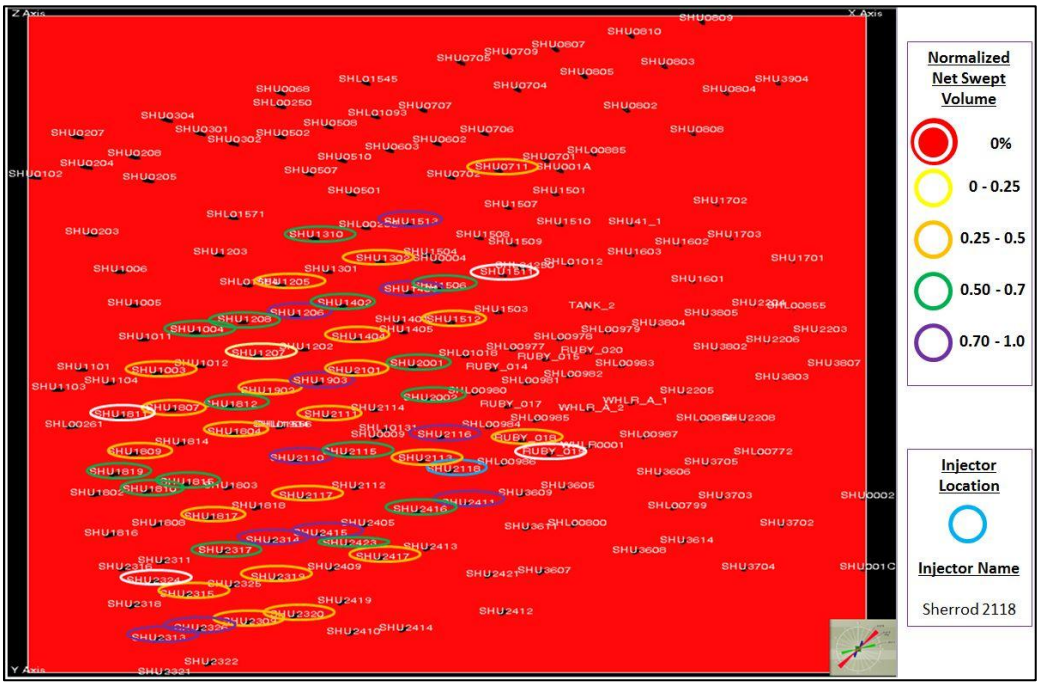

Figure 4.28: Normalized swept volume map for 'Sherrod 2118'

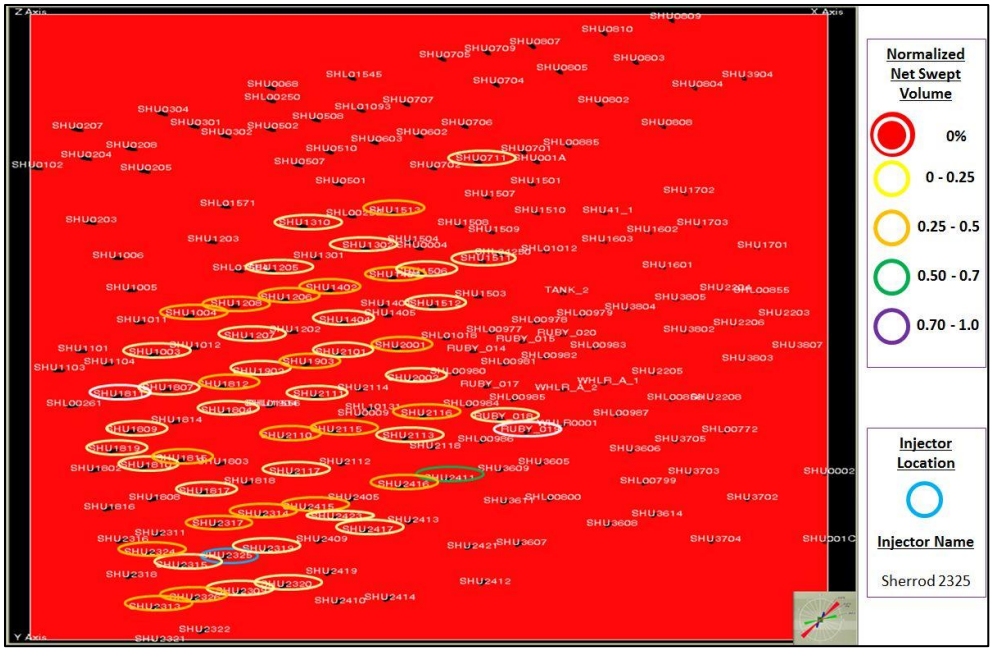

Figure 4.29: Normalized swept volume map for 'Sherrod 2325'

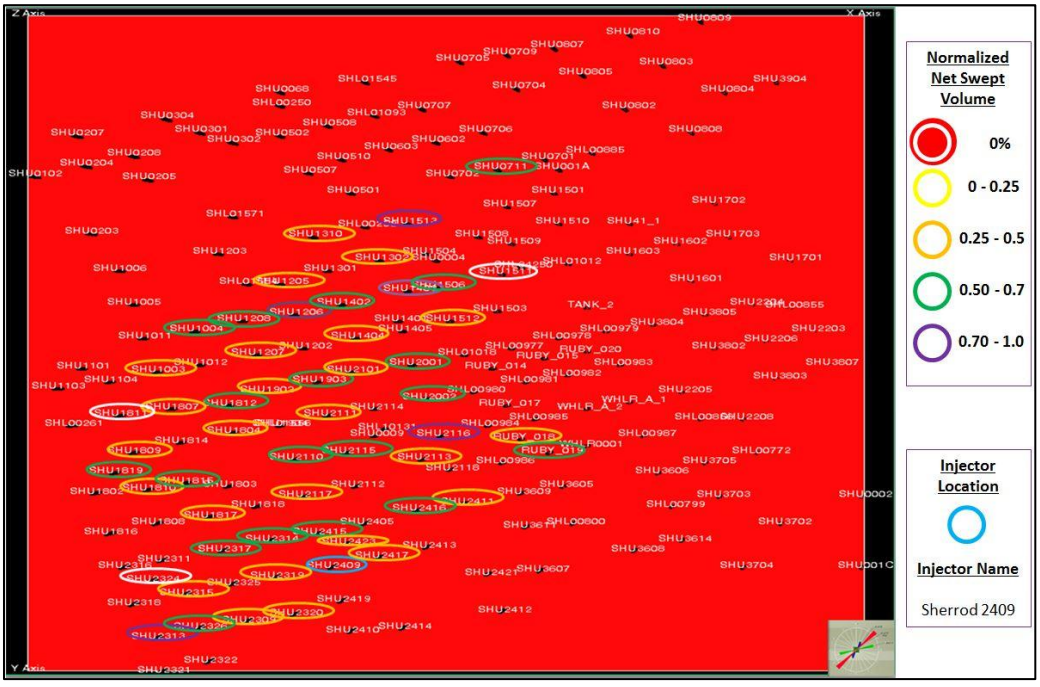

Figure 4.30: Normalized swept volume map for 'Sherrod 2409'

4.4 Moment Analysis: Interpretation & Limitation

The full field distribution of normalized net swept volume appears to be very close to a normal distribution. This is most likely a reflection of the distribution of fracture properties in the tracer area which are the main drive of the sweep. Well by well distributions of normalized swept volumes show the most frequent swept volume in the range of 0.3 to 0.7 of maximum. Only exceptions are wells Sherrod 701 and 2325 which have their maximum frequency of normalized swept volumes in the range from 0 to 0.2. This could be explained by one of the following: either these two wells are in poor communication with the sampled producers, or it is due to the relatively low injection rate of these two wells compared to all other injectors. Normalized swept volume was plotted against tracer recovery in Figure 4.17 and indicated no direct relation.

Normalized swept volumes of 0.7 and higher are observed only in few wells and constitute the upper-low frequency interval of the global swept volume distribution. Wells showing such high normalized swept volumes indicate locations where injected water is recovered relatively higher than other locations in the tracer test area. Mapping these observations give indication of directions of maximum sweep or major features controlling water movement in the field. Maps shown in Figures 4.18 through 4.30 highlight producers that exhibited low, moderate and high normalized net swept volumes for every tagged injector. If all maps were overlain, this will highlight important flow features in the pattern injection area. Connecting wells with high swept volumes (normalized swept volumes ≥ 0.50) consistently show four major flow features oriented $N76^{o}E$. These major flow features shown in Figures 4.31 through 4.50 were detected by

10 out of the 13 tagged injectors. For these 10 injectors to be widely spaced covering large area of the field and consistently detecting these four flow features, it is an indication that these four features governs water movement in the tracer test area. Honoring high swept volumes from Method of Moments, two fracture realizations could exist explaining the inter-connectivity between these four flow features and the 10 tagged injectors. Figures 4.31 through 4.40 show a very likely fracture realization where a NE-SW fracture system connects injectors with these four major flow features. Figures 4.41 through 4.50 show a less likely fracture realization where a NW-SE fracture system connects injectors with these main features.

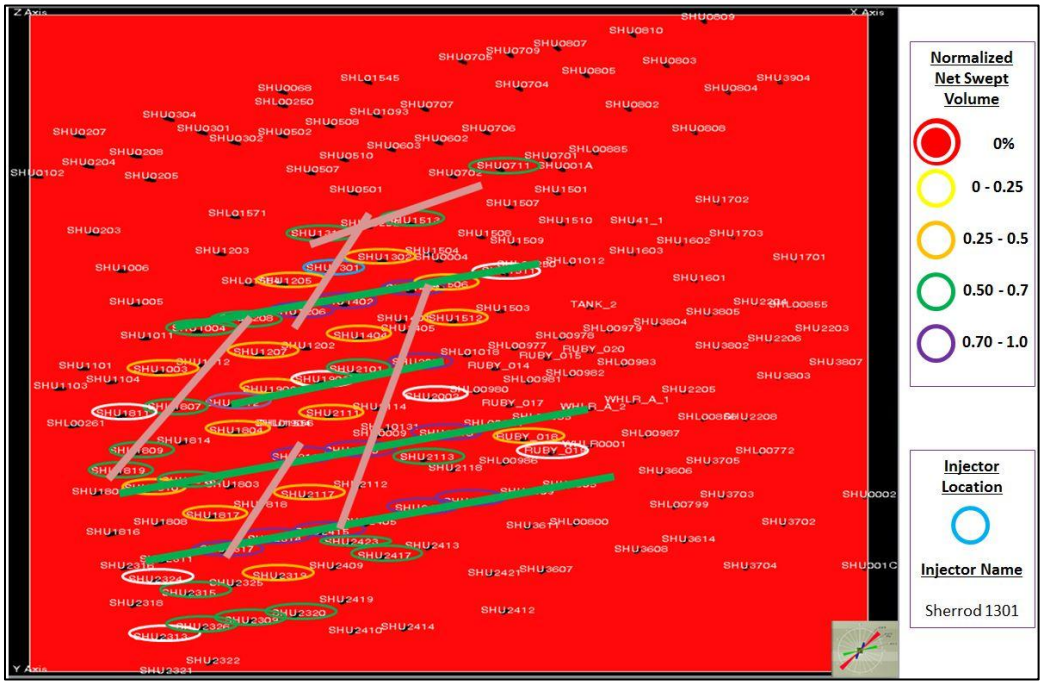

Figure 4.31: 'Sherrod 1301' connectivity with major flow features (green lines) through NE-SW fractures

Figure 4.32: 'Sherrod 1012' connectivity with major flow features (green lines) through NE-SW fractures

Figure 4.33: 'Sherrod 1202' connectivity with major flow features (green lines) through NE-SW fractures

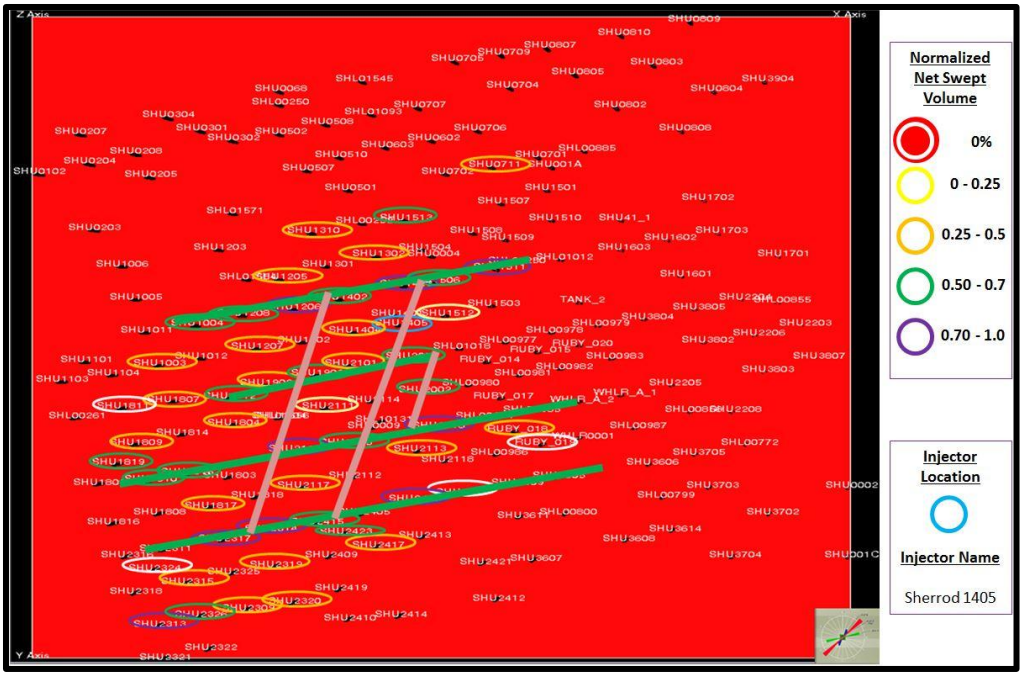

Figure 4.34: 'Sherrod 1405' connectivity with major flow features (green lines) through NE-SW fractures

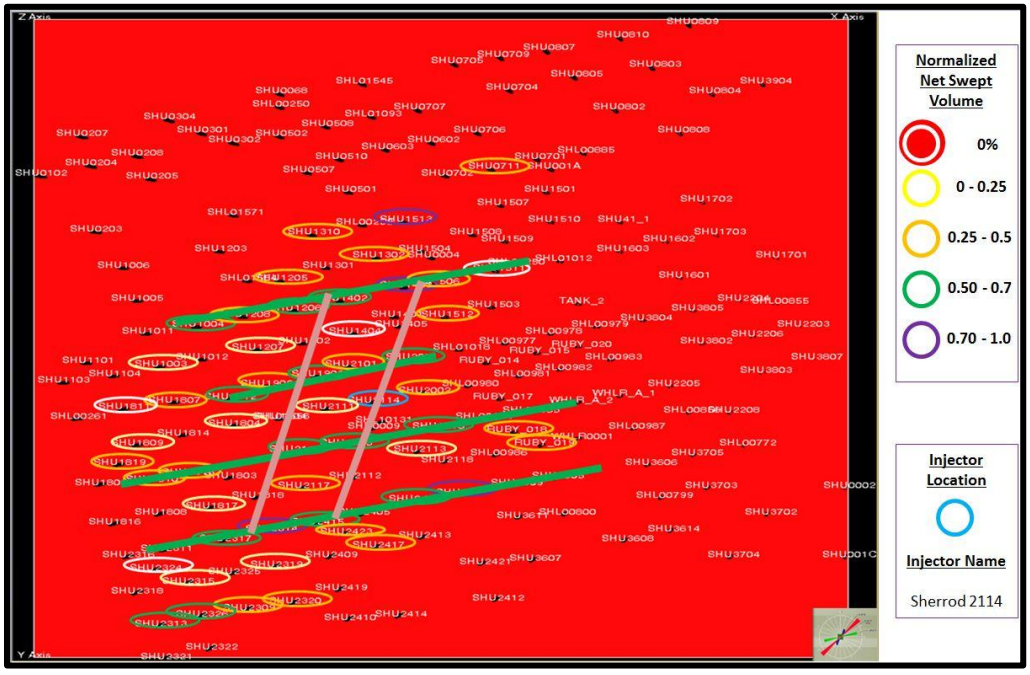

Figure 4.35: 'Sherrod 2114' connectivity with major flow features (green lines) through NE-SW fractures

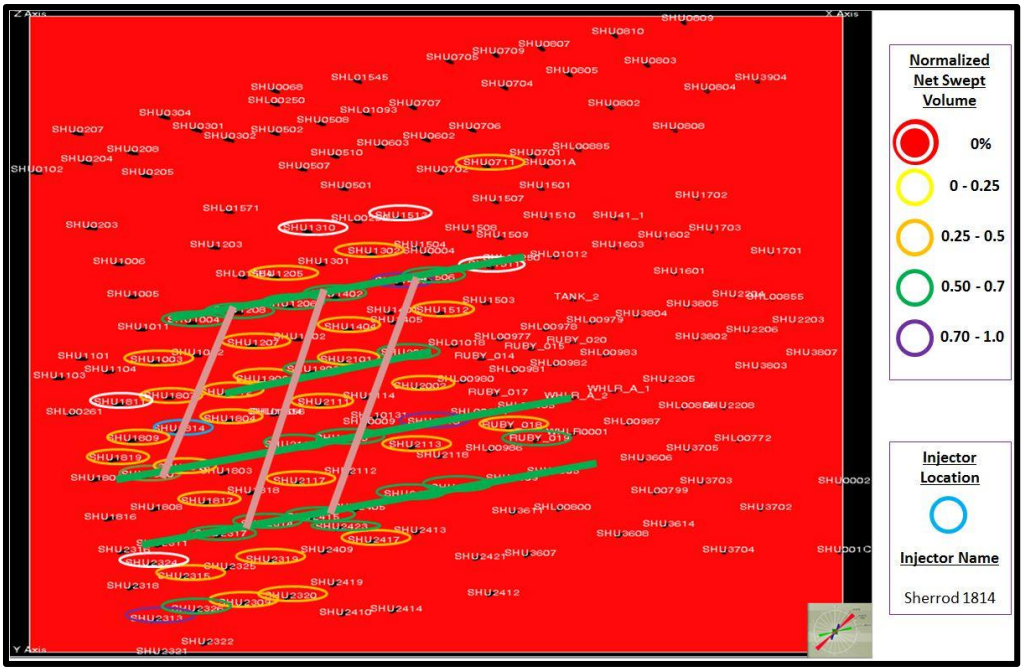

Figure 4.36: 'Sherrod 1814' connectivity with major flow features (green lines) through NE-SW fractures

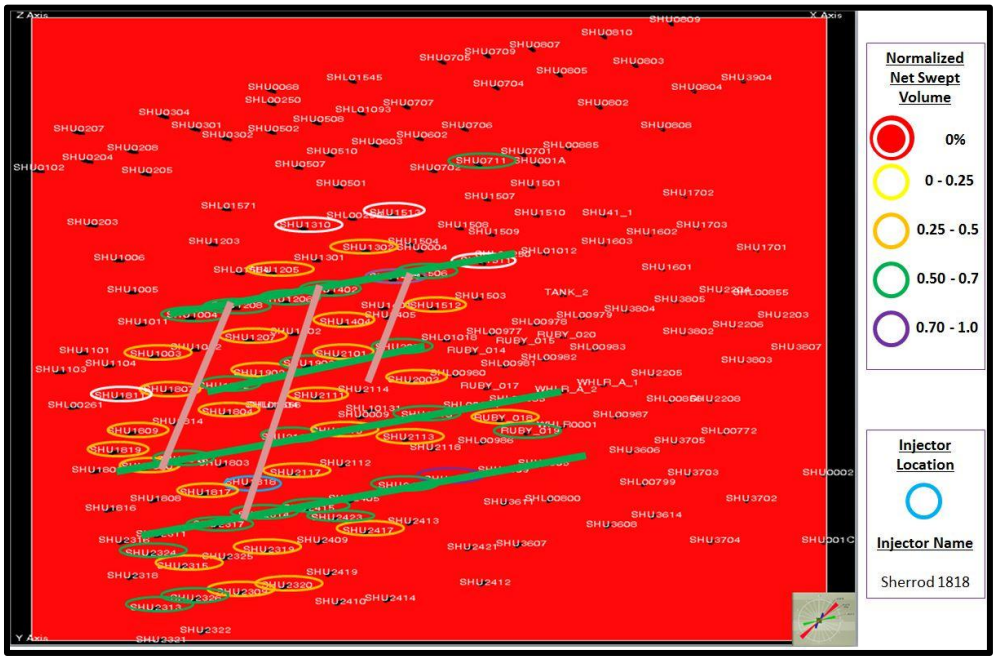

Figure 4.37: 'Sherrod 1818' connectivity with major flow features (green lines) through NE-SW fractures

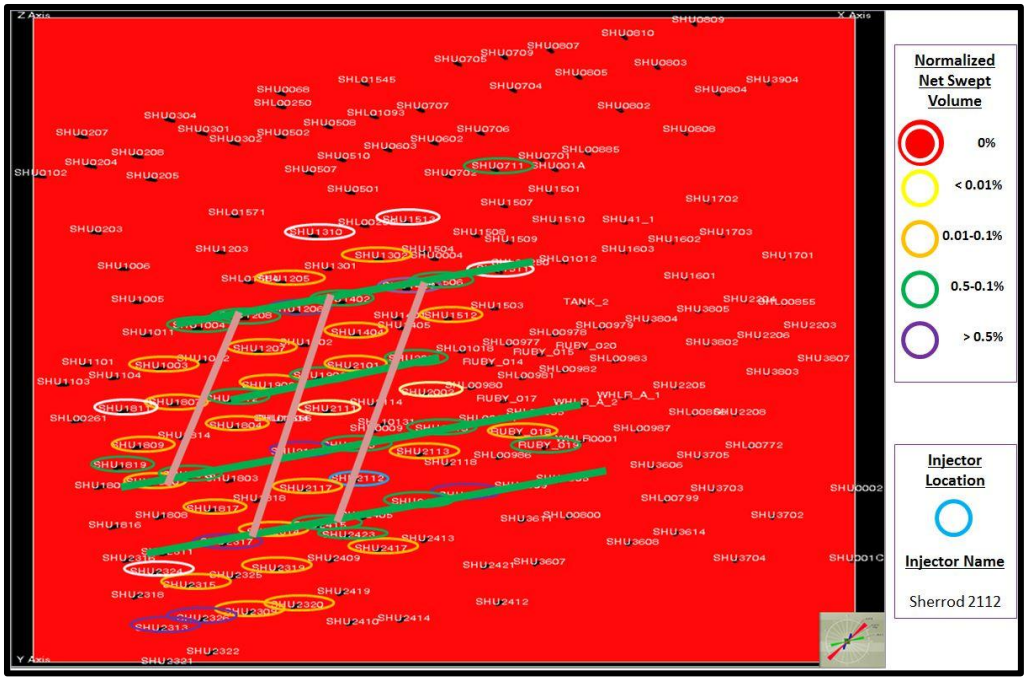

Figure 4.38: 'Sherrod 2112' connectivity with major flow features (green lines) through NE-SW fractures

Figure 4.39: 'Sherrod 2118' connectivity with major flow features (green lines) through NE-SW fractures

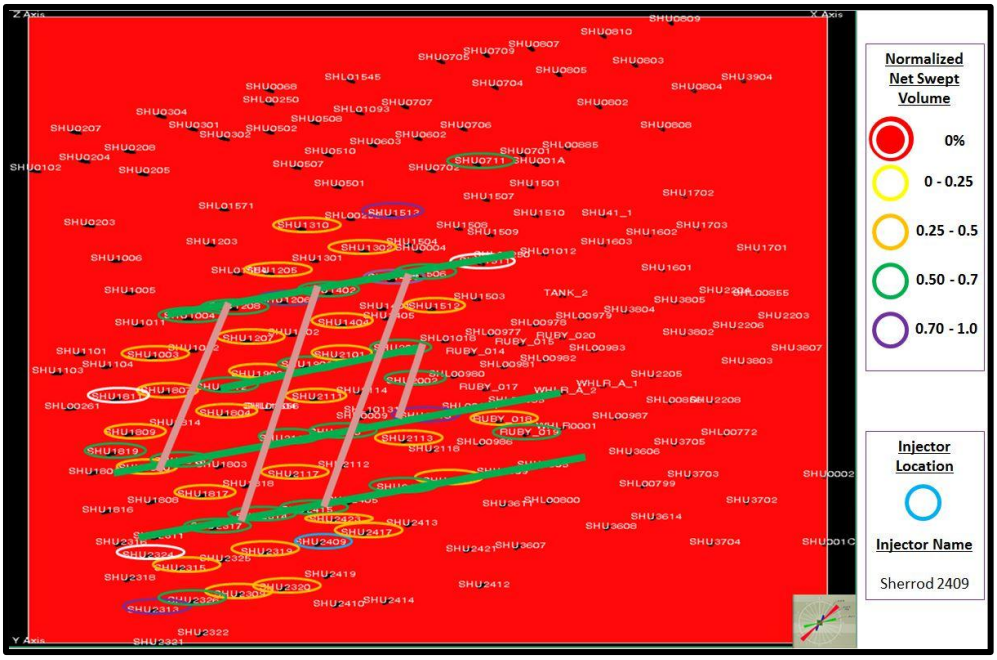

Figure 4.40: 'Sherrod 2409' connectivity with major flow features (green lines) through NE-SW fractures

Figure 4.41: 'Sherrod 1301' connectivity with major flow features (green lines) through NW-SE fractures

Figure 4.42: 'Sherrod 1012' connectivity with major flow features (green lines) through NW-SE fractures

Figure 4.43: 'Sherrod 1202' connectivity with major flow features (green lines) through NW-SE fractures

Figure 4.44: 'Sherrod 1405' connectivity with major flow features (green lines) through NW-SE fractures

Figure 4.45: 'Sherrod 2114' connectivity with major flow features (green lines) through NW-SE fractures

Figure 4.46: 'Sherrod 1814' connectivity with major flow features (green lines) through NW-SE fractures

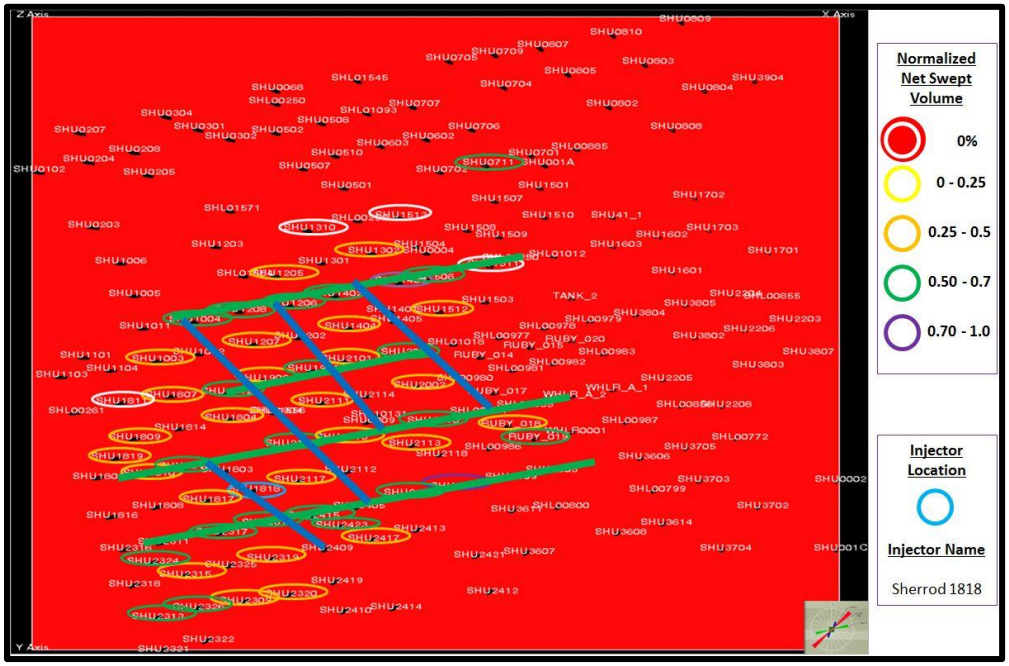

Figure 4.47: 'Sherrod 1818' connectivity with major flow features (green lines) through NW-SE fractures

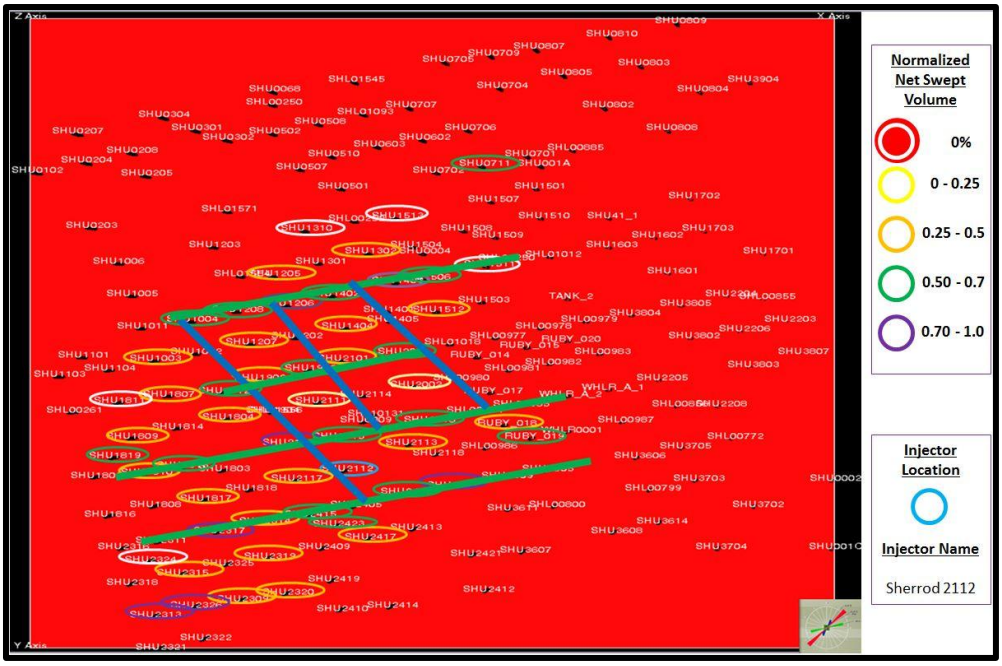

Figure 4.48: 'Sherrod 2112' connectivity with major flow features (green lines) through NW-SE fractures

Figure 4.49: 'Sherrod 2118' connectivity with major flow features (green lines) through NW-SE fractures

Figure 4.50: 'Sherrod 2409' connectivity with major flow features (green lines) through NW-SE fractures

Several severe limitations in method of moment analysis do exist. First, it is purely volumetric. As a result, important details in a tracer response such as tracer recovery, velocity, multiple peaks, or anomalies in breakthrough time are not captured. Second, it assumes that tracer response will exhibit exponential decline at the end of test. Due to large number of tracers showing peaking trend rather than decaying trend, a decision was made not to extrapolate tracer data to assure consistency when comparing and normalizing all results. Third, Method of Moments has a strong bias toward higher values of injection rates. For example, injectors showing relatively low swept volume could give a false indication of poor communication (e.g. Sherrod 2325). While in

reality, the relatively low swept volumes could be just a result of using a relatively lower injection rate. Thus, an attempt to analyze mass percentage of tracer recovered rather than swept volumes will be investigated in the next section.

4.5 Tracers Recovery : Statistical Analysis & Categorizing Responses

The fraction of tracer recovered at a given producer equals the fraction of injected water being produced at that producer. This key relation is an important tool to analyze wells' water production performance to assess the fraction of water produced due to direct communication by the surrounding tagged injectors and the fraction of water produced due to reservoir water saturation higher than irreducible. The following expressions were used to calculate mass of tracer recovered and its relation to injected water produced:

$$Tracer\ Recovered\ (g) =$$

$$Tracer\ Concentration\ (ppt) x \frac{1ppm}{10^6 ppt} x \frac{1mg/L}{1ppm} x \frac{1g}{1000mg} x \frac{158.9L}{1bbl} x \Delta Wp \quad \text{.....(12)}$$

$$\frac{tracer\ recovered\ (g)}{tracer\ injected\ (g)} = fraction\ of\ injection\ rate\ produced \quad \text{.....(13)}$$

A summary of total tracer recovered for each of the 13 tracer is shown in Figure 4.51. The overall tracer recovery is poor with none of the 13 tracers exceeding 10% recovery. Such low tracers' recoveries are not expected in a reservoir where highly conductive fractures are believed to be the main drive for the high water-cut observed in the field. Two possible explanations exist for such tracers recoveries: First, tagged injected water flow outside the pattern injection area. Second, tracer responses are excessively diluted and do not represent actual water contributed by pattern injectors. True reason will be

investigated in later sections. Table 4.4 show total tracer recovered at each producer. Colors used in the table will be explained later when mapping these observations. To make Table 4.4 more meaningful and easy to interpret, the frequencies of tracer recoveries are summarized in Table 4.5 and plotted as a distribution in Figure 4.52. The global distribution of tracer recoveries, Figure 4.52, shows that majority of tracer responses in Sherrod inter-well tracer test exhibit less than 0.01% tracer recovery (52.2% of tracer responses). If a tracer response between a pair of injector and producer exhibit 0.01% tracer recovery, this mean that only 0.01% of the water injected will appear as produced water. Tracer responses with such low recoveries provide minimum information about water movement in the field and can be treated as noise. This will be illustrated quantitatively in section 4.6. The next three intervals in the global distribution of tracer recoveries cover tracer recoveries from 0.01% to 0.1%. Although tracer recovery still low and expected to provide insignificant information about water movement, it is showing a different frequency trend compared to tracers with < 0.01% recovery. Comparing the three intervals with each other in Table 4.5 suggests that these three intervals could be combined into one category based on repetitive frequencies and similarities in number of observations (e.g. tracers IWT-1900, IWT-1200, IWT-2100). In a similar manner, tracer recoveries between 0.1-0.5% as well as tracer recoveries higher than 0.5% could be combined into two additional categories. Although the last two categories still show low tracer recoveries, they are expected to be containing the maximum useful information about water movement in Sherrod Area. Each one of the tracer recovery category is given a unique color to be used in mapping and these colors

are the one used in Tables 4.4 and 4.5 and Figure 4.52. In summary, by using frequency tables and global distribution of tracer recoveries, tracer responses can be categorized into four categories: responses with less than 0.01% recovery, responses with 0.01%-0.1% tracer recovery, responses with 0.1-0.5% tracer recovery, and responses with higher than 0.5% tracer recovery.

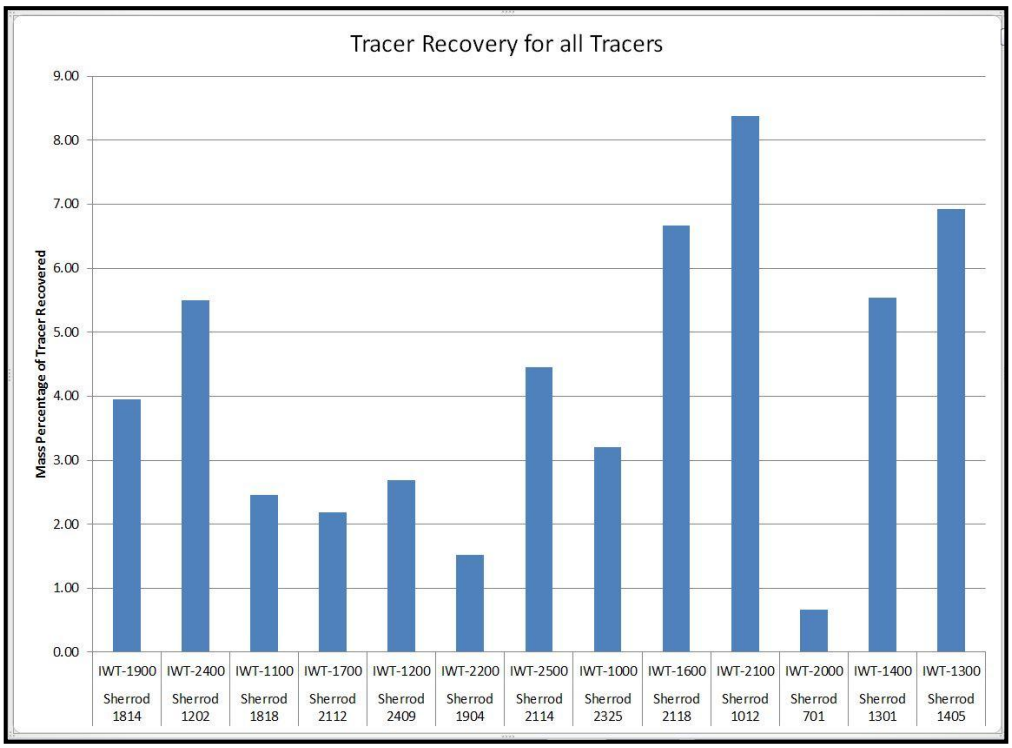

Figure 4.51: Recoveries of the 13 injected tracers

	1814	1202	1818	2112	2409	1904	2114	2325	2118	1012	701	1301	1405
	IWT-1900	IWT-2400	IWT-1100	IWT-1700	IWT-1200	IWT-2200	IWT-2500	IWT-1000	IWT-1600	IWT-2100	IWT-2000	IWT-1400	IWT-1300
Ruby 18	0.082	0.134	0.027	0.024	0.071	0.002	0.105	0.106	2.864	0.303	0.001	0.032	0.130
Ruby 19	0.002	0.006	0.001	0.001	0.004	0.000	0.006	0.009	0.453	0.026	0.000	0.000	0.009
Sherrod 711	0.007	0.018	0.003	0.003	0.009	0.000	0.019	0.020	0.011	0.063	0.623	0.002	0.030
Sherrod 1003	0.256	0.340	0.076	0.061	0.196	0.017	0.354	0.229	0.221	2.184	0.010	0.119	0.324
Sherrod 1004	0.002	0.003	0.001	0.001	0.002	0.000	0.004	0.003	0.002	0.120	0.000	0.001	0.005
Sherrod 1205	0.034	0.059	0.010	0.010	0.031	0.000	0.063	0.044	0.037	0.143	0.000	2.291	0.060
Sherrod 1206	0.003	0.005	0.001	0.001	0.003	0.000	0.005	0.005	0.004	0.429	0.000	0.005	0.009
Sherrod 1207	0.143	1.705	0.047	0.041	0.121	0.007	0.267	0.171	0.142	0.912	0.004	0.071	0.224
Sherrod 1208	0.027	0.040	0.008	0.006	0.021	0.001	0.041	0.030	0.025	1.078	0.001	0.016	0.044
Sherrod 1302	0.035	0.069	0.012	0.012	0.035	0.000	0.066	0.055	0.046	0.175	0.000	2.631	0.090
Sherrod 1310	0.000	0.000	0.000	0.000	0.000	0.000	0.000	0.000	0.000	0.001	0.000	0.006	0.000
Sherrod 1402	0.011	0.764	0.005	0.004	0.011	0.000	0.023	0.019	0.014	0.054	0.000	0.005	0.027
Sherrod 1403	0.001	0.126	0.000	0.000	0.001	0.000	0.002	0.003	0.001	0.007	0.000	0.000	0.015
Sherrod 1404	0.046	0.895	0.016	0.016	0.049	0.001	0.086	0.061	0.050	0.190	0.001	0.019	1.541
Sherrod 1506	0.000	0.001	0.000	0.000	0.001	0.000	0.001	0.001	0.001	0.004	0.000	0.000	0.173
Sherrod 1511	0.000	0.000	0.000	0.000	0.000	0.000	0.000	0.000	0.000	0.000	0.000	0.000	0.013
Sherrod 1512	0.085	0.126	0.026	0.026	0.080	0.003	0.140	0.095	0.088	0.281	0.002	0.034	2.452
Sherrod 1513	0.000	0.000	0.000	0.000	0.000	0.000	0.000	0.000	0.000	0.001	0.000	0.007	0.001
Sherrod 1804	0.936	0.116	0.021	0.017	0.056	0.815	0.120	0.080	0.069	0.268	0.002	0.027	0.117
Sherrod 1807	0.004	0.004	0.001	0.001	0.002	0.000	0.005	0.003	0.003	0.195	0.000	0.001	0.004
Sherrod 1809	0.847	0.135	0.028	0.022	0.066	0.006	0.135	0.089	0.082	0.249	0.004	0.046	0.128
Sherrod 1810	0.029	0.003	0.001	0.000	0.002	0.000	0.003	0.029	0.002	0.007	0.000	0.001	0.005
Sherrod 1811	0.000	0.000	0.000	0.000	0.000	0.000	0.000	0.000	0.000	0.008	0.000	0.000	0.000
Sherrod 1812	0.344	0.089	0.003	0.002	0.006	0.004	0.014	0.012	0.009	0.036	0.000	0.003	0.018
Sherrod 1815	0.259	0.012	0.003	0.002	0.006	0.001	0.012	0.008	0.007	0.023	0.000	0.005	0.012
Sherrod 1817	0.033	0.060	0.922	0.008	0.041	0.001	0.072	0.046	0.043	0.132	0.000	0.011	0.058
Sherrod 1819	0.369	0.072	0.012	0.009	0.029	0.003	0.053	0.037	0.027	0.095	0.002	0.019	0.048
Sherrod 1902	0.001	0.066	0.000	0.000	0.000	0.000	0.001	0.001	0.001	0.002	0.000	0.000	0.001
Sherrod 1903	0.000	0.002	0.000	0.000	0.001	0.003	0.002	0.003	0.002	0.009	0.000	0.000	0.229
Sherrod 2001	0.010	0.025	0.004	0.005	0.012	0.000	0.687	0.022	0.017	0.064	0.000	0.004	0.030
Sherrod 2002	0.000	0.001	0.000	0.001	0.000	0.004	0.023	0.008	0.001	0.003	0.000	0.000	0.001
Sherrod 2101	0.005	0.011	0.002	0.002	0.007	0.000	0.011	0.011	0.008	0.030	0.000	0.002	0.490
Sherrod 2110	0.002	0.004	0.155	0.001	0.002	0.009	0.011	0.004	0.003	0.011	0.000	0.001	0.005
Sherrod 2111	0.139	0.215	0.045	0.054	0.118	0.529	1.404	0.143	0.128	0.364	0.005	0.076	0.172
Sherrod 2113	0.086	0.133	0.031	0.028	0.078	0.004	0.131	0.112	1.698	0.290	0.002	0.045	0.153
Sherrod 2115	0.004	0.007	0.321	0.001	0.004	0.000	0.011	0.006	0.004	0.018	0.000	0.002	0.008
Sherrod 2116	0.005	0.014	0.003	0.617	0.009	0.101	0.320	0.023	0.013	0.062	0.000	0.002	0.035
Sherrod 2117	0.018	0.033	0.316	0.700	0.015	0.000	0.036	0.026	0.024	0.078	0.000	0.007	0.037
Sherrod 2309	0.009	0.013	0.003	0.002	0.176	0.000	0.015	0.009	0.010	0.027	0.000	0.004	0.012
Sherrod 2313	0.000	0.001	0.000	0.000	0.000	0.000	0.001	0.113	0.001	0.002	0.000	0.000	0.001
Sherrod 2314	0.003	0.007	0.065	0.252	0.004	0.000	0.007	0.220	0.005	0.018	0.000	0.001	0.010
Sherrod 2315	0.022	0.023	0.009	0.004	0.013	0.001	0.026	0.272	0.016	0.049	0.000	0.006	0.023
Sherrod 2317	0.004	0.009	0.245	0.001	0.006	0.000	0.009	0.061	0.007	0.023	0.000	0.002	0.011
Sherrod 2319	0.057	0.095	0.025	0.018	0.714	0.002	0.107	0.676	0.062	0.217	0.001	0.025	0.107
Sherrod 2320	0.001	0.003	0.001	0.001	0.095	0.000	0.003	0.003	0.002	0.008	0.000	0.000	0.004
Sherrod 2324	0.000	0.000	0.002	0.000	0.000	0.000	0.000	0.002	0.000	0.000	0.000	0.000	0.000
Sherrod 2326	0.003	0.004	0.002	0.001	0.003	0.000	0.004	0.032	0.004	0.006	0.000	0.002	0.003
Sherrod 2411	0.001	0.002	0.001	0.000	0.018	0.000	0.002	0.002	0.001	0.004	0.000	0.001	0.002
Sherrod 2415	0.003	0.005	0.002	0.222	0.003	0.000	0.006	0.261	0.004	0.015	0.000	0.001	0.009
Sherrod 2416	0.003	0.008	0.003	0.002	0.005	0.000	0.008	0.010	0.432	0.028	0.000	0.001	0.012
Sherrod 2417	0.013	0.022	0.004	0.004	0.312	0.000	0.023	0.017	0.017	0.047	0.000	0.005	0.022
Sherrod 2423	0.005	0.010	0.002	0.002	0.252	0.000	0.011	0.010	0.007	0.025	0.000	0.002	0.014

Table 4.4: Tracer recoveries at each producer

Injector Number	1814	1202	1818	2112	2409	1904	2114	2325	2118	1012	701	1301	1405	Total
Mass of Tracer Recovered (%)	IWT-1900	IWT-2400	IWT-1100	IWT-1700	IWT-1200	IWT-2200	IWT-2500	IWT-1000	IWT-1600	IWT-2100	IWT-2000	IWT-1400	IWT-1300	
<0.01	25	21	29	32	25	33	19	19	24	15	23	30	17	312
[0.01-0.025)	4	7	6	6	6	1	11	9	9	6	1	5	10	81
[0.025-0.05)	6	3	6	3	5	0	3	7	5	8	0	5	7	58
[0.05-0.1)	4	7	2	2	6	0	5	6	4	6	0	2	3	47
[0.1-0.25)	2	7	2	1	4	1	6	7	3	8	0	1	9	51
[0.25-0.5)	4	1	2	1	2	0	3	2	2	6	0	0	2	25
[0.5-1.0)	2	2	1	2	1	2	1	1	0	1	1	0	0	14
[1.0-2.0)	0	1	0	0	0	0	1	0	1	1	0	0	1	5
2.0+	0	0	0	0	0	0	0	0	1	1	0	2	1	5

Table 4.5: Frequencies of Recoveries for all Tracers Responses

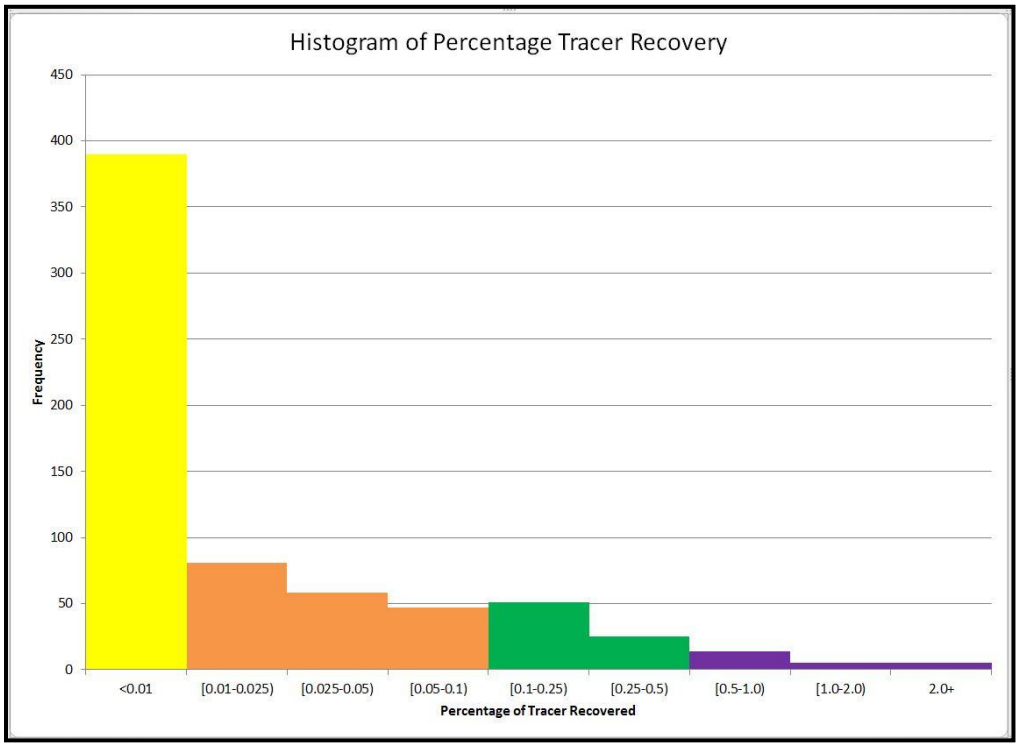

Figure 4.52: Distribution of recoveries from all tracers' responses

4.6 Linking Tracers Recovery To Wells' Water Rate Performance

To illustrate quantitatively the significance of tracers in explaining wells' water performance, one inverted nine spot pattern is taken as a case study (Figure 4.53). Enclosed in this pattern area one of the unique tracer responses where the pair Sherrod 1012- Sherrod1003 showed the highest tracer concentration produced in Sherrod inter-well tracer test.

In this case study, water production from each one of the producers within this inverted nine spot pattern is decomposed into two components: tagged water rate and untagged water rate. The tagged water rate is the water being contributed by all of the tracer-tagged injectors and is calculated by simply multiplying tracer recovery at each producer with injection rate of the contributing injector. The untagged water rate is the water rate of the well after removing the water flowing from tagged injectors. This is used to analyze the significance of tracers in explaining wells water production. In general, for a pair of wells producer "P" and injector "I", the fraction of water injected at well "I" which appear as water production rate at well "P" is given by :

$$q_{w\ (at\ well\ P\ from\ well\ I)} = {}^{m_{ip}}/_{M_i}\ x\ i_{w\ (well\ I)} \quad \text{.....(14)}$$

where q_w is water rate in stb/d , "m_{ip} / M_i" is fraction of tracer recovered at producer "P", and i_w is water injection rate of injector "I". It must be highlighted that the fraction of tracer recovered is highly affected by extrapolating the tracer response assuming exponential decay. Thus, consistency and precaution must be considered while evaluating tracer recovery. Moreover, tracer recovery is a strong function of distribution of fluxes in the reservoir which changes whenever the distribution of injected water

changes. Here it is assumed to be constant because there is no significant variation of injection rates during tracer injection period. Figures 4.54 through 4.61 show location of each producer in the pattern, its decomposed water rate, and contributing injectors. A sample calculation for producer “Sherrod 1207” is shown in Table 4.6. Calculations for the remaining 7 producers are shown in Appendix F.

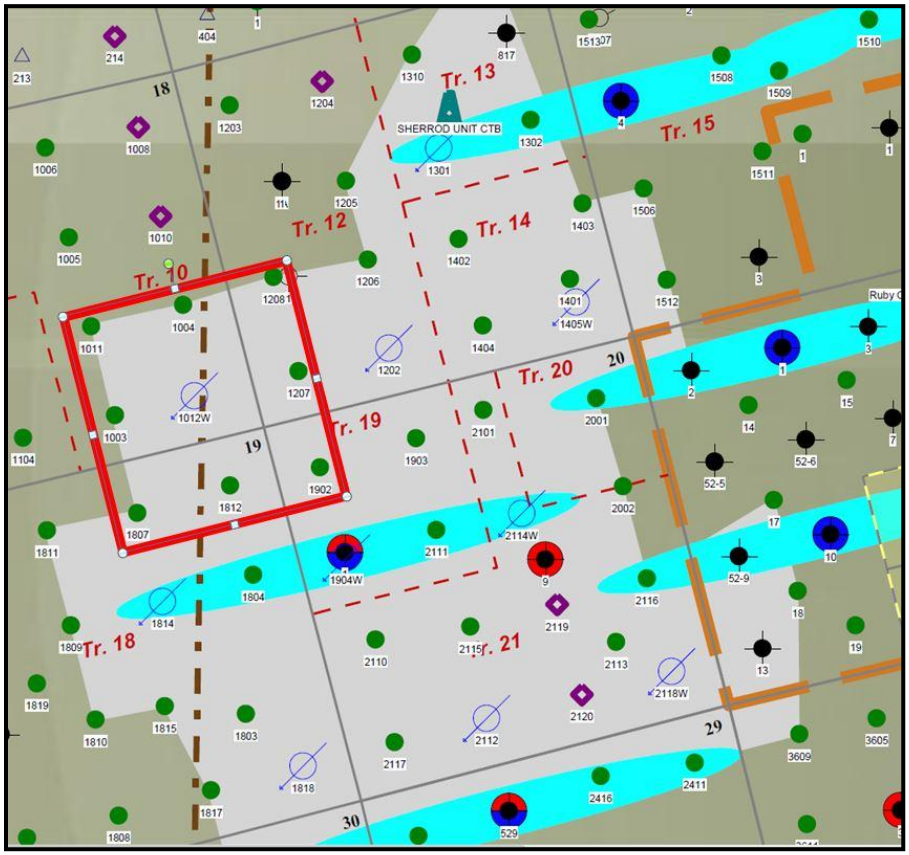

Figure 4.53: Pattern used as a case study in linking tracer recovery with wells water performance

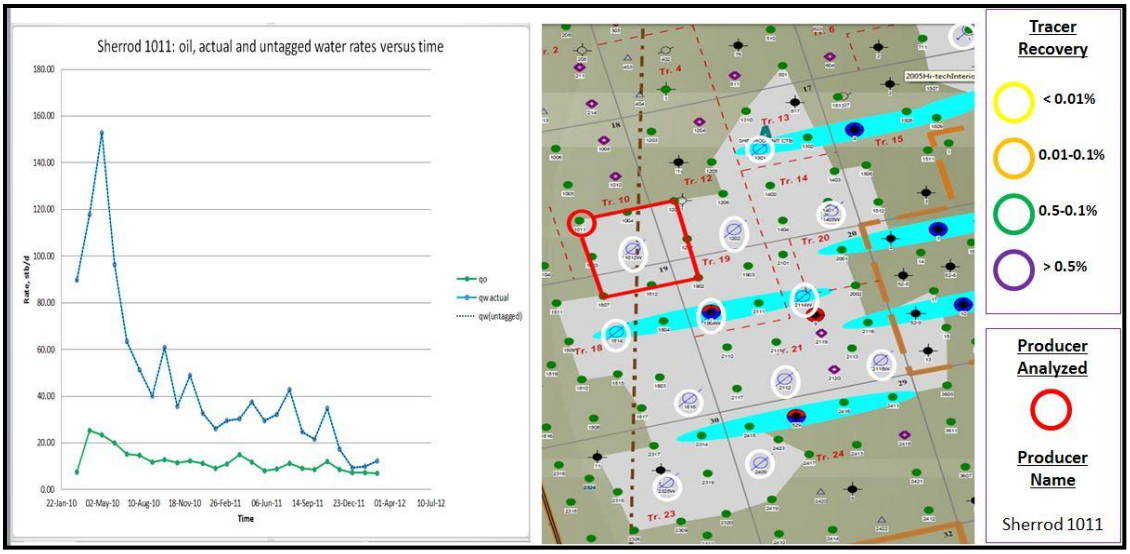

Figure 4.54: Sherrod 1011, contributing injectors, and water rate decomposition.

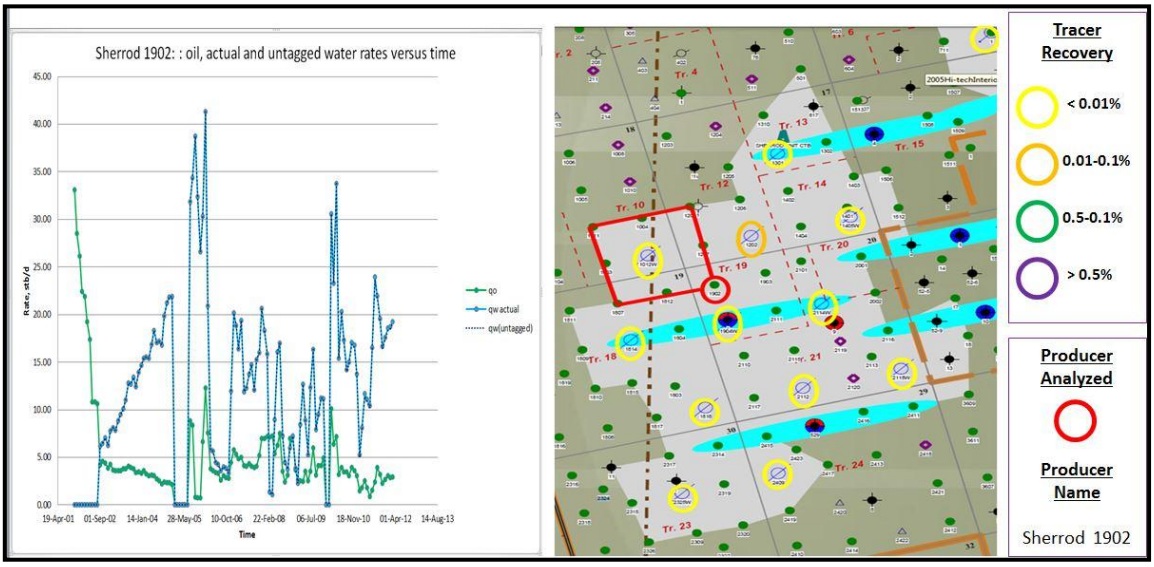

Figure 4.55: Sherrod 1902, contributing injectors, and water rate decomposition.

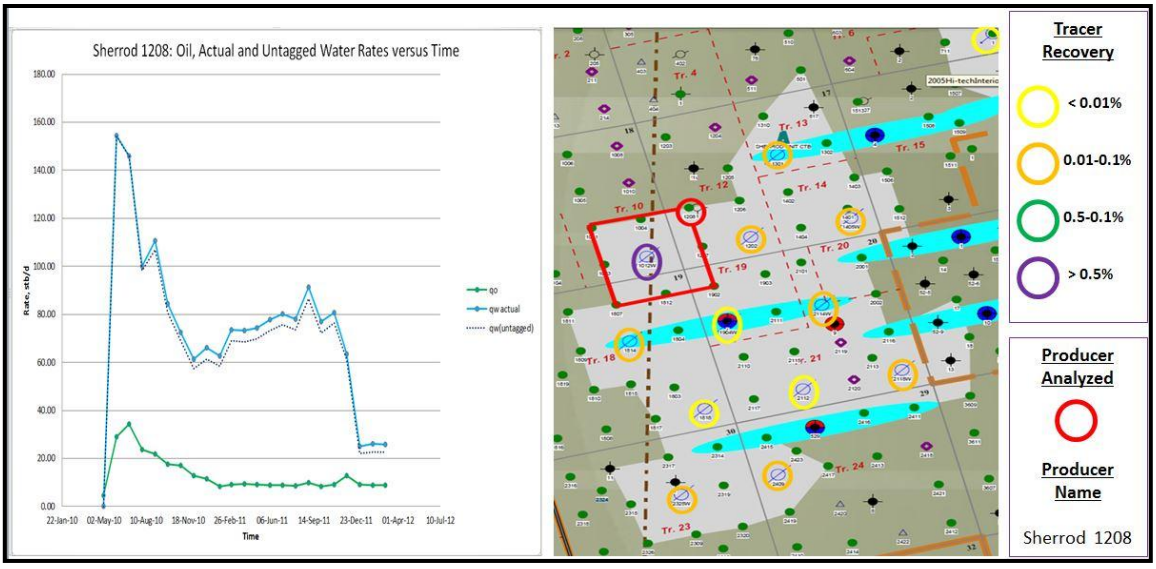

Figure 4.56: Sherrod 1208, contributing injectors, and water rate decomposition.

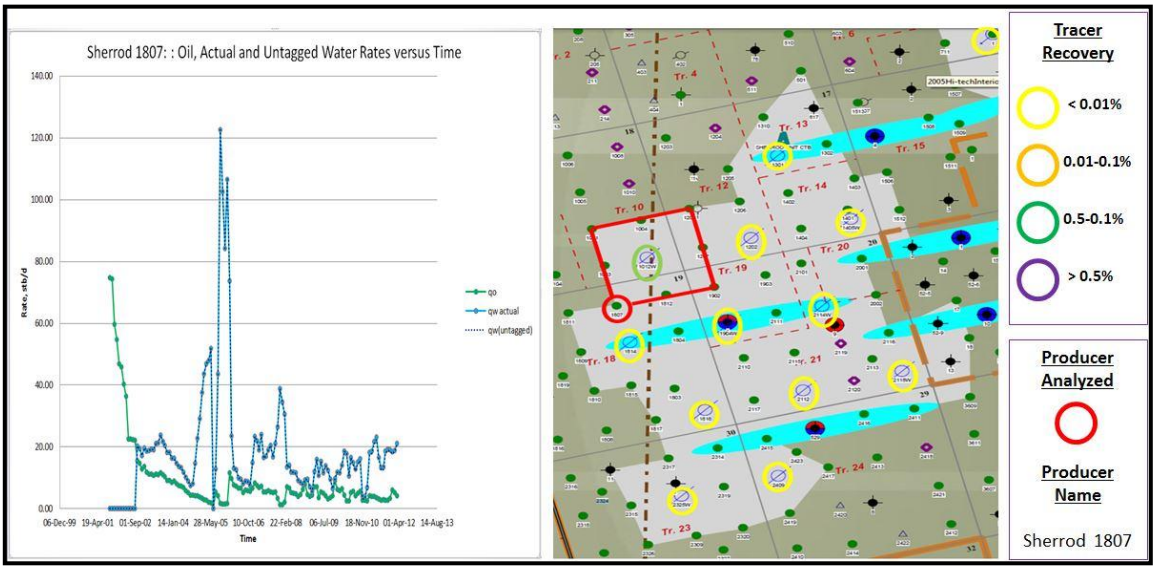

Figure 4.57: Sherrod 1807, contributing injectors, and water rate decomposition

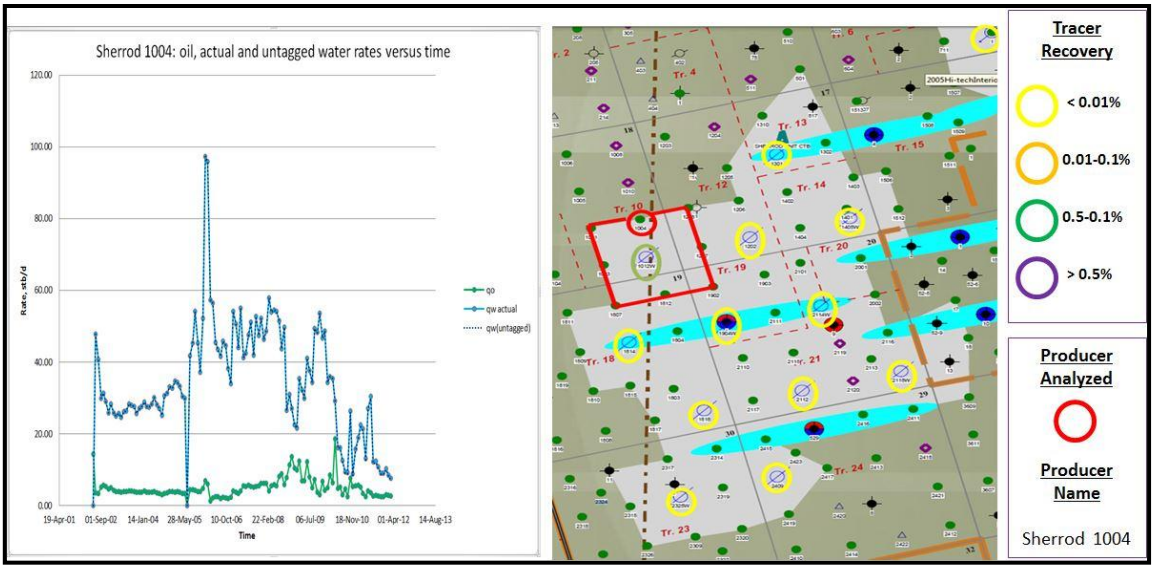

Figure 4.58: Sherrod 1004, contributing injectors, and water rate decomposition

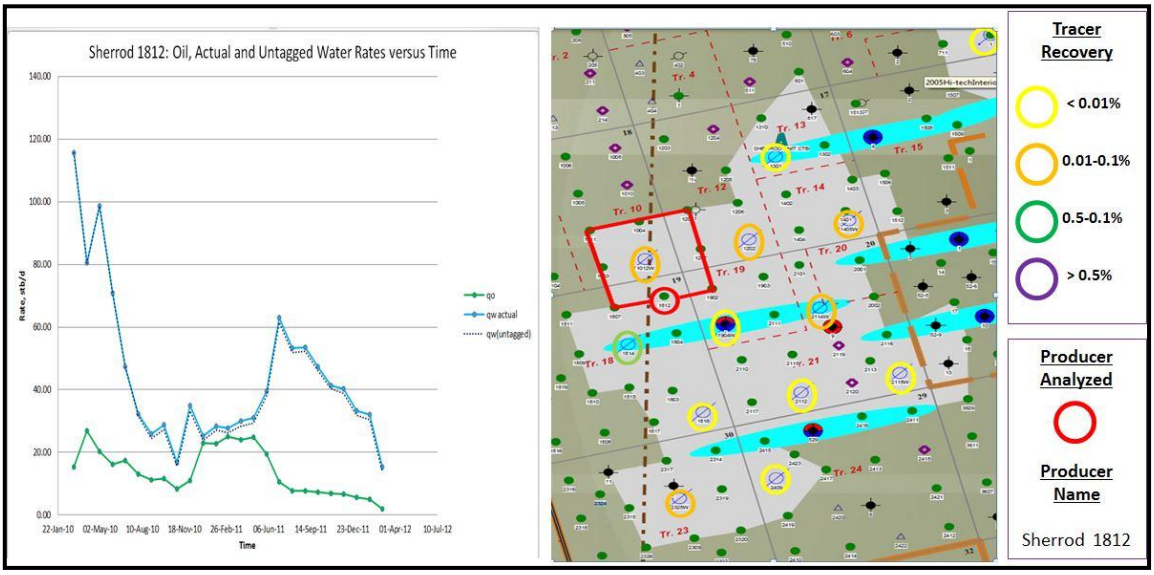

Figure 4.59: Sherrod 1812, contributing injectors, and water rate decomposition

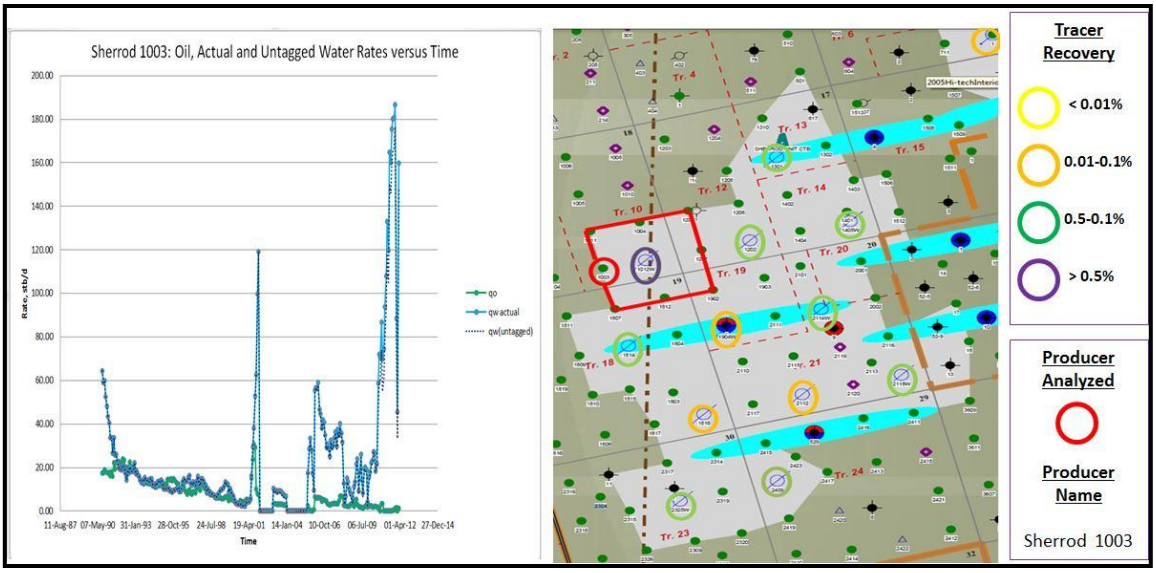

Figure 4.60: Sherrod 1003, contributing injectors, and water rate decomposition

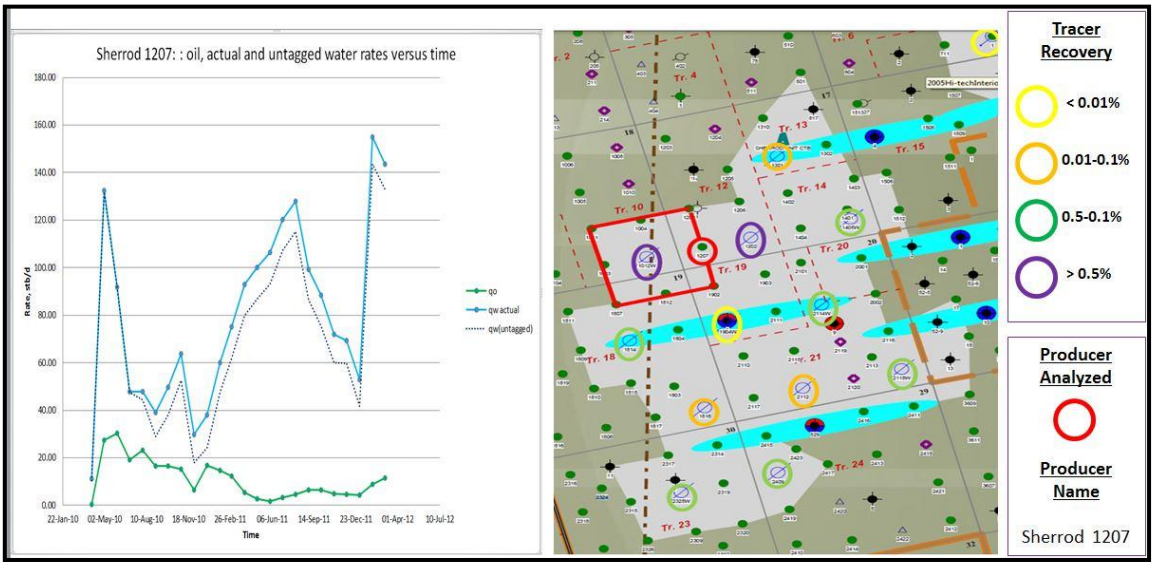

Figure 4.61: Sherrod 1207, contributing injectors, and water rate decomposition

Sherrod 1207																	
Date	Daily Oil	Daily Wtr	qw(1814)	qw(1202)	qw(1818)	qw(2112)	qw(2409)	qw(1904)	qw(2114)	qw(2325)	qw(2118)	qw(1012)	qw(1405)	qw(701)	qw(1301)	qw(tagged)	qw(untagged)
01-Apr-10	0.32	11.15	0.00	0.00	0.00	0.00	0.00	0.00	0.00	0.00	0.00	0.00	0.00	0.01	0.56	0.57	10.58
01-May-10	27.30	132.36	0.00	0.00	0.00	0.00	0.00	0.00	0.00	0.00	0.00	0.00	0.00	0.01	0.42	0.42	131.94
01-Jun-10	30.25	91.83	0.00	0.00	0.00	0.00	0.00	0.00	0.00	0.00	0.00	0.00	0.00	0.01	0.24	0.25	91.59
01-Jul-10	19.21	47.96	0.00	0.00	0.00	0.00	0.00	0.00	0.00	0.00	0.00	0.00	0.00	0.00	0.30	0.31	47.66
01-Aug-10	23.06	47.96	0.20	2.81	0.00	0.00	0.00	0.00	0.00	0.00	0.00	0.00	0.29	0.00	0.19	3.50	44.45
01-Sep-10	16.52	39.09	0.44	5.12	0.08	0.07	0.21	0.02	0.30	0.18	0.21	2.65	0.69	0.00	0.20	10.17	28.92
01-Oct-10	16.44	49.78	0.43	5.60	0.16	0.12	0.40	0.01	0.67	0.38	0.42	2.54	0.73	0.00	0.22	11.68	38.09
01-Nov-10	15.30	63.69	0.41	5.49	0.15	0.12	0.38	0.02	0.61	0.28	0.41	2.45	0.46	0.00	0.21	10.99	52.70
01-Dec-10	6.47	29.88	0.46	5.72	0.14	0.13	0.39	0.02	0.64	0.48	0.35	2.64	0.69	0.00	0.24	11.91	17.97
01-Jan-11	16.81	38.02	0.48	6.34	0.15	0.14	0.40	0.02	0.96	0.35	0.51	3.23	0.82	0.00	0.26	13.65	24.37
01-Feb-11	14.79	59.92	0.43	5.72	0.15	0.13	0.38	0.02	0.83	0.28	0.47	2.92	0.76	0.00	0.23	12.31	47.61
01-Mar-11	12.20	75.09	0.48	6.07	0.16	0.14	0.42	0.02	0.86	0.23	0.50	3.21	0.79	0.00	0.25	13.15	61.94
01-Apr-11	5.39	93.03	0.47	5.97	0.16	0.14	0.41	0.02	0.83	0.24	0.51	3.21	0.80	0.00	0.25	13.01	80.02
01-May-11	2.69	100.01	0.49	5.94	0.16	0.14	0.42	0.02	0.93	0.33	0.50	3.15	0.79	0.00	0.25	13.11	86.90
01-Jun-11	1.78	106.44	0.46	5.96	0.14	0.14	0.42	0.02	0.94	0.32	0.50	3.20	0.79	0.00	0.25	13.12	93.32
01-Jul-11	3.29	120.21	0.47	6.02	0.15	0.14	0.42	0.02	0.65	0.29	0.50	3.21	0.81	0.00	0.25	12.93	107.29
01-Aug-11	4.73	127.85	0.39	5.76	0.13	0.13	0.38	0.02	0.95	0.24	0.49	3.13	0.78	0.00	0.24	12.66	115.19
01-Sep-11	6.36	99.18	0.38	5.15	0.13	0.13	0.35	0.02	0.94	0.35	0.50	3.53	0.79	0.00	0.25	12.54	86.64
01-Oct-11	6.51	88.52	0.34	6.18	0.11	0.13	0.33	0.01	0.89	0.42	0.45	3.29	0.81	0.00	0.25	13.21	75.31
01-Nov-11	4.96	72.10	0.34	5.39	0.12	0.13	0.44	0.02	0.85	0.39	0.54	3.05	0.64	0.00	0.24	12.15	59.95
01-Dec-11	4.70	69.36	0.45	4.44	0.15	0.09	0.42	0.02	0.82	0.31	0.52	1.41	0.71	0.00	0.22	9.57	59.79
01-Jan-12	4.36	52.78	0.48	5.42	0.16	0.13	0.36	0.02	0.83	0.24	0.42	1.97	0.71	0.00	0.20	10.94	41.84
01-Feb-12	8.84	154.96	0.46	5.31	0.14	0.12	0.34	0.02	0.86	0.53	0.39	2.10	0.77	0.00	0.26	11.31	143.65
01-Mar-12	11.39	143.65	0.46	4.92	0.14	0.12	0.30	0.02	0.87	0.48	0.39	1.93	0.76	0.00	0.25	10.65	132.99

Table 4.6: Sample water rate decomposition calculation for ‘Sherrod 1207’

A total of 77 tracer responses were obtained from 7 out of the 8 producers in the inverted nine spot understudy. Tracer responses in this pattern are in the range of 0.001-2.1% which covers the four tracer recovery categories defined earlier in section 4.5.

Producers located on a NW-SE trend with respect to the pattern injector showed no tracer response for case of ‘Sherrod 1011’ and weak tracer responses for case of ‘Sherrod 1902’ (Figures 4.54 and 4.55). This is believed to be due to the absence of a NW-SE fracture system within this pattern. As a result of the weak tracer responses, tagged water rate in “Sherrod 1902” is only 1% on average of the actual water rate. Thus, for these two wells, none of the tagged injectors explains the source of water being produced and the actual water rate almost matches the untagged water rate.

In a similar manner, producers located on a N-S trend with respect to the pattern injector showed mainly weak tracer responses. Only one exception exists where

producer ‘Sherrod 1004” showed a moderate recovery tracer response in the range of “0.1-0.5%”. This exception reflects the existence but rarity of N-S fracture trend which connects injector “Sherrod 1012” to “Sherrod 1004”. It should be noted that producer ‘Sherrod 1812’ show a moderate tracer show through its connection with an injector outside the pattern through a NE-SW fracture. As a result of low tracer recovery, “Sherrod 1004” and “Sherrod 1812” show a small separation between actual and untagged water rates. On average, tagged water at these producers is 3.3-3.6% of actual water rate.

Producers “Sherrod 1807” and “Sherrod 1208” in Figures 4.56 and 4.57 showed moderate to high tracer recoveries reflecting the existence of a NE-SW trend which connects the producers with the injector inside the pattern. Injectors outside the pattern show weak communication with these two producers. The well with high tracer recovery, “Sherrod 1208”, shows tagged water rate of 6.4% of actual water rate on average compared to 5.6% for the well with moderate tracer recovery, “Sherrod 1807” .

Producers “Sherrod 1003” and “Sherrod 1207” which are located on an E-W trend with respect to the injector inside the pattern reflect more the complexity of the water movement in the reservoir (Figures 4.60 and 4.61). Along the E-W fracture system, 9 out of the 12 tagged injectors outside the pattern shows significantly higher water contribution and moderate recovery tracer responses. This reflects a complex fracture network where far injectors as well as nearby injectors have a direct impact on pattern performance. Tagged water rates are in the range of 13.4-14% on average of the actual

water rate. The nature of this fracture network will be investigated in more depth when tracers from all other producers are mapped in section 4.8.

In summary, the inverted nine spot pattern studied in this section highlights several aspects of the tracer test area. First, tracer recovery is poor rising a question of where the injected water is going. Second, water-cuts are high raising a question about the source of the water produced. Third, for a field where water injection rates are in the range of 120-390 bbl/day, tracer recoveries of < 0.1% reflects infinitesimally small water movement of a fraction of a barrel. Modeling this scale of volumes is irrelevant and does not fit the purpose of this study. Thus, these tracer responses which belong to the lower two tracer recovery categories will not be mapped or simulated and more focus will be put on tracer recoveries of "0.1-0.5%" and "0.5%+". Forth, preferential path for tracers in Sherrod area is in the NE-SW and E-W direction reflecting major fracture system carrying water in this direction. Tracer movement through a N-S or NW-SE direction does exist but it is rare. Fifth, producers located on the E-W fracture set reflect more the complexity of the global fracture network as far injectors as well as nearby injectors contribute more significantly to wells' performance by showing higher tracer responses.

4.7 Characteristics of Tracers Responses

In this section, breakthrough times, tracer velocities, as well as general characteristics of tracer response curves such as number of peaks observed in a response is studied. Breakthrough times were studied independently of velocities because they capture some trends in data that might not be clear from velocity interpretation alone (e.g. intermittent

tracer production and probability of tracer response being affected by dilution). Characteristic of tracers' responses is studied by tracer recovery category as well as from a global point of view.

4.7.1 Tracers' Velocities

A histogram of all tracer velocities obtained during Sherrod inter-well tracer test is shown in Figure 4.62. This histogram also includes producers that did not show any tracer response and those are represented as zero velocity tracers.

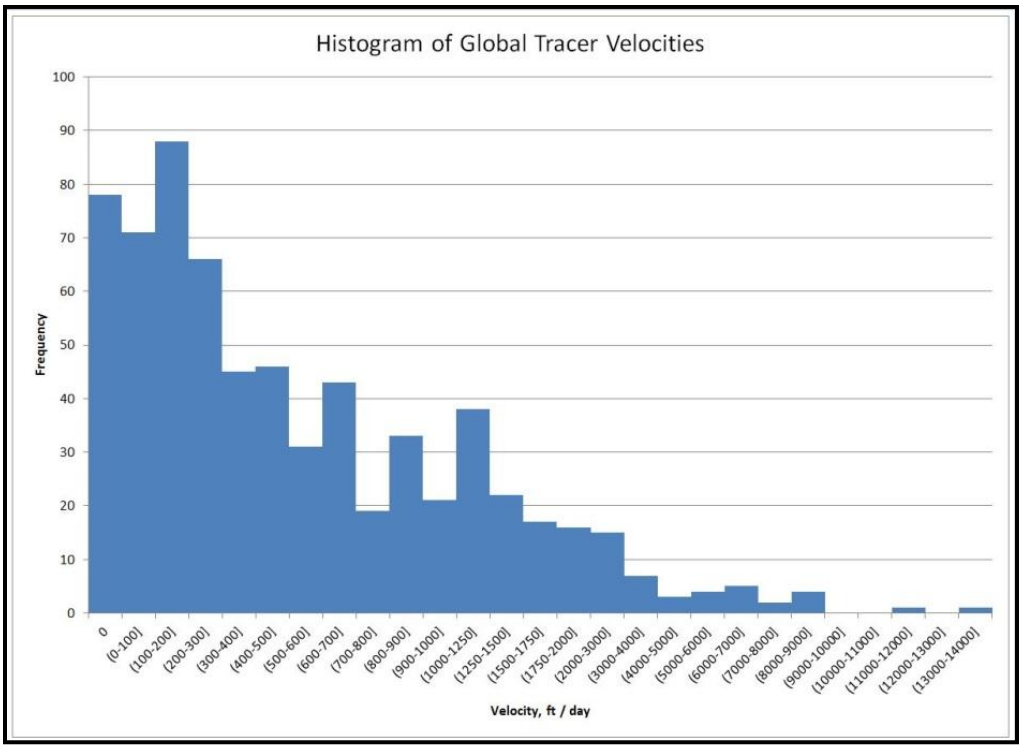

Figure 4.62: Histogram of global tracers velocities

The distribution of tracer velocities covers a wide range from zero velocities to ultra-high velocities of 13,288 ft/day with majority of observations lying in the lower velocities interval. Three trends could be observed from the global velocity distribution: First trend is from 0 to 600 ft/day which covers 63% of responses. Second trend is between 600 to 5000 ft/day which covers 35% of responses and the third trend covers the remaining range between 5000 to 13,288 ft/day. The three trends are highlighted in figure 4.63 below. This most likely reflects three fracture sets controlling water movement in the reservoir each with different average conductivity.

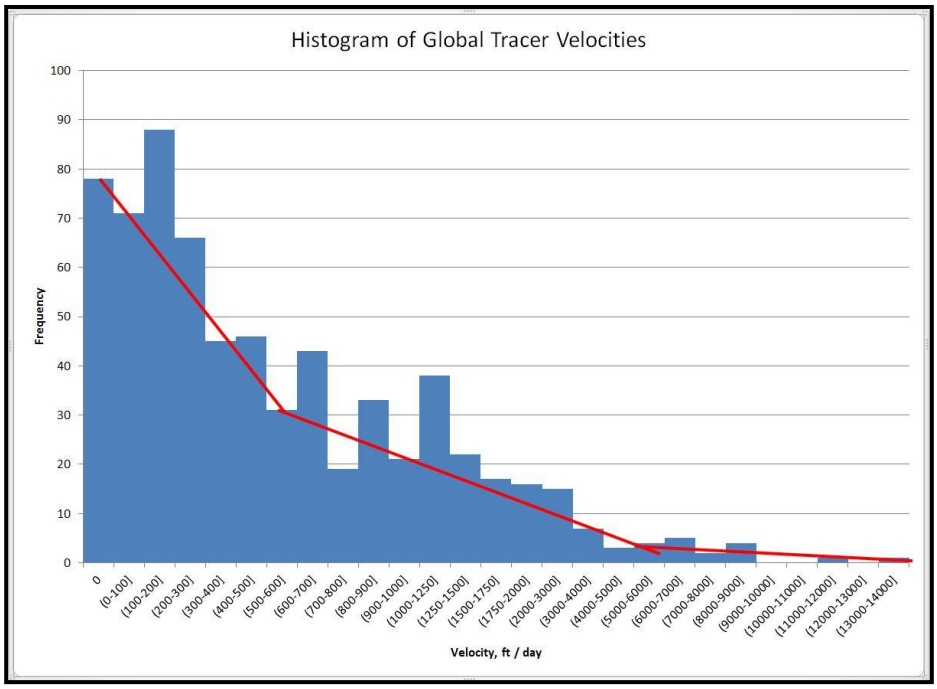

Figure 4.63: Three trends observed in distribution of tracers velocities

In an attempt to investigate the relation between tracers' velocities with their recovery, distributions of tracer velocities by recovery category is shown in Figures 4.64 through 4.67.

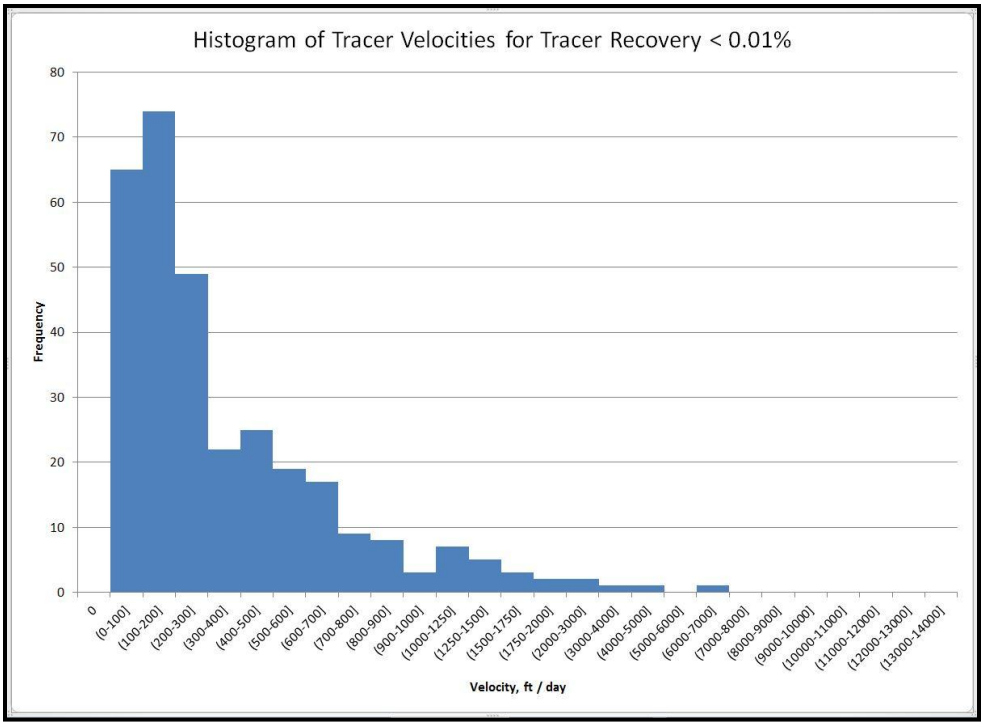

Figure 4.64: Distribution of tracers' velocities (tracer recovery < 0.01%)

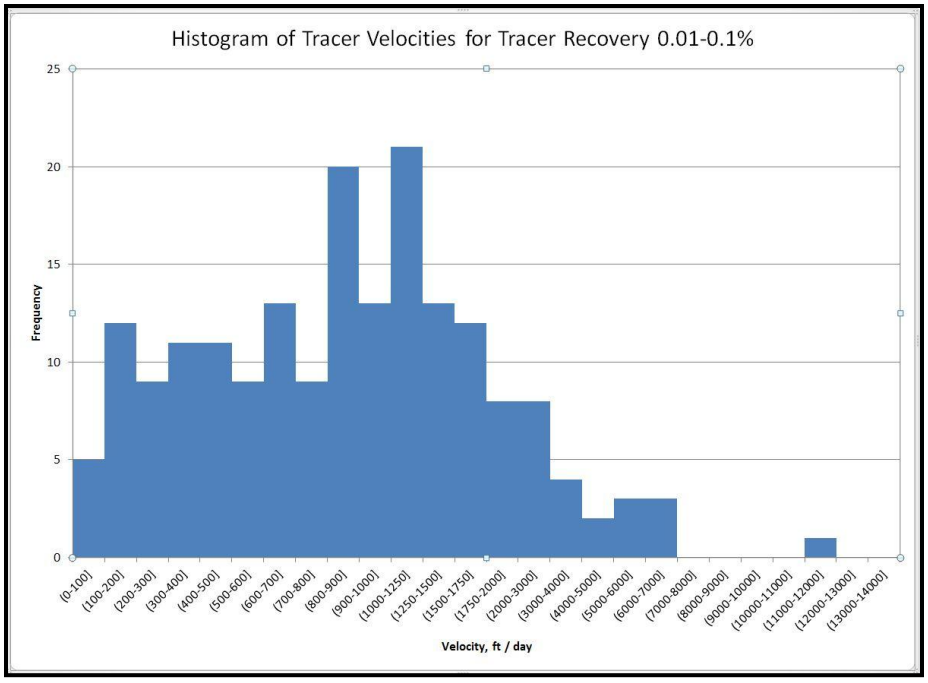

Figure 4.65: Distribution of tracers' velocities (tracer recovery 0.01-0.1%)

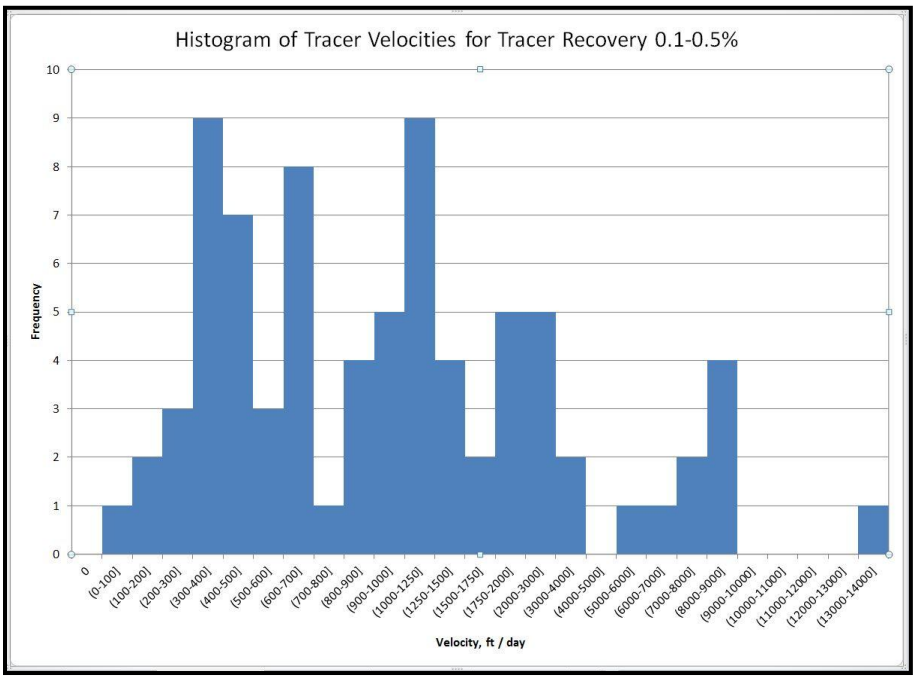

Figure 4.66: Distribution of tracers' velocities (tracer recovery 0.1-0.5%)

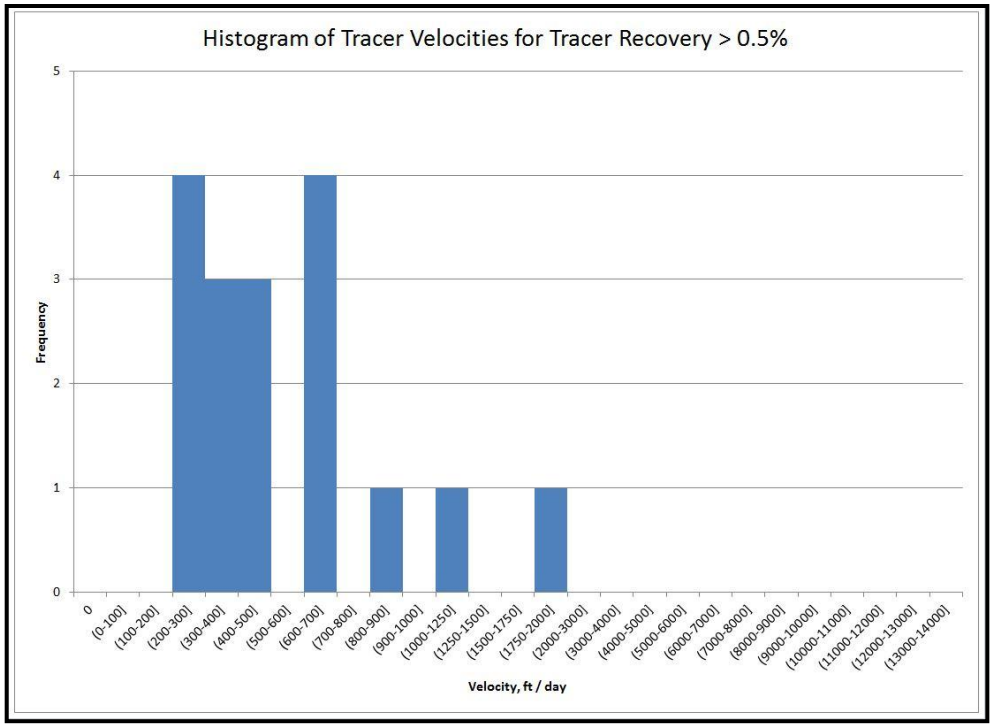

Figure 4.67: Distribution of tracers' velocities (tracer recovery > 0.5%)

The distribution of tracers velocities for the lowest tracer recovery group in Figure 4.64 show a smooth declining trend covering a wide range of velocities between 0 to 7,000 ft/day. This distribution is very close to the exponential distribution. The wide range and the distribution of velocities most probably reflect that these tracers are flowing through fractures with a wide range of conductivity and pore volumes.

For responses with tracer recoveries between 0.01-0.1%, the distribution of tracers velocities shown in Figure 4.65 also covers a wide range of velocities but the shape shows different type of distribution. The shape of velocity distribution is very close to bimodal normal distribution and this most probably reflect that tracers are flowing

through two types of fracture systems each with a different mean pore volume and conductivity.

For tracer recoveries between 0.1-0.5%, distribution of tracers velocities shown in Figure 4.66 reflect a wide range similar to the earlier ones with velocities between 100 to 14,000 ft / day. However, the shape of the distribution is different than the previous ones and it shows a distribution very close to a tri-modal normal distribution. The three normal distributions most probably reflect three sets of fracture systems each with different mean connectivity and fracture pore volume.

For the tracer recoveries higher than 0.5% in Figure 4.67, due to severe limitation of sampling, it is hard to link the histogram with any type of distribution.

In summary, distribution of tracer velocities reflects two important points: First, as higher tracer amount is recovered, a higher resolution picture is obtained about the systems of fractures transmitting the injected water in the reservoir. Second, distribution of velocities is a good tool in the construction of the geological model to estimate number of fracture populations as well as their mean pore volume and connectivity.

4.7.2 Tracers' Breakthrough Time

The global distribution of tracer breakthrough time is shown in Figure 4.68. It shows that majority of tracer responses were obtained in the first two weeks of the project (64% of tracer responses). In addition, it shows a consistent discontinuity starting from the third week of the test and continues in a cyclic manner showing almost a bi-weekly trend. This could indicate one of two things: First interpretation, the late tracer responses

appearing in cyclic manner could be a result of water recycling. In this case, these tracers do not reflect a reservoir response and should be ignored. Second interpretation, these late responses could be a result of less conductive fracture systems and the gap reflect a large difference in conductivity between these sets of fracture. In this case, the late tracers should be considered in fracture characterization. This issue could be investigated by analyzing breakthrough time for each tracer recovery group. Distributions of breakthrough times for each tracer recovery group are shown in Figures 4.69 through 4.72.

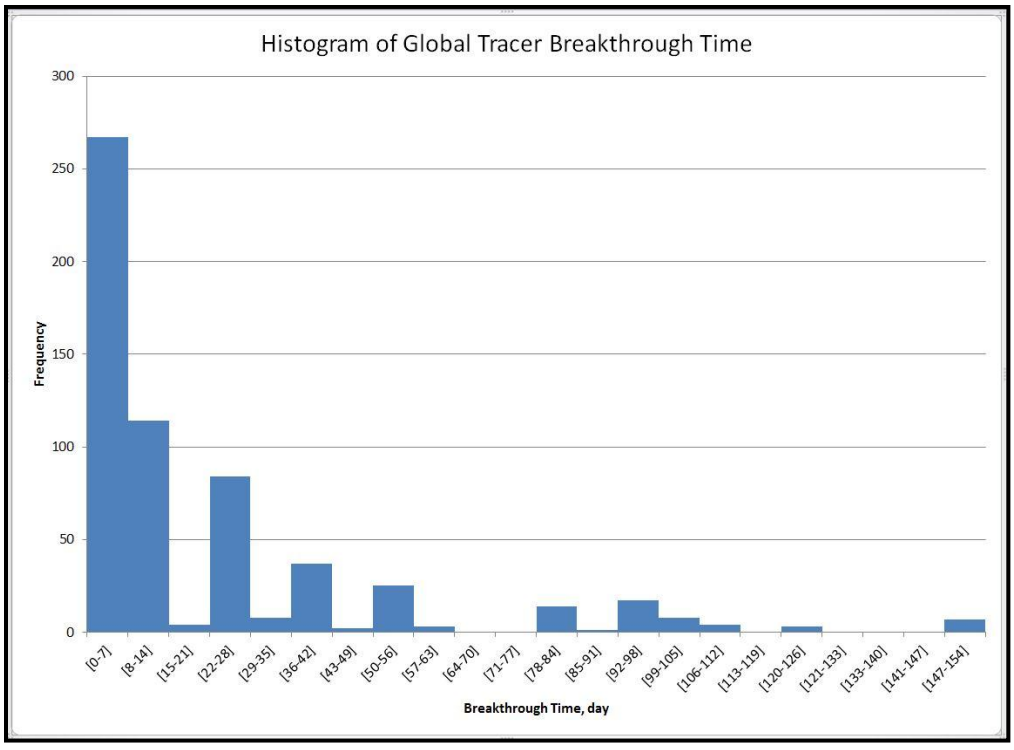

Figure 4.68: Distribution of tracers' breakthrough time

For tracer responses with less than 0.01% tracer recovery, the distribution of tracer breakthrough times shown in Figure 4.69 capture the cyclic trend observed in the global breakthrough distribution discussed earlier. Significant numbers of tracer responses were obtained in the first two weeks covering 38% of the low recovery tracer responses. The bi-weekly cyclic trend starts after the second week where peaks at fourth, sixth, and eighth week of test providing 21%, 11%, and 8% of total responses under "<0.01%" tracer recovery. The nature of these decline peaks and the systematic gaps between them strongly support that majority of tracer responses belonging to this tracer recovery group are highly affected by water recycling.

For tracer responses with 0.01-0.1% tracer recovery, the distribution of tracer breakthrough times shown in Figure 4.70 is different than the earlier group. The cyclic peaks of tracers breakthrough is significantly reduced and is diminishing. This indicates the higher the tracer recovered the less the response is affected by water recycling. Similar to the previous group, majority of breakthroughs occurs in the first two weeks of the tracer test (88.8% of responses). The remaining responses are produced in from the third to the 12^{th} week of the test.

Distributions of breakthrough time for tracer responses with 0.1-0.5% as well as 0.5%+ tracer recoveries are shown in Figures 4.71 and 4.72. Both distributions show that the cyclic behavior of tracers' breakthrough has completely diminished and all tracer responses occur in the first and second week of the test. Hence, the relation between cyclic tracer breakthroughs and water recycling is confirmed.

In summary, the global distribution of tracer breakthroughs shows majority of tracer responses appearing within the first two weeks of the tracer test (64% of responses). By the end of the second week of the test, tracers' breakthroughs exhibit a cyclic behavior peaking bi-weekly. Such cyclic behavior strongly correlates with tracer recovery, indicating that these cyclic peaks of breakthrough are associated with water recycling. As a result, for fracture characterization, only tracers obtained during the first two weeks of the test should be used as late tracer responses do not reflect a reservoir response and hence should be ignored.

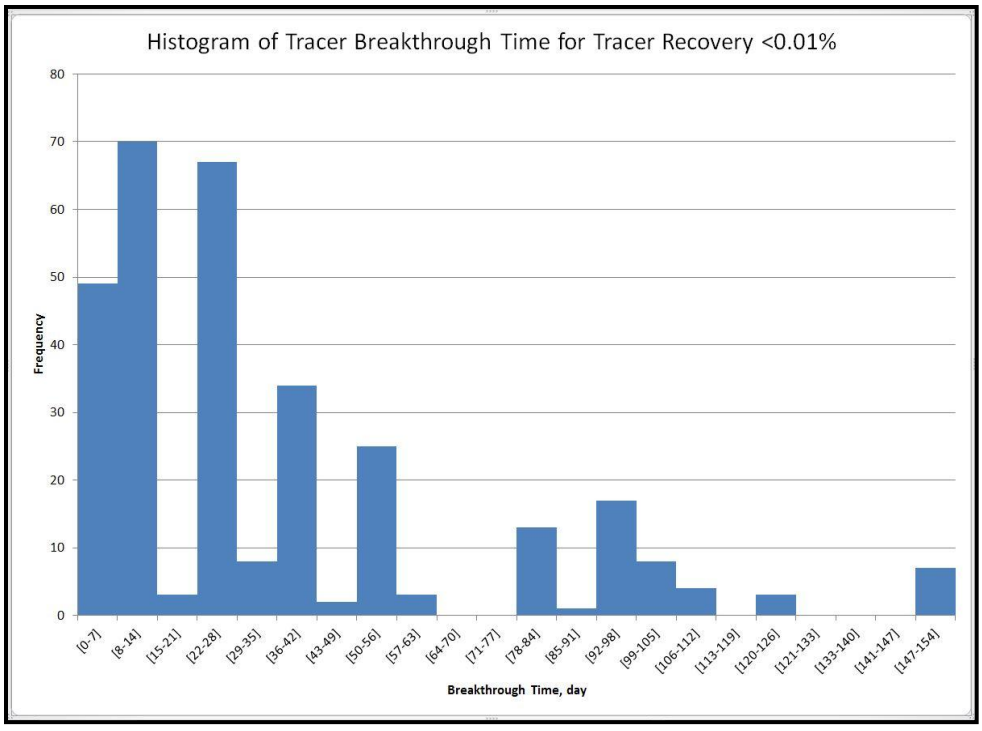

Figure 4.69: Distribution of tracers' breakthrough time (tracer recovery < 0.01%)

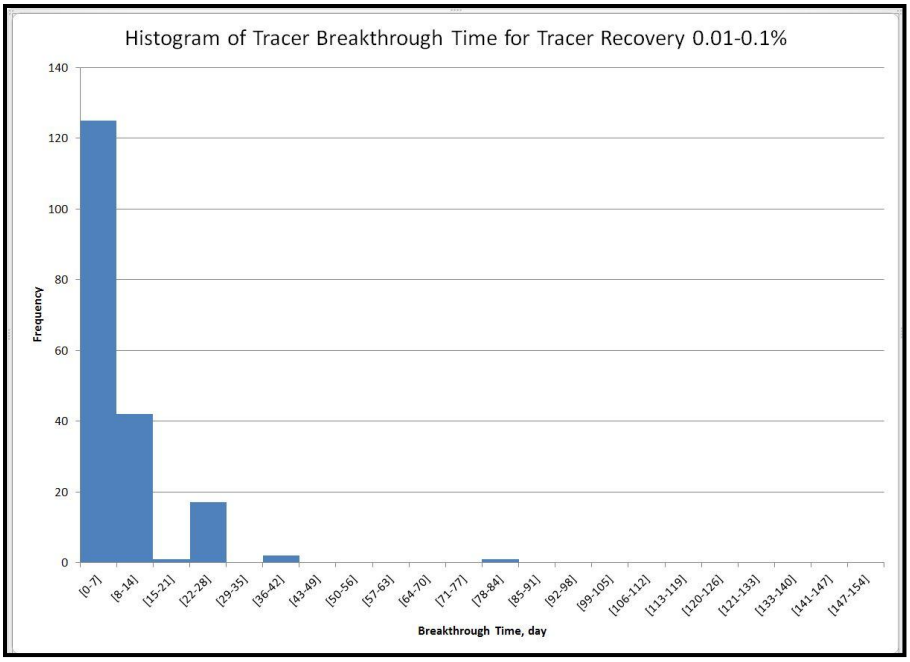

Figure 4.70: Distribution of tracers' breakthrough time (tracer breakthrough 0.01-0.1%)

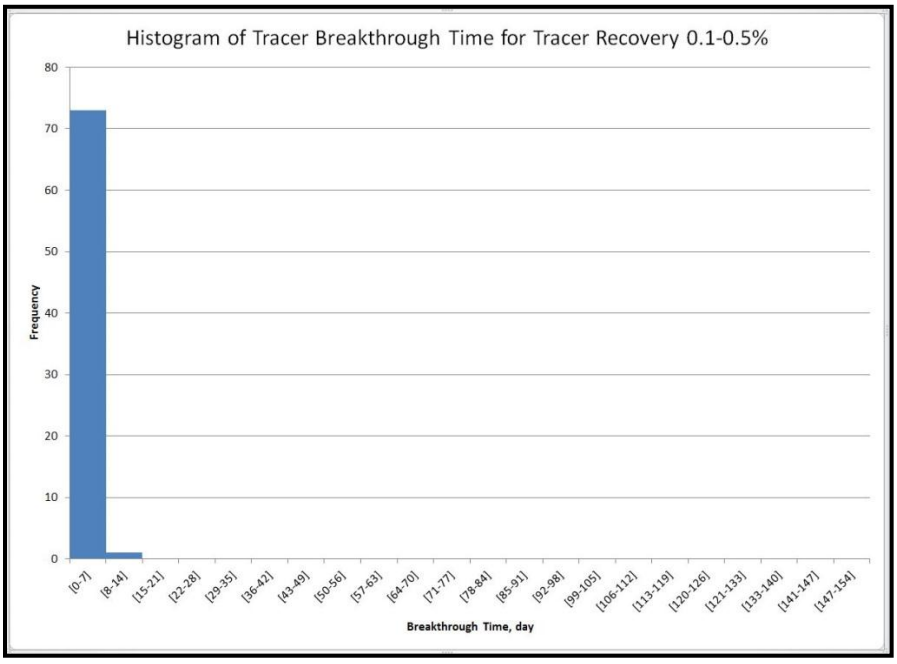

Figure 4.71: Distribution of tracers' breakthrough time (tracer recovery 0.1-0.5%)

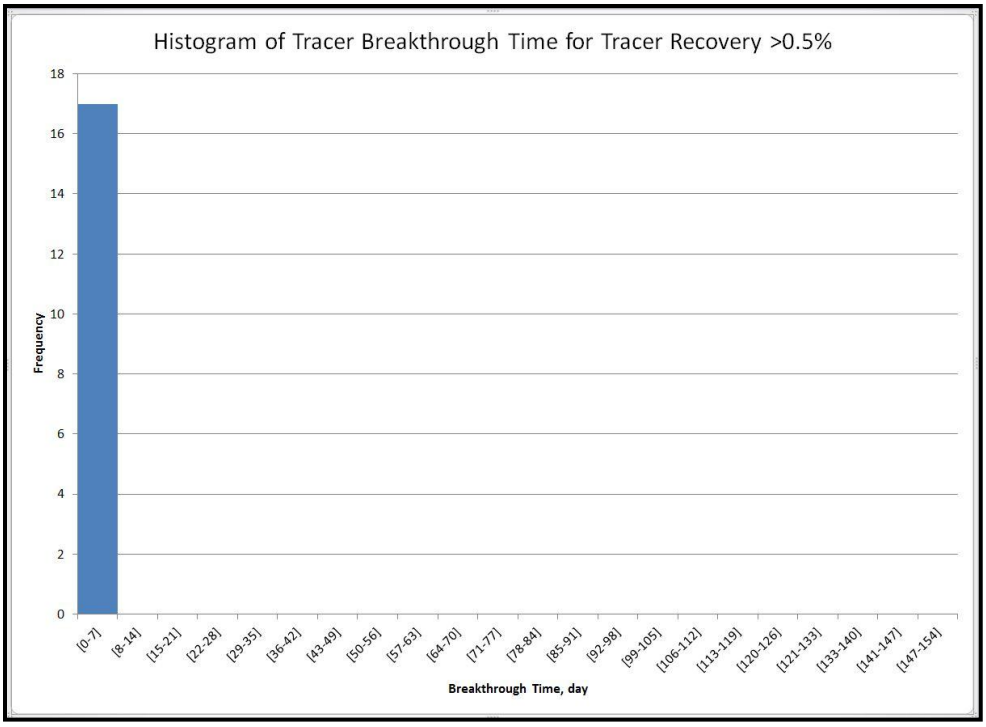

Figure 4.72: Distribution of tracers' breakthrough time (tracer recovery > 0.5%)

4.7.3 Tracer Responses with Multiple Peaks

Multiple peaks in a tracer response reflect the degree of layering in the reservoir system. To evaluate how many layers are needed to explain tagged water movement in Sherrod Area of Spraberry Field, the number of peaks for all early tracer responses occurring during the first two weeks of the tracer test is evaluated and shown in Table 4.7 below.

Global analysis of the 377 tracer responses obtained in the first two weeks of the test shows 87.3%, or 329 responses exhibiting a single peak. This indicates that the movement of tagged water from a given injector to a given producer could be explained

using a single layer model. Dual peak tracer responses are rare and observed only in 11.4% of the early responses (43 out of 377 responses). A dual peak tracer response indicate that the movement of tagged water from a given injector to a given producer could be explained using a two layer model. Triple peak responses are rarer than dual peak responses. Only 5 out of the 377 early tracer responses, or 1.3% of the early responses, showed a triple peak tracer response. In general, the number of peaks explains the number of layers needed to explain tagged water movement between an injector and a producer. Examples of single peak, dual peak, and triple peak tracer responses are shown in Figures 4.73 through 4.75.

An attempt to link number of peaks in a tracer response with its tracer recovery is shown in Table 4.8. Table 4.8 shows that tracer responses with less than 0.01% tracer recoveries do not exhibit multiple peaks. On the other hand, for tracer responses with 0.01-0.1% tracer recoveries, 9 out of 158 tracer responses exhibit dual peak but no response with triple peaks. Tracer responses with 0.1-0.5% and 0.5%+ tracer recoveries show larger number of dual peaks and triple peaks responses indicating that the higher the tracer recovery of a tracer response, the more information the response carry about the characteristics of the path followed.

In summary, majority of tracer responses show single peak tracer response (87.3% of total early responses). Thus, movement of tagged water from a given injector to a given producer could be explained most of the time using a single layer model. Dual peaks and triple peaks tracer responses present only 11.4% and 1.3% of total early responses, respectively. These less frequent responses could be explained by two and three layers

models. Number of peaks in a tracer response shows a strong correlation with tracer recovery indicating that as tracer recovery increase, the higher resolution the tracer response provide about the layering of the system

.

No of peaks	Frequency	Relative Frequency (%)
1	329	87.3%
2	43	11.4%
3	5	1.3%

Table 4.7: Frequency of number of peaks in tracers' responses

Tracer Recovery	# of peaks	Frequency	Relative Frequency (%)
< 0.01%	1	119	100%
	2	0	0
	3	0	0
0.01-0.1%	1	158	94.6%
	2	9	5.4%
	3	0	0
0.1%- 0.5%	1	47	63.6%
	2	25	33.7%
	3	2	2.7%
0.5%+	1	5	29.4%
	2	9	52.9%
	3	3	17.6%

Table 4.8: Peaking in tracers responses per tracer recovery category

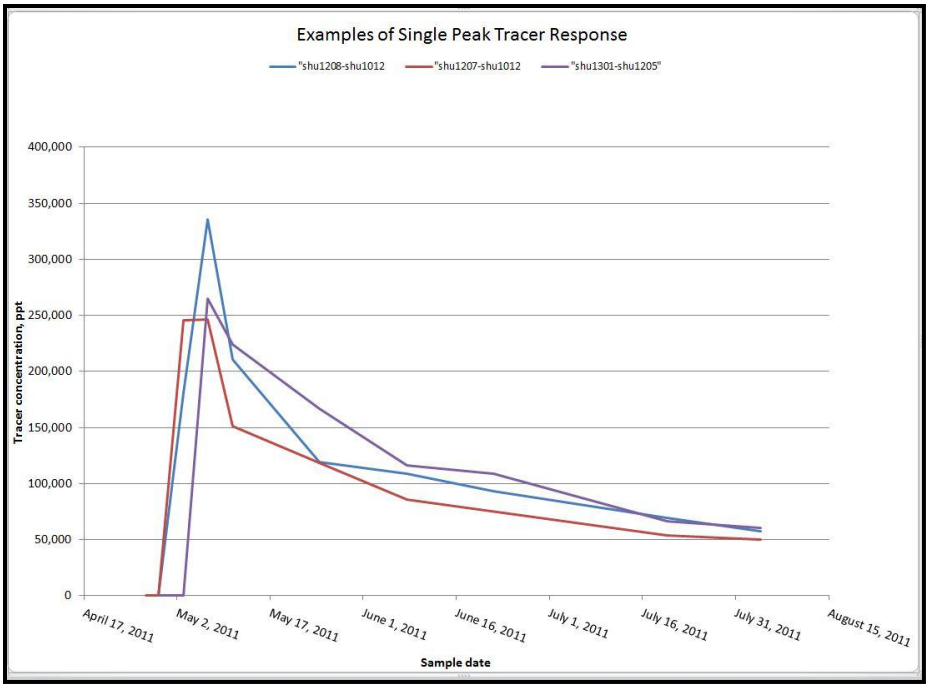

Figure 4.73: Examples of Single Peak Tracer Response

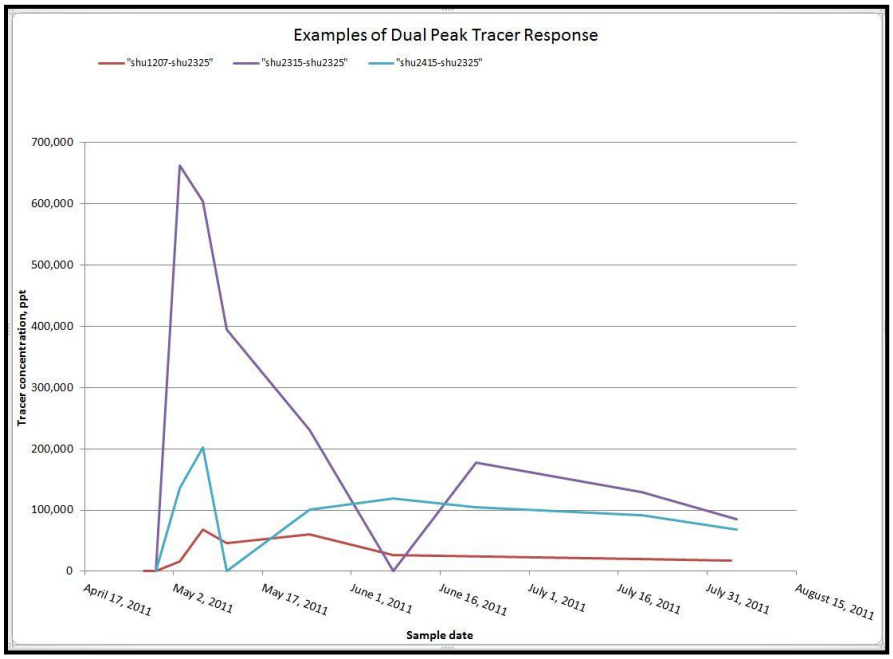

Figure 4.74: Examples of Dual Peak Tracer Response

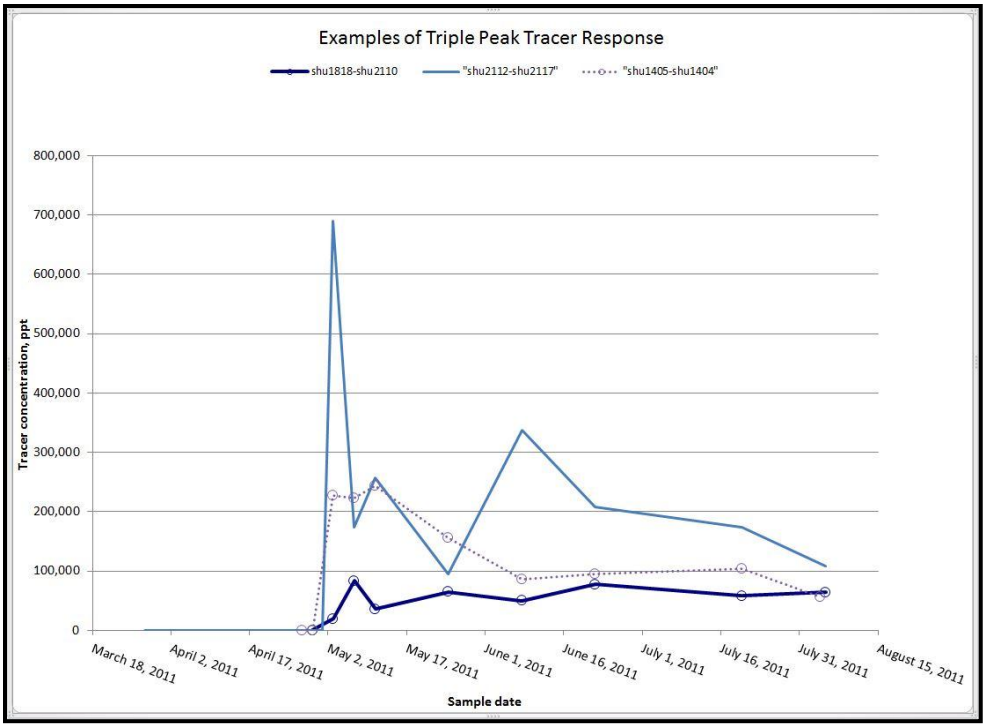

Figure 4.75: Examples of triple peak tracer response

4.8 Mapping Tracer Recoveries

In order to understand tracer movement through different fracture systems in the field, tracer shows are mapped for every injector. Each tracer show was given one out of four color codes to indicate magnitude of tracer recovery at each producer. Figures 4.76 through 4.92 show most likely fracture realizations built by linking moderate tracer shows and by linking high tracer shows for each injector. Creating an independent fracture system based on tracer recovery category is done because high tracer recoveries consistently show simple near wellbore water movement. On the other hand, moderate

tracer recoveries consistently show more complex water movement covering larger areas of the field.

Tracer injected through Sherrod 701 show poor overall tracer recovery as indicated in Figure 4.76. This could be justified by the location of the injector which is drilled outside the pattern injection area. The only high tracer show is observed at Sherrod 711 which indicates the presence of an E-W fracture connecting the two wells. Similarly for the tracer injected through Sherrod 1301 which exist in the north-east side of the pattern injection area, the only high tracer shows observed at wells adjacent to the injector in the E-W direction (Figure 4.77).

Tracers injected through the first line of pattern injectors (Sherrod 1012, Sherrod 1202, and Sherrod 1405) show two types of tracer movement: First, simple tracer movement in the vicinity of the wellbore in the E-W and NE-SW direction indicated by high tracer recoveries. Second, tracer movement in a complex fracture system where nearby producers as well as far producers show stronger communication with pattern injector. This type of tracer movement is indicated by moderate tracer recoveries and it reflects multiple fracture orientations. It is important to mention that one producer outside the pattern injection area show strong connection with these three injectors which supports that injected water is flowing outside Sherrod Area (Figures 4.78-4.83).

Second line of injectors which includes Sherrod 2114, Sherrod 1904, and Sherrod 1814 exhibit both similarities and differences in tracers' movement compared to the first line of injectors. For example, tracer injected through Sherrod 2114 show the two types of tracer movement indicated. On the other hand, Sherrod 1904 show only simple tracer

movement in the E-W direction. Sherrod 1914 shows only moderate tracer recoveries all enclosed in a small area around the injector (Figures 4.84-4.87).

Third line of injectors which includes Sherrod 2118, Sherrod 2112, and Sherrod 1818 shows very similar tracer movement to the second line of injectors. For example, tracer injected through Sherrod 2118 which exist in the east side of the tracer study area show very similar tracer behavior compared to Sherrod 2114 in the second line of injectors. Sherrod 2112 show similar tracer movement behavior compared to Sherrod 1914 in the second line of injectors. Sherrod 1818 show similar tracer movement behavior compared to Sherrod 1814 in the second line of injectors (Figures 4.88-4.90).

The last line of injectors in the south of the tracer study area includes two injectors: Sherrod 2409 and Sherrod 2325. Both of these injectors show strong communication with wells outside pattern injection area. In addition, tracers movement in both of the two injectors indicate the presence of a wide range of fracture orientation extending for long distances from injectors (Figures 4.91-4.92).

In summary, mapping tracer recoveries highlight two types of tracers' movement in the reservoir: simple tracer movement and complex tracer movement. The simple tracer movement is indicated by high tracer recoveries and is limited to the vicinity of the injector's wellbore in the E-W and NE-SW directions. The complex tracer movement is indicated by moderate tracer recoveries and it highlights that injected water flow outside the pattern injection area. In addition, it highlights the complex inter-connectivity between majority of pattern injectors with near and far producers in the pattern injection area. Fracture realizations from high and moderate tracer shows for all injectors are

integrated in Figures 4.93 through 4.94 to visualize the global fracture network in the field.

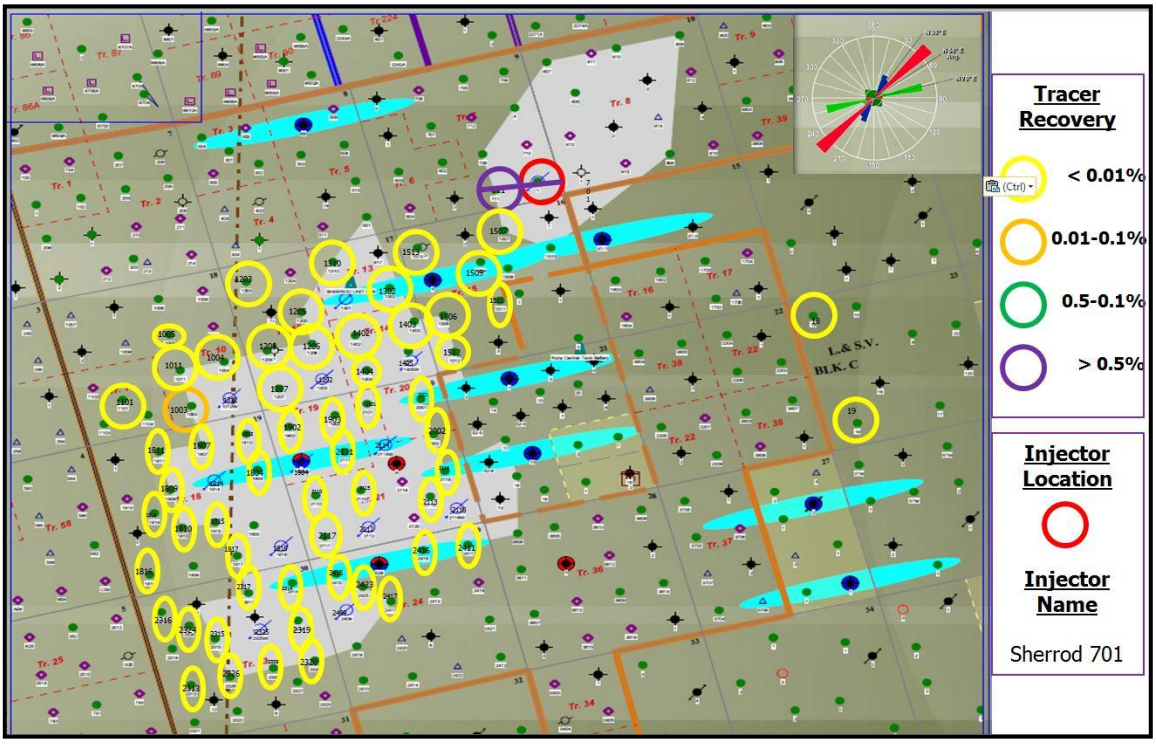

Figure 4.76: Fracture realization from ‘Sherrod 701’ high tracer shows

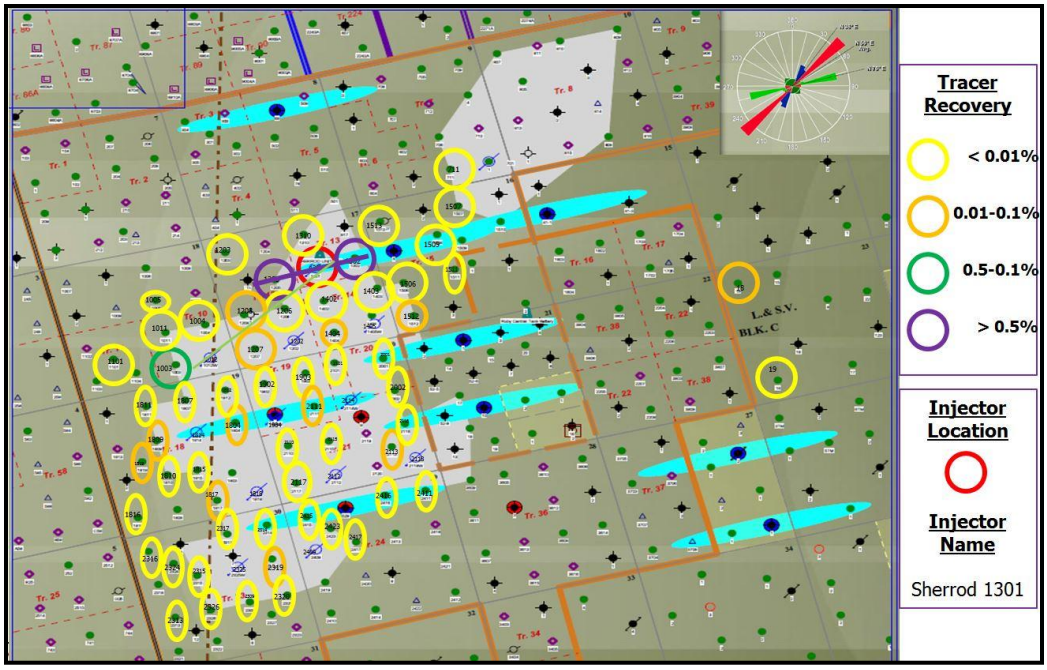

Figure 4.77: Fracture realization from 'Sherrod 1301' high & moderate tracer shows

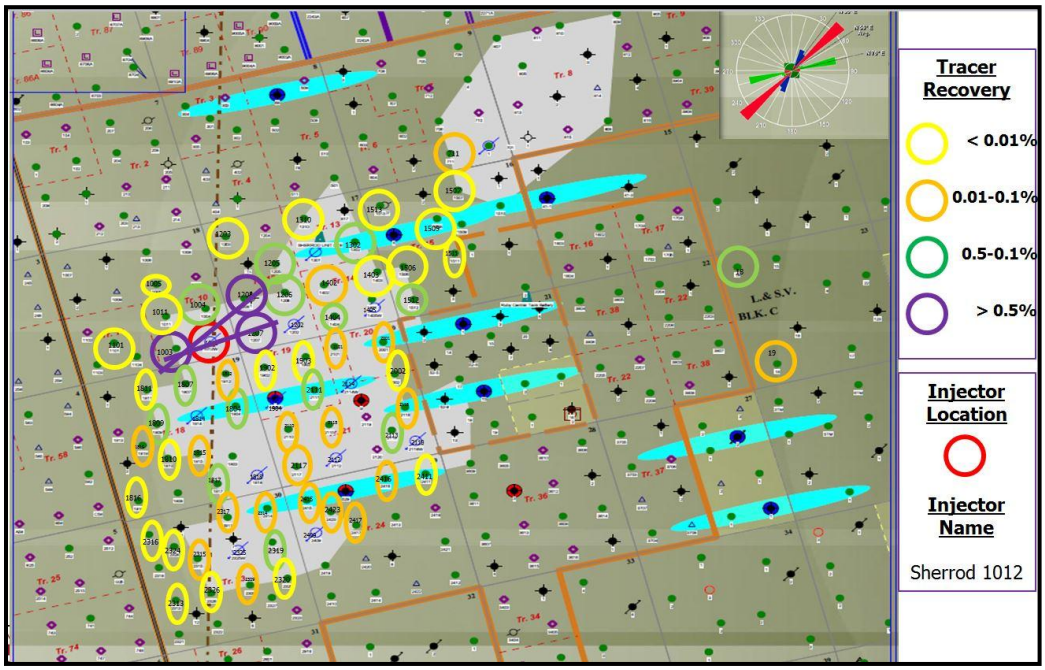

Figure 4.78: Fracture realization from 'Sherrod 1012' high tracer shows

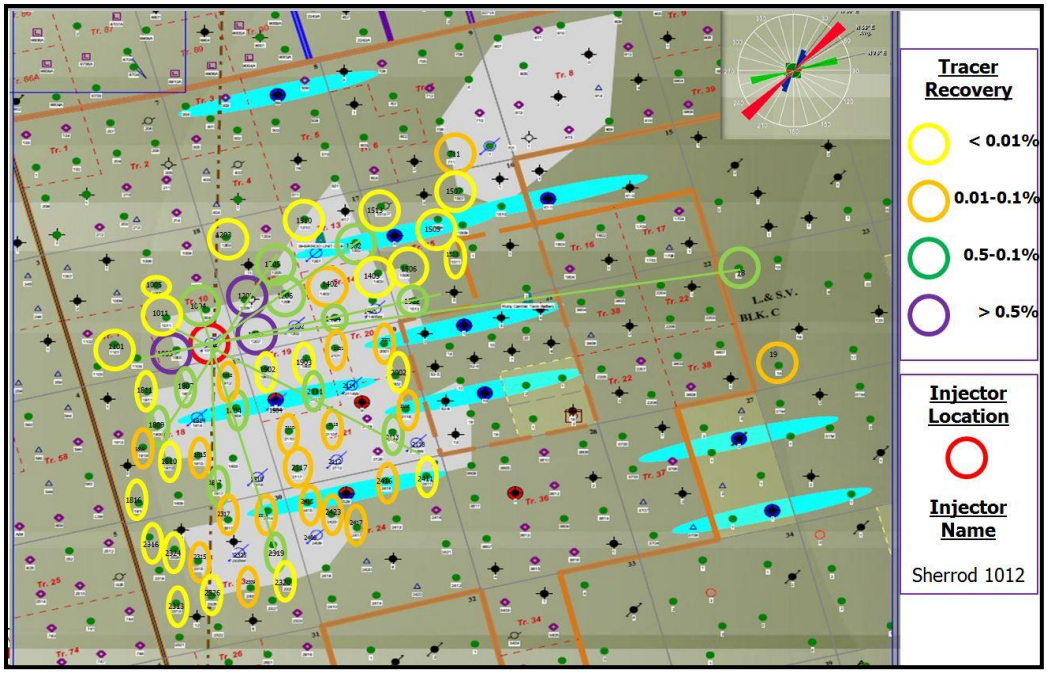

Figure 4.79: Fracture realization from 'Sherrod 1012' moderate tracer shows

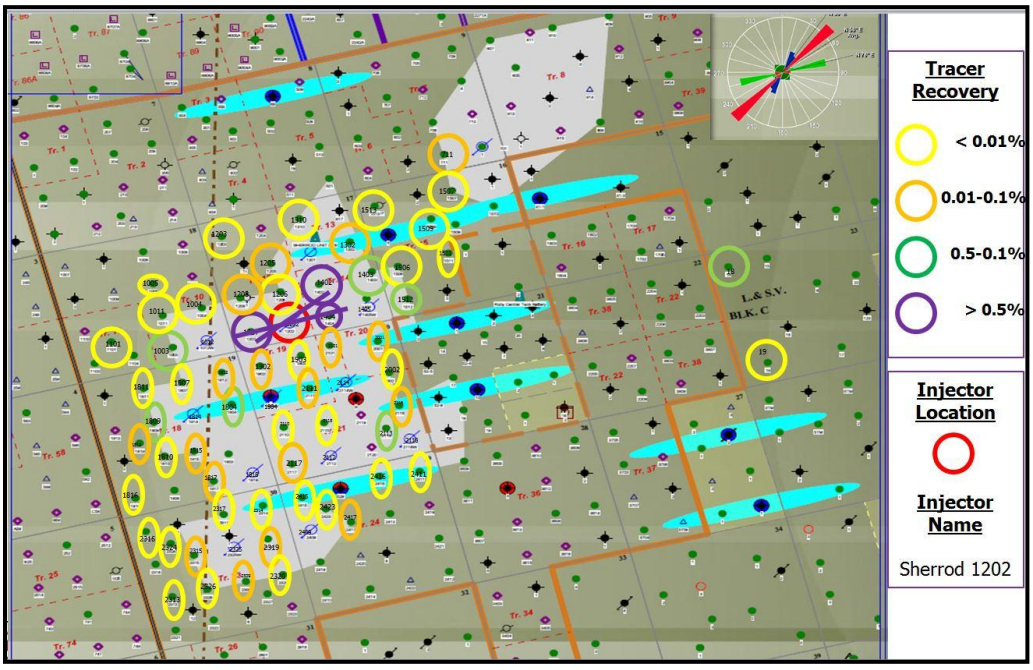

Figure 4.80: Fracture realization from 'Sherrod 1202' high tracer shows

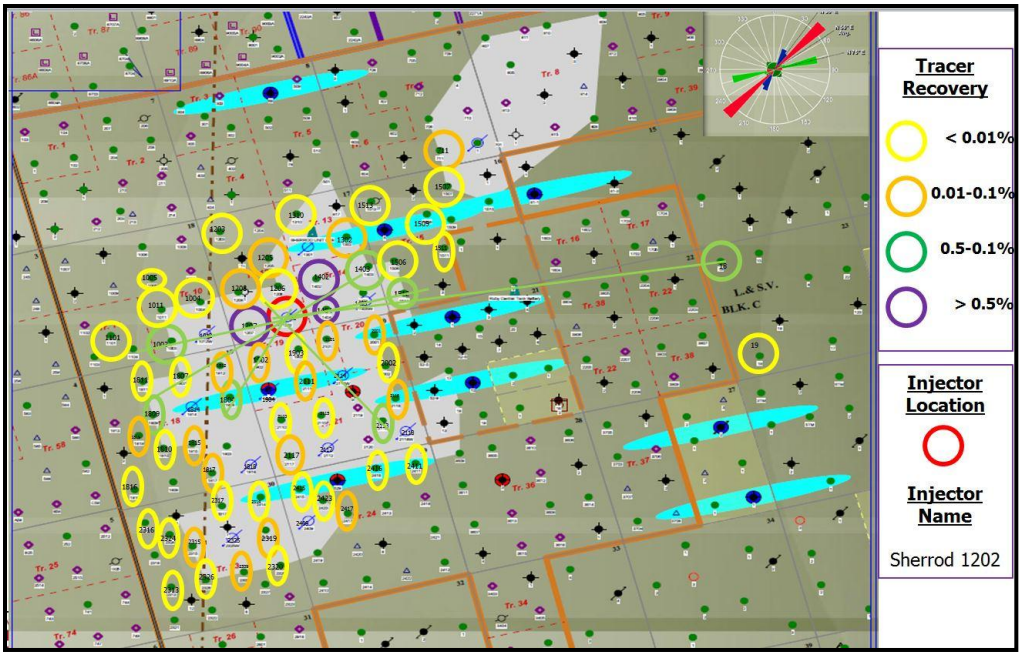

Figure 4.81: Fracture realization from ‘Sherrod 1202’ moderate tracer shows

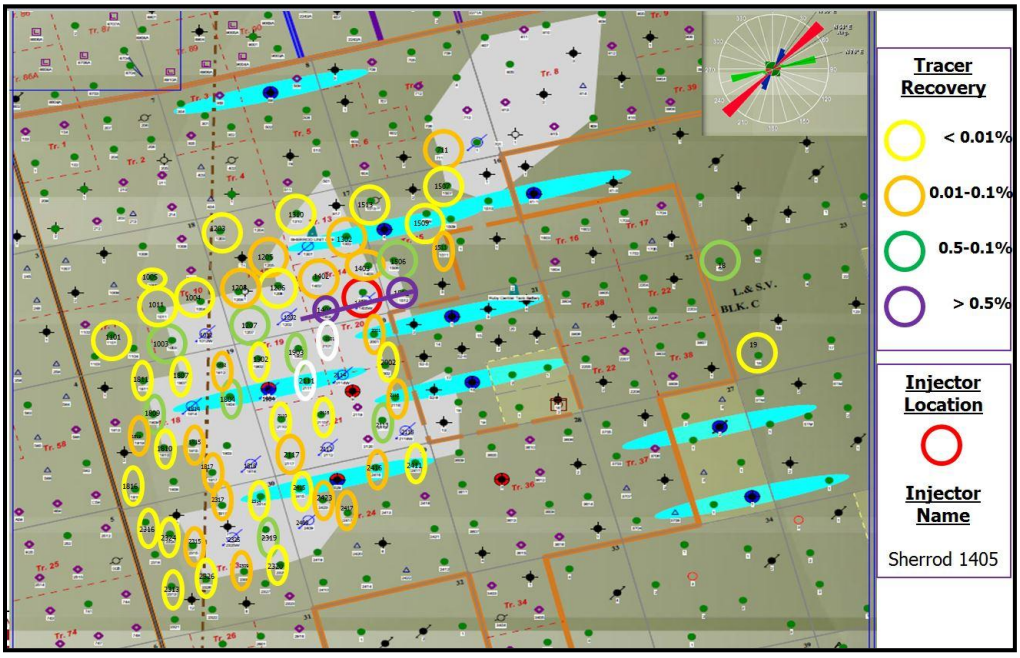

Figure 4.82: Fracture realization from ‘Sherrod 1405’ high tracer shows

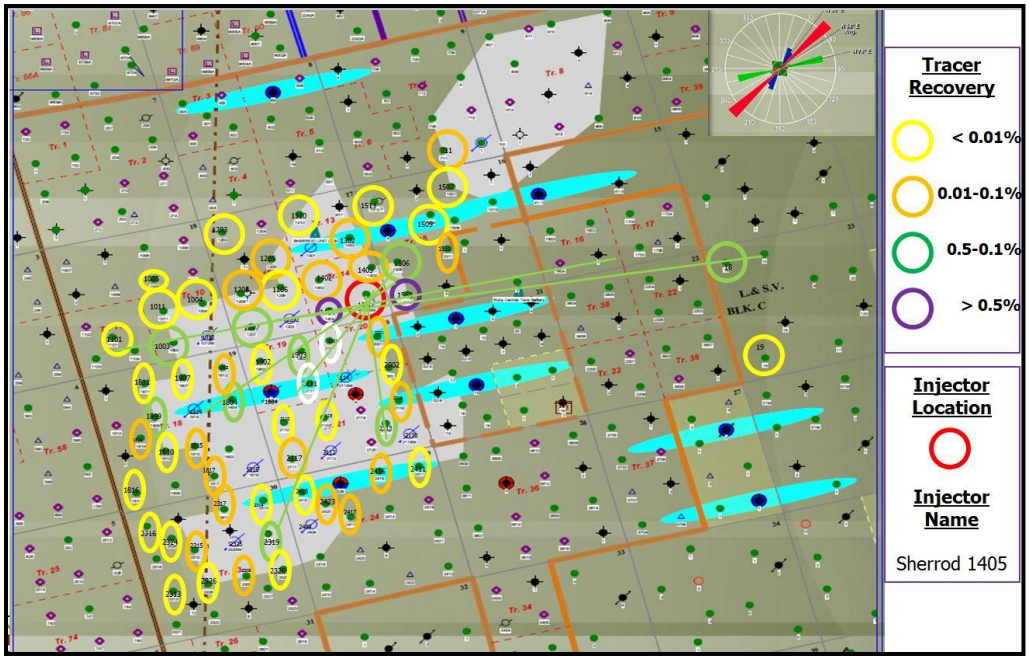

Figure 4.83: Fracture realization from ‘Sherrod 1405’ moderate tracer shows

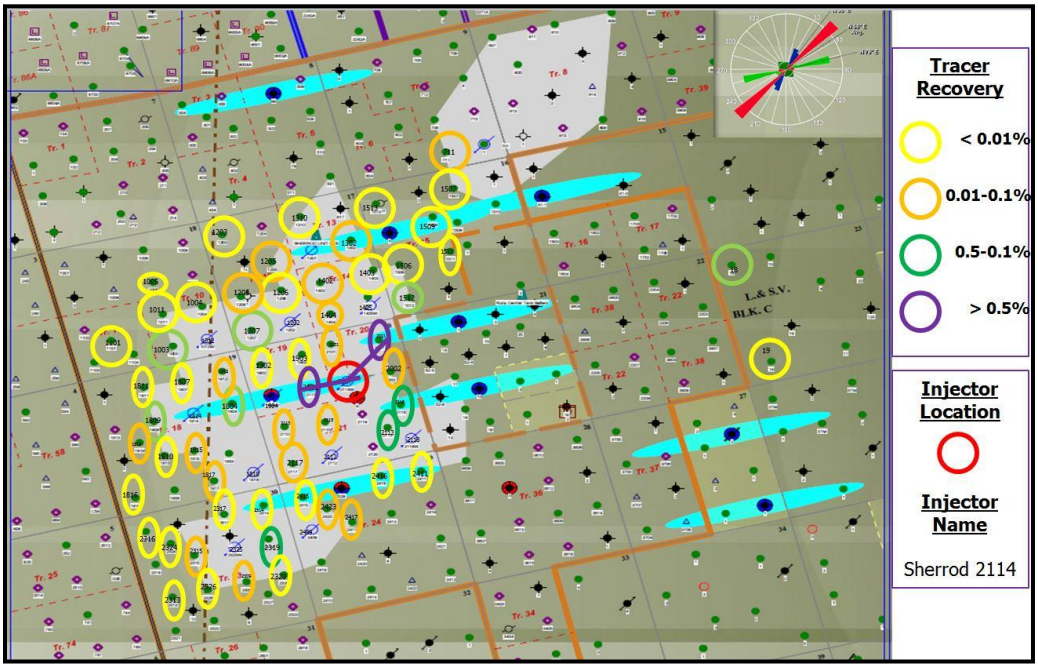

Figure 4.84: Fracture realization from ‘Sherrod 2114’ high tracer shows

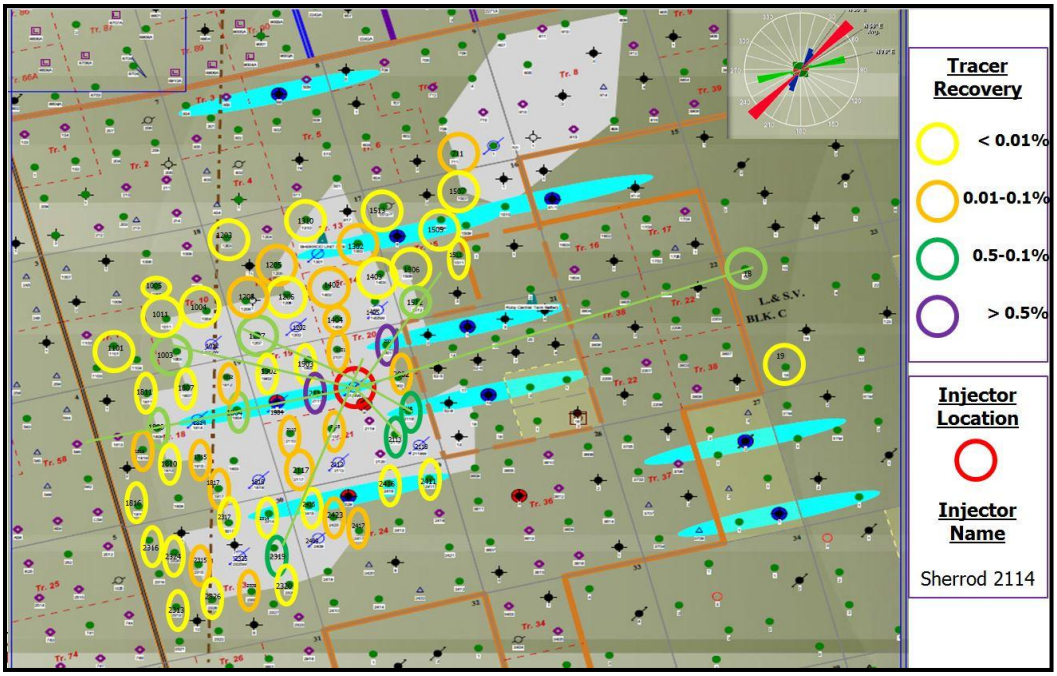

Figure 4.85: Fracture realization from ‘Sherrod 2114’ moderate tracer shows

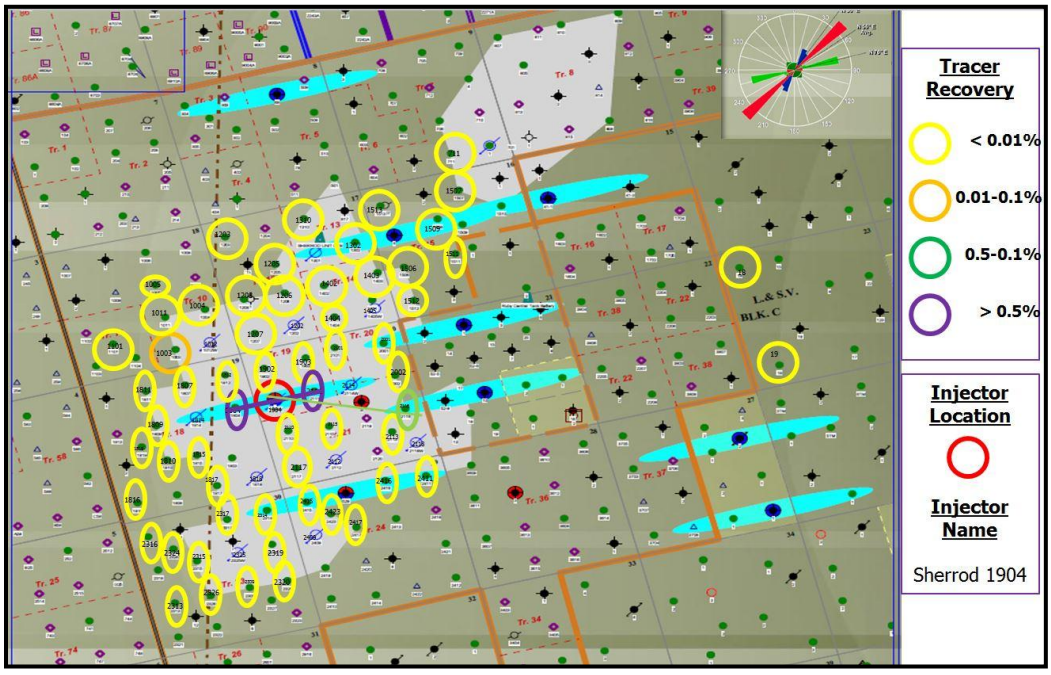

Figure 4.86: Fracture realization from ‘Sherrod 1904’ high tracer shows

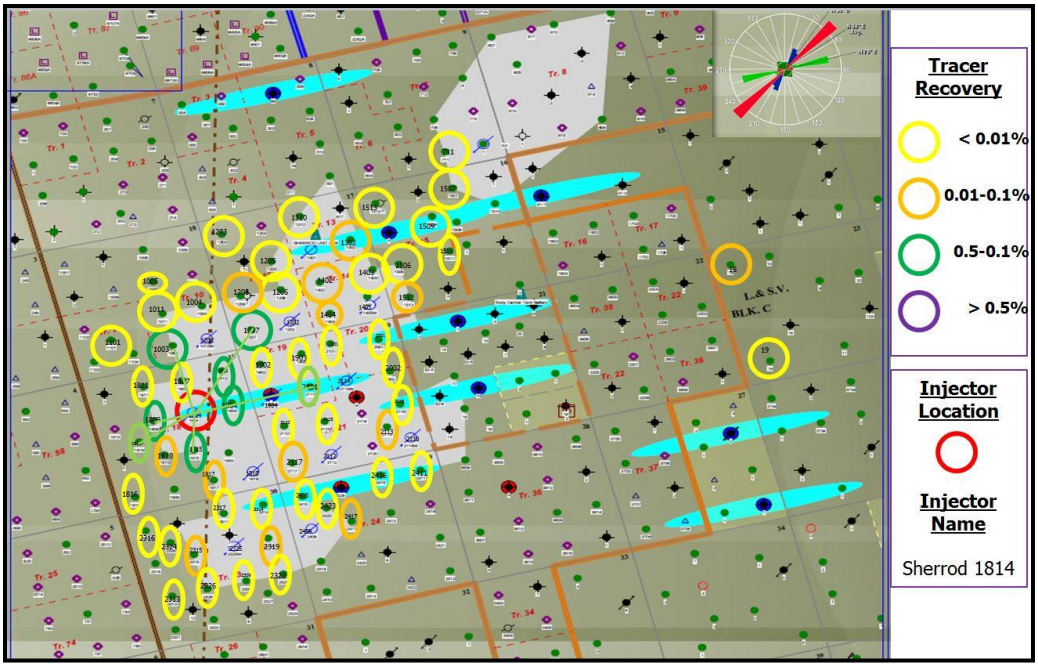

Figure 4.87: Fracture realization from 'Sherrod 1814' moderate tracer shows

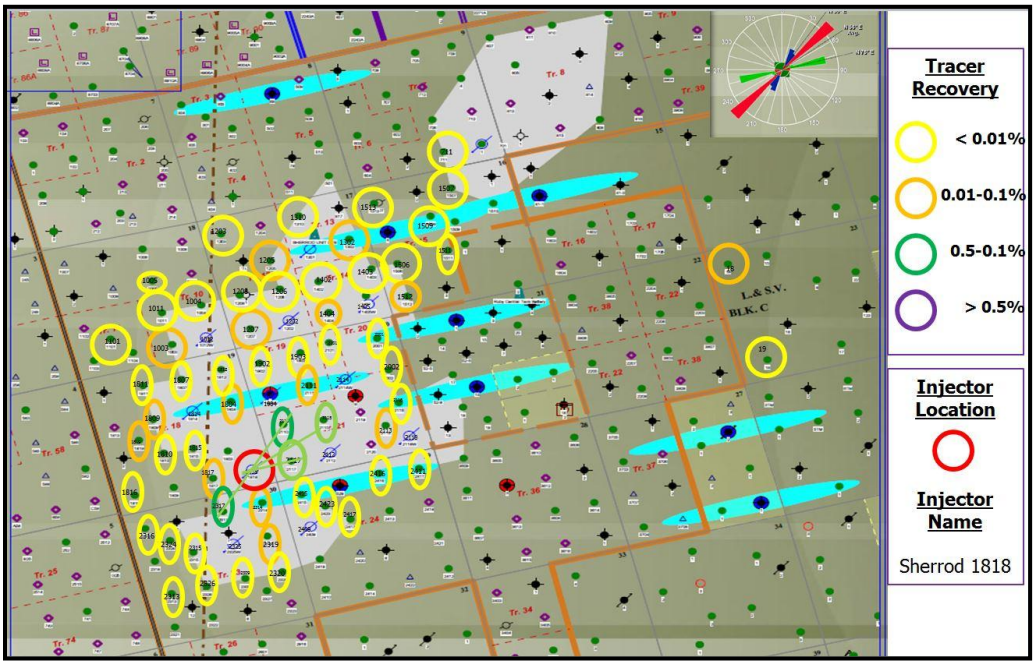

Figure 4.88: Fracture realization from 'Sherrod 1818' moderate tracer shows

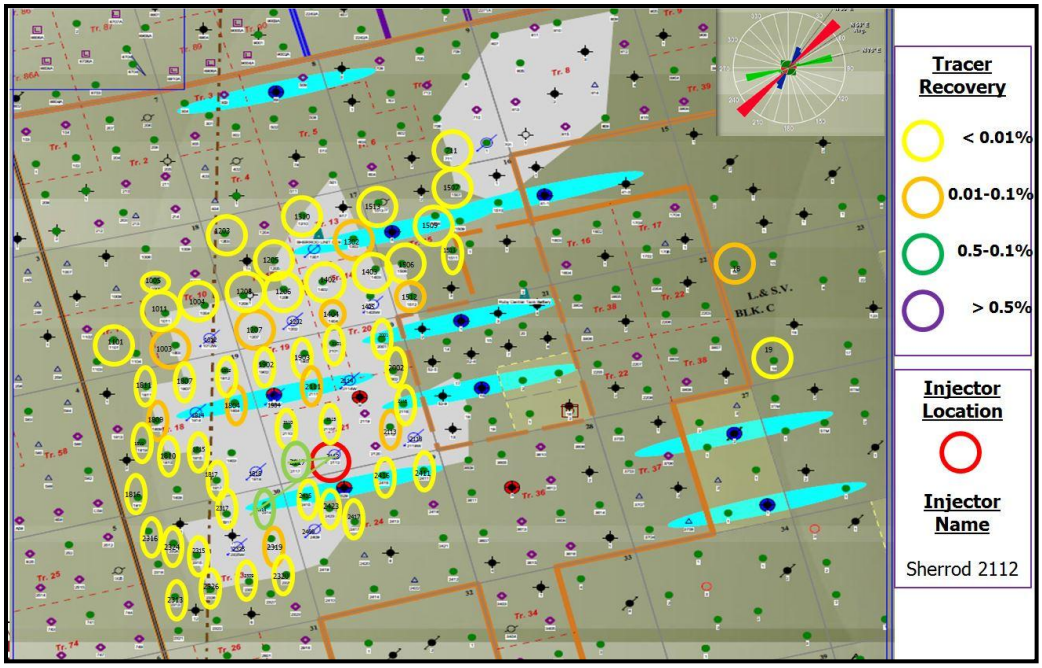

Figure 4.89: Fracture realization from ‘Sherrod 2112’ moderate tracer shows

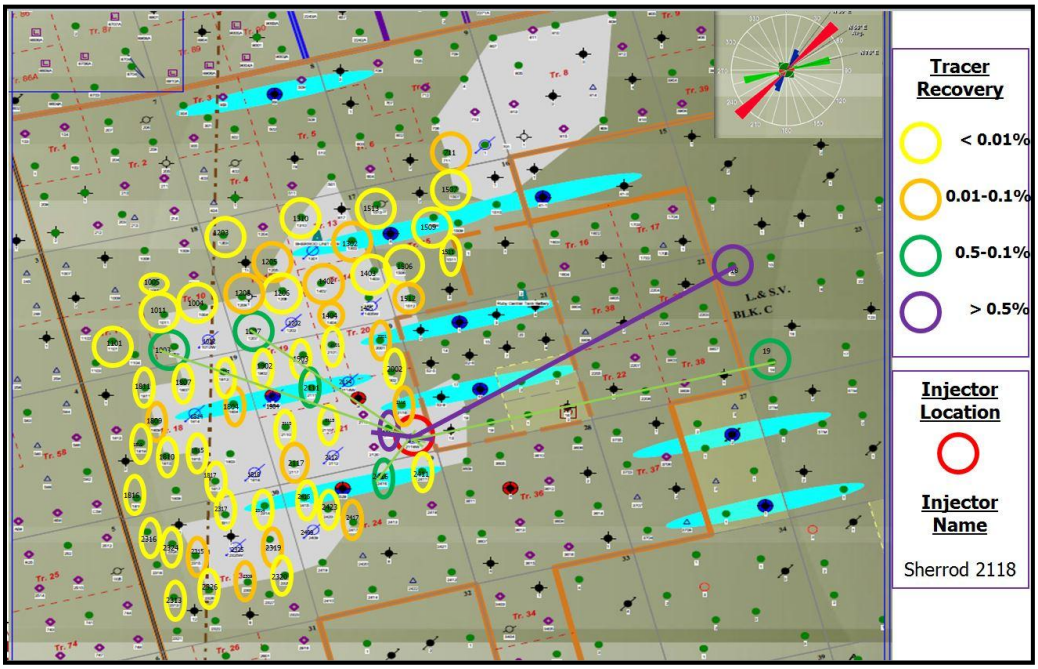

Figure 4.90: Fracture realization from ‘Sherrod 2118’ high & moderate tracer shows

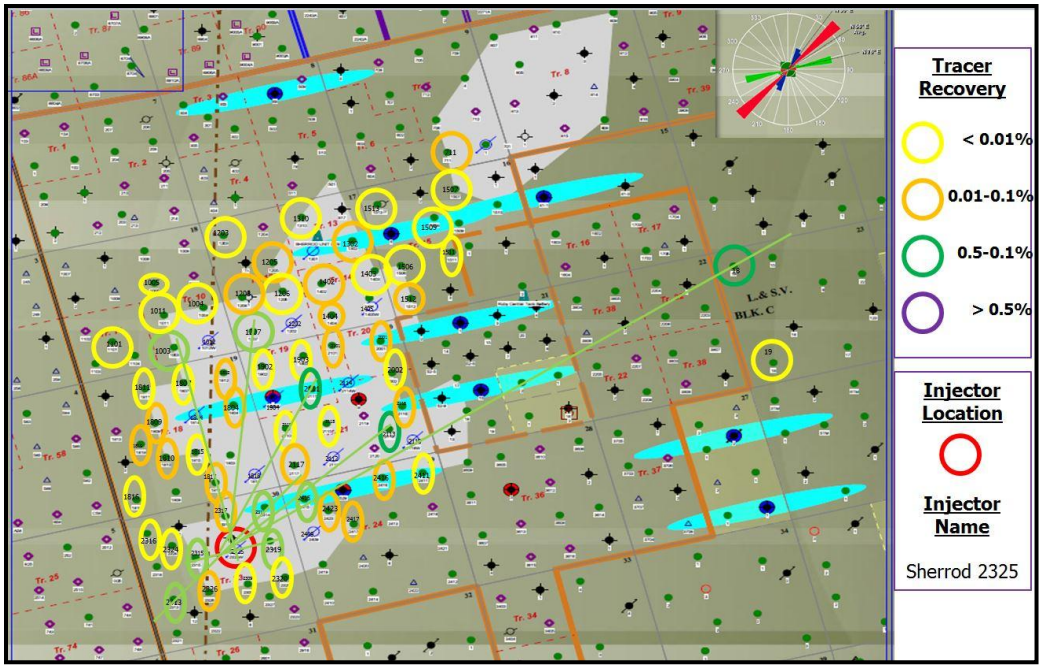

Figure 4.91: Fracture realization from 'Sherrod 2325' moderate tracer shows

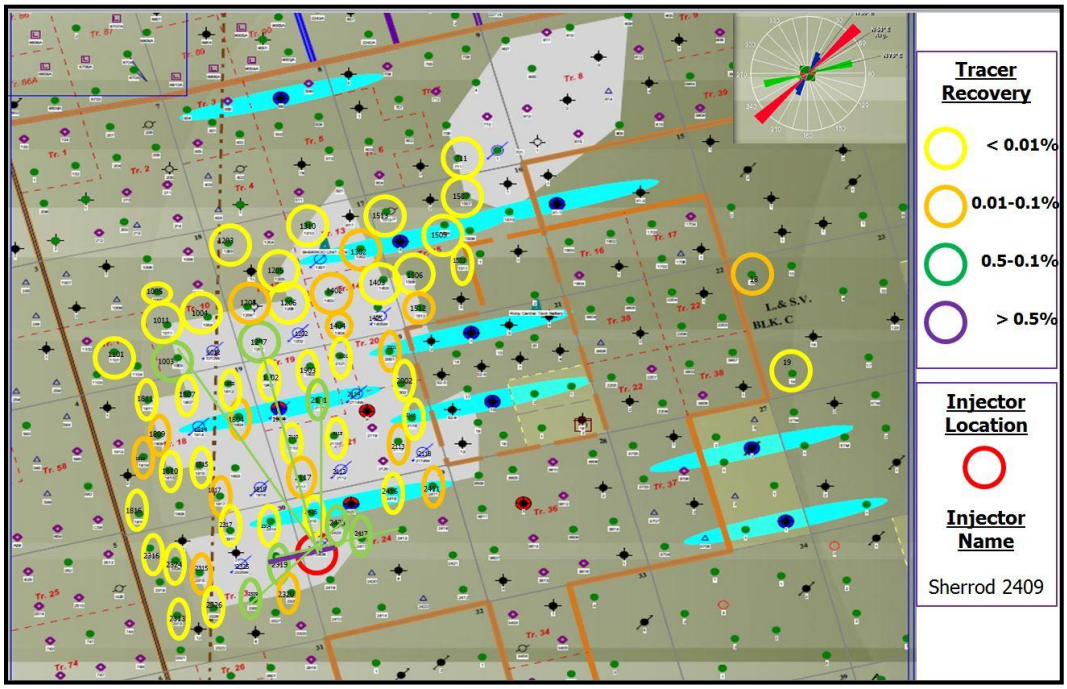

Figure 4.92: Fracture realization from 'Sherrod 2409' high & moderate tracer shows

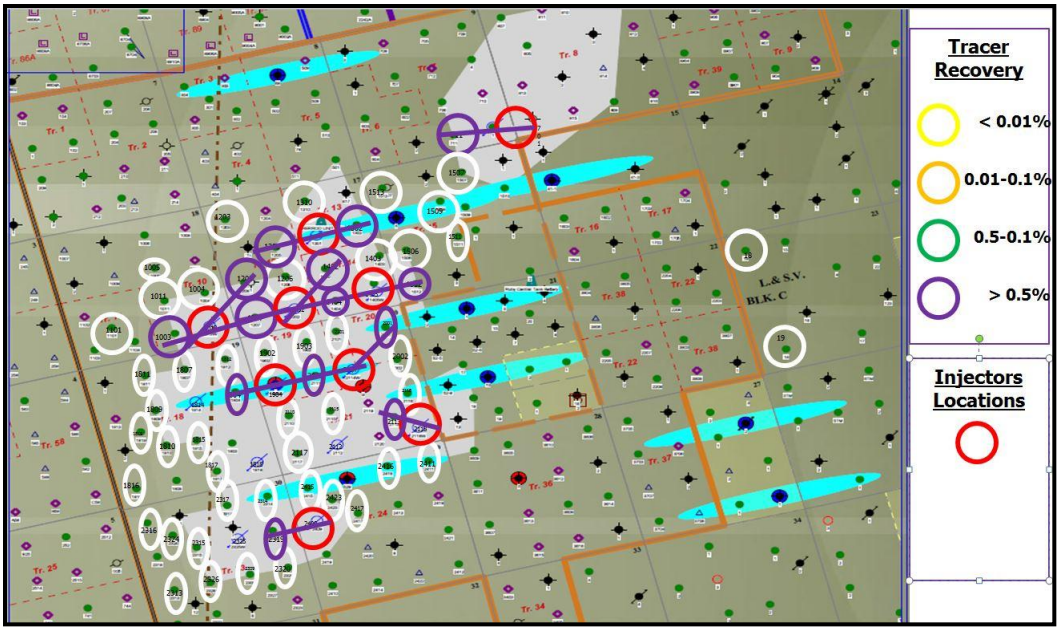

Figure 4.93: Global fracture network by integrating high tracer shows

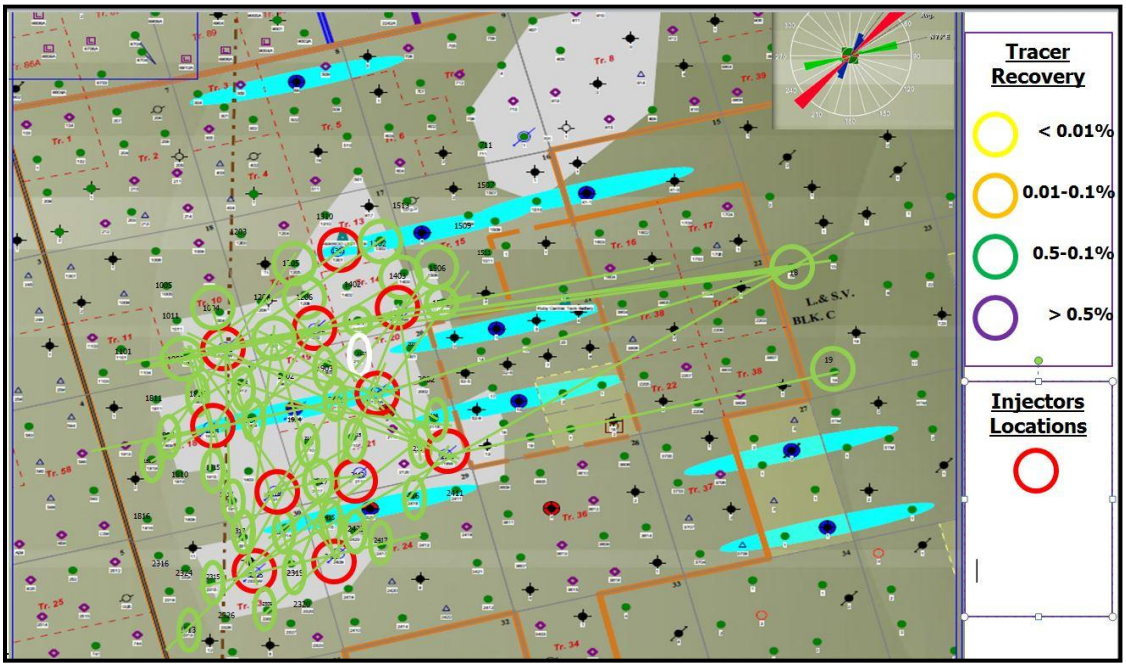

Figure 4.94: Global fracture network by integrating moderate tracer shows

4.9 Field Production Performance

Sherrod Area of Spraberry Field shown in Figure 4.95 was first put on production in July 1951. Field performance plots in Figures 4.96 and 4.97 show that field oil production was dry for about 22 years until six wells exhibited simultaneous water breakthrough in January 1973. Early water production data shows complex water-cut behavior indicating the presence of a complex fracture network. Examples of such water-cut behavior are shown in Figures 4.98 and 4.99. After around 32 years of primary depletion, water injection in the field started in January 1983 with only one power water injector. One additional injector was introduced in 1990 and three more were introduced in late 2001 / early 2002. After adding the last three injectors, 44 wells exhibited simultaneous water breakthrough in 2002 with majority of wells showing high water-cuts in the range 70-85% water-cut. This unique phenomena of simultaneous water breakthrough of a large number of wells covering large area of the field indicates the complex inter-connectivity between injectors and producers despite the vast distances between them. Field water injection and water production performance are shown in Figures 4.100 and 4.101. The figures show that field water production is closely following field water injection which indicates a poor overall waterflood performance. A list of early injectors and a map of their locations is shown in Figure 4.102.

In 2010, a decision was made to develop a large area of Sherrod using 11 inverted 9-spot patterns. This was done by converting 5 producers and drilling 6 new injectors. A list of the new injectors and a map of their locations is shown in Figure 4.103 below. Producers drilled in early 2010 showed high initial water-cuts in the range of 80-90%

indicating pre-production water invasion in the area. The recently added injectors show either insignificant or adverse impact on oil rates and water-cuts of the recent 2010 wells. Figure 4.104 show an example where oil rates and water-cuts of a well, Sherrod 1011, appear to be unaffected by the active pattern injector next to it. Figure 4.105 show an example of a well, Sherrod 2111, where the pattern injector have caused the well to die by increasing water-cut to above 99%. The normalized injection rate appearing in the figure is obtained by dividing pattern injection rate by maximum value. Poor performance of recent 2010 injectors was the main reason for the design and execution of Sherrod inter-well tracer test. Main objectives of the inter-well tracer test are to understand the reasons of poor performance of 2010 injectors. In addition, the test is used to check for communication between injectors outside the pattern area with producers inside the pattern area.

In summary, analysis of field production performance highlights several aspects of this field. First, field water production is closely following the field water injection indicating a poor waterflooding performance. Second, the three injectors added in late 2001 and early 2002 caused large number of wells to simultaneously breakthrough. These wells cover almost entire Sherrod Area and no dry production observed in Sherrod from that point forward. Third, recent inverted 9-spot patterns introduced in 2010 show high initial water-cuts and poor injection performance raising questions about source of water produced and injected water movement. Forth, precaution should be taken while dealing with early field production data. One reason is because production data prior to January 1970 shows exactly the same monthly average allocated rates. This highlight the

inaccurate rate allocation practices during this period. Second reason is because old maps of Sherrod Area indicate the presence of 9 abandoned injectors with no information about their history. These wells are shown in Figure 4.106 and believed to be the main cause of simultaneous water breakthrough of 6 wells in 1973.

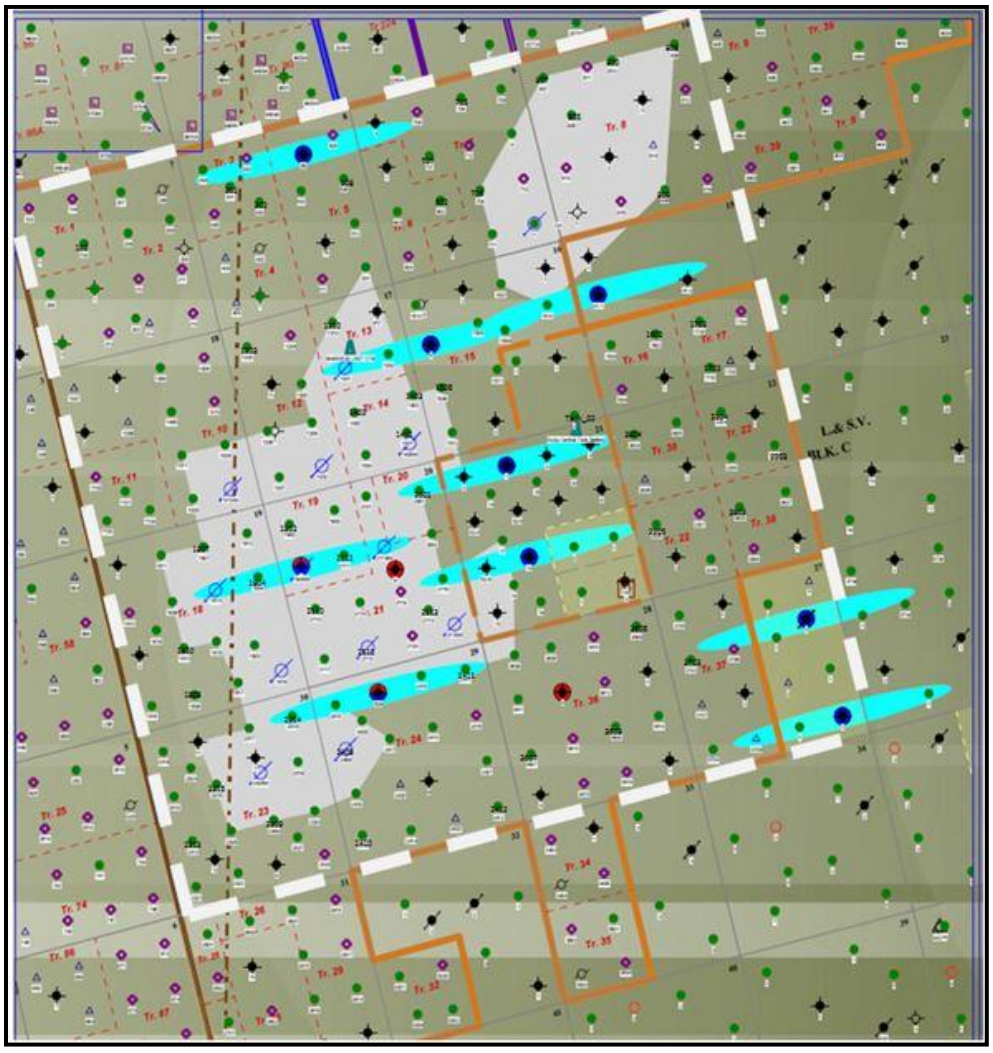

Figure 4.95: Boundary of the full field model used in this study

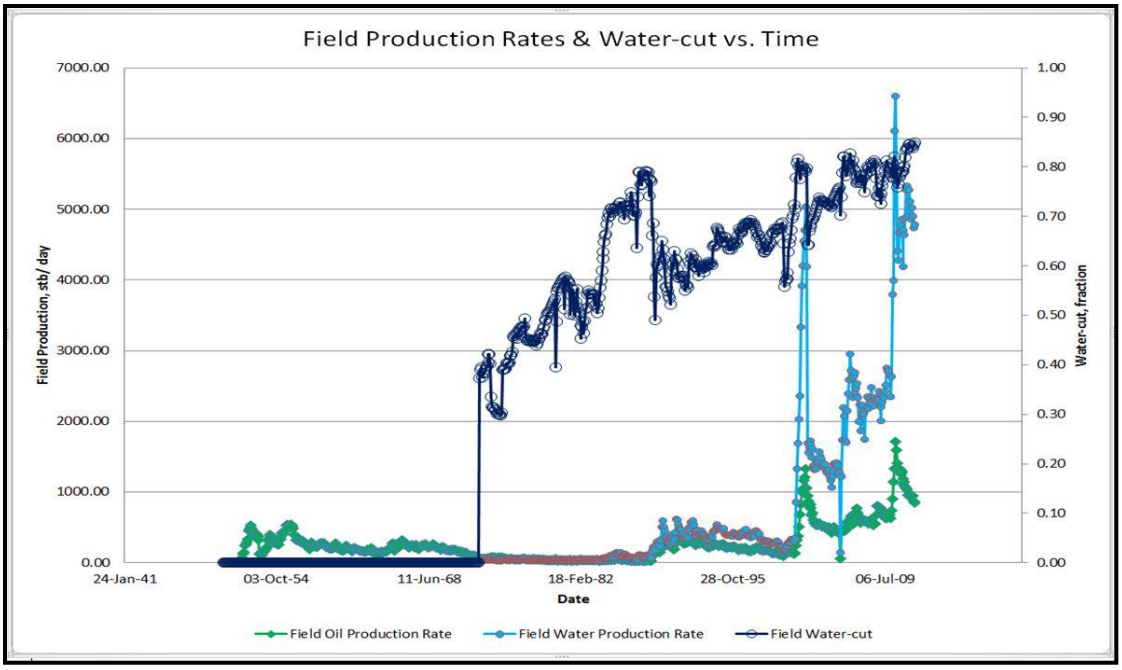

Figure 4.96: Field oil and water production rates and field water-cut with time.

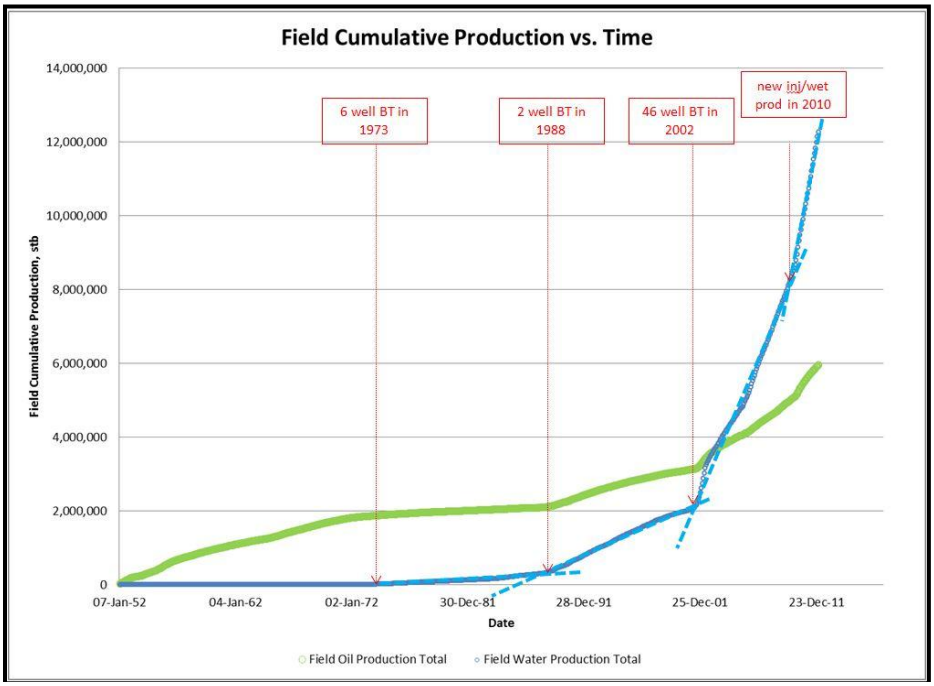

Figure 4.97: Field oil and water cumulative production

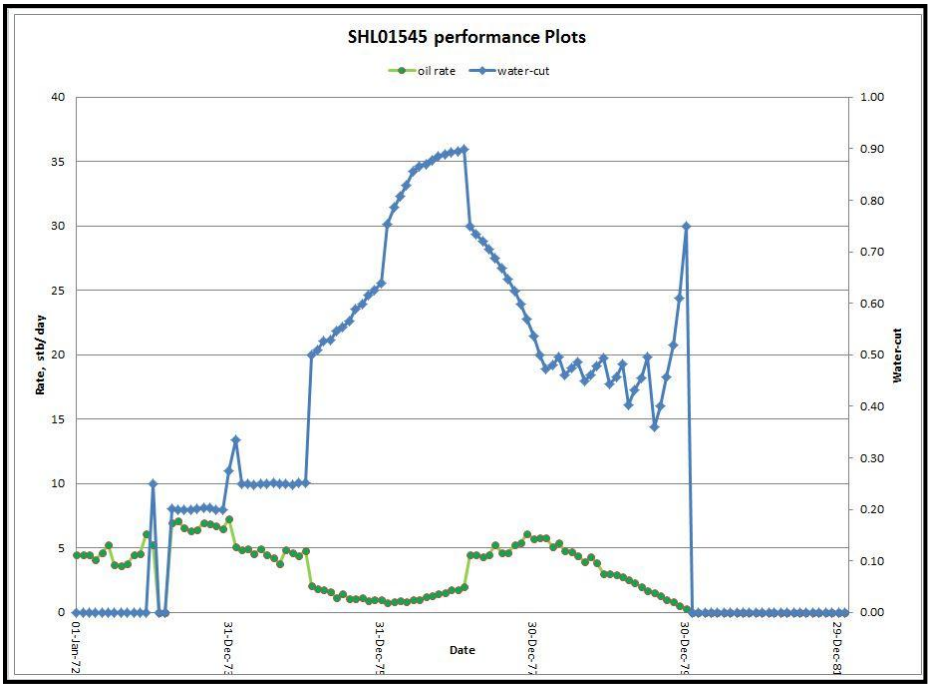

Figure 4.98: Example (1) of early complex water-cut behavior

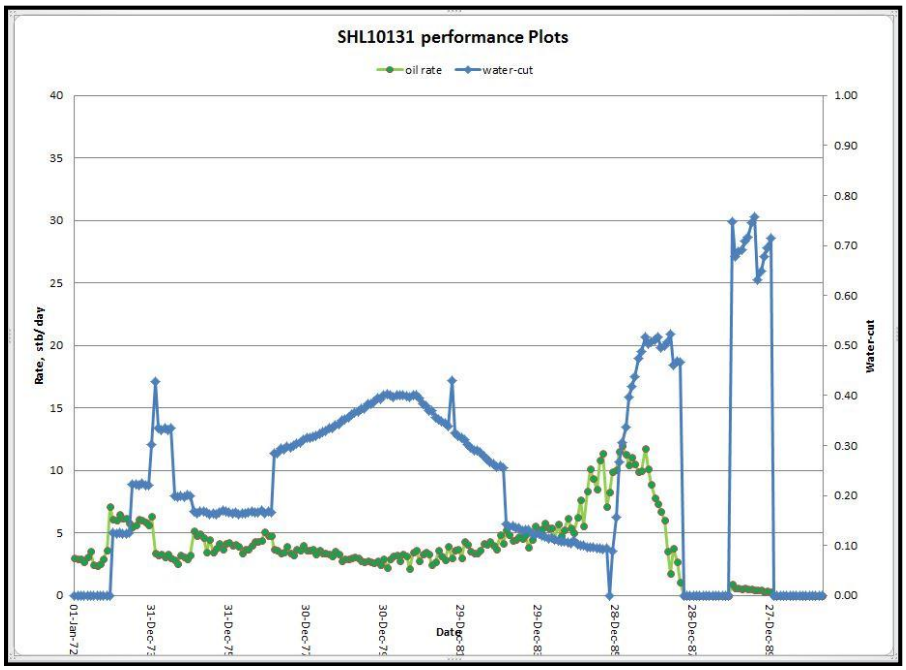

Figure 4.99: Example (2) of early complex water-cut behavior

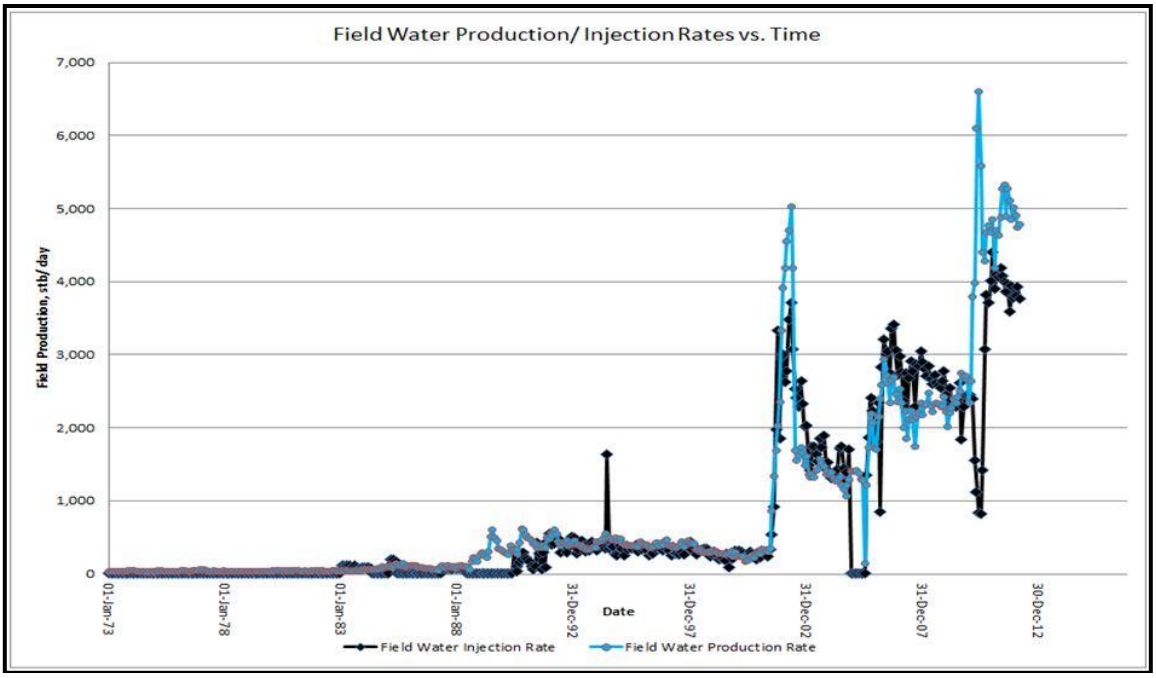

Figure 4.100: Field water production and injection rates

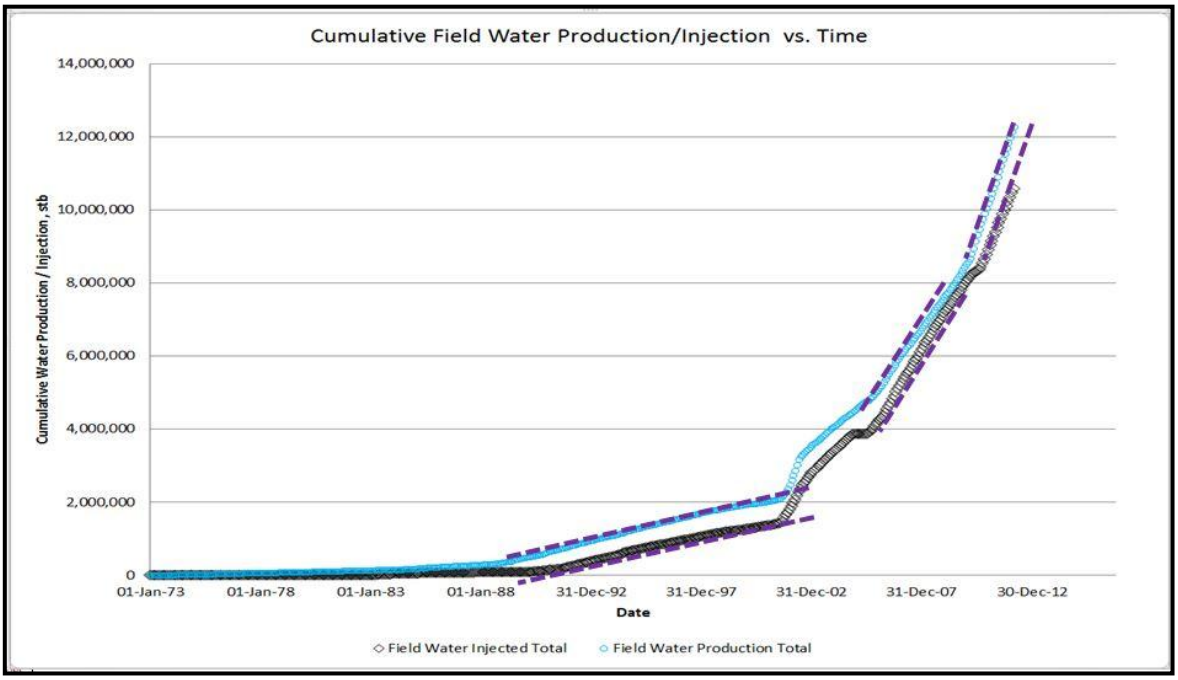

Figure 4.101: Field cumulative water production and injection Rate

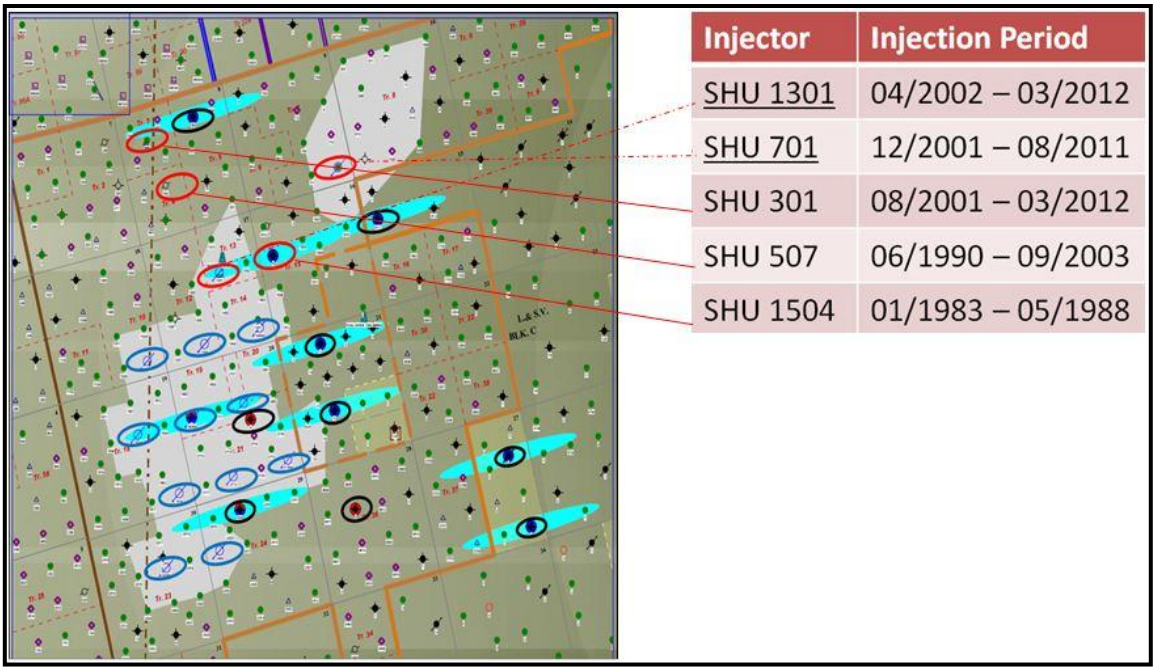

Injector	Injection Period
SHU 1301	04/2002 – 03/2012
SHU 701	12/2001 – 08/2011
SHU 301	08/2001 – 03/2012
SHU 507	06/1990 – 09/2003
SHU 1504	01/1983 – 05/1988

Figure 4.102: Available early injection data (locations highlighted in red)

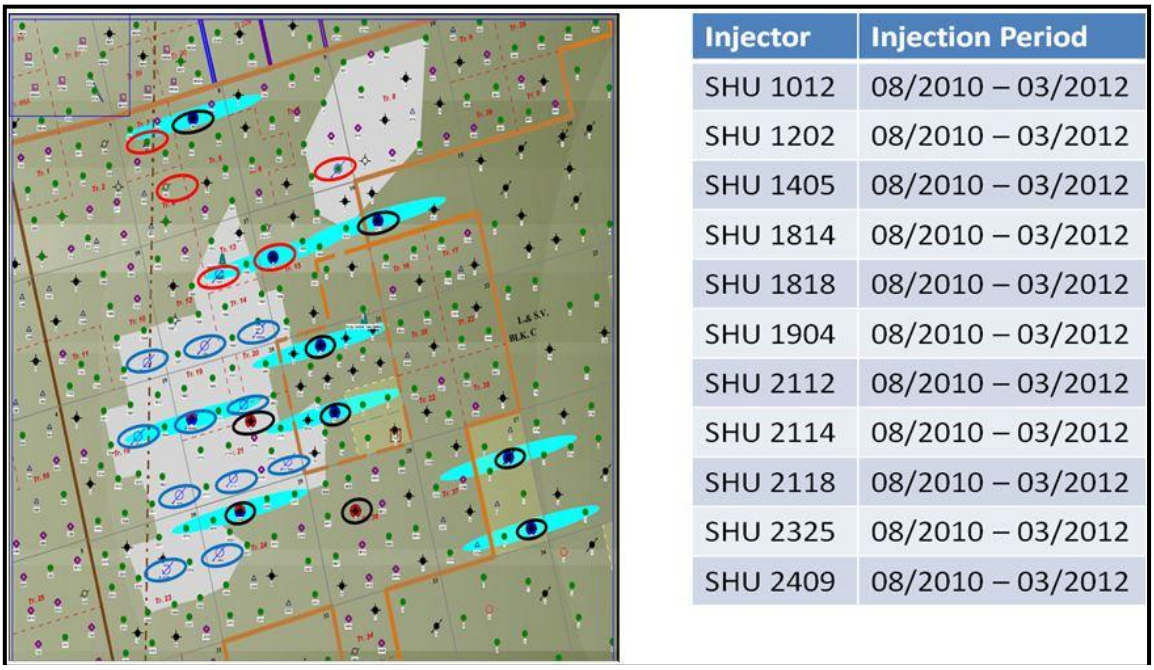

Injector	Injection Period
SHU 1012	08/2010 – 03/2012
SHU 1202	08/2010 – 03/2012
SHU 1405	08/2010 – 03/2012
SHU 1814	08/2010 – 03/2012
SHU 1818	08/2010 – 03/2012
SHU 1904	08/2010 – 03/2012
SHU 2112	08/2010 – 03/2012
SHU 2114	08/2010 – 03/2012
SHU 2118	08/2010 – 03/2012
SHU 2325	08/2010 – 03/2012
SHU 2409	08/2010 – 03/2012

Figure 4.103: Late injection data (locations highlighted in blue)

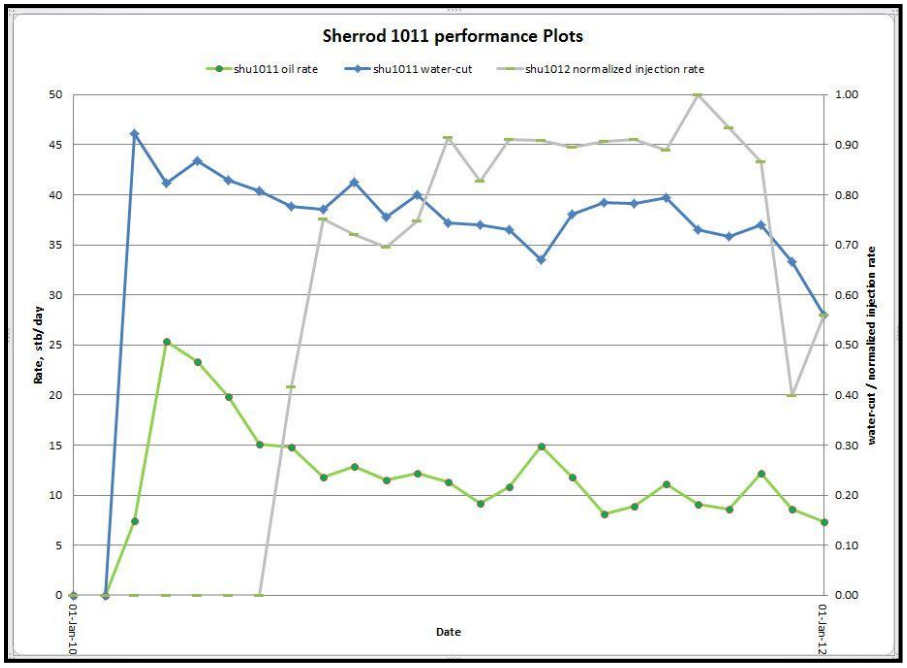

Figure 4.104: Performance plot of a 2010 producer with normalized injection rate

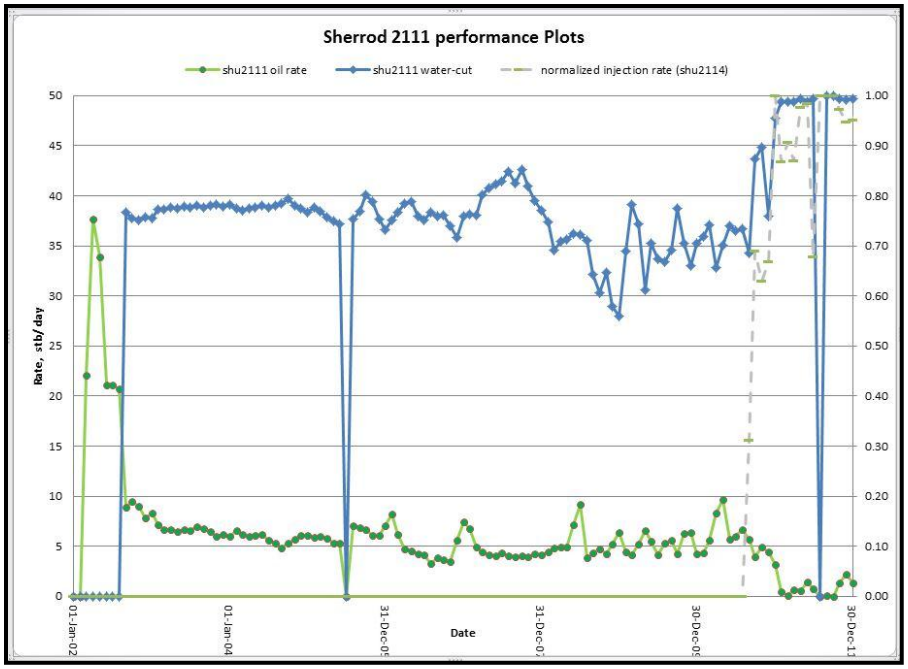

Figure 4.105: Performance plot of a 2010 producer with normalized injection rate

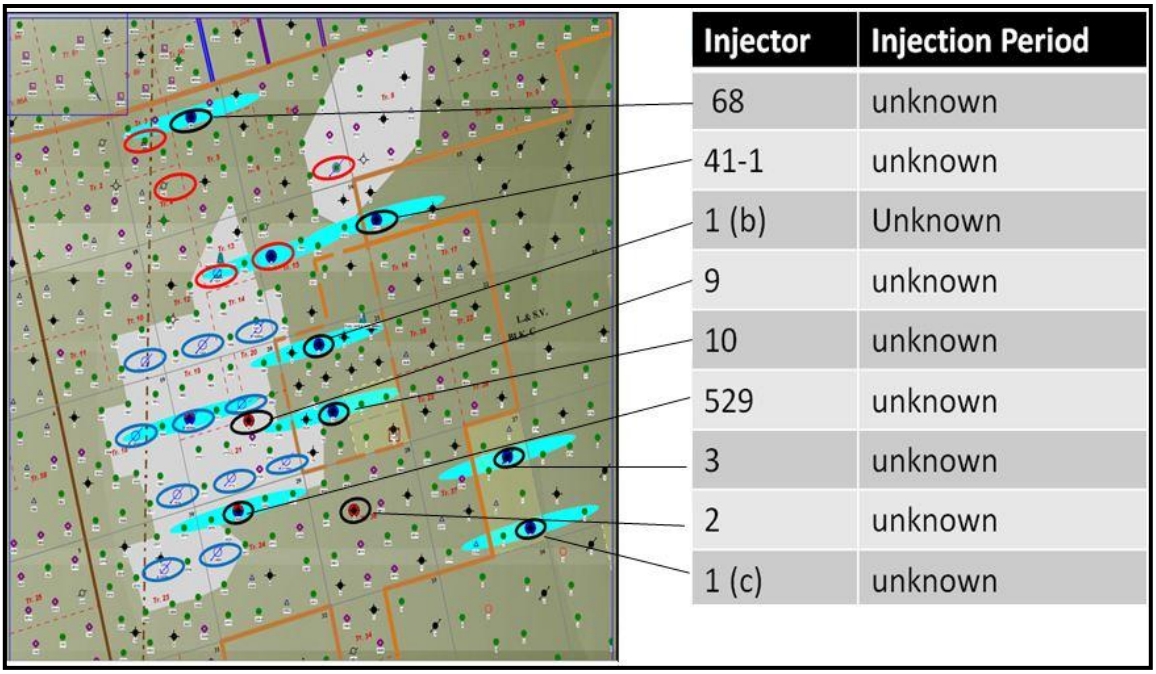

Injector	Injection Period
68	unknown
41-1	unknown
1 (b)	Unknown
9	unknown
10	unknown
529	unknown
3	unknown
2	unknown
1 (c)	unknown

Figure 4.106: Abandoned injection with no injection history

4.10 A Highlight on Sherrod Dry Production History

The purpose of this section is to highlight and map simultaneous water breakthrough of dry producers observed throughout the history of the field. Simultaneous breakthrough of a group of wells after a field event is a very important observation that will help to assess connectivity between wells. In addition, small simulation sector models for these groups of wells and their offending injector(s) could be created and analyzed using inversion modeling or manual history matching. A summary of dry producers with their water breakthrough year is summarized in Table 4.9.

Number of dry wells	BT year
6	1973
2	1988
1	2000
45	2002
1	2003
1	2005

Table 4.9: Summary of dry wells showing water breakthrough

4.10.1 Simultaneous Water Breakthrough of Dry Wells in 1973

Six wells with dry production exhibited simultaneous water breakthrough in 1973. A list of the 6 wells' names and their date of breakthrough is shown in Table 4.10 below. Water-cut of these wells exhibit high degree of fluctuation while oil rates are very stable. Example of such water-cut behavior is shown in Figure 4.107 below. This abnormal water-cut behavior indicates that water is flowing to these wells through fractures. In addition, locations of these wells on a NE-SW trend indicate the presence of a major fracture trend governing early water movement in this direction. Figure 4.108 shows wells' locations and the most likely fracture realization that connects the observations.

These simultaneous early water breakthroughs without any active injection system during the 1970s support the hypothesis of the presence of an external water source feeding Sherrod Area. Modeling external water source is highly uncertain due to uncertainty in water entry location, uncertainty in start of injection, and uncertainty of

effective injection rate. Uncertainty could be reduced by utilizing wells' water production rates and water-cut anomalies. However, since old maps of Sherrod Area indicate the presence of 9 abandoned injectors with no information about their injection history, it is very likely that this missing very early injection data is responsible for these breakthroughs. As a result, these breakthroughs cannot be modeled due to the absence of needed injection data.

Well Name	BT Date
Shu0301	Jan-1973
SHL01545	Jan-1973
SHL10131	Jan-1973
SHU0704	Jan-1973
SHU3802	Jan-1973
SHL00780	Oct-1973*

Table 4.10: Well list for 1973 simultaneous water breakthrough

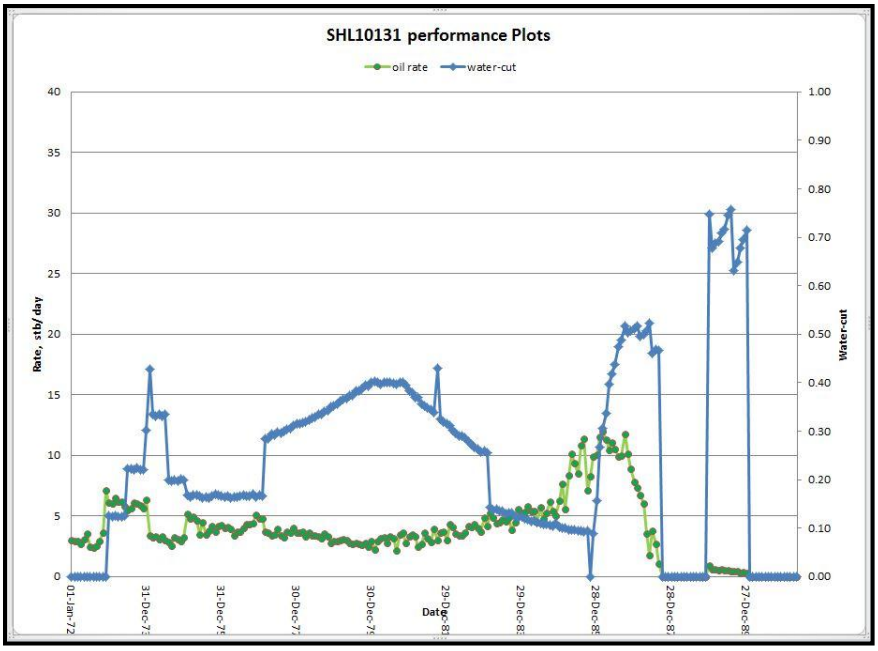

Figure 4.107: Example of water-cut behavior for a well exhibited water breakthrough in 1973

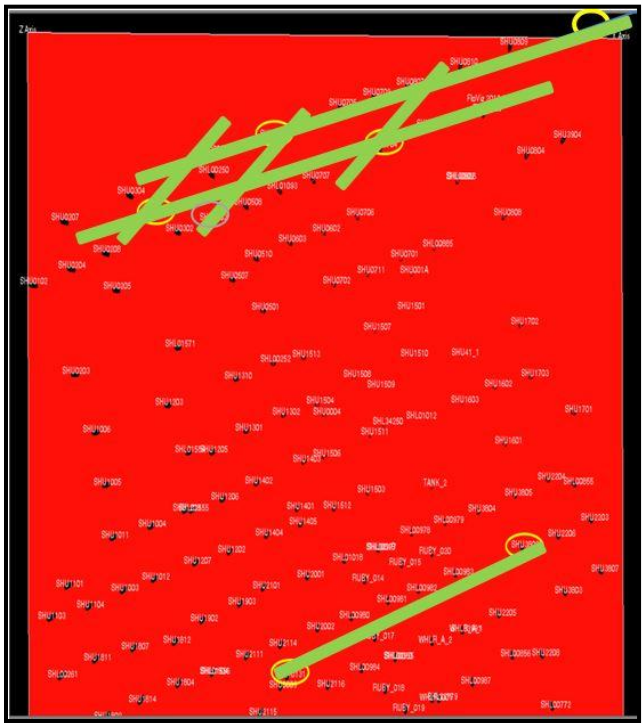

Figure 4.108: Fracture realization from 1973 simultaneous water breakthrough

4.10.2 Simultaneous Water Breakthrough of Dry Wells in 2002

Forty four wells with dry production exhibited simultaneous water breakthrough in 2002. This abnormal simultaneous water breakthrough occurred directly after the introduction of three injectors in late 2001 – early 2002. A list of the 44 wells' names and their breakthrough dates are shown in Table 4.11 below. Water-cut of these wells exhibit abnormal increase from 0 to 70-85% in one month for majority of wells. Example of such water-cut behavior is shown in Figure 4.109 below. This global breakthrough and sudden increase in water-cut indicates that these wells are interconnected through a complex fracture network. Figure 4.110 show the sparse locations of the 44 wells along with the three injectors introduced shortly before the breakthrough. Breakthroughs cover almost the entire field area giving a strong indication that water is moving almost areally through a high permeability streak. Another support for the areal movement of water is, with the exception of two wells, no well showed dry production in Sherrod after the 2002 water breakthrough.

In order to investigate the direct connection between the three injectors introduced in late 2001 – early 2002 and the field-wide simultaneous water breakthrough in 2002, water production rates of individual wells are summed and compared against different combination of active wells injection rates in the period between 2002 to 2009 year end. Table 4.12 show active injectors during 2002 water breakthroughs and their injection period.

A comparison between the sum of water production rates from the 44 producers and total water injection rate from the four active injectors is shown in Figure 4.111. Several

key observations could be made from the figure: First, group water breakthrough occur 7 months after start of injection of the 4 injectors. Second, average water production rate of 1,000 stb/day appear to be significantly lower than total injection rate of the four injectors. Third, there are similarities in rate fluctuation between the two but those are not clear due to the large gap between the curves. Thus, the comparison will be done on a smaller scale by using individual or smaller combinations of active injection rates. Forth, field water injection was shut-in between December 2004 and July 2005. Group water production continues to be high and appear to be unaffected by field injection shut-in. During this shut-in period, water-cut of individual producers show three types of trends: wells showed increase in water-cut, wells showed decrease in water-cut, and wells showed no change in water-cut. Figures 4.112 through 4.114 show examples of the three water-cut trends. A decrease in wells' water-cut is expected as the four active injectors were shut-in. However, an increase in water-cut of significant number of producers cannot be explained without the presence of an external water source feeding Sherrod Area. If such external water source does exist and it is affecting Sherrod Area producers, this will create problems in future management of Sherrod Area.

A comparison between individual wells injection rates with the group water production rate is shown in Figures 4.115 through 4.121. Figure 4.115 shows that group water production follows precisely Sherrod 1301 injection rate between July 2006 and December 2007. In addition, Figure 4.116 shows that group water production also follow precisely Sherrod 701 injection rate for the same period. This is because both injectors have same injection rates during the same period. On the other hand, Figure 4.117 shows

that early shut-in of Sherrod 507 injection have no impact on group water production rate. Thus, it should not be used as part of any comparison. Moreover, Figure 4.118 shows that Sherrod 301 was also shut-in for a two short periods of time between November 2003 – August 2004 and December 2004 – July 2005. These two shut-in periods did not show apparent impact on the group water production rate making Sherrod 301 less likely to contribute significantly to the group water production. However, late group water production rate matches injection rate of Sherrod 301. This indicates that injector's contribution to water production might changes with changes in fluxes caused by shutting some producers or changing the distribution of water injected in the area.

Comparing different combinations of wells injection rates with the group water production rate in Figures 4.119 through 4.121 show that more sections of the group water production curves could be matched. This indicate that the contribution of each injector to field water production changes with time as a result of changes in flux directions in the field when adding new wells, shutting old wells, or modifying rates of active injectors and producers.

In summary, analysis of water production rate of the group of wells that exhibited simultaneous water breakthrough in 2002 shows two key findings: First, two out of four active injectors during 2002 are responsible for majority of the group water production rate. This is evidenced by the match obtained between group water production rate and different combination of wells injection rates. Second, field injection shut-in period between December 2004 and July 2005 highlights water influx to Sherrod Area from an

external water source. This is evidenced by the abnormal increase in water-cut of several producers during the field injection shut-in period.

Sn	Well Name	BT date	Sn	Well Name	BT date
1	Sherrod 102	Jul-2002	23	Sherrod 2001	Jul-2002
2	Sherrod 302	Jul-2002	24	Sherrod 2110	Nov-2002
3	Sherrod 508	Jul-2002	25	Sherrod 2111	Sep-2002
4	Sherrod 602	Sep-2002	26	Sherrod 2112	Sep-2002
5	Sherrod 705	Sep-2002	27	Sherrod 2113	Sep-2002
6	Sherrod 706	Sep-2002	28	Sherrod 2203	Sep-2002
7	Sherrod 707	Sep-2002	29	Sherrod 2204	Sep-2002
8	Sherrod 807	Sep-2002	30	Sherrod 2205	Sep-2002
9	Sherrod 808	Sep-2002	31	Sherrod 2309	Sep-2002
10	Sherrod 809	Aug-2002	32	Sherrod 2313	Jul-2002
11	Sherrod 810	Aug-2002	33	Sherrod 2314	Sep-2002
12	Sherrod 1203	Jul-2002	34	Sherrod 2315	Sep-2002
13	Sherrod 1301	Jul-2002	35	Sherrod 2410	Sep-2002
14	Sherrod 1402	Jul-2002	36	Sherrod 2411	Jul-2002
15	Sherrod 1506	Sep-2002	37	Sherrod 2412	Jul-2002
16	Sherrod 1602	Jul-2002	38	Sherrod 3606	Sep-2002
17	Sherrod 1702	Jul-2002	39	Sherrod 3607	Jul-2002
18	Sherrod 1804	Oct-2002	40	Sherrod 3608	Jul-2002
19	Sherrod 1807	Oct-2002	41	Sherrod 3703	Aug-2002
20	Sherrod 1808	Oct-2002	42	Sherrod 3803	Jul-2002
21	Sherrod 1810	Sep-2002	43	Sherrod 3804	Jul-2002
22	Sherrod 1902	Sep-2002	44	Sherrod 3904	Jul-2002

Table 4.11: Well list for 2002 simultaneous water breakthrough

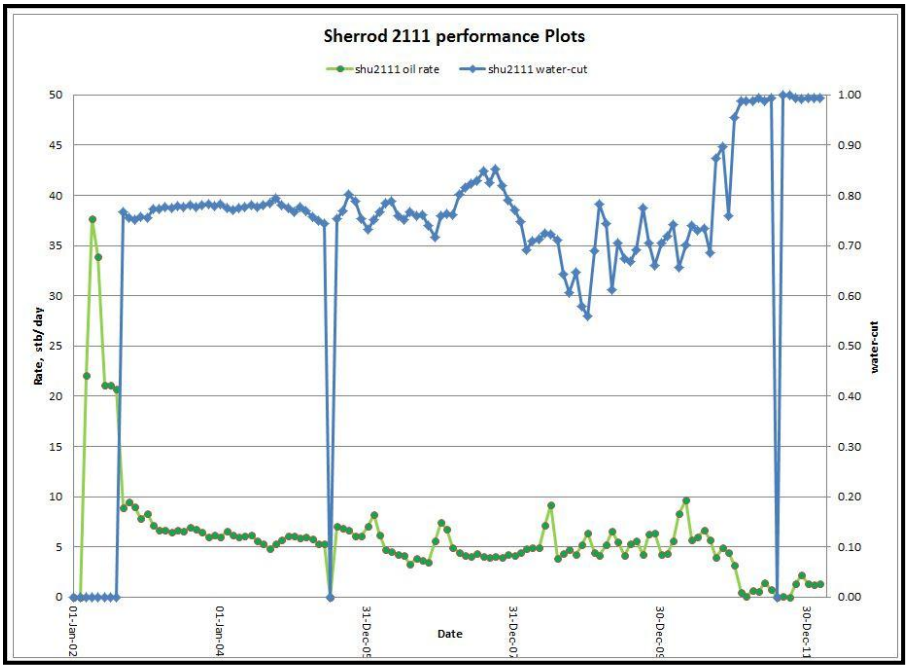

Figure 4.109: Example performance plot for a 2002 breakthrough well

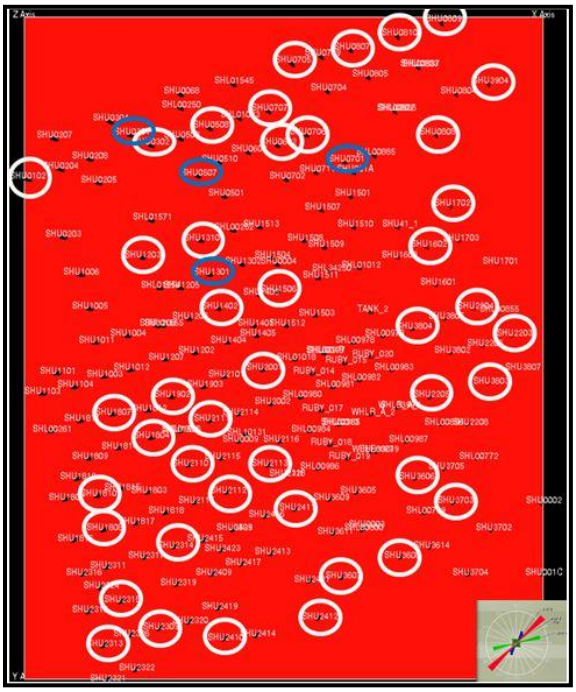

Figure 4.110: Water breakthroughs in 2002 highlighted on the full field model

Active Injector	Tagged?	Start	End
Shu 507	X	06/1990	09/2003
Shu 301	X	08/2001	active
Shu 701	√	12/2001	08/2011
Shu 1301	√	04/2002	active

Table 4.12: Active injectors during the field-wide water breakthrough in 2002

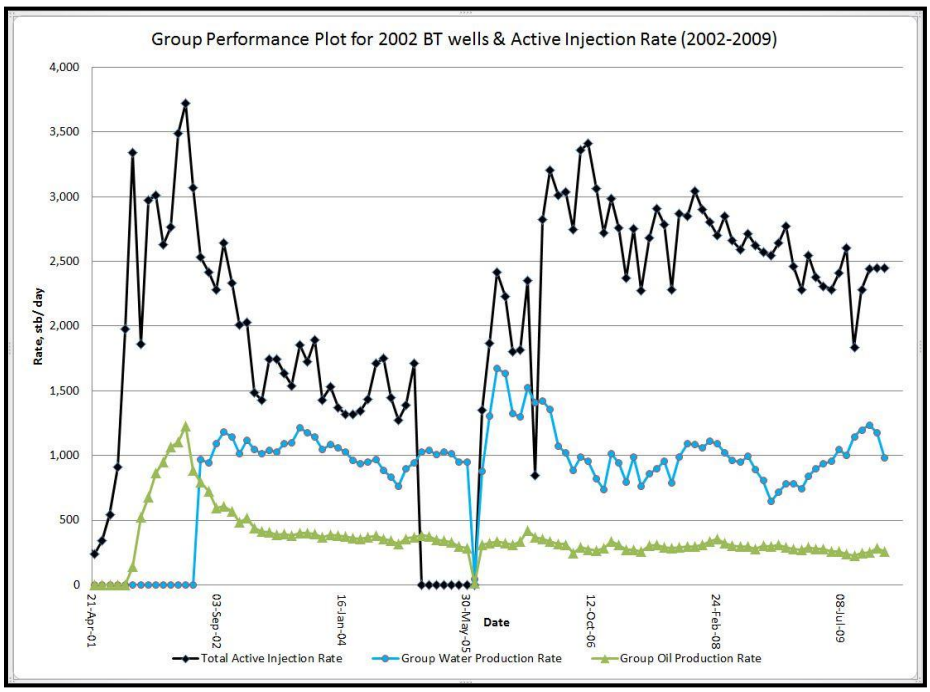

Figure 4.111: Total active injection rate with 2002 wells group production rates

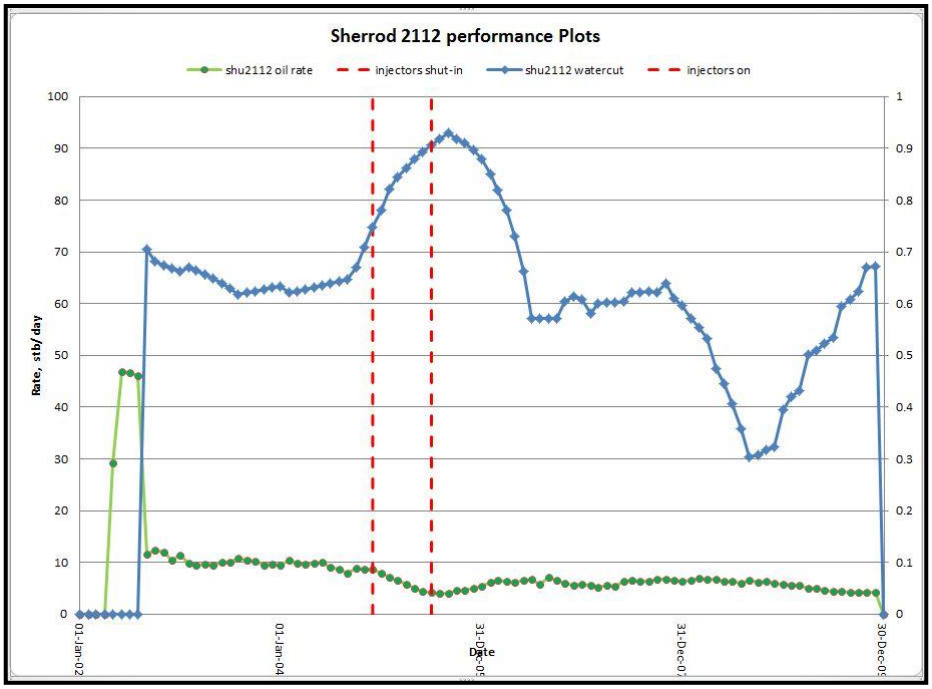

Figure 4.112: Example of water-cut increase during field injection shut-in

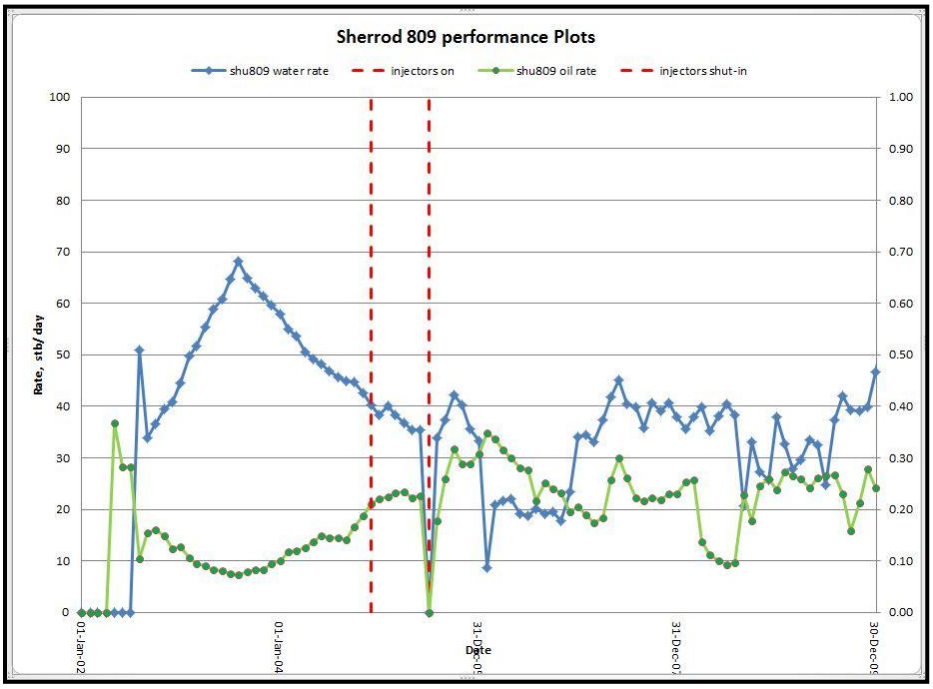

Figure 4.113: Example of water-cut decrease during field injection shut-in

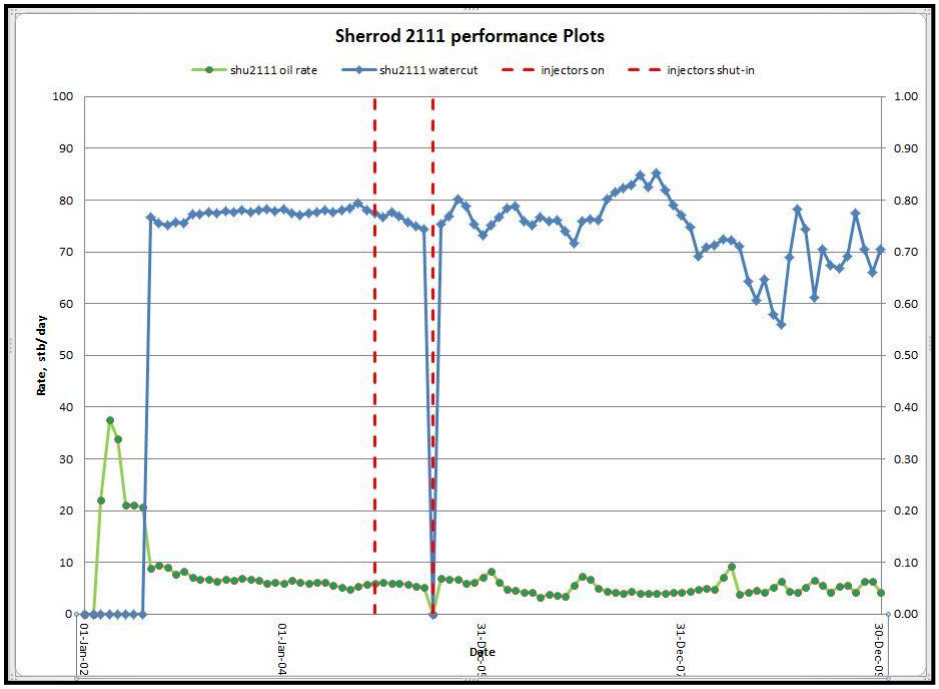

Figure 4.114: Example of no change in water-cut during field injection shut-in

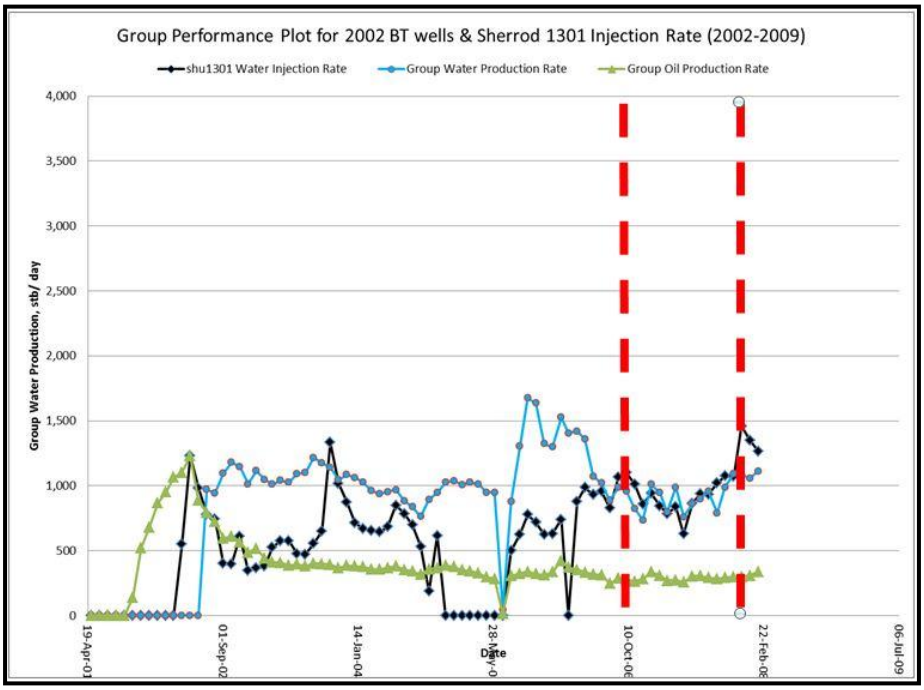

Figure 4.115: 'Sherrod 1301' injection rate with 2002 wells group production rates

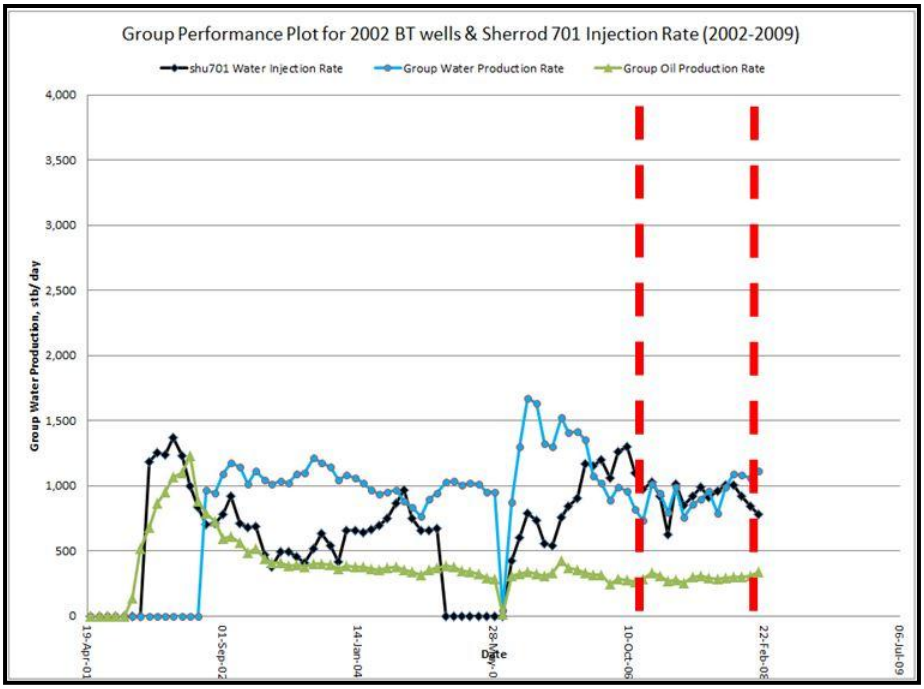

Figure 4.116: 'Sherrod 701' injection rate with 2002 wells group production rates

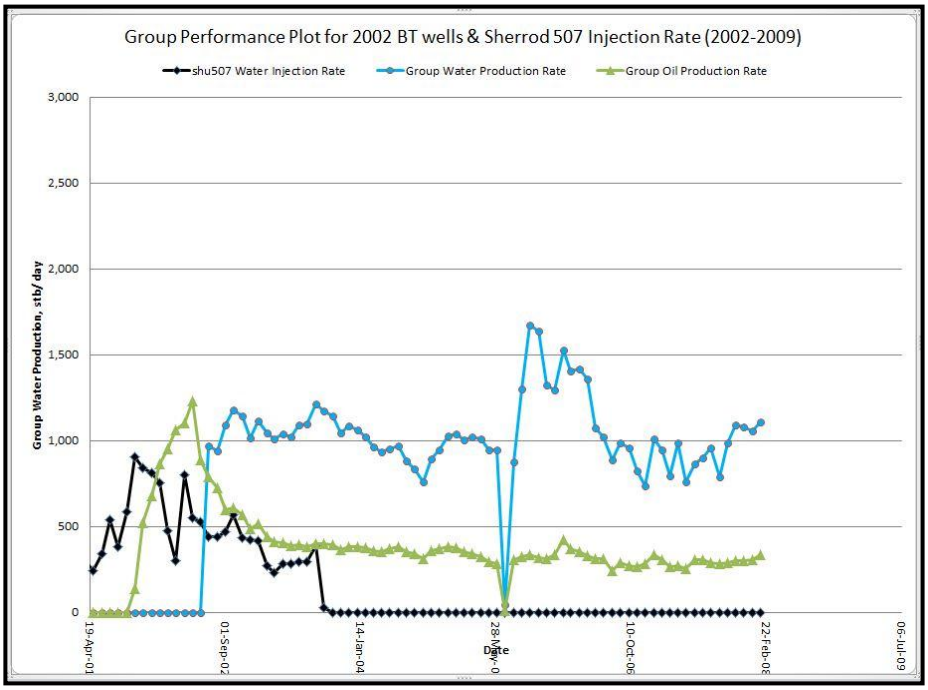

Figure 4.117: 'Sherrod 507' injection rate with 2002 wells group production rates

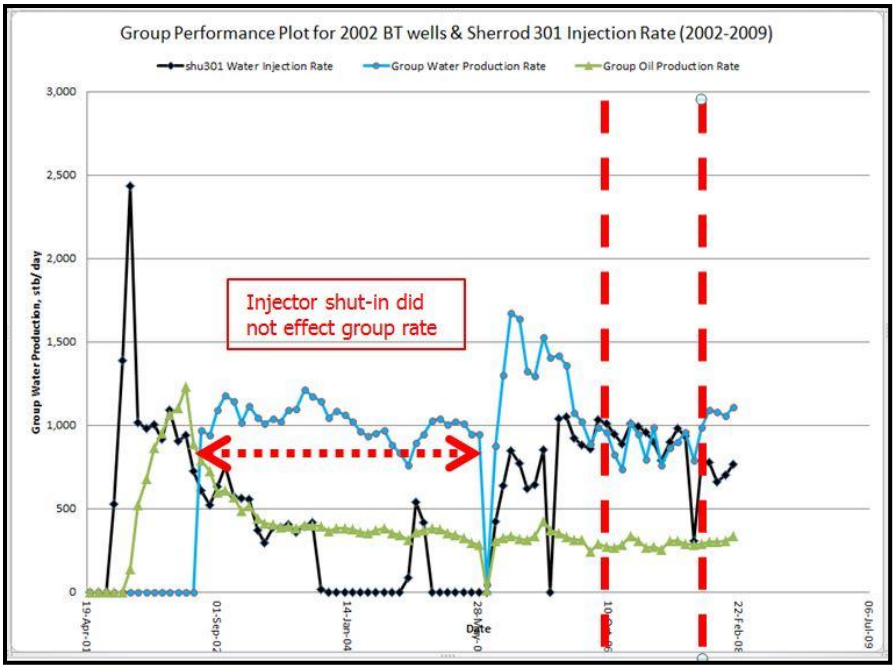

Figure 4.118: 'Sherrod 301' injection rate with 2002 wells group production rates

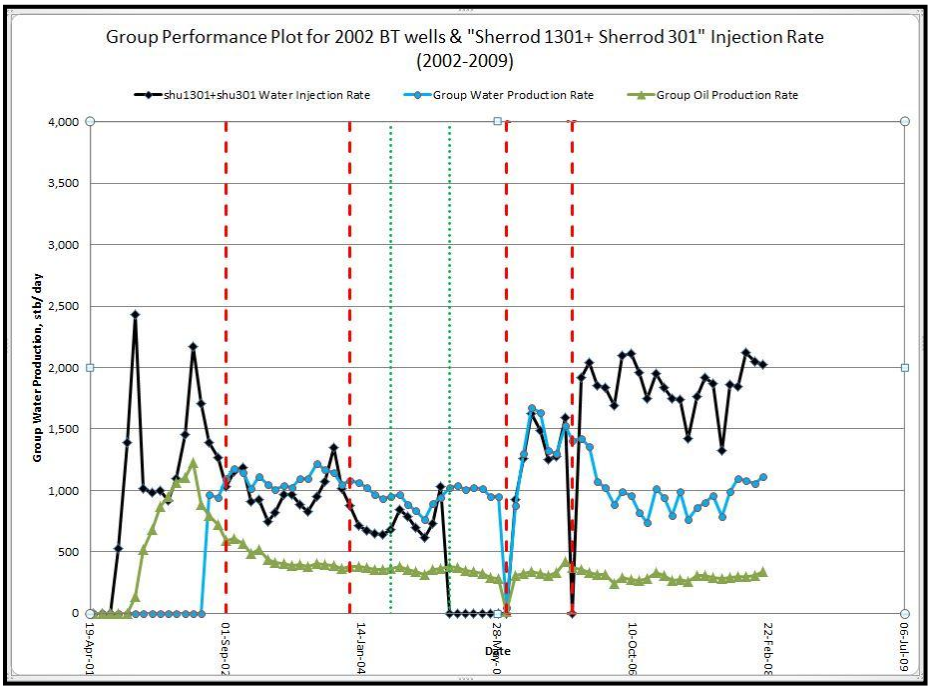

Figure 4.119: Multi-well injection rate with 2002 wells group production rates

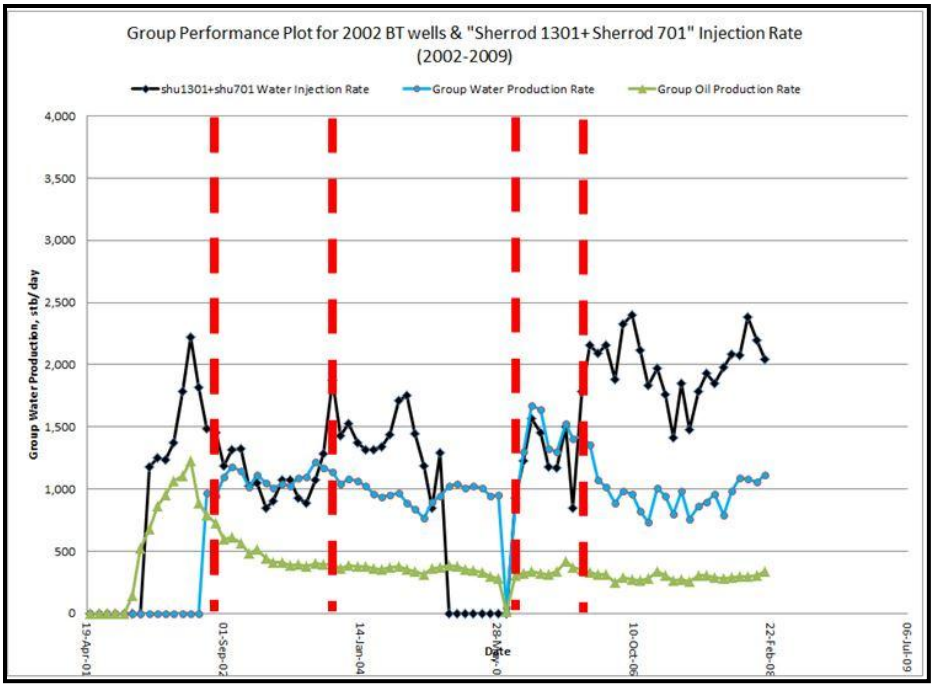

Figure 4.120: Multi-well injection rate with 2002 wells group production rates

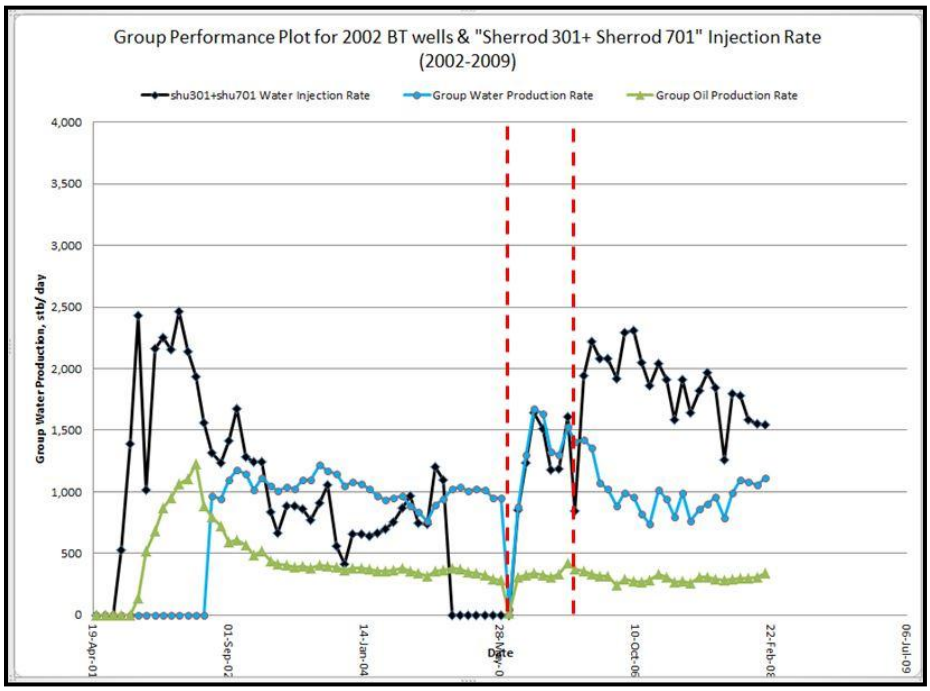

Figure 4.121: Multi-well injection rate with 2002 wells group production rates

4.11 Water-cut Signatures

Water production in oil or gas reservoirs could be explained by one of two phenomena: increase in matrix\fracture water saturation, or water conning. While water-cut driven by water conning could be controlled by reducing oil rate, water-cut driven by high water saturation in the rock shows only increasing trend and is unaffected by changes in oil rate. A large number of producers in Sherrod Area exhibit abnormal water-cut behavior. Examples of abnormal water-cut behavior includes declining water-cut with time, high fluctuation in water-cut during stable oil production period, wells showing 100% water-cut for a limited period of time. Examples of wells showing declining water-cut trends and their locations are shown in Figures 4.122 and 4.123 below. Examples for the other two types of water-cut behavior are shown in Figures 4.124 and 4.125. Small fluctuations in water-cut could be attributed to measurement error usually associated with water rate allocation. However, large fluctuation in water-cut or a declining water-cut cannot be explained in term of reservoir saturation. The only explanation for these water-cut behaviors is the direct communication of producers with active injectors through a facture system. In this case, fluctuations or a sharp decline in water-cut reflect changes in injection rate of the offending injector. Thus, these water-cuts provide another support for the presence of external water source feeding these wells as those wells show no or very weak communication with Sherrod injectors as shown by tracer recoveries.

Another water-cut signature to be highlighted is the similarity that exists between water-cut responses for different producers located on the same tracer path. Three

examples are shown in Figures 4.126 through 4.128 for producers located along N-E, and E-W fracture directions. These similarities are useful to group wells in any future history matching study.

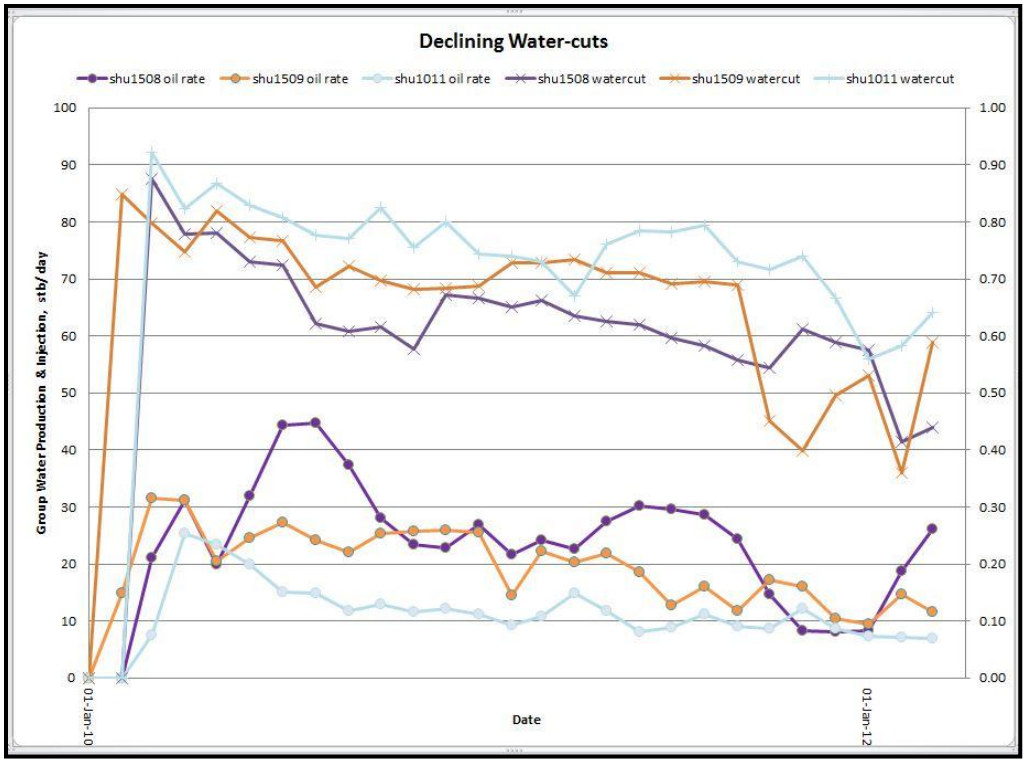

Figure 4.122: Example wells showing declining water-cut trend

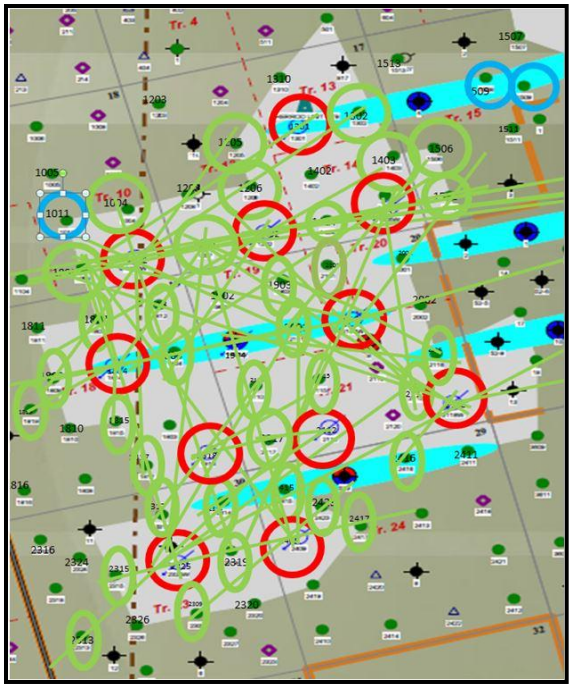

Figure 4.123: Locations of wells showing declining water-cut

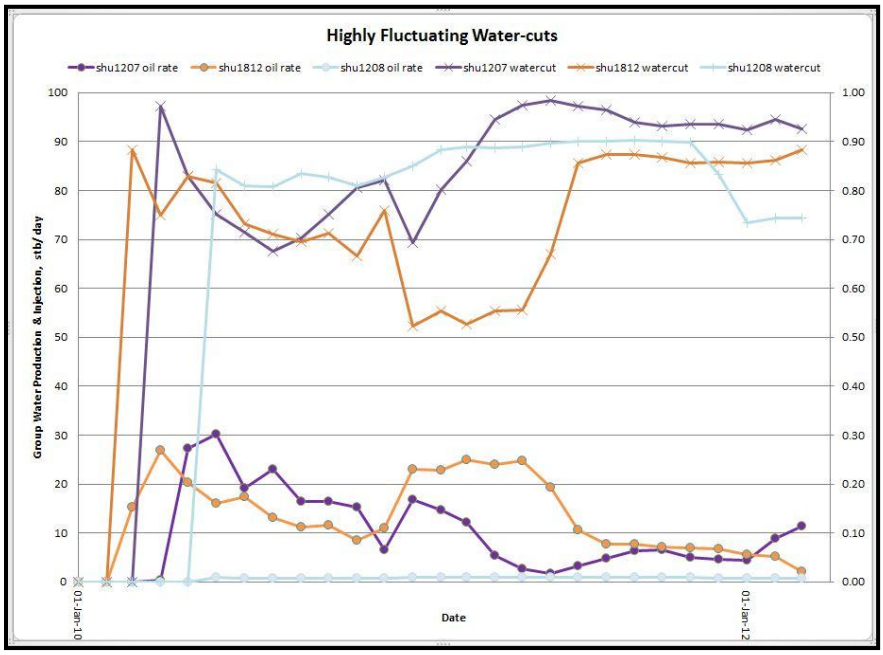

Figure 4.124: Examples of wells showing highly fluctuating water-cuts

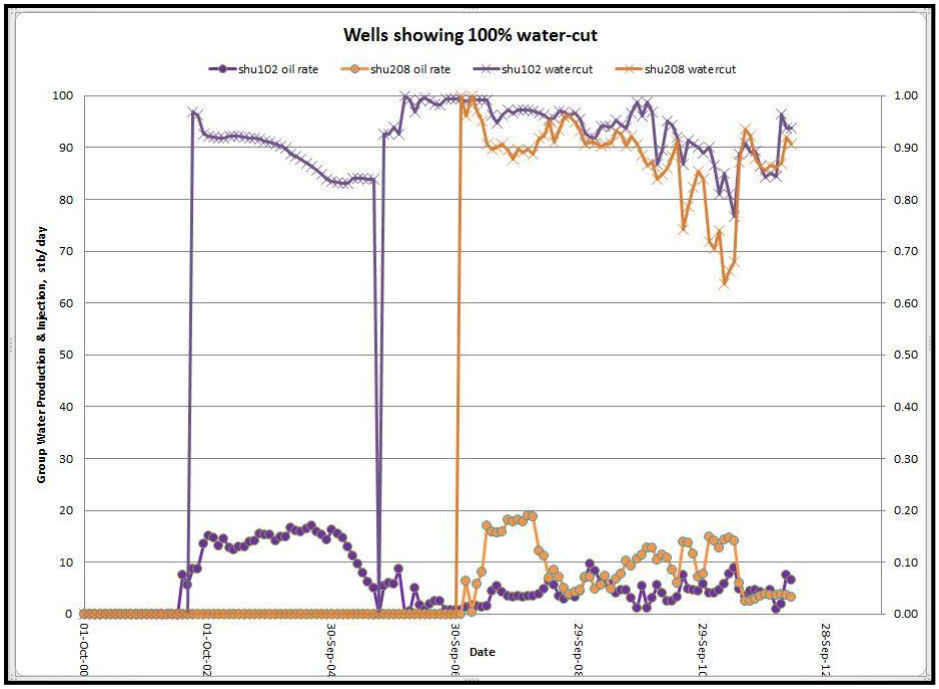

Figure 4.125: Examples of wells showing 100% water-cut for a short period

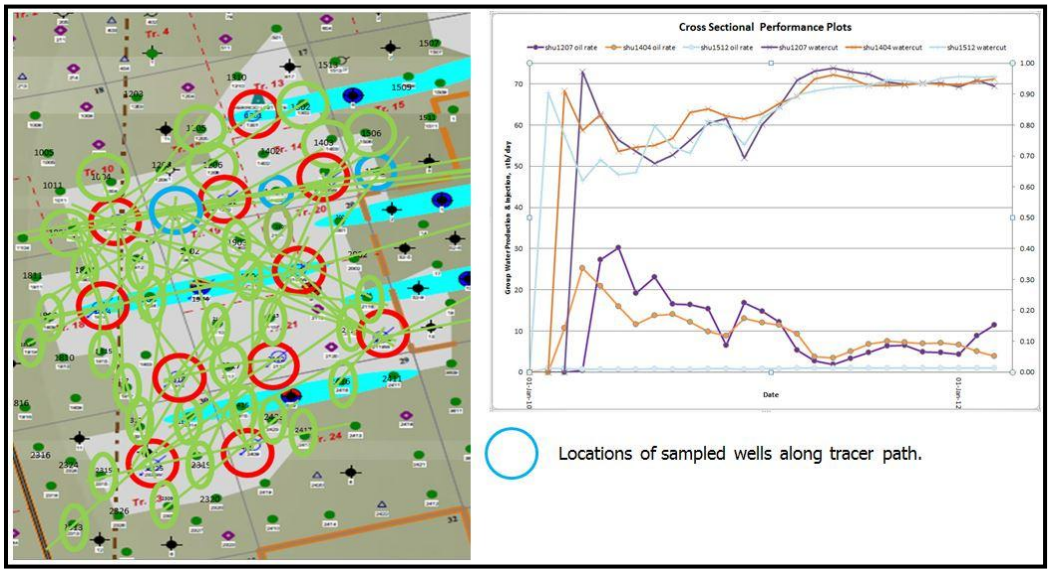

Figure 4.126: Wells showing similarities in water-cut along tracer path (example1)

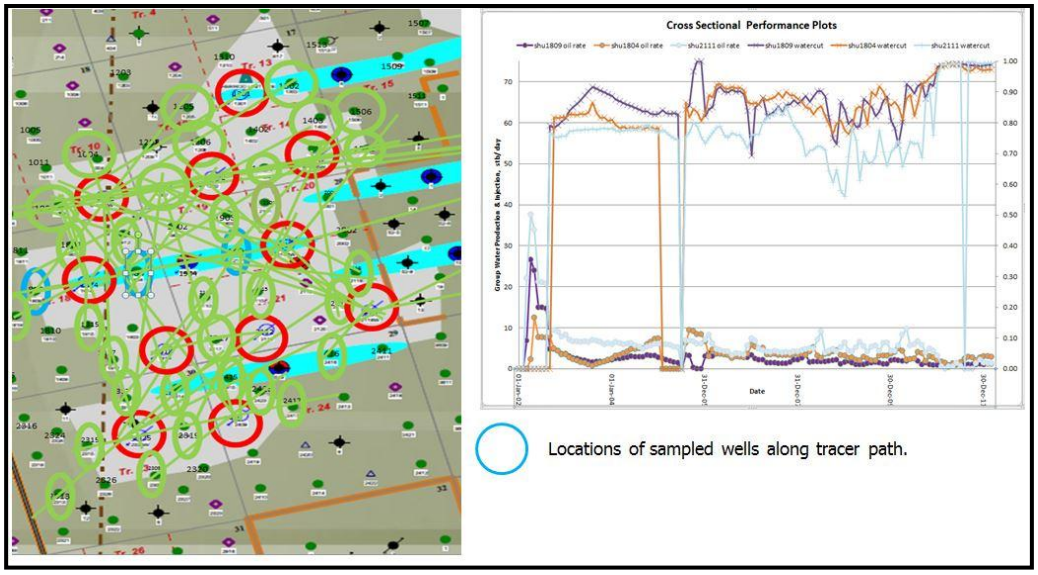

Figure 4.127: Wells showing similarities in water-cut along tracer path (example 2)

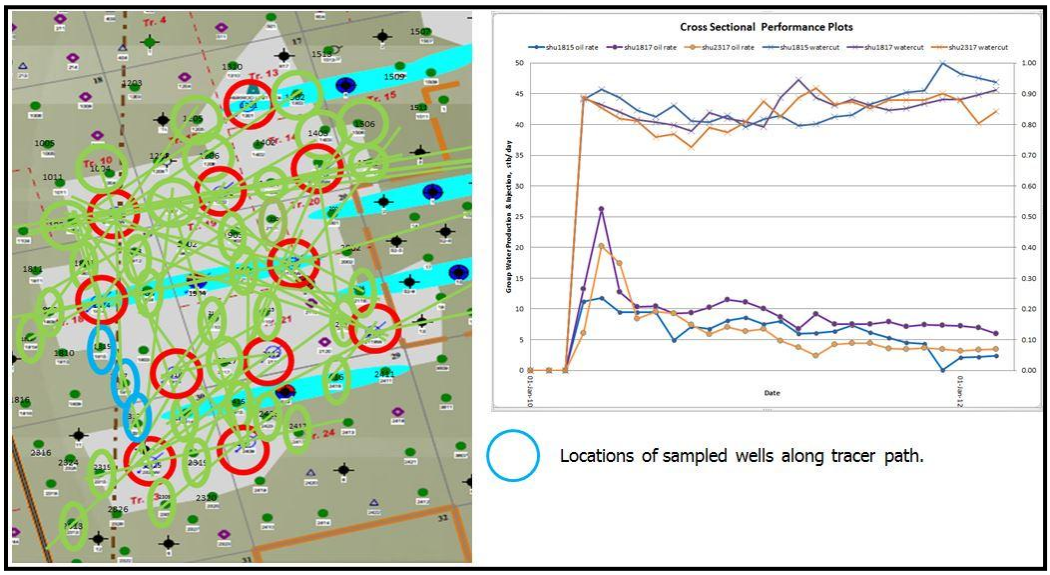

Figure 4.128: Wells showing similarities in water-cut along tracer path (example 3)

4.12 Summary of Analytical Interpretation Techniques

The findings from analytical interpretation techniques could be summarized as follows:

1. Maximum sweep directions obtained from Methods of Moments indicate the presence of four major flow features inter-connected with 10 out of the 13 tagged injectors. These flow features are oriented N76^{o}E and governs majority of water movement in the field.
2. No correlation exists between tracer recovery and net swept volumes from Methods of moments.
3. Poor overall tracer recovery with no tracer out of the 13 injected tracer recovered by more than 9% recovery.
4. Tracer responses could be categorized into four groups based on the distribution of tracer recovery at all producers.
5. For a field where wells injection rates are in the range of 100-400 stb/d, tracer responses with less than 0.1% recovery explains water movement of less than 1 bbl / day and thus should be ignored.
6. Producers located on the E-W fracture trend reflect more the complexity of the fracture network where far injectors as well as nearby injectors contribute significantly to producers.
7. Studying characteristics of tracer responses based on tracer recovery highlight several aspects of tracer responses
    a. No correlation between tracer velocity and tracer recovery

b. Tracer responses with less than 0.01% recovery is highly effected by water recycling. As tracer recovery of the tracer response increase, the water recycling effect decrease.

c. Number of peaks in a tracer response correlates strongly with tracer recovery. This indicates that a higher recovery tracer response captures more the layering between a pair of injector and producer.

8. Sherrod Area of Spraberry Field exhibit very poor waterflood performance. This is evidenced by field water production which follows precisely the field water injection rate.

9. Sherrod Area of Spraberry Field receives water influx from an external water source. This is supported by the following observations:

a. The abnormal increase in water-cut for a number of wells during field water injection shut-in between December 2004 and July 2005

b. The declining water cut trend for a number of wells that did not show any tracer from water-cuts as high as 85% to as low as 40%.

c. The abnormal higher than 99% water-cut appearing for a short period of time for a number of wells surrounding tracer study area.

d. The high fluctuation of water-cut values between as high as 90% to as low as 50% for a number of wells without changes in active injection rates that justify such behavior.

e. Simultaneous water breakthrough of a group of 6 wells in 1973 without data showing an active injection system in the area.

10. Simultaneous breakthrough of 44 wells in 2002 is dominated by fracture saturation. This is supported by the match between group water production rate and different combinations of injection rates of active injectors.

11. Majority of pattern injectors, 6 out of 11, show that part of the injected water flow outside Sherrod Area toward east. Although tracers indicate small volumes, these volumes could be underestimated by excessive tracer dilution

5. CONSTRUCTION OF SIMULATION MODELS

5.1 Construction of Base Case Model

Construction of a base case model requires knowledge about matrix & fracture properties, fluid properties, rock-fluid and matrix-fracture interaction properties, and knowledge of reservoir structure in the area understudy.

Matrix properties such as porosities, permeabilities, and net thicknesses of 5U and 1U sand units were taken from a general knowledge of these properties in areas surrounding Sherrod in Spraberry Field such as O'Danial and Patrson Units. On the other hand, fracture and fracture-matrix interaction properties were treated as highly uncertain parameters determined solely by the history match. Properties used for base case are listed in Table 5.1 below.

Sherrod PVT model was built based on 5 reservoir fluid studies from different areas in Spraberry Field. Out of the 5 oil samples used for the study, four were obtained using bottom hole sampling and only one was recombined at surface. Smoothed PVT functions used for the base case are shown in Tables 5.2 & 5.3.

Fluid-matrix interaction functions were used from both experimental measurements and correlations. As mentioned earlier in chapter 2, oil-water imbibition capillary pressure measurements using static-equilibrium, mercury injection, and centrifuge method was done on core samples from Judkins Area in Spraberry Field. Static equilibrium is believed to be the most representative capillary pressure measurement and hence, it was used for the base case while considering some uncertainty. For matrix relative permeability curves, they were constructed by using correlations which relies on

residual saturations obtained from imbibition oil-water capillary pressure measurements and the weak water wettability behavior indicated in previous studies. The correlation used was as follows:

$$k_{ro} = (1 - S_n)^{no} \quad \text{.....(15)}$$

$$k_{rw} = k_{rwe}\, S_n{}^{nw} \quad \text{.....(16)}$$

$$S_n = \frac{S_w - S_{wr}}{1 - S_{or} - S_{wr}} \quad \text{.....(17)}$$

where S_n is normalized water saturation, S_w is matrix water saturation, S_{wr} is irreducible water saturation, S_{or} is residual oil saturation, K_{ro} is oil relative permeability, exponent "no" is oil saturation exponent, K_{rw} is water relative permeability, K_{rwe} is water relative permeability at residual oil saturation, and exponent "nw" is water saturation exponent. Constants used in the correlations above are reported in Table 5.4 below. Oil-water capillary pressure and relative permeability curves used for the matrix system of the base case are shown in Figures 5.1 and 5.2 below. For the fracture system, capillary pressure was assumed to be zero and relative permeability curves were assumed to be straight lines as typically done in simulation studies of naturally fractured reservoirs.

Property	Matrix	Fracture
Permeability, md	1	200
Porosity,	0.15	0.005
Ky / Kx	1	1
Thickness, ft	11	
Top Depth, ft	6930	
Rock Compressibility, 1/psi	4.0×10^{-6}	
Shape Factor, σ	.01	

Table 5.1: Matrix and fracture properties used for base case

Pressure	GOR	FVF	μ_o	Co	Uo
141.7	0.033	1.0496	1.821	3.00E-05	6.63E-05
268.7	0.066	1.0640	1.563	3.00E-05	6.63E-05
395.7	0.102	1.0802	1.364	3.00E-05	6.63E-05
522.8	0.140	1.0979	1.210	3.00E-05	6.63E-05
649.8	0.180	1.1169	1.087	3.00E-05	6.63E-05
776.8	0.221	1.1372	0.989	3.00E-05	6.63E-05
903.8	0.264	1.1586	0.907	3.00E-05	6.63E-05
1030.9	0.308	1.1811	0.839	3.00E-05	6.63E-05
1157.9	0.353	1.2045	0.782	3.00E-05	6.63E-05
1284.9	0.400	1.2289	0.732	3.00E-05	6.63E-05
1411.9	0.447	1.2542	0.689	3.00E-05	6.63E-05
1538.9	0.495	1.2804	0.651	3.00E-05	6.63E-05
1666	0.543	1.3074	0.618	2.82E-05	6.63E-05
1793	0.593	1.3352	0.588	2.57E-05	6.63E-05
1920	0.643	1.3637	0.562	2.35E-05	6.63E-05
2136	0.730	1.4140	0.522	2.04E-05	6.63E-05
2352	0.819	1.4663	0.489	1.80E-05	6.63E-05
2568	0.909	1.5206	0.460	1.61E-05	6.63E-05
2784	1.0013	1.5767	0.435	1.45E-05	6.63E-05
3000	1.0948	1.6347	0.412	1.32E-05	6.63E-05

Table 5.2: Oil PVT functions used in base case

Pressure	FVF	μ_g
141.7	20.7247	0.01119
268.7	10.6667	0.01146
395.7	7.0649	0.01169
522.8	5.2140	0.01200
649.8	4.0878	0.01238
776.8	3.3315	0.01281
903.8	2.7899	0.01330
1030.9	2.3846	0.01385
1157.9	2.0715	0.01447
1284.9	1.8242	0.01517
1411.9	1.6256	0.01594
1538.9	1.4644	0.01679
1666	1.3324	0.01771
1793	1.2235	0.01868
1920	1.1333	0.01971
2136	1.0124	0.02153
2352	0.9220	0.02341
2568	0.8528	0.02529
2784	0.7989	0.02715
3000	0.7561	0.02897

Table 5.3: Gas PVT functions used in base case

Constant	Value
Irreducible Water Saturation, S_{wr}	0.22
Residual Oil Saturation, S_{or}	0.43
Water relative permeability at residual, K_{rwe}	0.8
Oil saturation exponent, “no”	2.5
Water saturation exponent, “nw”	2.5

Table 5.4: Constants used to build matrix oil-water relative permeability curves

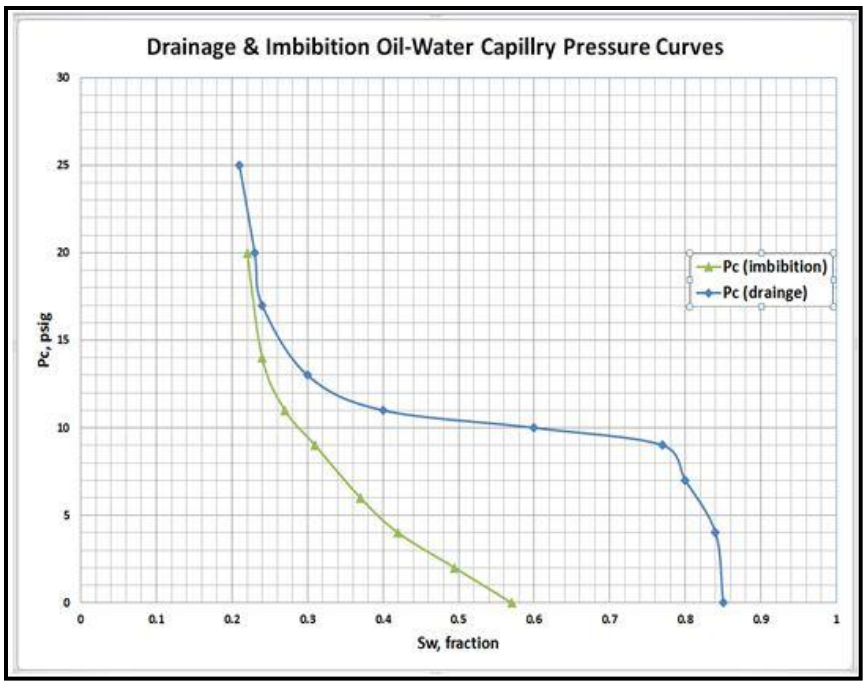

Figure 5.1: Imbibition oil-water capillary pressure used for base case

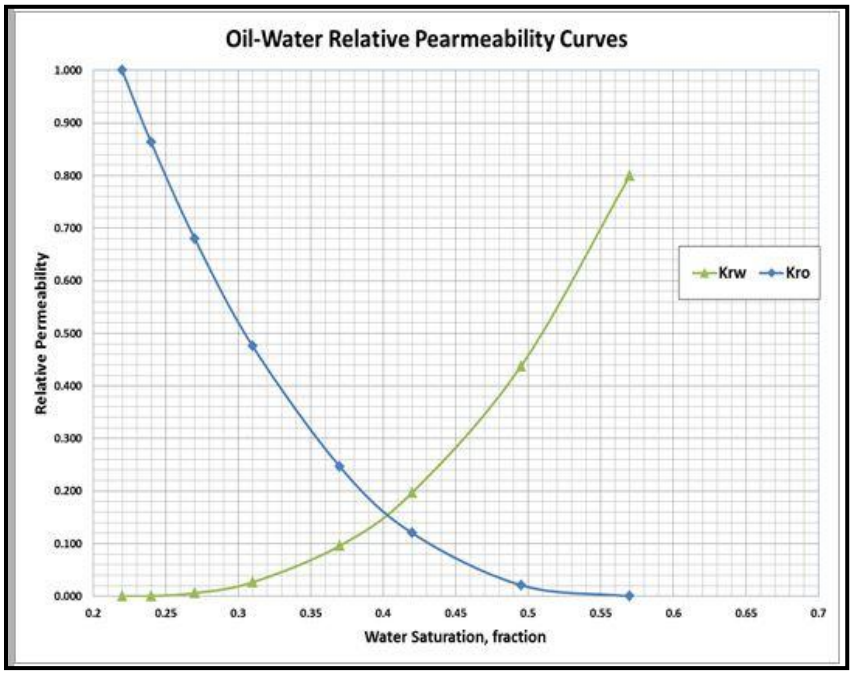

Figure 5.2: Oil-water relative permeability curves used for base case

5.2 Dual Porosity Simulators with Tracer Options

Three different simulators with tracer option in dual porosity reservoirs were available at the time of the study: Eclipse E-100 developed by Shlubmerger, tNavigator developed by Rock Fluid Dynamics, and UTCHEM developed by University of Texas at Austin. One inverted 9-Spot pattern located on north-east of Sherrod was used as a case study to compare performance of the three simulators. The pattern as wells as the sector model is shown in Figure 5.3 below.

At the time of the study, application of tracer option in UTCHEM was limited to single phase flow for dual porosity reservoirs. Thus, the case study chosen is not applicable for testing. Moreover, tracer option in dual porosity reservoir was a new option in tNavigator and has not been tested thoroughly. tNavigator was tested using different values of fracture permeability and shape factor for the case understudy. Testing results show that tNavigator have unstable solver. Round off error in initial reservoir pressure creates large differences in pattern water performance. In addition, tracer solution showed oscillations between positive and negative values. These discrepancies in results are shown in Figures 5.4 and 5.5 below. Discrepancies were reported to tNavigator support and a decision was made to use Eclipse E100.

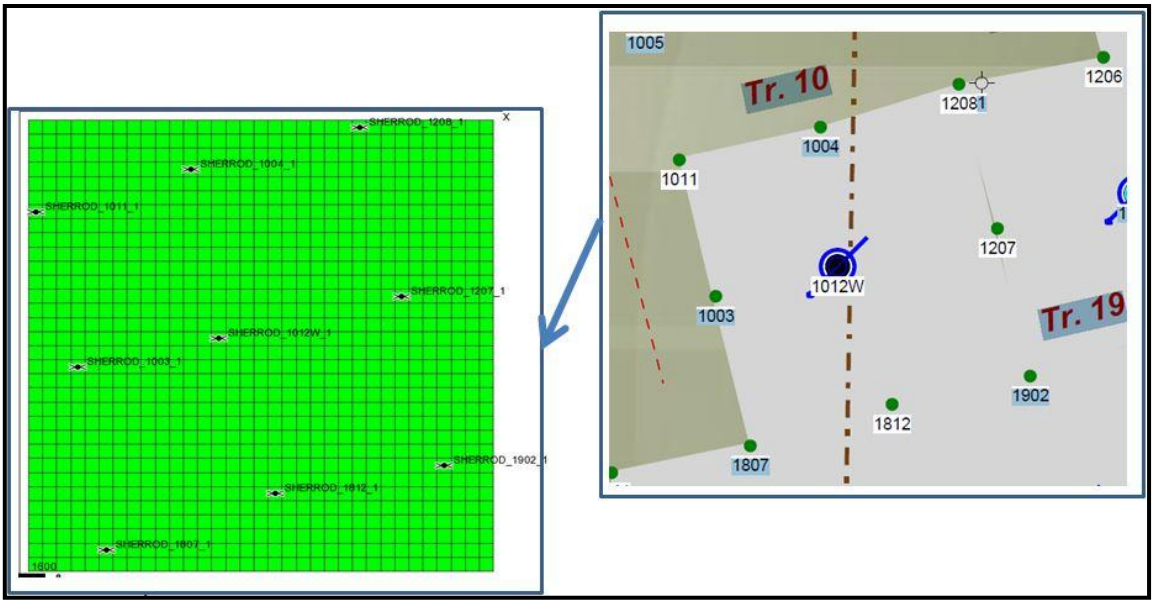

Figure 5.3 Sector model chosen as a case study for different simulators

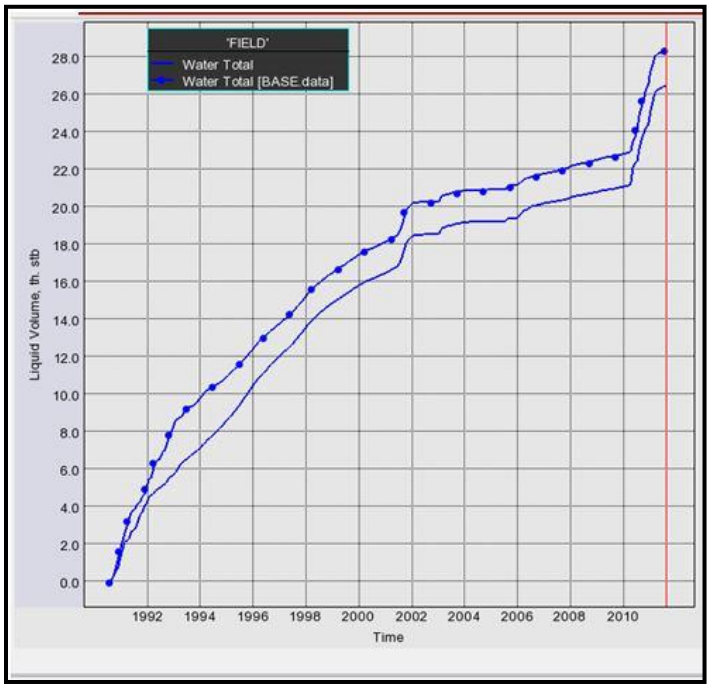

Figure 5.4: tNavigator water-cut solution effected by round off error

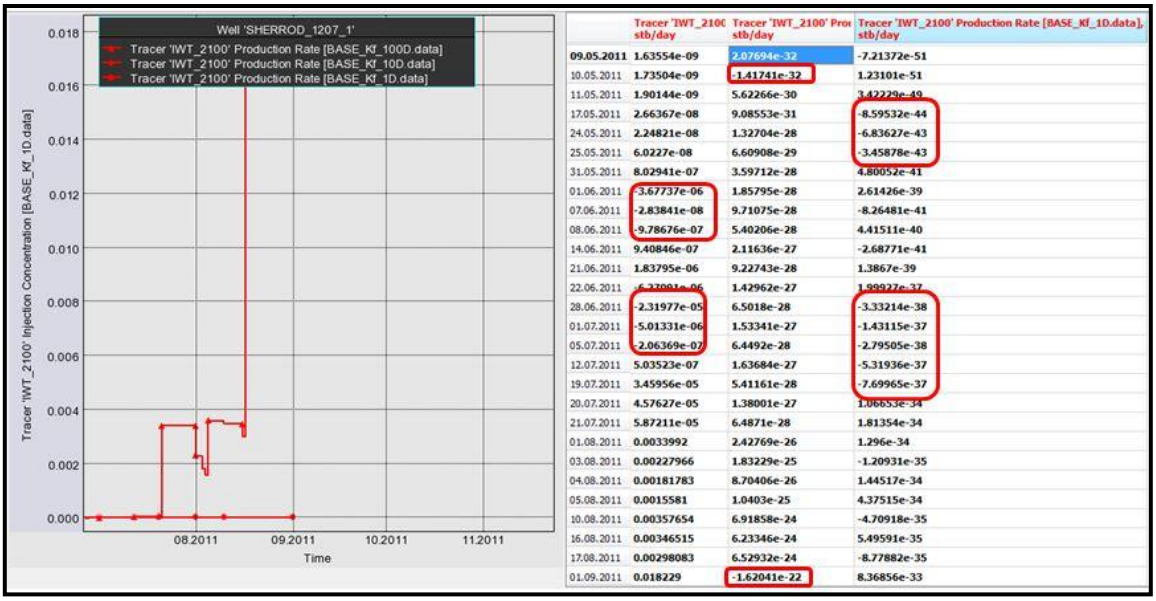

	Tracer 'IWT_2100' stb/day	Tracer 'IWT_2100' Prod stb/day	Tracer 'IWT_2100' Production Rate [BASE_Kf_1D.data], stb/day
09.05.2011	1.63554e-09	2.07694e-32	-7.21372e-51
10.05.2011	1.73504e-09	-1.41741e-32	1.23101e-51
11.05.2011	1.90144e-09	5.62266e-30	3.42229e-49
17.05.2011	2.66367e-08	9.08553e-31	-8.59532e-44
24.05.2011	2.24821e-08	1.32704e-28	-6.83627e-43
25.05.2011	6.0227e-08	6.60908e-29	-3.45878e-43
31.05.2011	8.02941e-07	3.59712e-28	4.80052e-41
01.06.2011	-3.67737e-06	1.85795e-28	2.61426e-39
07.06.2011	-2.83841e-08	9.71075e-28	-8.26481e-41
08.06.2011	-9.78676e-07	5.40206e-28	4.41511e-40
14.06.2011	9.40846e-07	2.11636e-27	-2.68771e-41
21.06.2011	1.83795e-06	9.22743e-28	1.3867e-39
22.06.2011	-6.37091e-06	1.42962e-27	1.99927e-37
28.06.2011	-2.31977e-05	6.5018e-28	-3.33214e-38
01.07.2011	-5.01331e-06	1.53341e-27	-1.43115e-37
05.07.2011	-2.06369e-07	6.4492e-28	-2.79505e-38
12.07.2011	5.03523e-07	1.63684e-27	-5.31936e-37
19.07.2011	3.45956e-05	5.41161e-28	-7.69965e-37
20.07.2011	4.57627e-05	1.38001e-27	1.06653e-34
21.07.2011	5.87211e-05	6.4871e-28	1.81354e-34
01.08.2011	0.0033992	2.42769e-26	1.296e-34
03.08.2011	0.00227966	1.83229e-25	-1.20931e-35
04.08.2011	0.00181783	8.70406e-26	1.44517e-34
05.08.2011	0.0015581	1.0403e-25	4.37515e-34
10.08.2011	0.00357654	6.91858e-24	-4.70918e-35
16.08.2011	0.00346515	6.23346e-24	5.49591e-35
17.08.2011	0.00298083	6.52932e-24	-8.77882e-35
01.09.2011	0.018229	-1.62041e-22	8.36856e-33

Figure 5.5: Oscillation in tNavigator tracer solution with unrealistic values

5.3 Two-Well Simulation Models & Sensitivities

5.3.1 Objectives

Two-well simulation models are sector models to model connectivity between a pair of injector and producer. Examples of possible two-well models are shown in Figure 5.6 below. The overall objectives of two-well simulation models include:

1. Assess flow path characteristic by matching tracer breakthrough and peak concentration through high resolution simulation models.
2. Utilization of fraction of water in communication between two pairs of wells (if applicable).
3. Assess dilution and saturation uncertainty by modifying initial saturation and concentration injected (if needed).

4. Use pseudo wells to model loss of tracer & water injected outside study area (if needed).

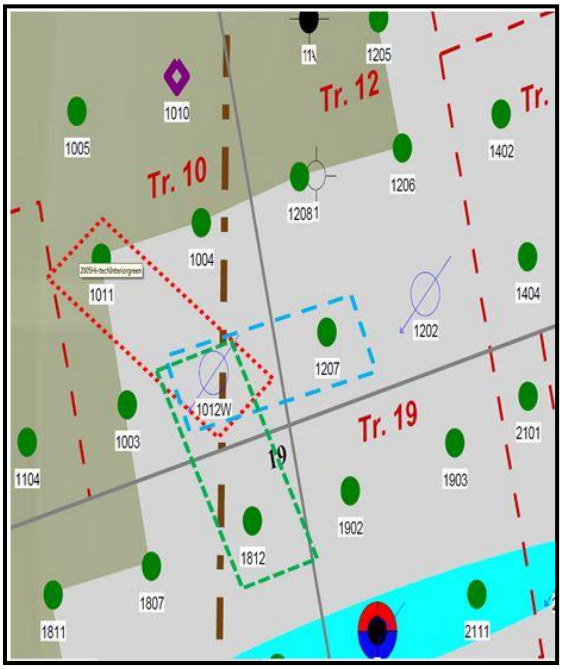

Figure 5.6: Examples of two-well simulation models

5.3.2 Approach Limitations

Two-well simulation models have the following limitations:

1. Effect of the interaction of the two wells with their surrounding via the complex fracture network is not captured.
2. Over-simplify connectivity
3. High uncertainty in drainage area surrounding the two wells

5.3.3 Case Studies

Three different phenomena observed in the field will be taken as case studies: First, tracer flow with ultra-high velocities from 6 injectors to producer "Ruby 18" which exists outside pattern injection area. This tracer movement is illustrated in Figures 5.7 and 5.8. Second, tracers flow with ultra-high velocities from the same injectors, but toward producer "Sherrod 1809" which exist on the opposite direction of "Ruby 18". This tracers' movement is illustrated in Figure 5.9. Third, the simple tracers movement indicated by tracers' responses with high recoveries (> 0.5%). This simple tracers' movement is illustrated in Figure 5.10 below using a schematic diagram showing tracer velocities and direction of movement around the first two rows of injectors north of pattern injection area.

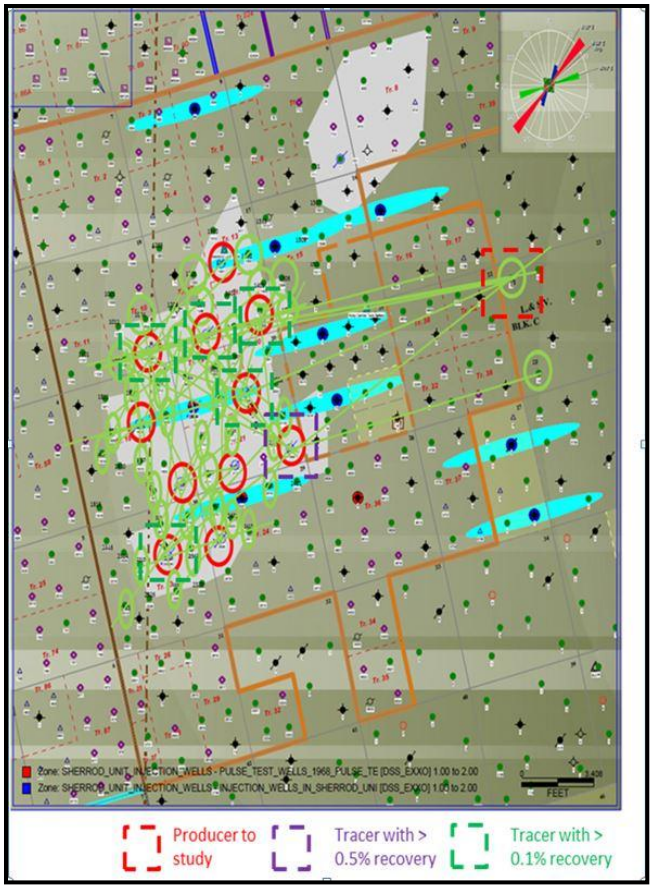

Figure 5.7: Field map of tracers movement toward 'Ruby 18' outside tracer study area

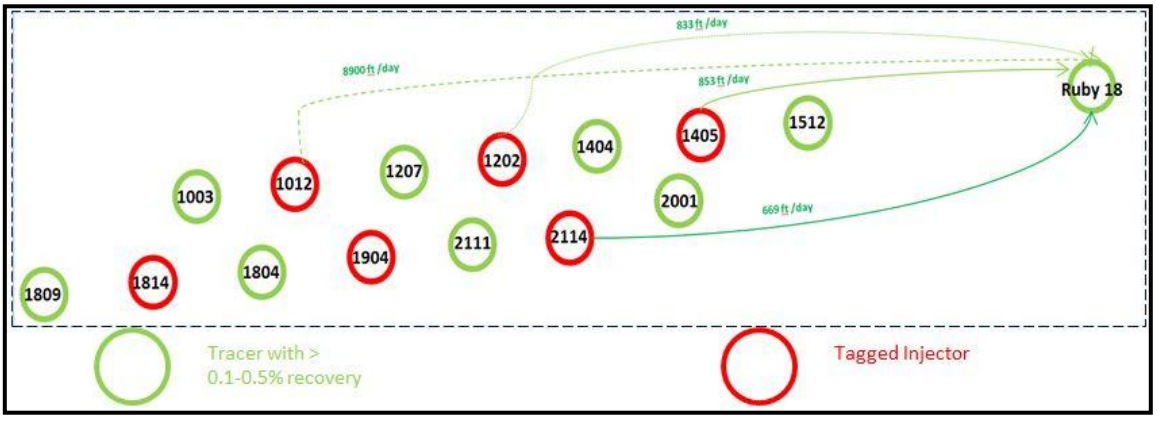

Figure 5.8: Diagram of tracers movement and velocities toward 'Ruby 18' outside tracer study area

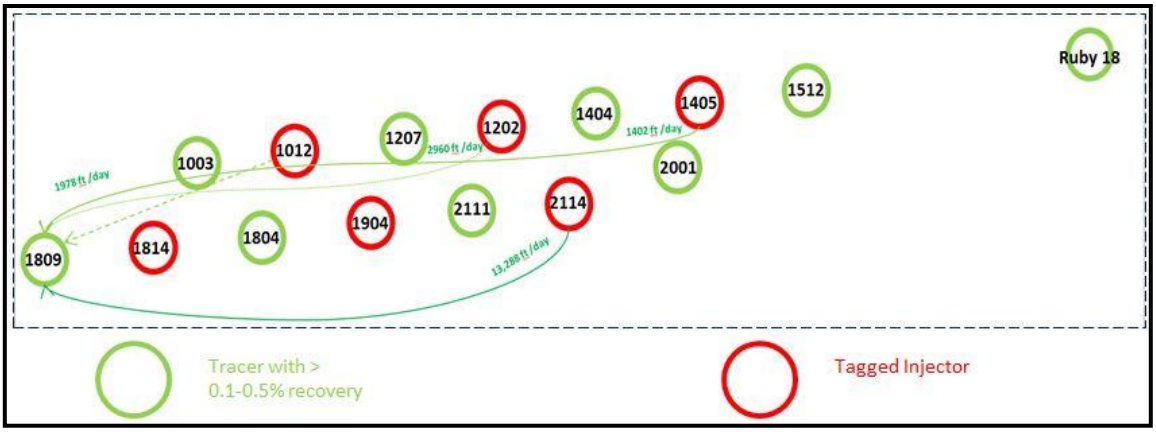

Figure 5.9: Diagram of tracers' movement and ultra-high velocities toward 'Sherrod 1809'.

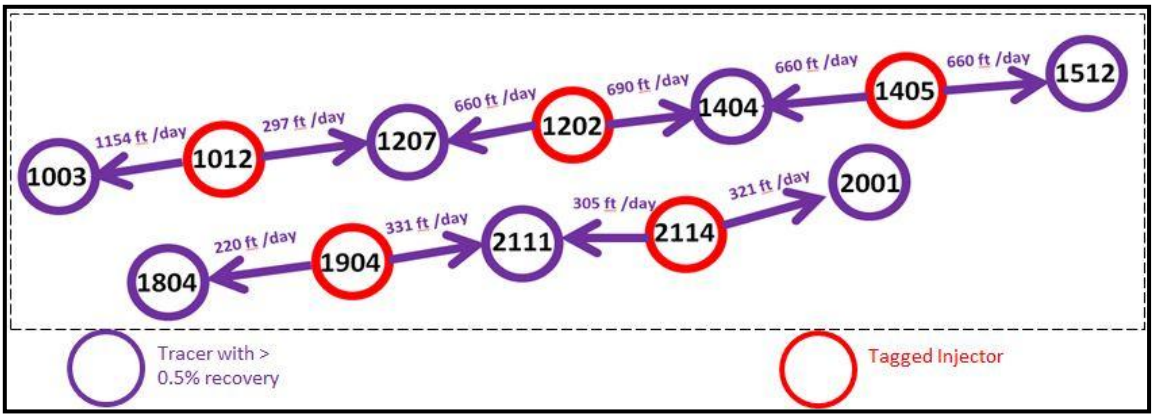

Figure 5.10: Tracers path and velocities for tracer recovery > 0.5%

5.3.4 Case Study I: Sensitivities & Tracer Flow outside Study Area

Multiple two-well simulation models were created to model tracer flow between a group of injectors and well 'Ruby 18' which exist outside pattern injection area. A list of injectors showing significant tracer recovery at 'Ruby 18' and their tracers' velocities are shown in Table 5.5 below. The tracer responses at Ruby18 are shown in Figure 5.11

below. This case study has two main objectives: First, investigate sensitivities of matrix and fracture parameters on tracer and water-cut responses. Second, model the ultra-high velocity, significant tracer recovery, and excessive tracer dilution observed between 'Ruby 18' and a group of injectors.

Injector	BT, days	Sampling uncertainty, days	Distance, ft	Velocity , ft/d
Sherrod 1202	8	4	6,664	833
Sherrod 1012	1	1	8,900	8,900
Sherrod 2114	6	4	4,012	669
Sherrod 1405	6	4	5,119	853
Sherrod 2325	5	4	9,274	1855
Sherrod 2118	5	4	2,081	416

Table 5.5: List of injectors with significant tracer show at 'Ruby 18'

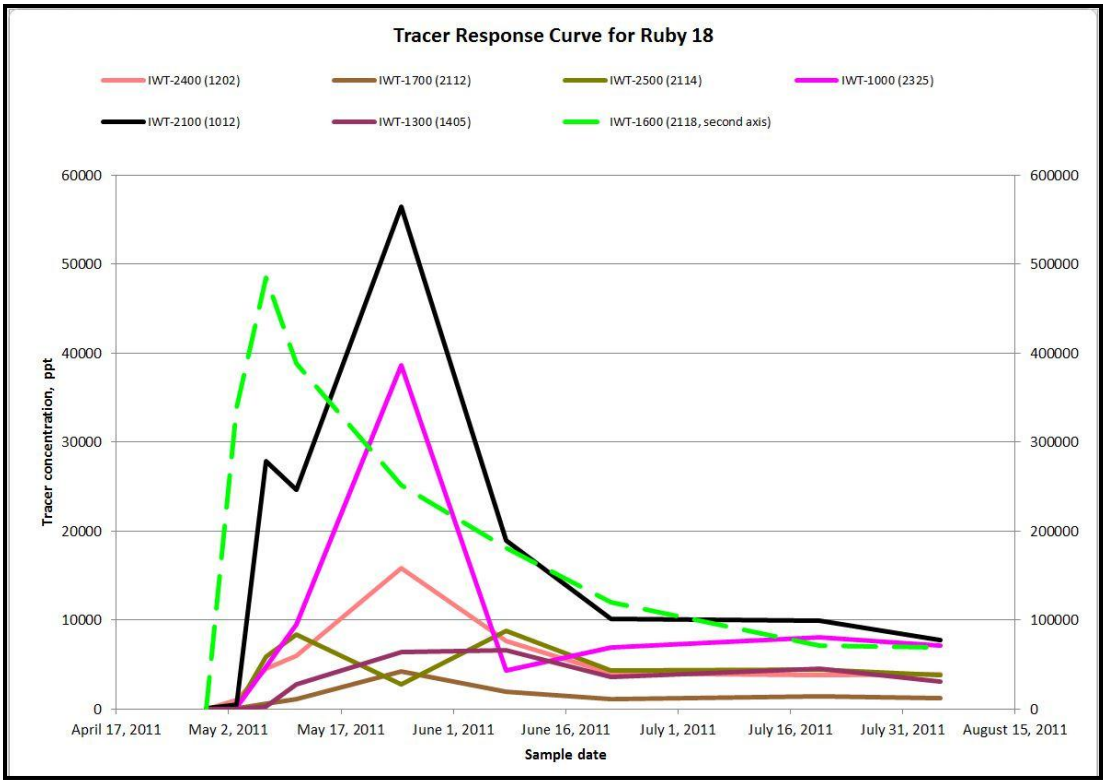

Figure 5.11: Tracer responses at 'Ruby 18' with significant tracer recovery

Base case for two-well simulation models was slightly changed to avoid running cases with no water and tracer breakthrough. This was done by slightly increasing initial water saturation and decreasing reservoir thickness. 'Sherrod 1012-Ruby18' simulation model was used to run sensitivities on initial water saturation, matrix and fracture properties, drainage area, grid resolution, and reservoir dispersive characteristics. Locations of the two wells are shown in Figure 5.12 below.

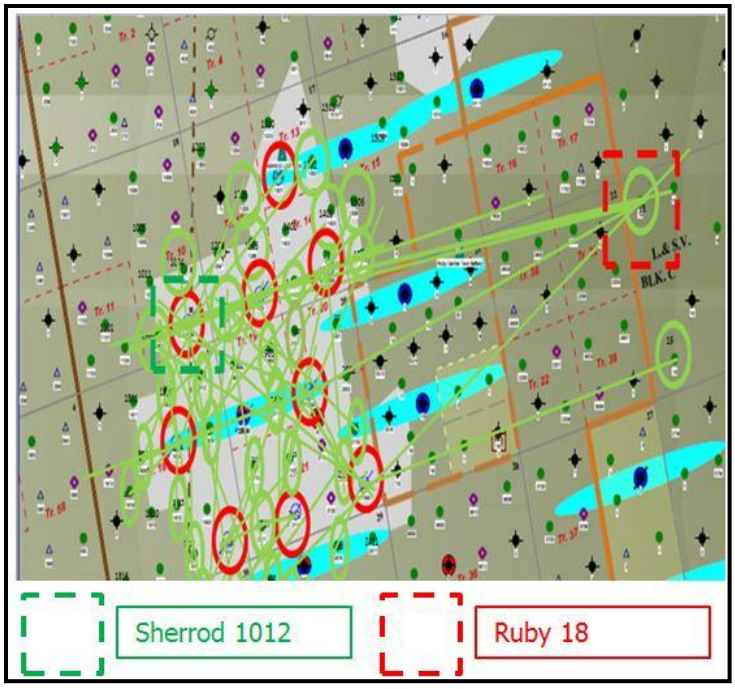

Figure 5.12: Map showing locations of 'Sherrod 1012' and 'Ruby 18'

5.3.4.1 Sensitivities on Initial Water Saturation

Sensitivities on initial water saturation of the matrix-fracture system are shown in Figures 5.13 and 5.14 below. While initial water saturation showed no impact on tracer response, it caused the water-cut response to shift vertically upward. A water-cut match is obtained by using fracture-matrix initial water saturation of 90%. Figure 5.15 shows that historical oil rates are achievable even with such high matrix-fracture saturation. This gives an indication that water and oil rates are contributed primarily by pore volume of the fracture system and matrix has insignificant impact on well performance.

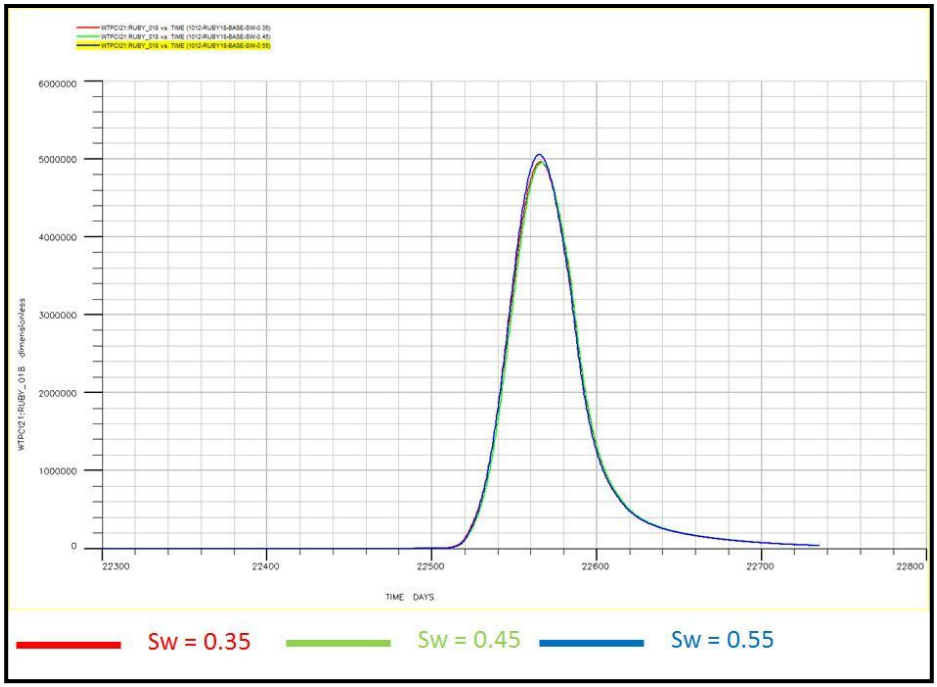

Figure 5.13: Effect of initial water saturation on tracer response at 'Ruby 18'

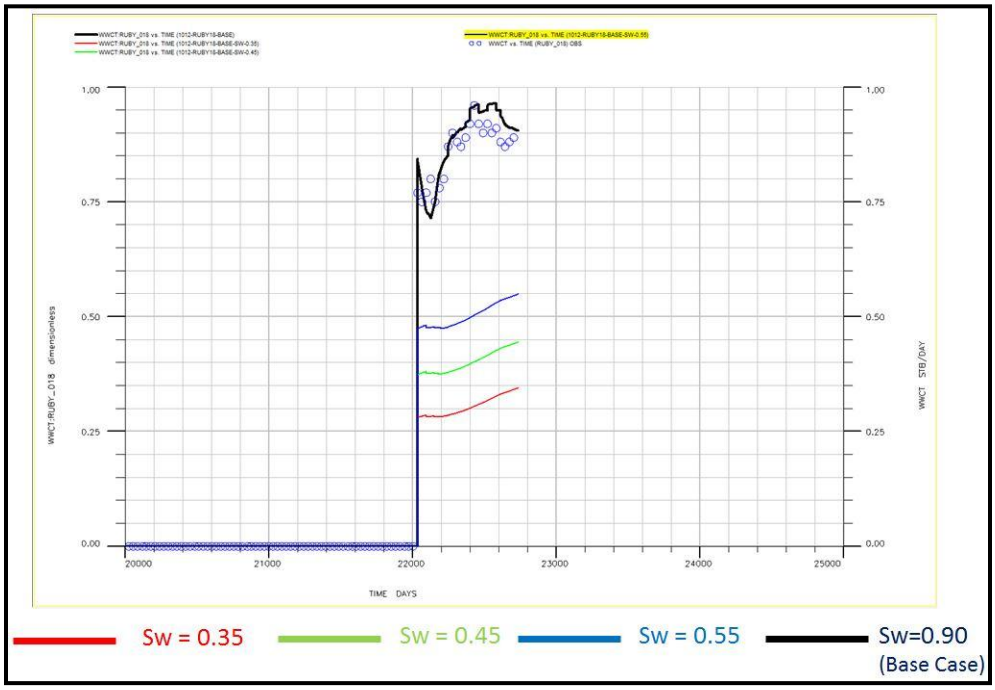

Figure 5.14: Effect of initial water saturation on 'Ruby 18' water-cut response

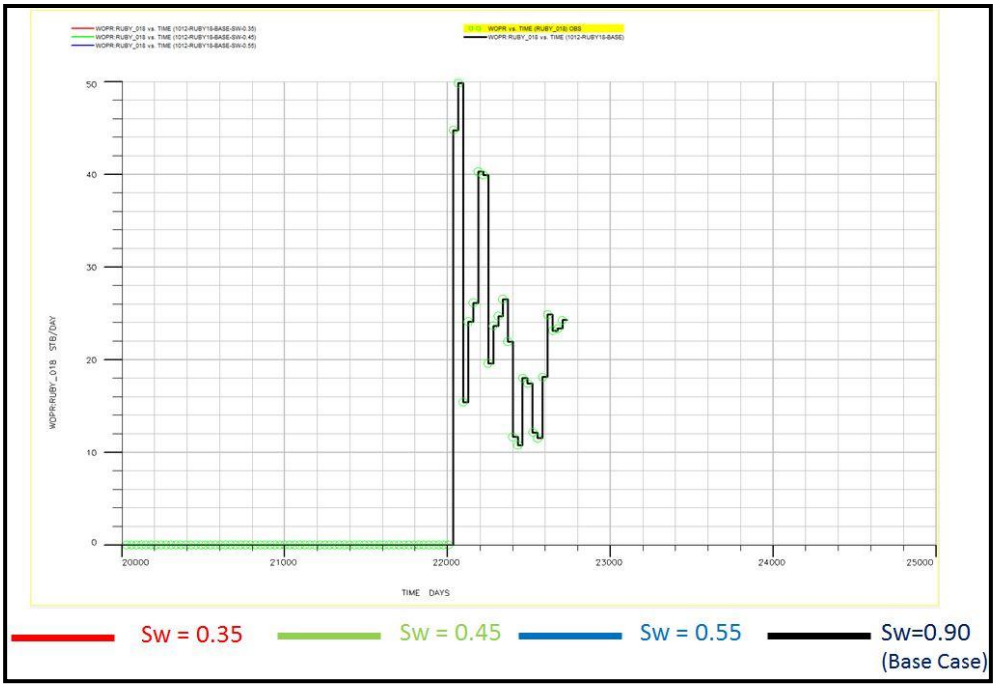

Figure 5.15: Effect of initial water saturation on deliverability of historical oil rate

5.3.4.2 Sensitivities on Fluid-Rock Interaction Functions

Sensitivities were made also on fluid-rock interaction functions. Maximum capillary pressure and exponents of oil-water relative permeability curves were varied to investigate their effect on the imbibition process of the matrix system. Capillary pressure and matrix relative permeability curves tested are shown in Figures 5.16 and 5.17, respectively. Both oil-water capillary pressure and relative permeability curve showed no impact on tracer responses. For capillary pressure, it plays a major role in controlling the distribution of injected water when initial saturation of the system is close to initial. In Sherrod, pre-production water invasion have caused initial saturation to be much higher than initial. Hence, capillary pressure is not expected to be of significant

importance. As for relative permeability curves, it did not show an impact due to the insignificant contribution of the matrix system to flow of oil and water as indicated earlier.

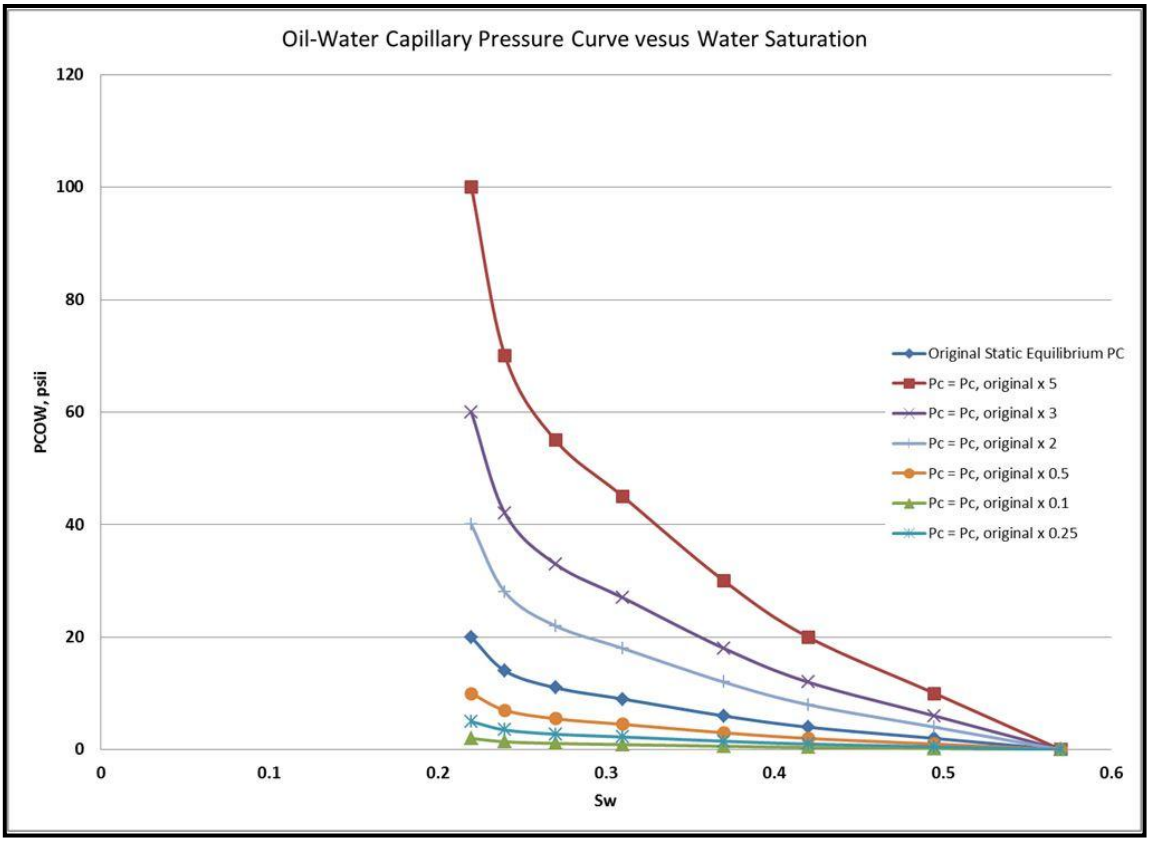

Figure 5.16: Sensitivities on imbibition capillary pressure curve

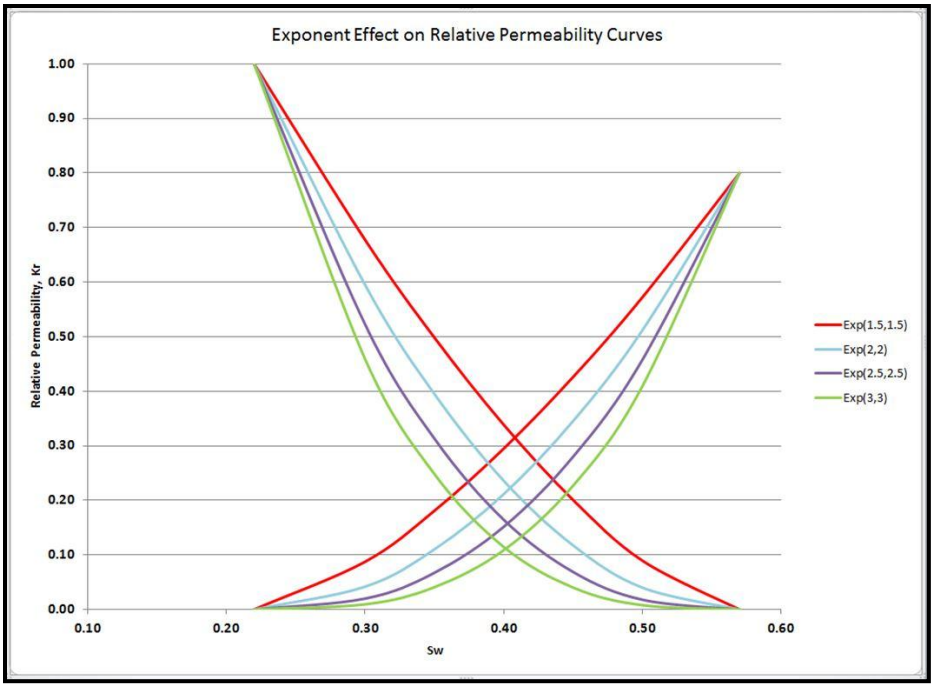

Figure 5.17: Sensitivity on matrix oil-water relative permeability curves

5.3.4.3 Sensitivities on Fracture Properties and Matrix-Fracture Interaction Function

Sensitivities made on fracture properties and matrix-fracture interaction function showed large impact on tracer responses for specific parameters. As for fracture permeability, it was varied from 200 md up to 10 darcies. Increasing fracture permeability showed no impact on tracer breakthrough time and insignificant impact on peak concentration produced and water-cuts. This is because tracer response is affected more by the system pore volume contacted rather than permeability. Performance plots are shown in Figures 5.18 and 5.19 below.

As for anisotropy in fracture permeability, K_{fy} / K_{fx} , it is highly effected by type of gridding and grid orientation. For sensitivity purposes, K_{fy} / K_{fx} was varied from 0.25 to

10.0 and the impact on tracer and water-cut are shown in Figures 5.20 and 5.21 below. Due to location of the wells on the corners of the model, a lower K_{fy} / K_{fx} cause the tracer to cover less drainage area and thus breakthrough faster. It was noticed for K_{fy} / K_{fx} below 0.25, oil rate constrain are not met. Moreover, for values equal or less than 0.01, solver start to crash due to severe convergence problems. Thus, fracture permeability anisotropy has an effect of limited range on tracer peak concentration and breakthrough.

As for Sigma, the shape factor, it shows no effect on tracer or water-cut response. Shape factor plays a major role in controlling the distribution of injected water-movement when initial saturation of the system is close to initial. In Sherrod, pre-production water invasion have caused initial saturation to be much higher than initial. Hence, shape factor did not show significant importance.

As for fracture pore volume, it appeared to be the most important parameter controlling tracer breakthrough time. If fracture pore volume was decreased, the tracer response will exhibit a faster breakthrough and a higher peak concentration produced. The higher peak simulated is because tracer contact smaller reservoir pore volume, while the faster tracer breakthrough is because less volume of water injected is required to achieve breakthrough. Figure 5.22 show the effect of changing fracture pore volume by changing thickness, while Figure 5.23 show the effect of changing fracture pore volume by changing fracture porosity. The effect of the two parameters is almost identical. Figure 5.24 overly thickness and fracture porosity effect and show that equal values of (φ_f h) product give same tracer solution given the same drawdown condition between a

given injector and producer. Figure 5.25 shows that fracture pore volume have no clear impact on water-cut.

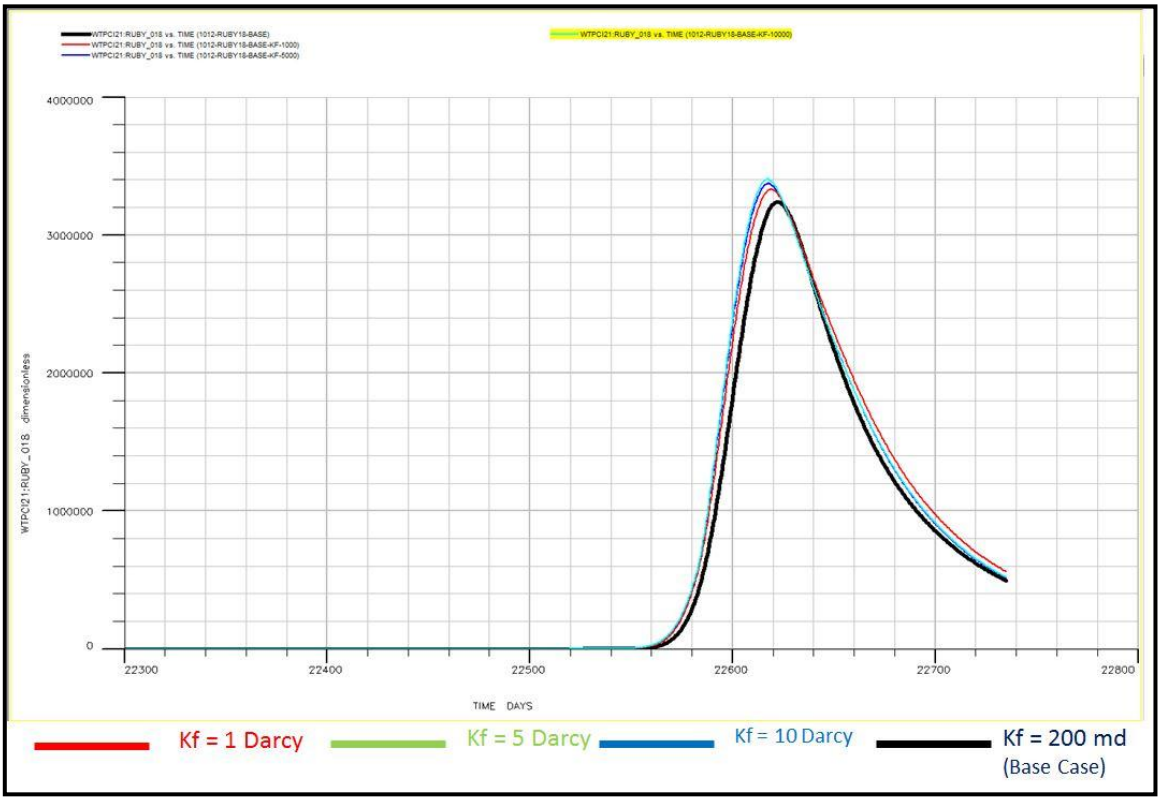

Figure 5.18: Effect of fracture permeability on tracer response

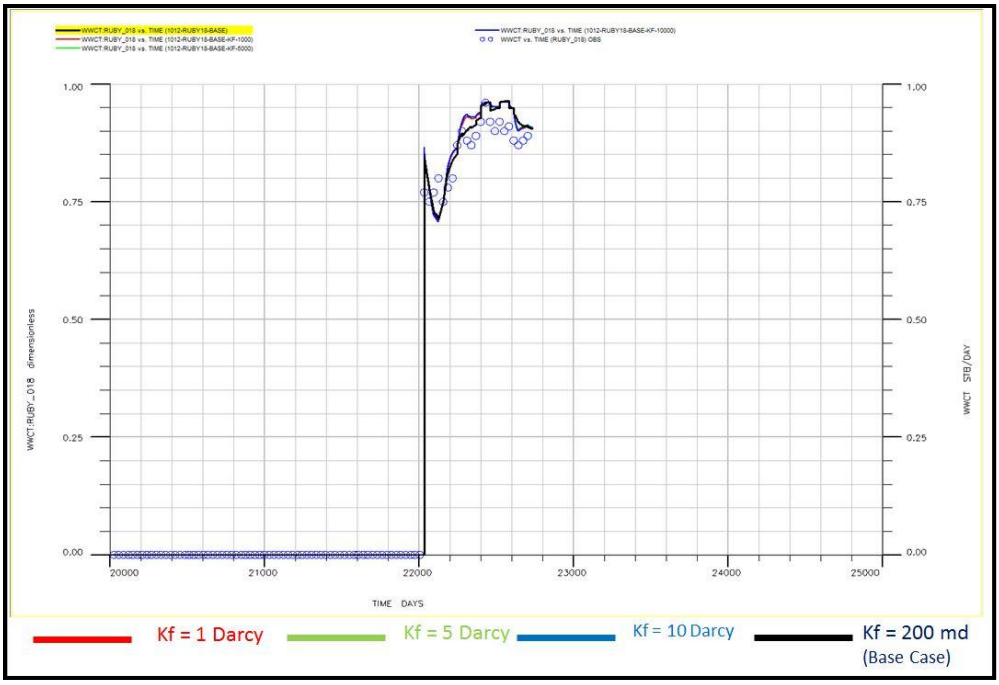

Figure 5.19: Effect of fracture permeability on water-cut

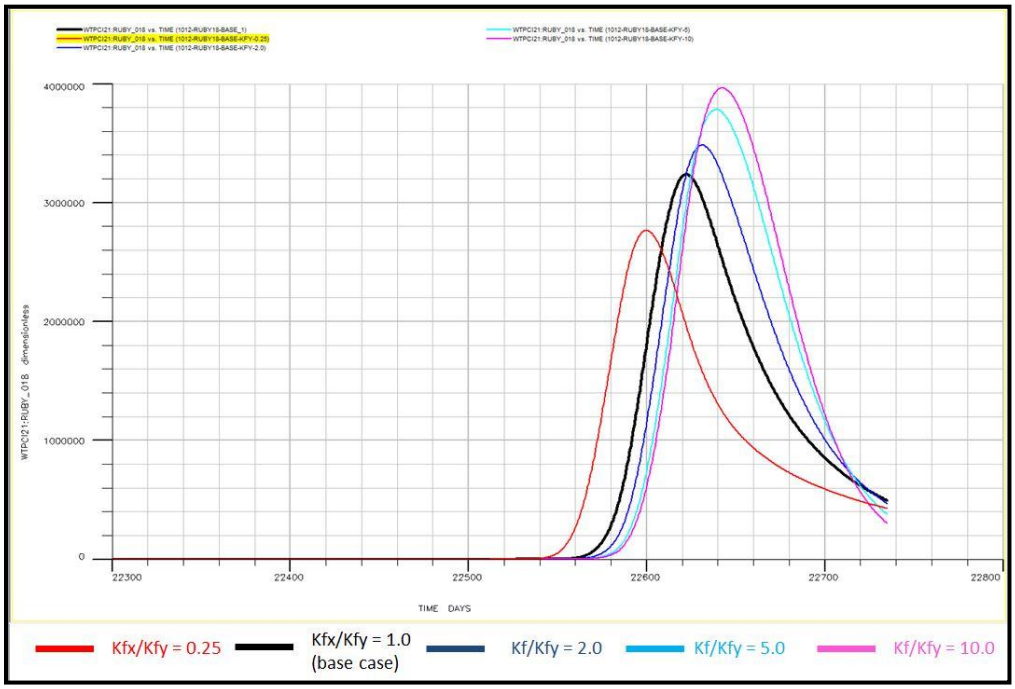

Figure 5.20: Effect of fracture permeability anisotropy on tracer response

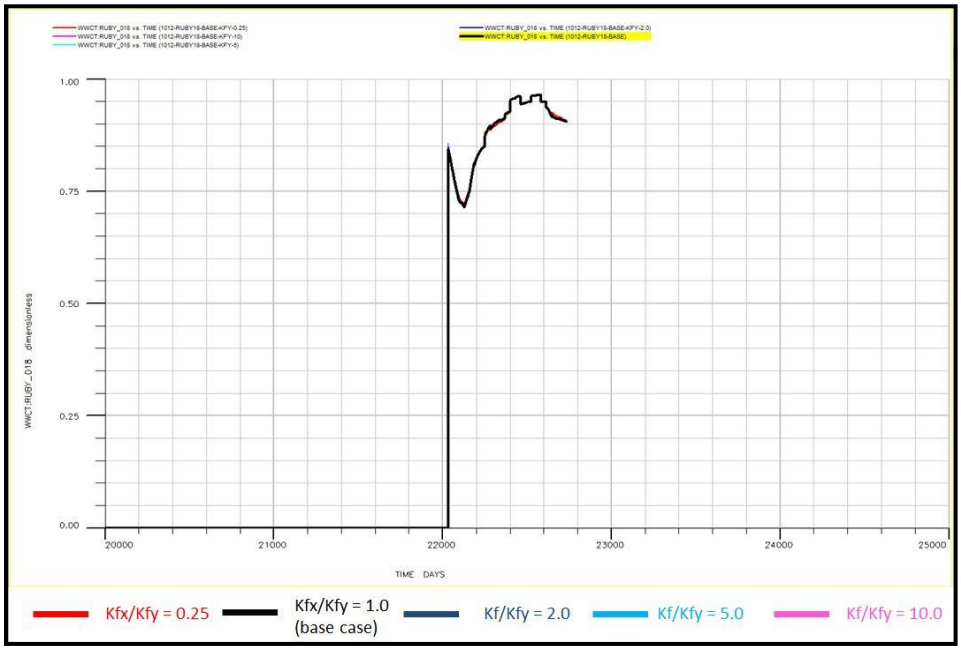

Figure 5.21: Effect of fracture permeability anisotropy on water-cut response

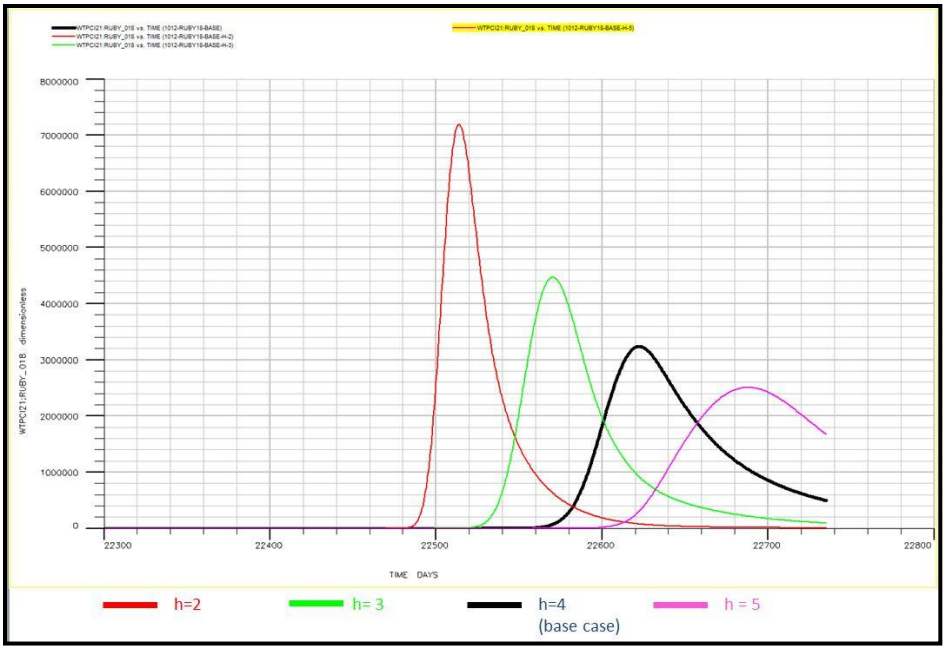

Figure 5.22: Effect of thickness on tracer responses

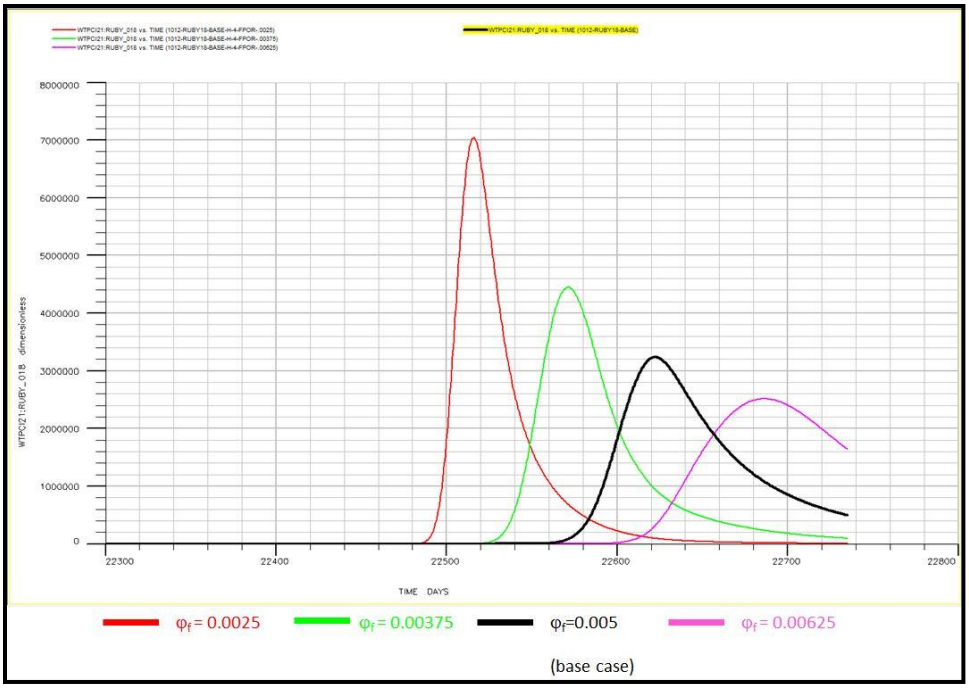

Figure 5.23: Effect of fracture porosity on tracer responses

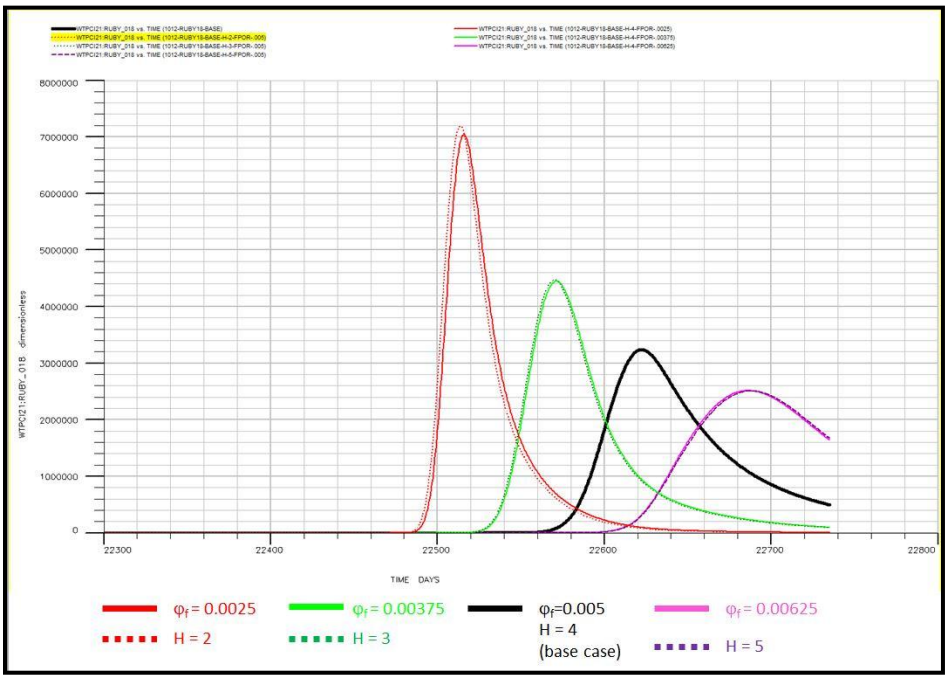

Figure 5.24: Identical tracer solutions for equal (φ_f h) product

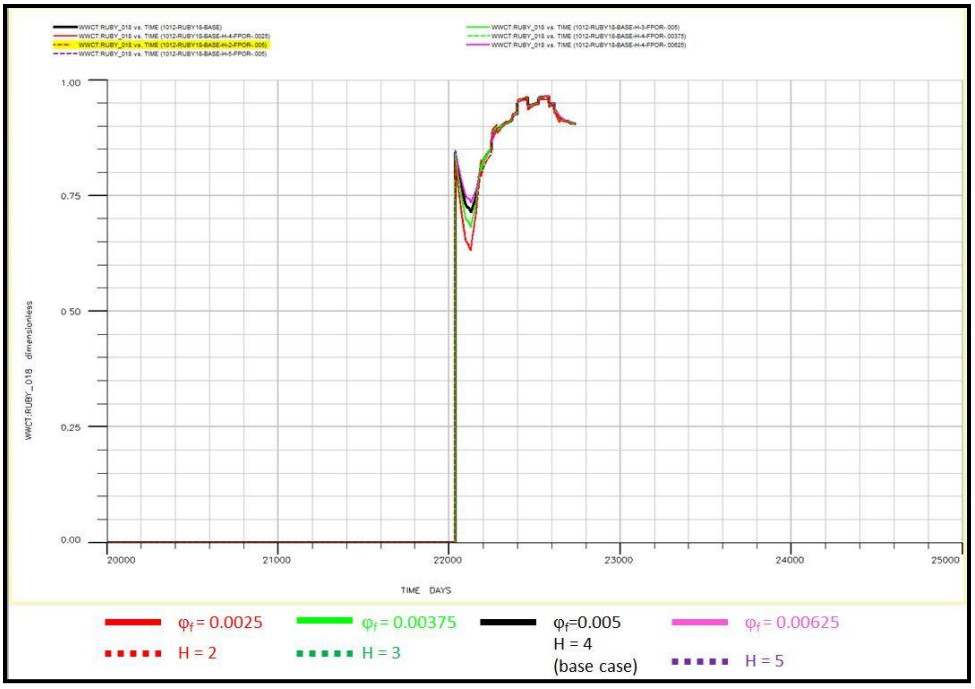

Figure 5.25: water-cuts of identical tracer solutions

5.3.4.4 Sensitivities on Matrix Properties

Sensitivities made on matrix properties showed weak impact on tracer and water-cut responses. As for matrix permeability, it was reduced and increased by a factor of 2 and 4. Figures 5.26 and 5.27 shows the weak impact of matrix permeability on tracer and water-cut responses. This is because these responses are dominantly controlled by the fracture system. Similarly, matrix porosity of base case was reduced and increased by a factor of 1.25 and 1.5. Figures 5.28 and 5.29 shows the weak impact of matrix porosity on tracer and water-cut responses. It should be noted that the weak impact of matrix porosity on water-production is due to the short production history of the pair understudy.

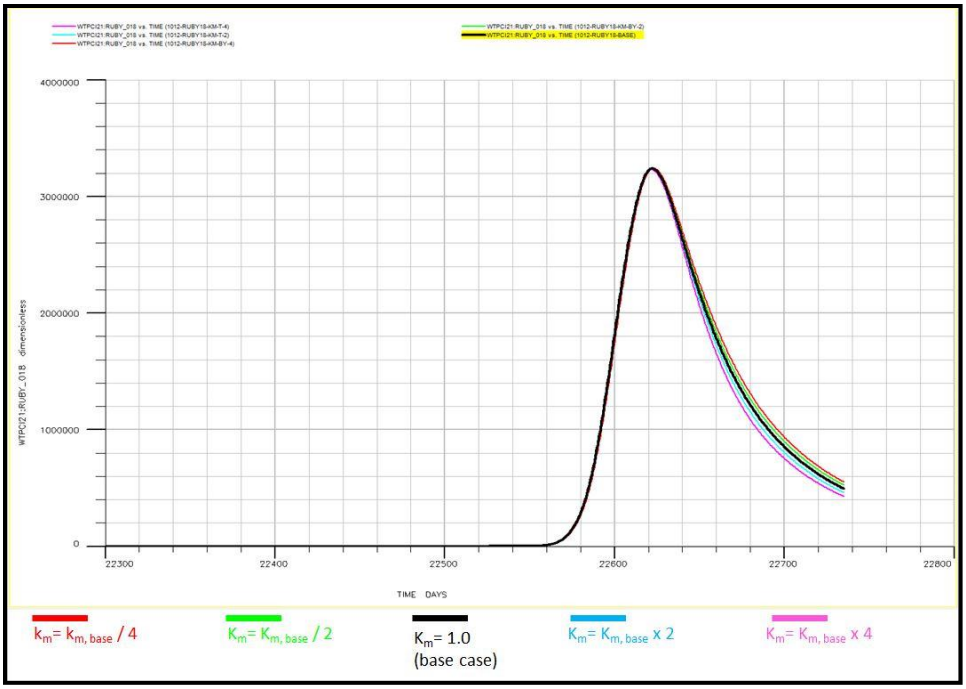

Figure 5.26: Effect of matrix permeability on tracer response

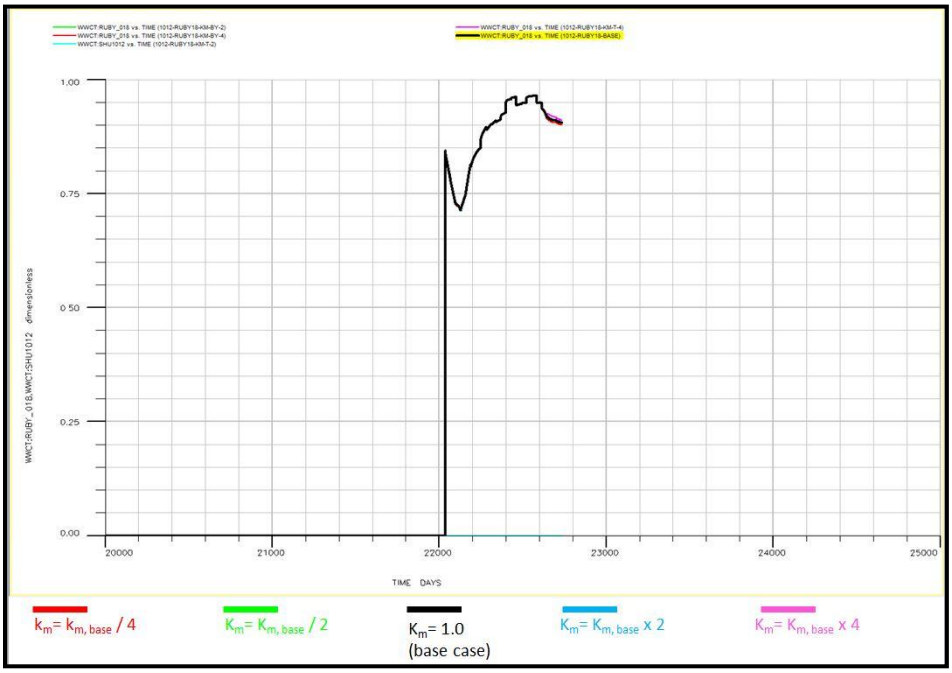

Figure 5.27: Effect of matrix permeability on water-cut

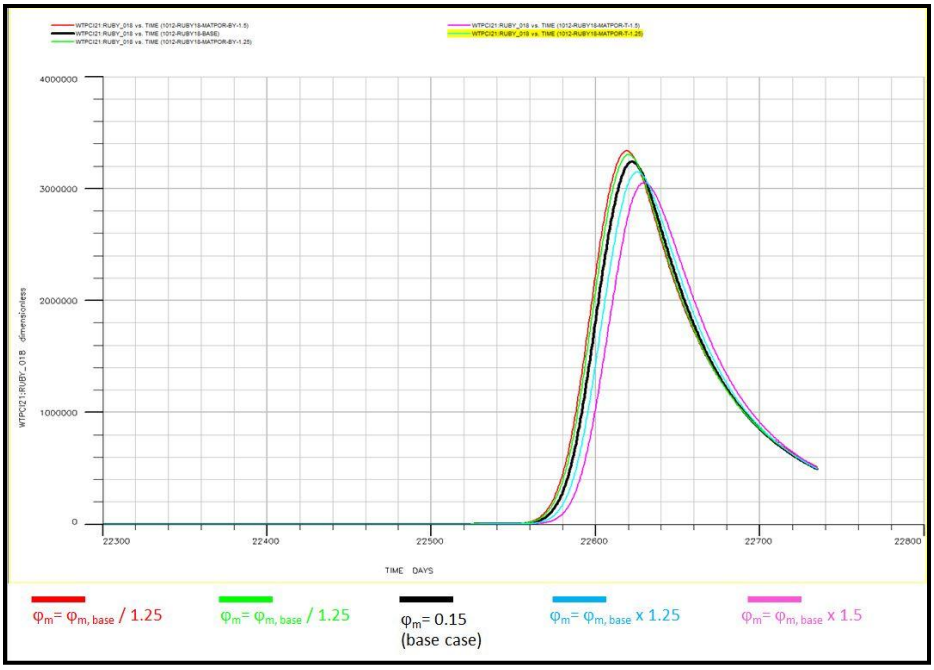

Figure 5.28: Effect of matrix porosity on tracer response

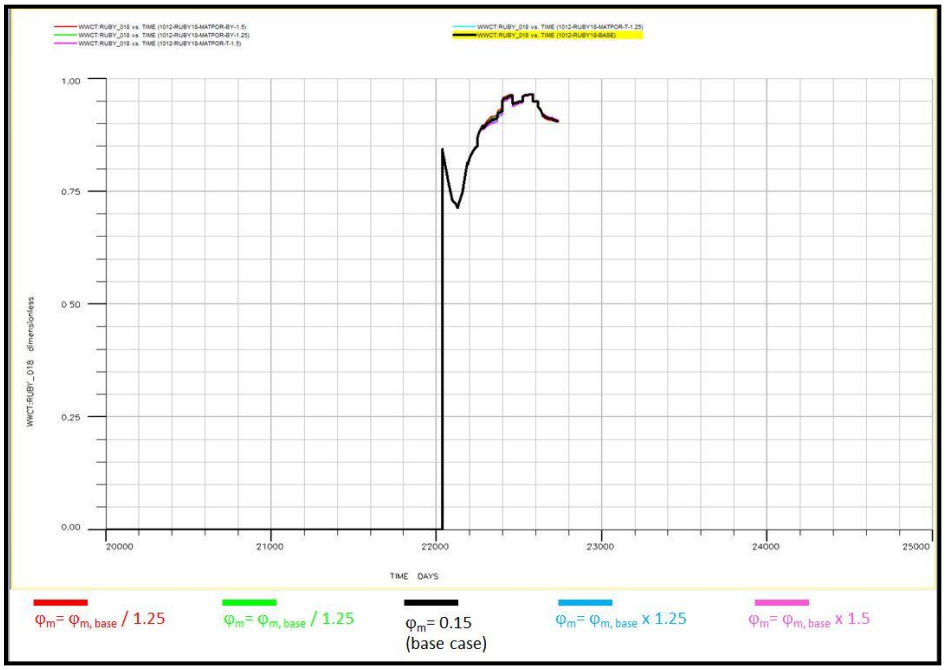

Figure 5.29: Effect of Matrix porosity on water-cut response

5.3.4.5 Sensitivities on Grid Design, Dilution, and Fraction of Water Injected

Sensitivities made on grid resolution, dilution, and fraction of injection rate in communication between the well pair showed a varying degree of impact on tracer responses. As for grid resolution, grid size of base case was reduced and increased by a factor of 1.5 and 2. As shown in Figure 5.30 below, changing size of grid cells have a large impact on tracer breakthrough time and peak concentration produced. This highlight that tracer breakthrough and peak concentration produced has a strong bias toward grid design.

As for drainage area surrounding the two wells, it was increased by a factor of 1.15 and 1.3 while keeping well distances the same. As shown in Figure 5.31 below, increasing drainage area showed large impact on tracer breakthrough and peak concentration produced. This is because a larger drainage areas cause the tracer to be more dispersed contacting more reservoir pore volume. As a result of contacting larger reservoir pore volume, breakthrough is delayed and the response appears to be more diluted.

To study the effect of dilution on tracer response, the process of mixing tracer with injected water is studied. Figure 5.32 show the effect of varying injection rate during the mixing process on the concentration injected. Concentration injected is a key input because it is used as a boundary condition to solve the tracer partial differential equation. For the concentration of tracer injected to be more diluted than what is initially calculated is very likely to happen. This is due to the inter-connectivity of a number of Sherrod pattern injectors which will cause the wellbore of the injector to receive water

from nearby wells. Effect of initial concentration injected on tracer response is shown in Figure 5.33 below. Initial concentration is only used to scale the response and it does not affect breakthrough time or shape of curve.

To investigate the effect of losing injected water to outside study area, a fraction of the actual injection rate is used to model water produced at 'Ruby 18' from 'Sherrod 1012'. Figure 5.34 shows the effect of using various fractions of 'Sherrod 1012' injection rates on tracer response. As fraction of injection rate is lowered, less drawdown is created between the pair of injector and producer. As a result, tracer breakthrough is delayed and peak concentration produced reflects a more diluted response.

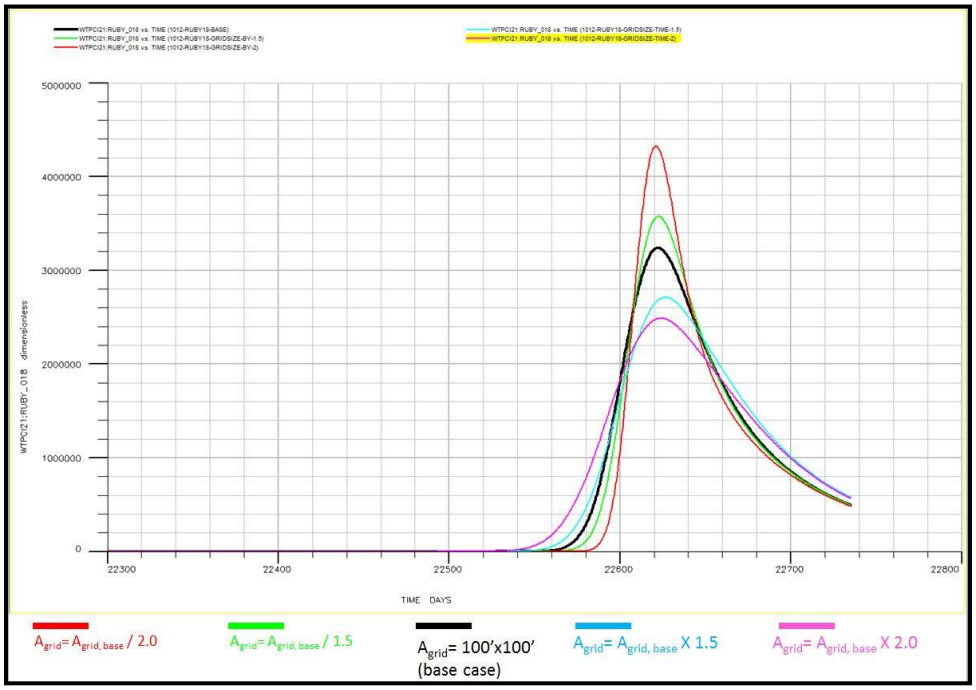

Figure 5.30: Effect of grid resolution on tracer response

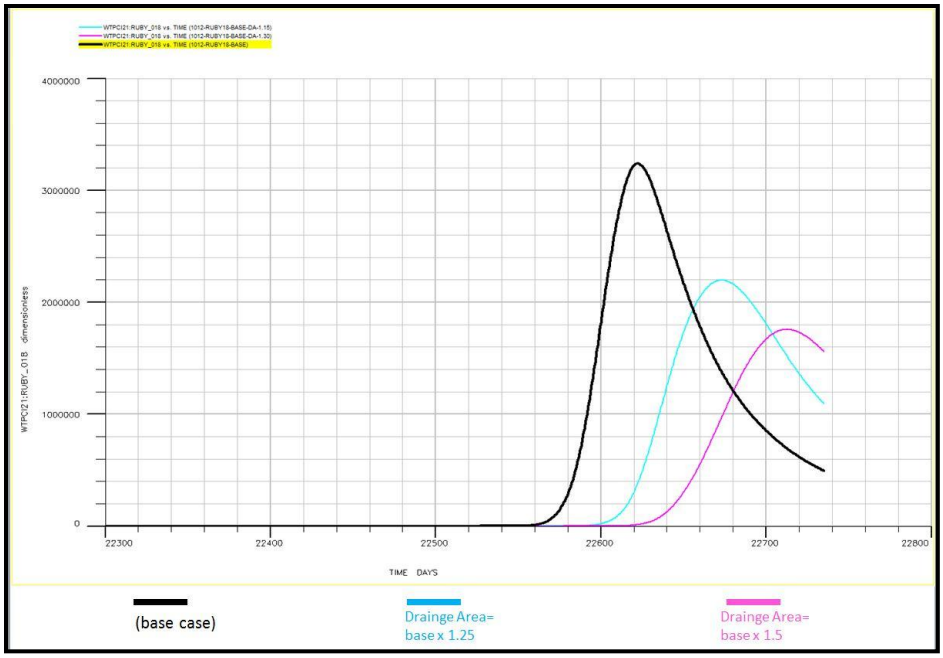

Figure 5.31: Effect of increasing drainage area around wells on tracer solution

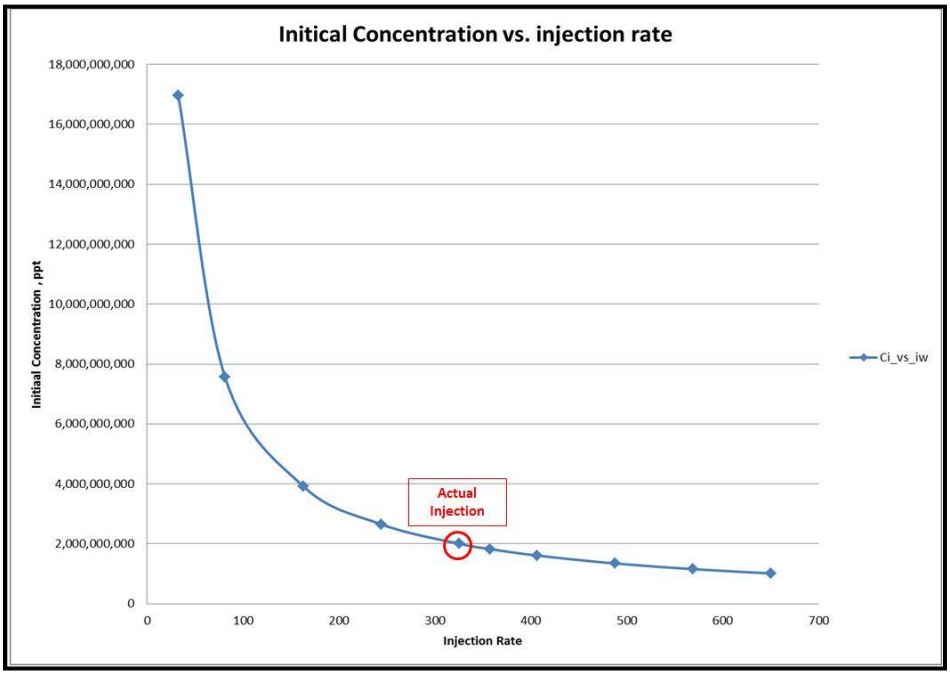

Figure 5.32: Effect of mixing injection rate used on injected concentration

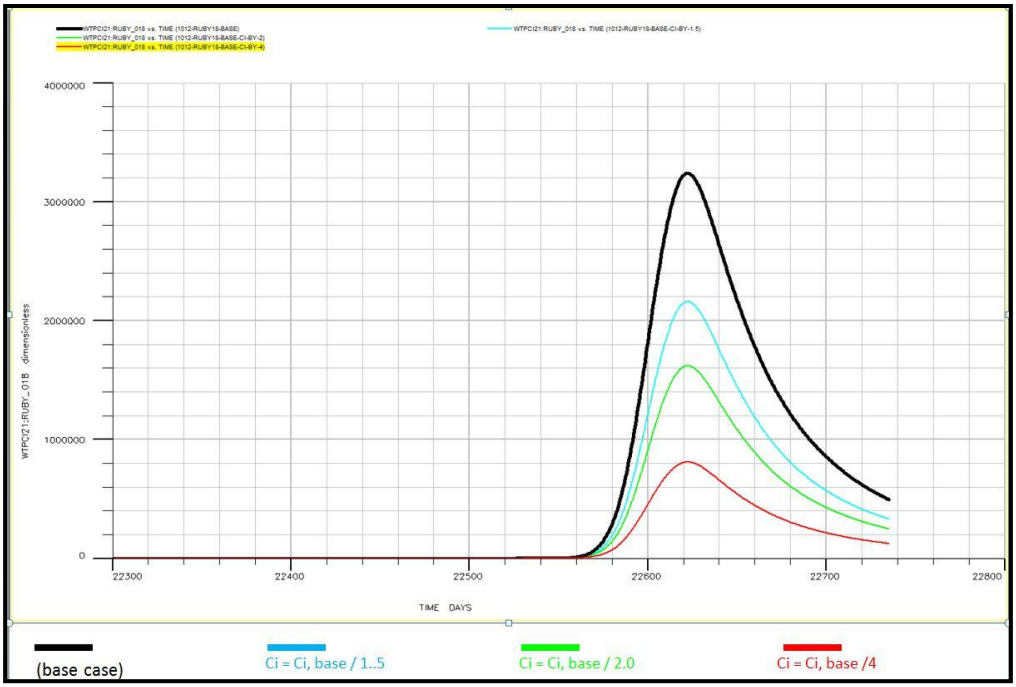

Figure 5.33: Effect of injection concentration on tracer response

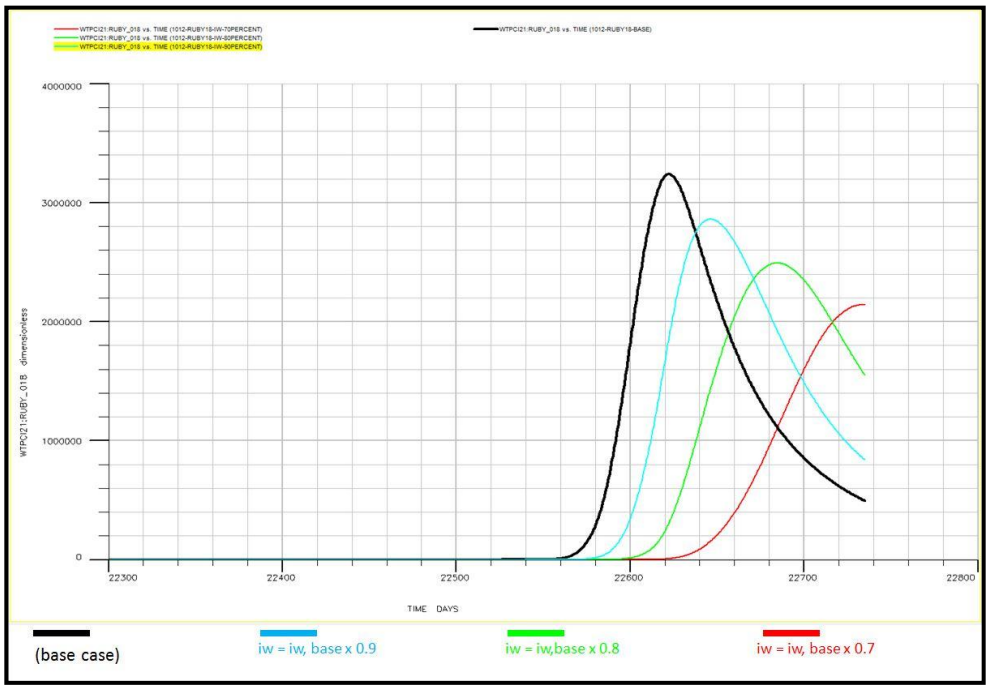

Figure 5.34: Effect of fraction of injection rate on tracer response

5.3.4.6 Sensitivities on Reservoir Dispersive Characteristics

Reservoir dispersive characteristics have two components: longitudinal dispersion, and transverse dispersion. Several studies indicated that transverse dispersion is insignificant with respect to longitudinal dispersion. Hence, only the first component is studied. With the absence of any information about longitudinal dispersion, the full range allowable by Eclipse dual porosity solver was tested. Sensitivity showed that solver is unable to handle longitudinal dispersion lower than 0.01 and higher than 400. Tracer responses for several values between the upper limit and lower limit are shown in Figure 5.35 below. Longitudinal dispersion has strong impact on breakthrough time, peak concentration, and width of the response.

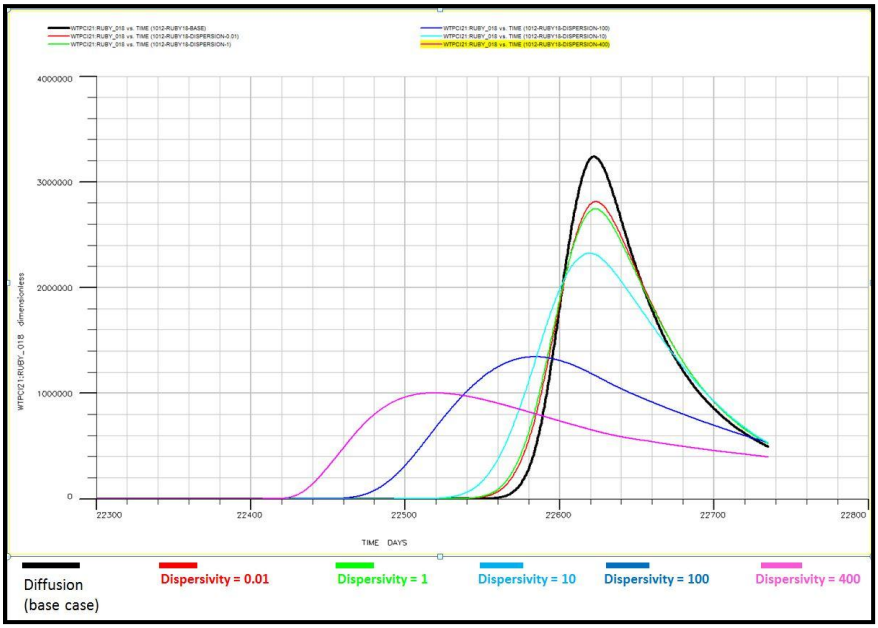

Figure 5.35: Effect of longitudinal dispersion on tracer response.

5.3.4.7 Summary of Tracer and Water-cut Sensitivities

A summary on sensitivities is shown in Table 5.6 below. Out of all reservoir parameters investigated, tracers responses are dominantly affected by fracture porosity-thickness product, fracture permeability anisotropy, and longitudinal dispersion. It is important to highlight that non-reservoir parameters also have significant impact on tracer response like dilution effect, grid cell resolution, drainage area of simulation model, and fraction of injected water in direct communication.

For water-cut response, it is affected dominantly by three parameters: water saturation of the fracture system, matrix porosity, and thickness. Unlike tracer response were non-reservoir parameters have large impact, water-cut is only affected by reservoir parameters.

Property	Tracer's BT	Tracer's Peak	Tracer's Width	Water Cut
Swi	X	X	X	√
thickness	√	√	√	√
φ_f	√	√	√	X
Dispersion	√	√	√	X
Dilution	X	√	√	X
K_f	X	X	X	X
K_{fy}/K_{fx}	√	√	√	X
Pc	X	X	X	X
σ	X	X	X	X
φ_m	X	~	~	√
K_m	X	X	X	X
K_{rwo}	X	X	X	X
Grid Resolution	√	√	√	√
Drainge Area	√	√	√	X
i_w fraction	√	√	√	X

Table 5.6: Summary of water-cut and tracer response sensitivities.

5.3.4.8 Matching Abnormal Tracer Velocity: Sherrod 1012 – Ruby 18

Tracer flow between the pair 'Sherrod 1012 – Ruby 18' exhibited unique tracer response. Tracer traveled with a velocity of 8,900 ft / day toward 'Ruby 18' which exist outside patterns injection area. Tracer appeared 1 day after tracer injection with the first water sample. Although breakthrough was fast, the tracer response exhibited excessive

dilution showing tracer recovery of only 0.3%. The tracer response and the locations of the two wells are shown Figures 5.36 and 5.37 below, respectively.

As tracer breakthrough time is primarily driven by fracture pore volume, Figure 5.38 below shows the linear relation observed while attempting to match tracer breakthrough time by changing (φ_f h). The slope of the line remains constant as long as the drawdown between the two wells remains unchanged. This linear relation obtained through large number of simulation runs indicates that a breakthrough of 1 day is not mathematically possible using fracture properties alone. This supports the hypothesis of the presence of an external water source flowing to Sherrod Area which creates both high tracer velocities and excessive dilution. This phenomenon is modeled by introducing a pseudo injector and a pseudo producer acting 1000 feet away from the two wells to create a higher drawdown or a 'stream'. Stream injection rates tested were between 0 – 18,000 stb/d. Pseudo producer operates at injection to production ratio (IPR) of 2 for all cases. Eclipse dual porosity solver start to crash for cases with stream injection rate higher than 18,000 stb/d. A schematic of the simulation model design is shown in Figure 5.39 below. Figure 5.40 summarizes simulation attempts to match a tracer breakthrough of 1 day and shows how the linear relation between (φ_f h) product and tracer breakthrough time changes under different drawdown conditions. Maximum achievable tracer velocity was 2,225 ft / day which represent only 25% of the actual velocity observed.

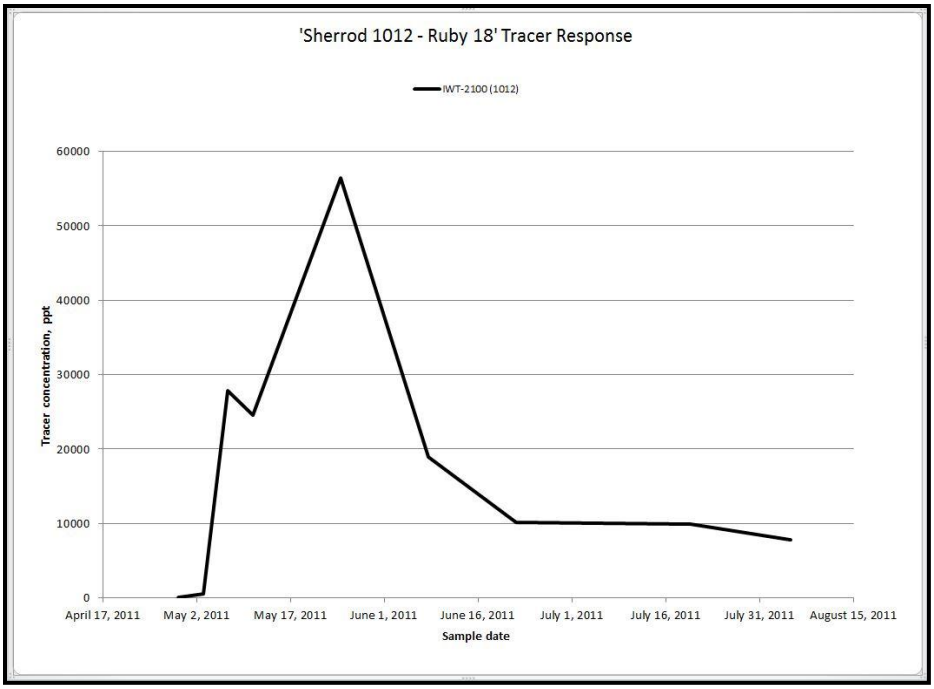

Figure 5.36: Tracer response at ‘Ruby 18’ from injector ‘Sherrod 1012’

’.

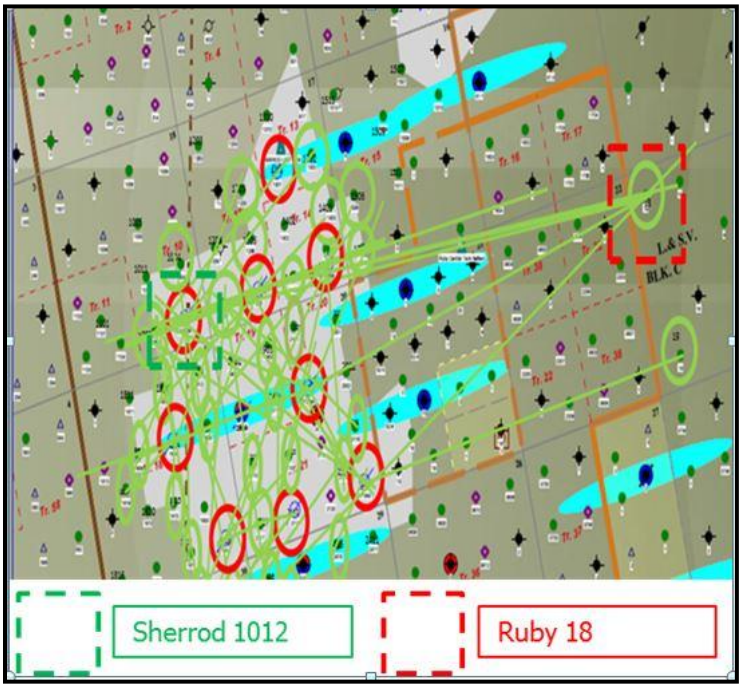

Figure 5.37: Locations of well pair: ‘Ruby 18’ and ‘Sherrod 1012’.

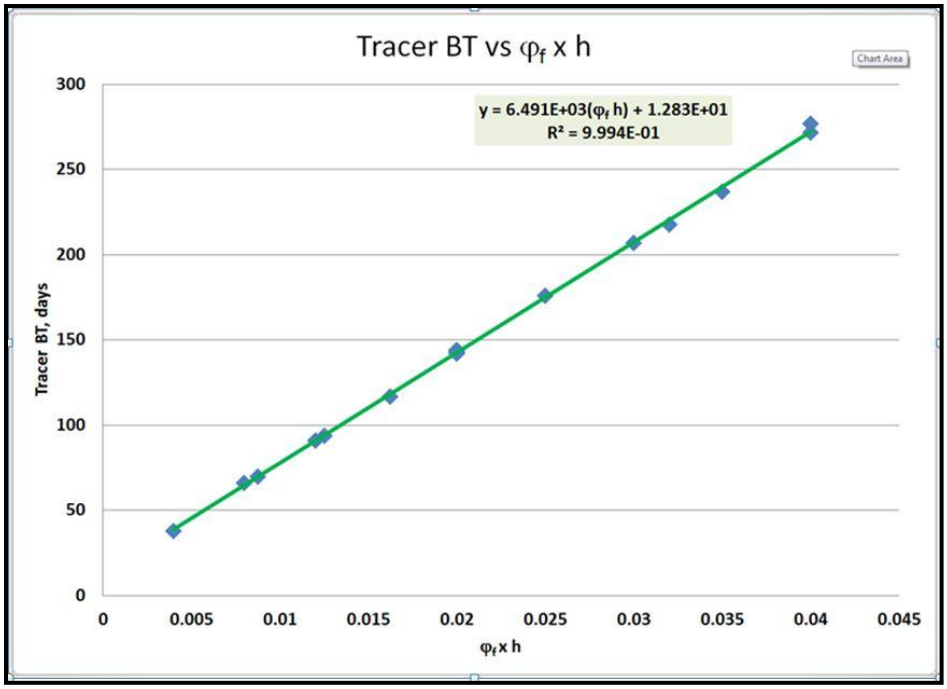

Figure 5.38: Linear relation observed between tracer breakthrough time and (φ_f h).

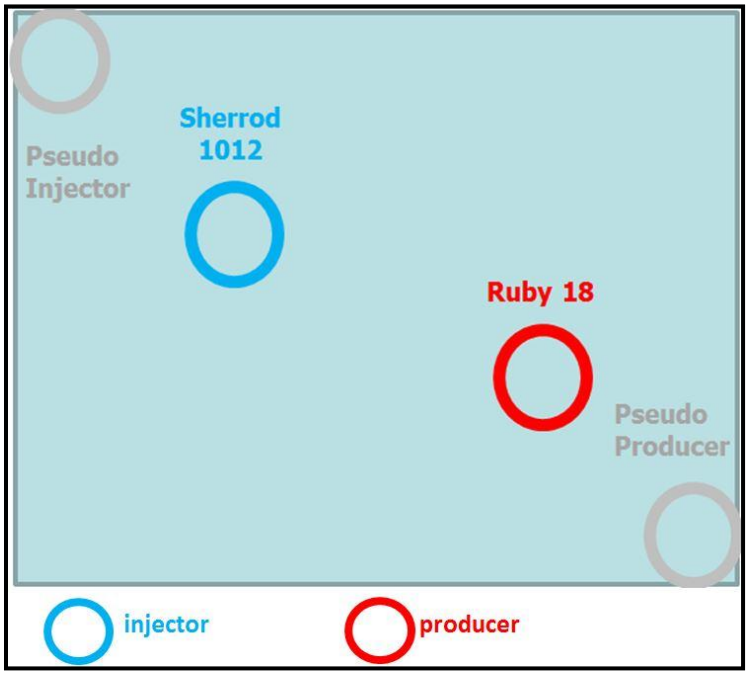

Figure 5.39: Schematic of 'Sherrod 1012 – Ruby 18' Simulation Model with pseudo wells

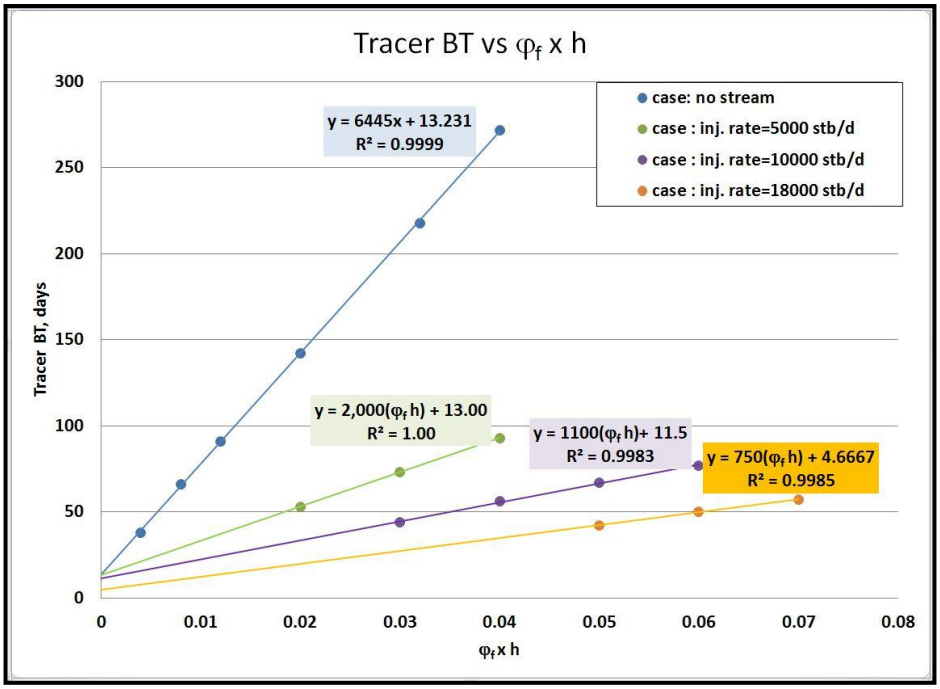

Figure 5.40: Tracer BT versus (φ_f h) for different drawdown conditions

5.3.4.9 Matching Tracer Flow outside Study Area

Matching moderate tracer velocities in the range of 669 – 853 ft /day was achievable by modifying (φ_f h) product as mentioned in the previous sub-section. Peak concentration was matched by modifying concentration injected to account for dilution caused by water flow from nearby injectors. Figure 5.41 show a match of the tracer response between the pair 'Sherrod 2114 - Ruby 18' using a fracture porosity-thickness product of 0.006. Figure 5.42 shows that the observed tracer response between the pair 'Sherrod 1405 – Ruby 18' appears as a dual peak tracer response due to miss-sampling. The three simulated peaks correspond to fracture porosity thickness product of 0.003, 0.00475, and 0.005, respectively. Locations of the wells Sherrod 2114, Sherrod 1405,

and Ruby 18 are shown in Figure 5.43 below. Assuming a fracture porosity of 0.5%, these tracers reflect movement in highly stratified and fractured thin layers with 0.6-1 ft extending for vast distances outside tracer study area.

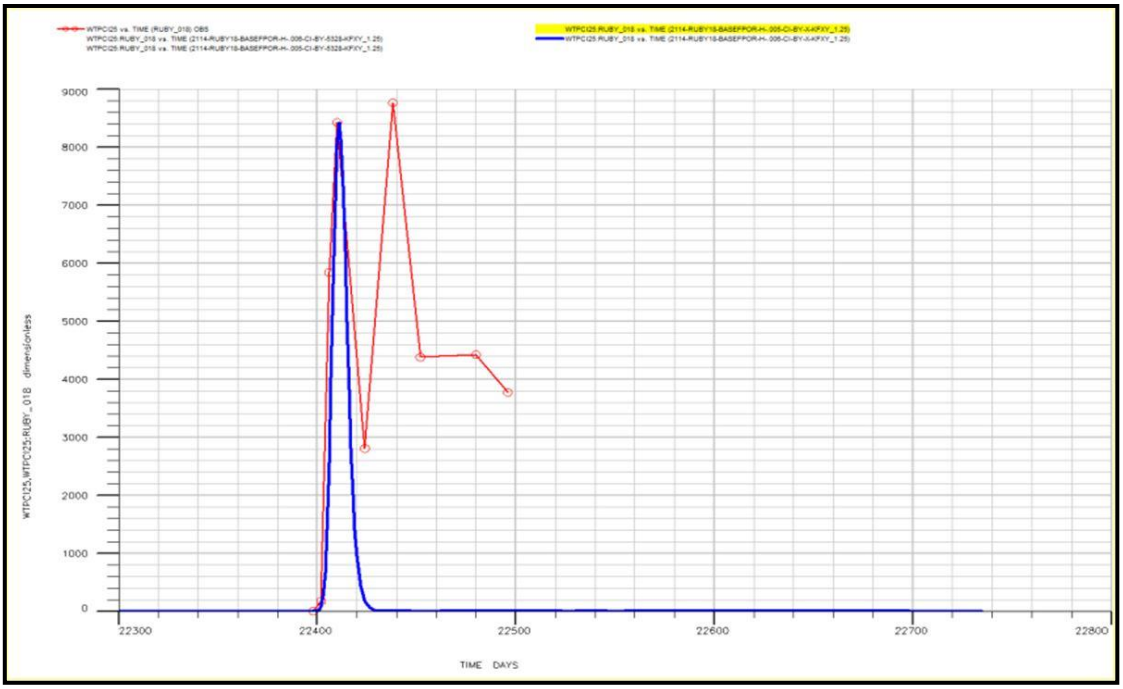

Figure 5.41: Tracer match for ‘Sherrod 2114-Ruby18’ response

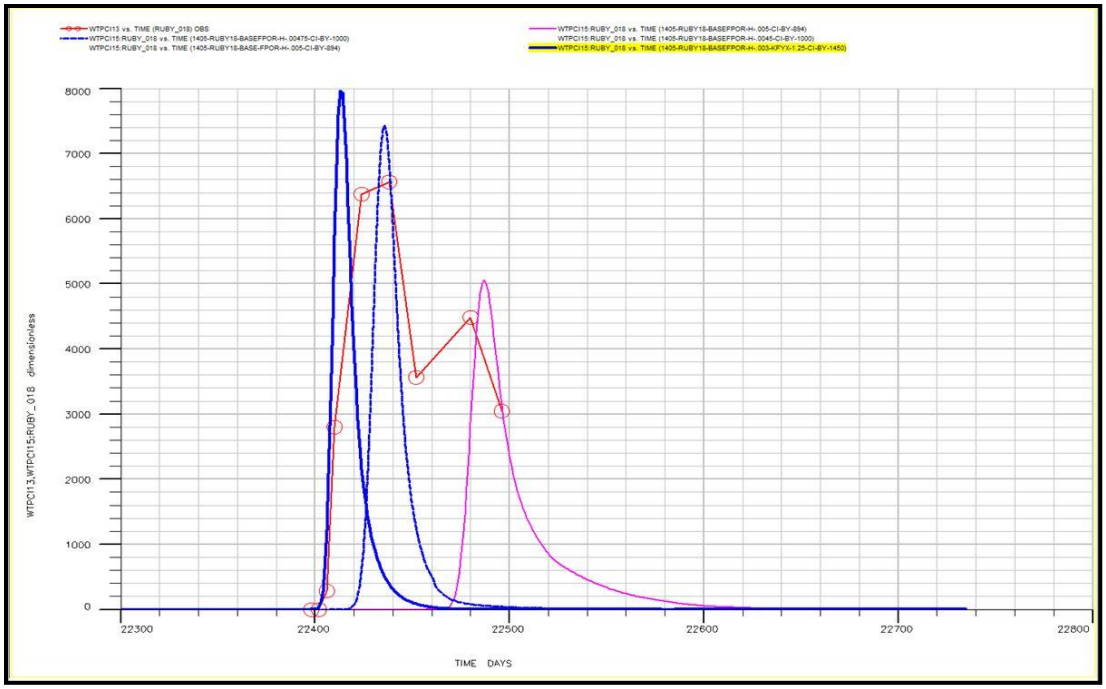

Figure 5.42: Tracer match for 'Sherrod 1405-Ruby18' response

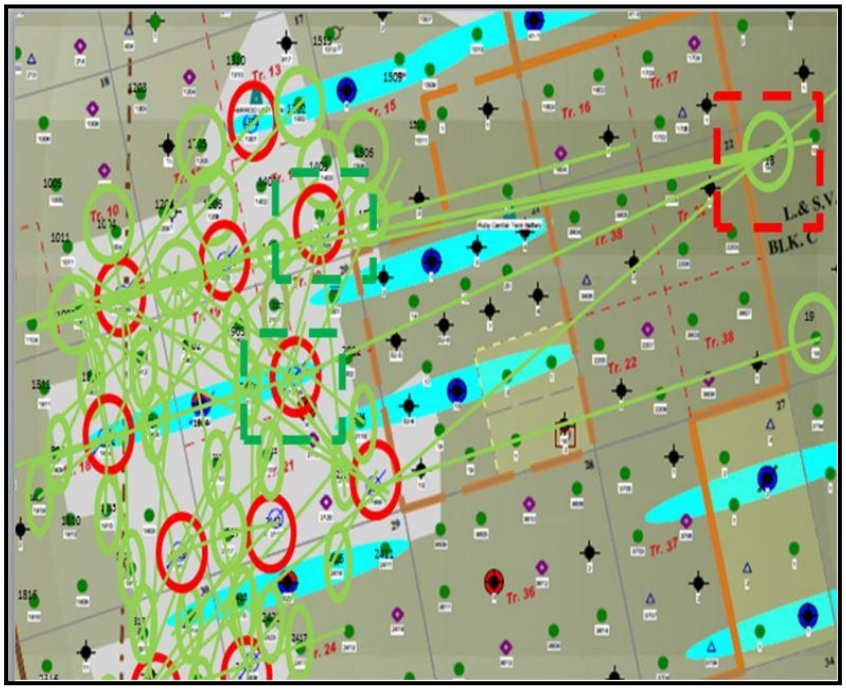

Figure 5.43: Sherrod 1405, Sherrod 2114, and Ruby18 wells' locations

5.3.5 Case Study II: Tracers Flow toward 'Sherrod 1809'

The same injectors that showed ultra-high tracer velocities toward 'Ruby 18' in case study I showed ultra-high velocity in an opposite direction toward 'Sherrod 1809'. Injectors contributing significantly to 'Sherrod 1809' and their observed tracers' velocities are listed in Table 5.7 below. These ultra-high tracer velocities acting in opposite directions are highlighted in the schematic diagram shown in Figure 5.44 below. In a similar manner to case study I, tracer breakthrough were matched by reducing (φ_f h) product, and peaks were matched by reducing concentration injected to account for dilution from nearby injectors. Figures 5.45 through 5.46 show matches for tracers responses and their respective locations. These tracers reflect movement in highly stratified and fractured thin layers in the range of 0.1-0.2 ft.

Injector	BT, days	Sampling uncertainty, days	Distance, ft	Velocity , ft/d
Sherrod 1012	1	2	3,696	3,696
Sherrod 1202	2	2	5,919	2,960
Sherrod 1405	6	4	8,412	1,402
Sherrod 1814	2	2	1,324	662
Sherrod 2114	0	0	6,511	13,288*

Table 5.7: Significant tracers show and tracers velocities at 'Sherrod 1809'

Figure 5.44: The two opposite in direction ultra-high tracer velocities observed from same injectors

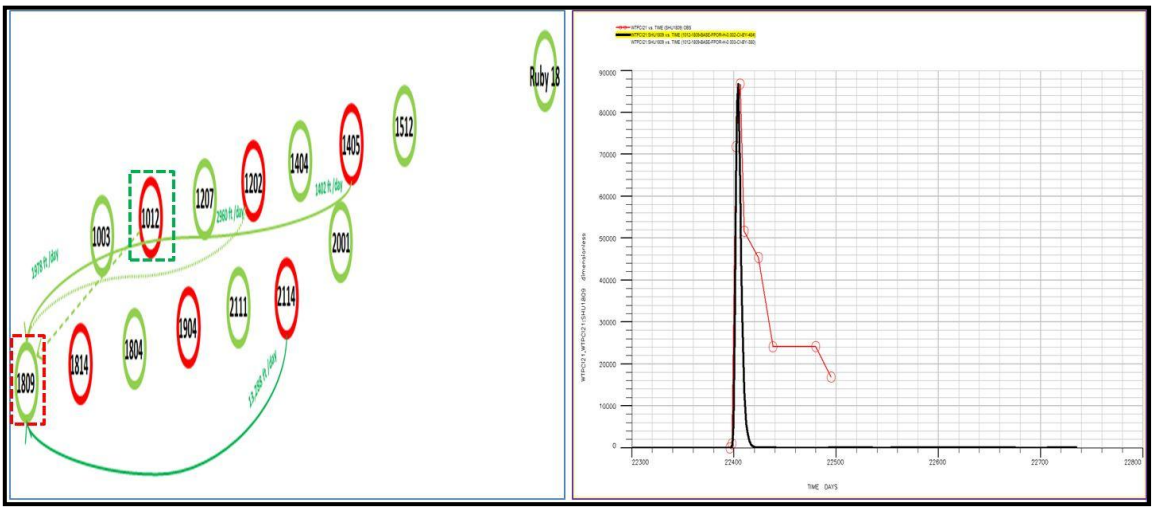

Figure 5.45: 'Sherrod 1012 – Sherrod 1809' tracer response match

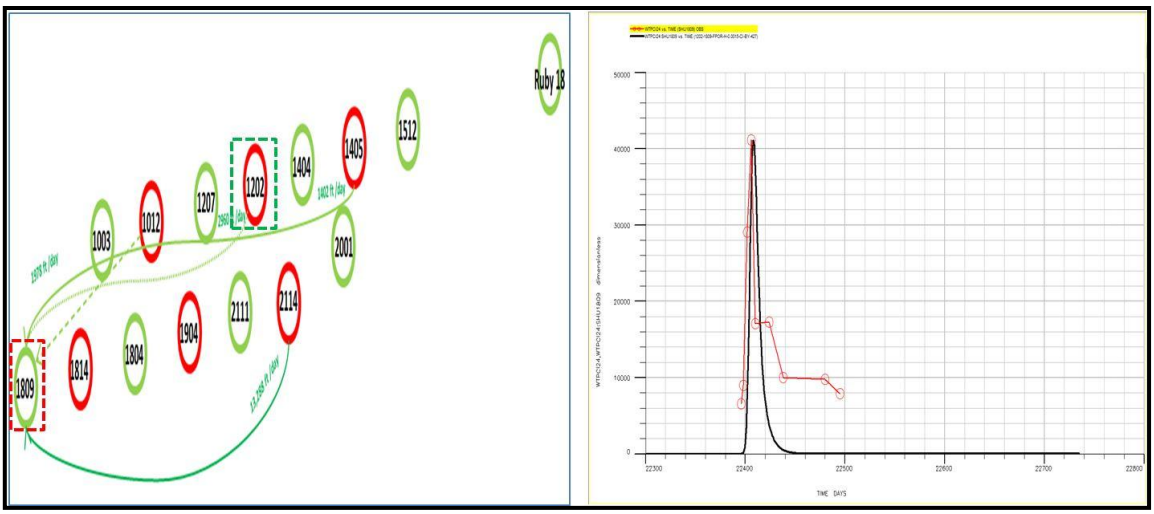

Figure 5.46: 'Sherrod 1202 – Sherrod 1809' tracer response match

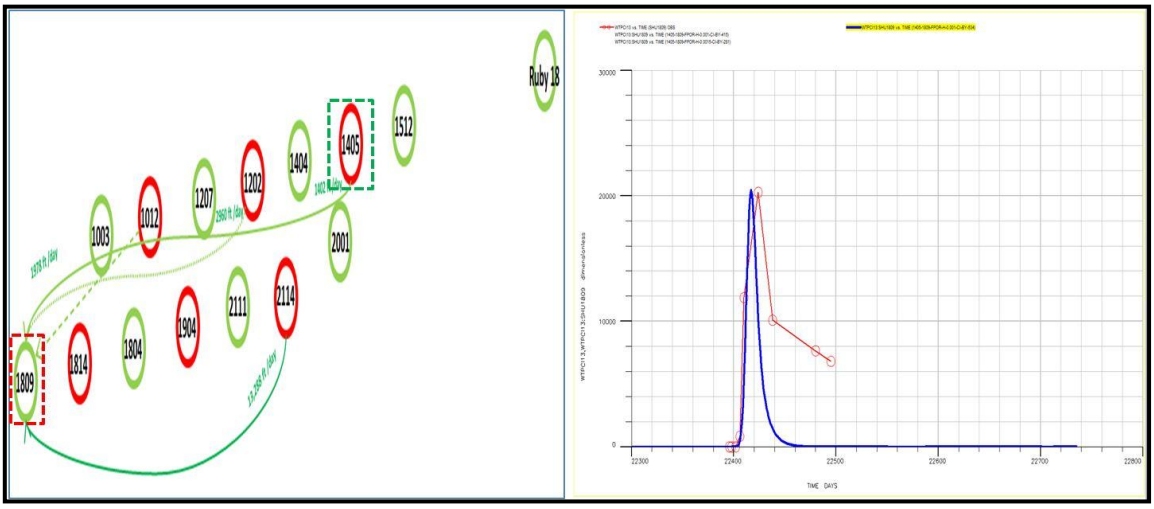

Figure 5.47: 'Sherrod 1405 – Sherrod 1809' tracer response match

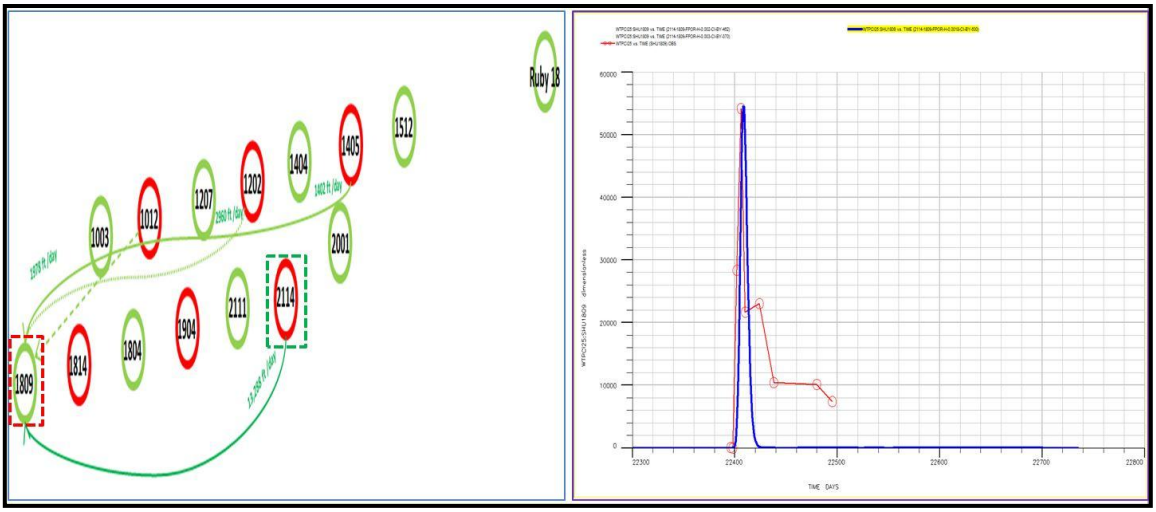

Figure 5.48: 'Sherrod 2114 – Sherrod 1809' tracer response match

5.3.6 Case Study III: Modeling Simple Tracer Movement

As indicated section 5.2.3 earlier, tracers' responses with relatively high recovery (> 0.5%) exhibit simple tracer movement in the vicinity of the tagged injectors. In a similar manner to the previous case studies, tracer breakthrough time was matched by changing (φ_f h) product, and peak concentration produced was matched by reducing concentration injected to account for dilution. Figures 5.49 through 5.52 show matches for tracers' responses and their respective wells' locations. Similarly to case studies 1 & 2, these tracers reflect movement in highly stratified and fractured layers but with relatively larger thicknesses in the range of 0.6-1.5 ft.

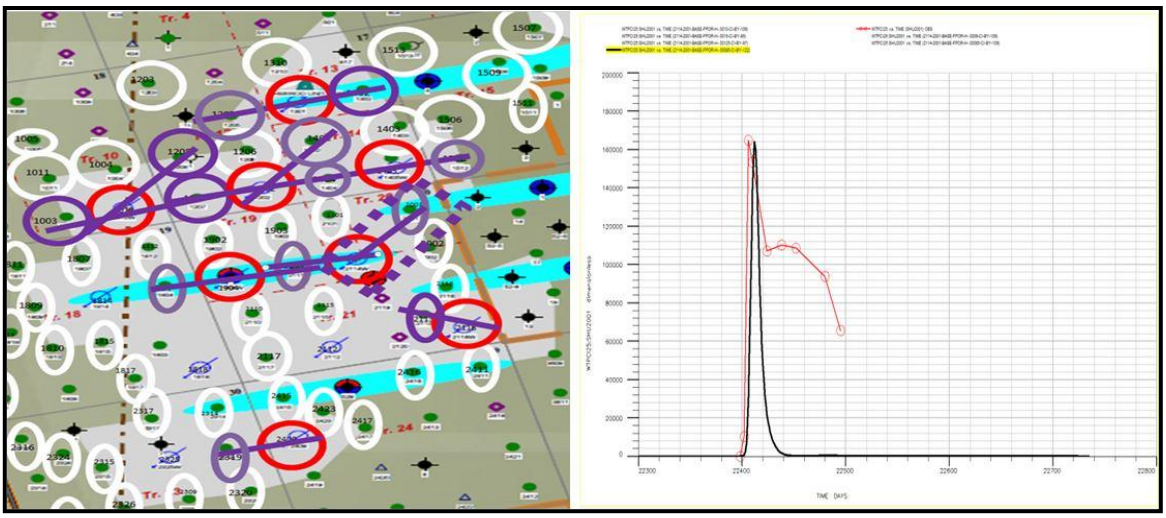

Figure 5.49: ‘Sherrod 2114 – Sherrod 2001’ tracer response match

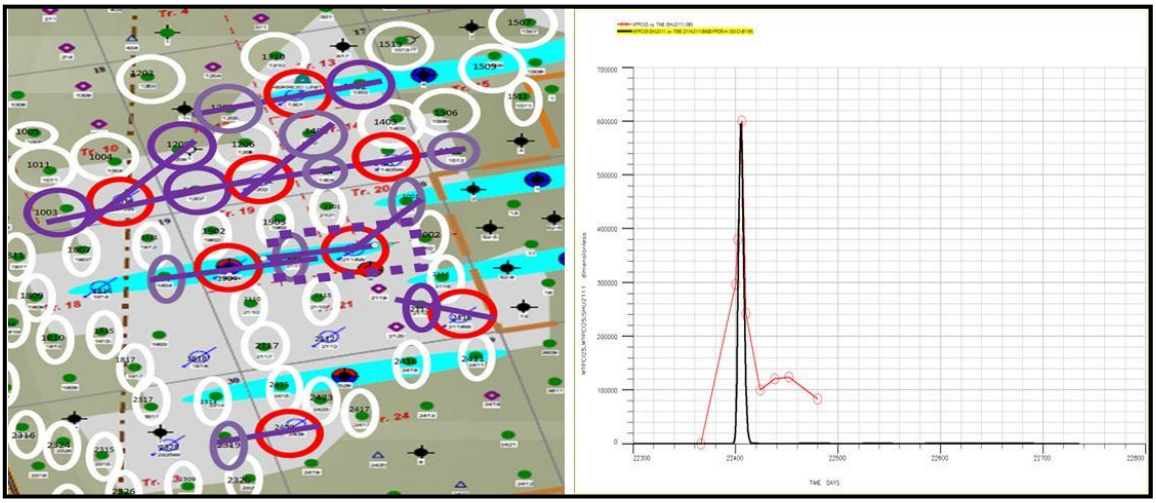

Figure 5.50: ‘Sherrod 2114 – Sherrod 2111’ tracer response match

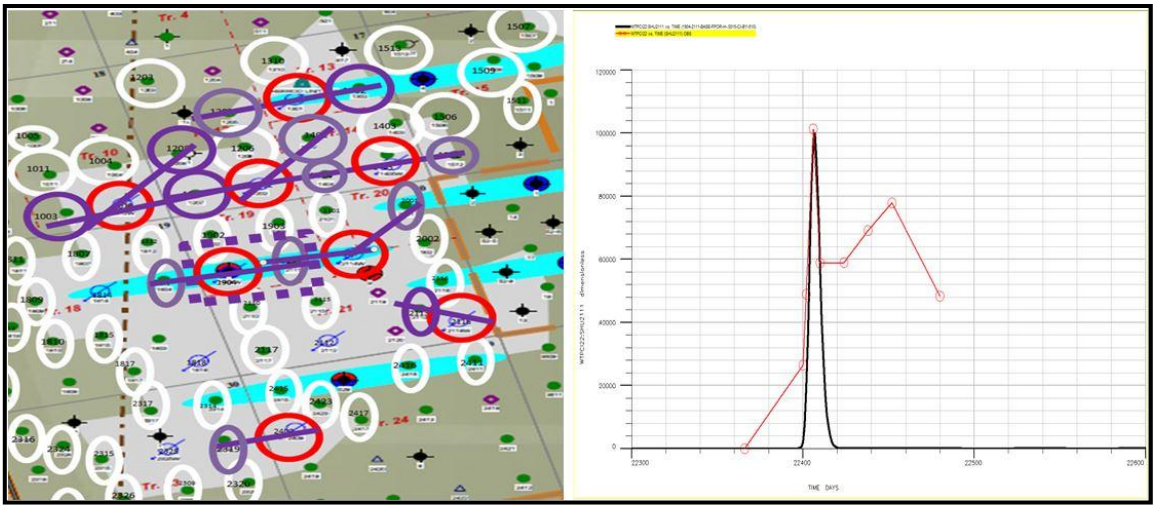

Figure 5.51: ‘Sherrod 1904 – Sherrod 2111’ tracer response match

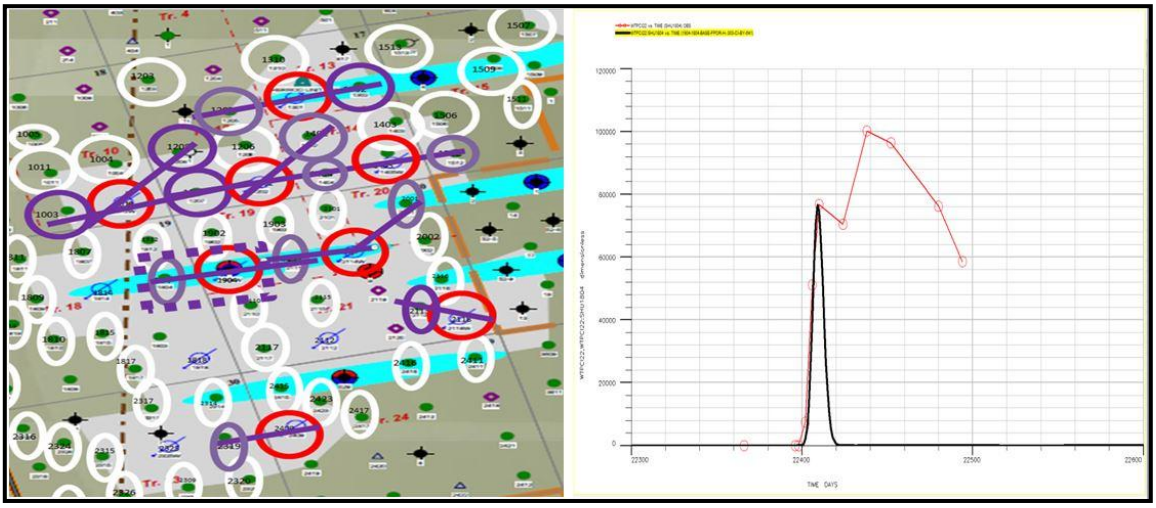

Figure 5.52: ‘Sherrod 1904 – Sherrod 1804’ tracer response match

5.4 Multi-layered Simulation Model per Tracer Injected

5.4.1 Objectives

Multi-layered simulation models are sector models to model connectivity between a tagged injector and all producers showing moderate and high tracer shows. Example of a possible simulation model incorporating all moderate and high tracer shows is shown in Figure 5.53 below. The overall objectives of these types of simulation models include:

1. Simplify the complex fracture network by matching responses of one injected tracer at a time.
2. Investigate the applicability of using multiple non-communicating layers to model each tracer response
3. Integrate fracture realizations from multiple simulation models to build the global fracture network

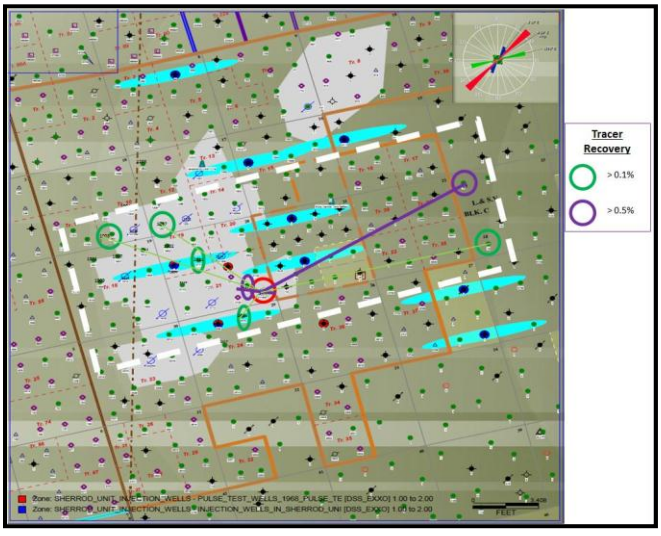

Figure 5.53: Example of a case study to incorporates moderate and high tracer shows in one model

5.4.2 Approach Limitations

The approach of modeling single tracer at a time using multi-layered simulation model has the following limitations:

1. Limitations in modeling the water dilution effect from nearby injectors.
2. Interaction of producers with other injectors is not captured.
3. Approach could lead to a very large number of simulation layers when multiple simulation models are integrated into one.

5.4.3 Case Study: Tracer Injected through 'Sherrod 1814'

Tracer injected through 'Sherrod 1814' shows moderate recoveries in a small area enclosed around the injector. This presents a simple case to test our approach. Figure 5.54 below show model area, injector location, and moderate tracer shows. Table 5.8 below show a list of producers with moderate tracer shows, tracer breakthrough time, and velocities of tracers produced.

Simulation model was built using 8 non-communicating layers. Each producer was completed in a different layer to minimize well interference, and to allow matching of each tracer response independently. Injector completion covers all the 8 layers. Figure 5.55 below show effect of varying (φ_f h) product on tracer breakthrough time for 4 out of the 8 producers.

The approach of matching multi-tracer responses using simulation models with multi non-communicating layers did not show success. The main reason is that the draw down created by producers and the injector was not high enough to make tracers flow at the

observed velocities. This highlights two key findings: First, using sector simulation models for individual patterns is not capable of modeling tracers velocities observed. Second, injection from nearby wells needs to be included in simulation model in order to match tracers' breakthrough times.

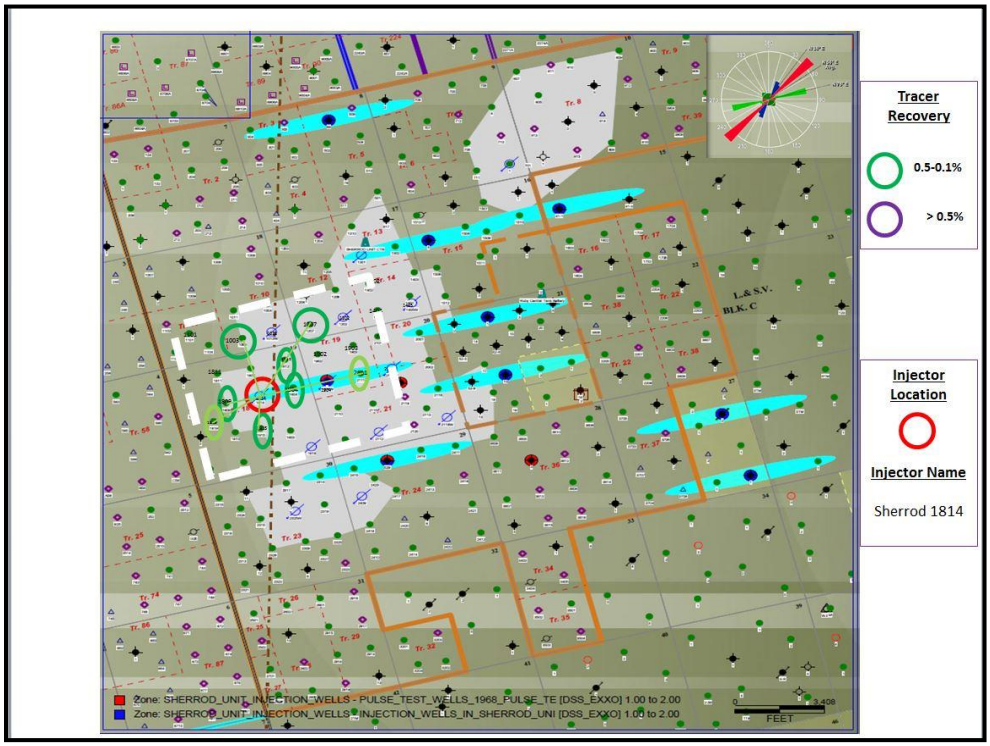

Figure 5.54: 'Sherrod 1814' moderate tracer shows

Producer	BT, days	Sampling uncertainty, days	Distance, ft	Velocity , ft/d
Sherrod 1003	4	2	2,701	675
Sherrod 1207	2	2	3,759	1,880
Sherrod 1804	2	2	1,330	665
Sherrod 1809	2	2	1,324	662
Sherrod 1812	4	4	1,863	466
Sherrod 1815	4	4	1,444	361
Sherrod 1819	8	8	2,076	260
Sherrod 2111	6	6	3,969	662

Table 5.8: List of wells showing significant tracer responses from 'Sherrod 1814'

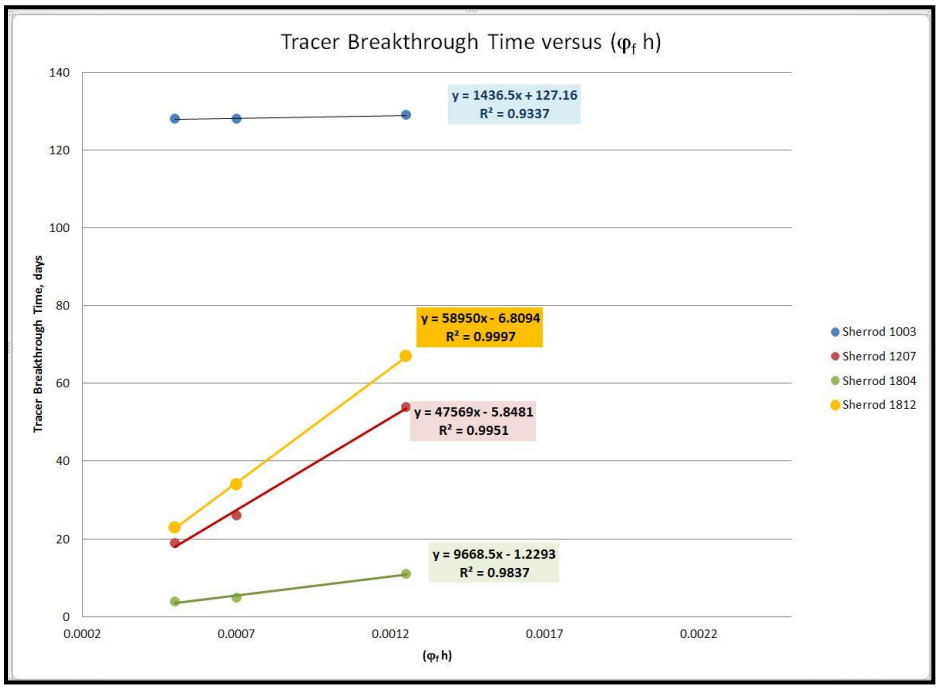

Figure 5.55: (φ_f h) product versus tracer breakthrough time (1814 pattern)

5.5 Modeling Simultaneous Water Breakthrough in 2002

A simulation model was built with the objective to match the simultaneous field-wide water breakthrough and the water production performance of 44 producers in 2002. Figure 5.56 below show locations of the 44 wells with respect to the map that shows paths of moderate tracer recoveries. Sensitivities studied earlier in section 5.2 showed that water-cut performance is dominantly controlled by three parameters: initial water saturation, thickness, and matrix porosity. Two approaches to model the problem were followed: First approach is to model wells performance using initially dry simulation model (initial saturation = S_{wir}). This approach has the advantage of capturing the early dry production of all wells. Second approach is to model wells performance using initially wet simulation model. This approach has more flexibility to model water performance after breakthrough.

The first approach showed some success in matching the water breakthrough time but did not show an acceptable water-cut match. Figure 5.57 below shows the best obtainable match for total water production rate using the first approach. It indicates that to achieve such a quick water breakthrough, the pore volume of the system has to be very small in the range of (φ-h) product of 0.75 or below. It should be noted that for a (φ-h) product below 0.55, the water production match at the late period of Figure 5.57 will be lost because simulated water production will be much higher than observed.

The second approach showed a remarkable success in matching the water production performance but left the early dry oil production period unexplained. Figures 5.58 and 5.59 show multiple matches of field water production and field water-cut, respectively.

The multiple matches indicate two important things: First, water performance is dominantly driven by water saturation in the fracture system. Second, the match indicate a moderate matrix pore volume system of (φ-h) product of 1.65. Different combinations of matrix porosity and thickness with the same product yield identical solution. Examples for water-cut matches of individual wells are shown in Figures 5.60 through 5.63.

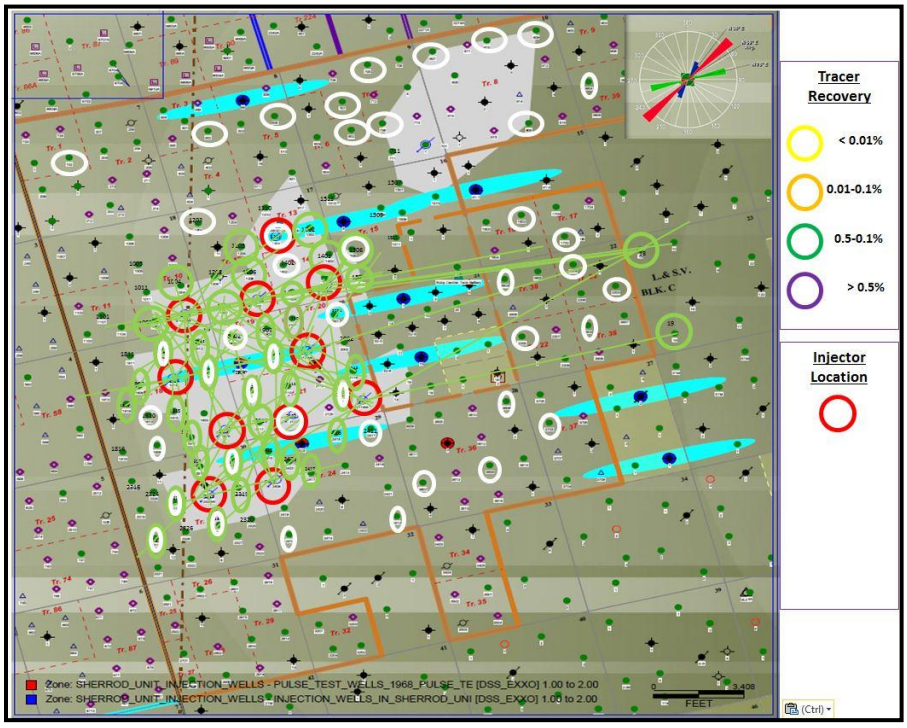

Figure 5.56: Locations of 2002 water breakthrough on tracer recovery map (white circles)

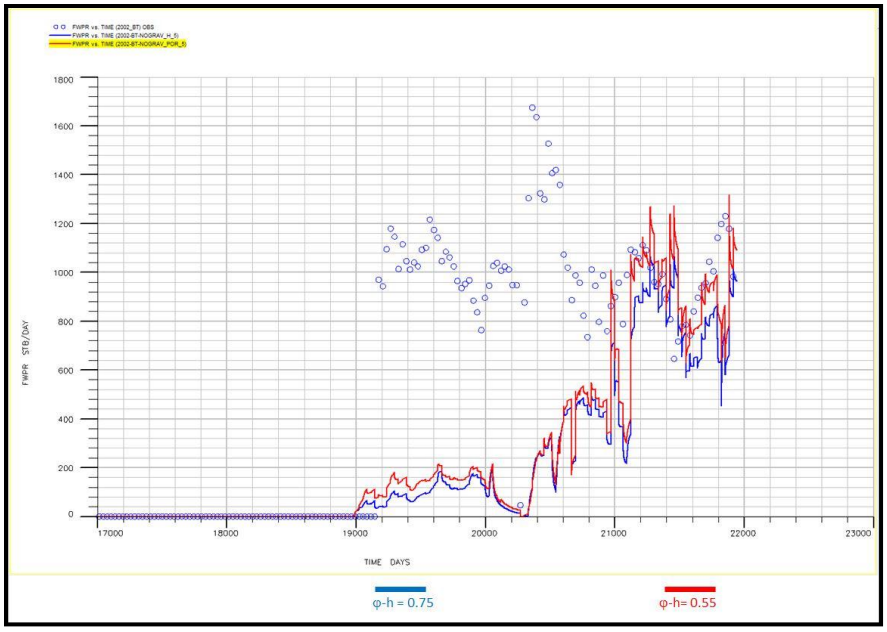

Figure 5.57: Best match for simultaneous water breakthrough in 2002 using dry model approach

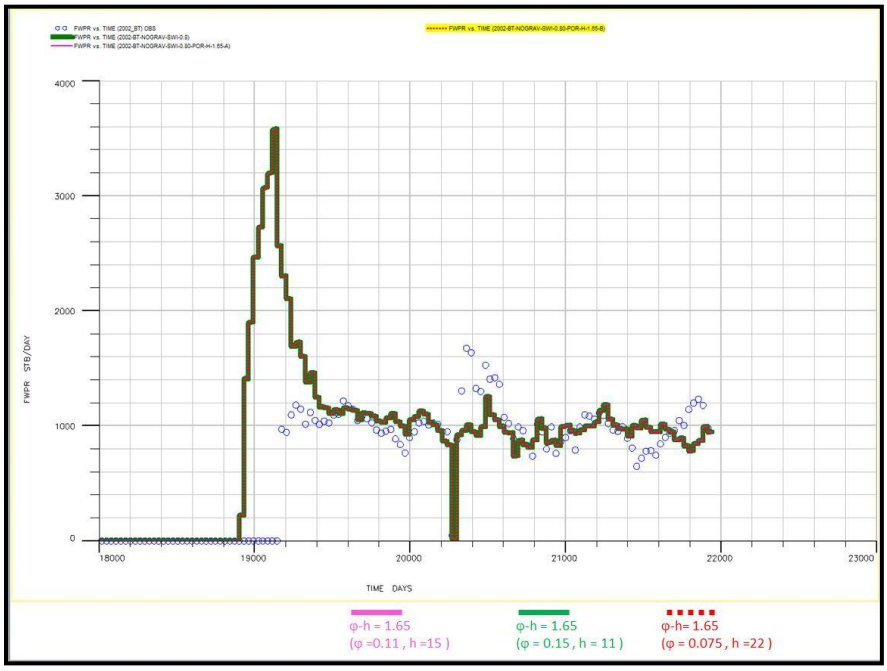

Figure 5.58: Multi-history matches (total water rate) for 2002 simultaneous water breakthrough using wet model approach

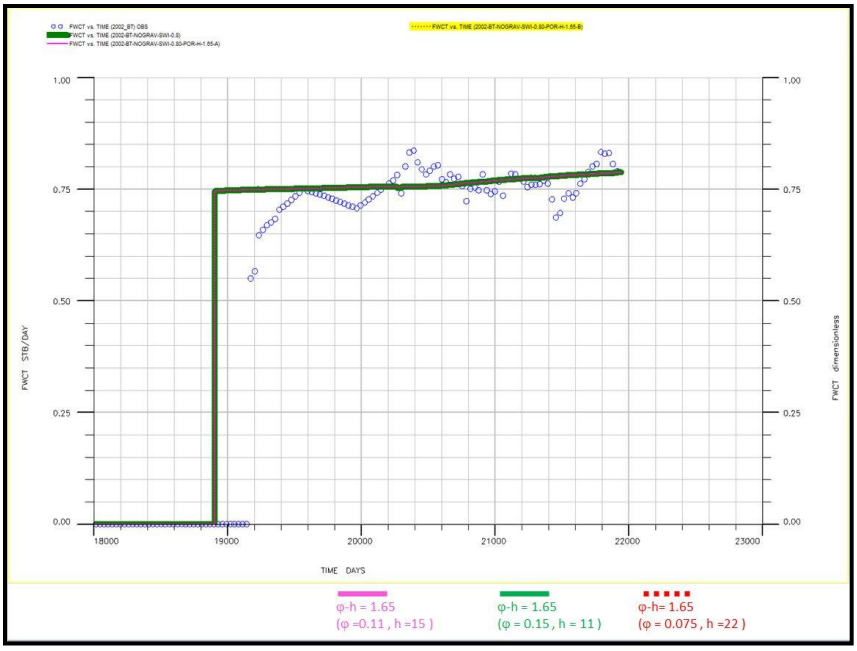

Figure 5.59: Multi-history matches (total water cut) for 2002 simultaneous water breakthrough using wet model approach

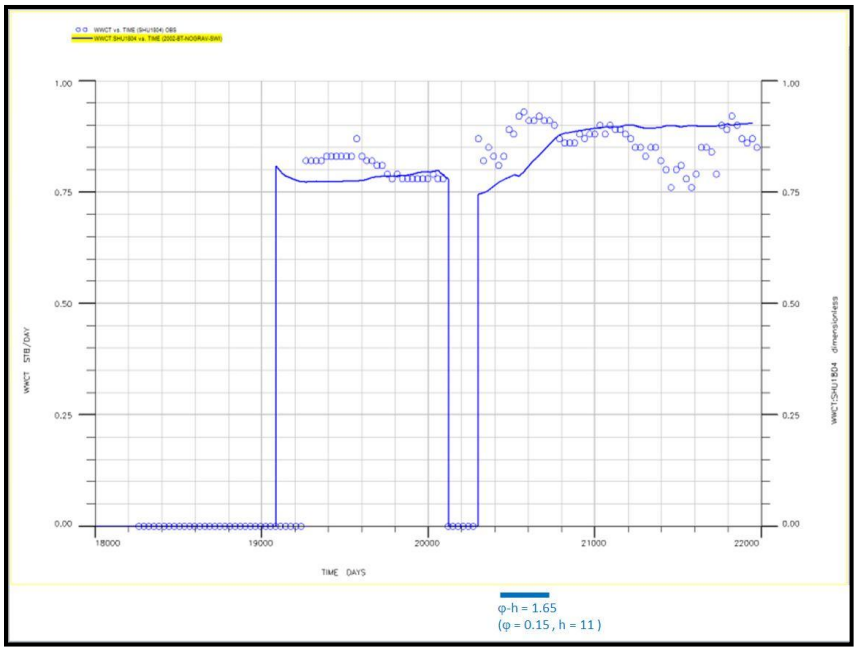

Figure 5.60: 'Sherrod 1804' water-cut match using wet model approach

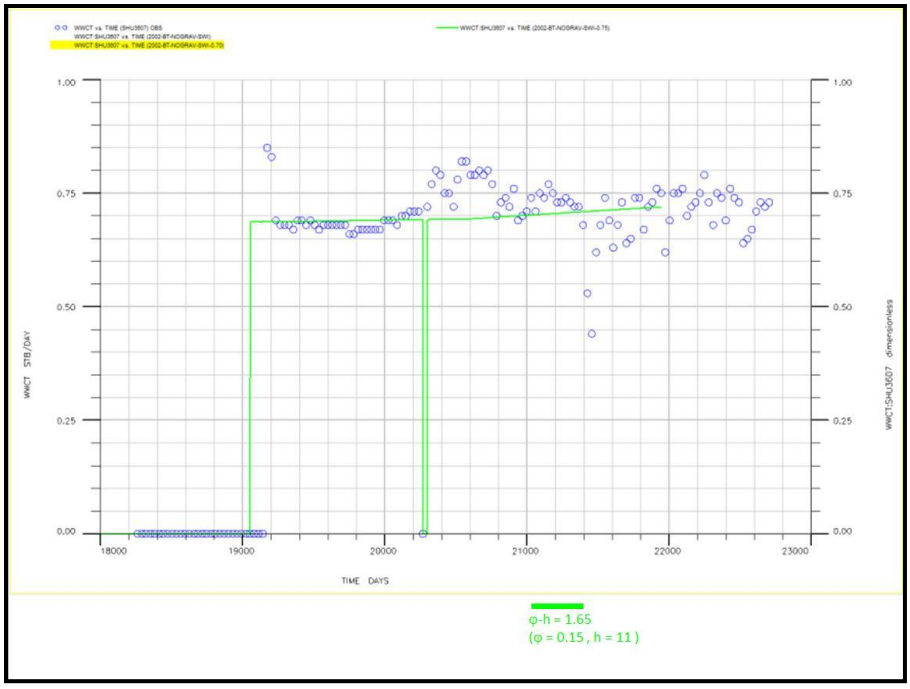

Figure 5.61: 'Sherrod 3607' water-cut match using wet model approach

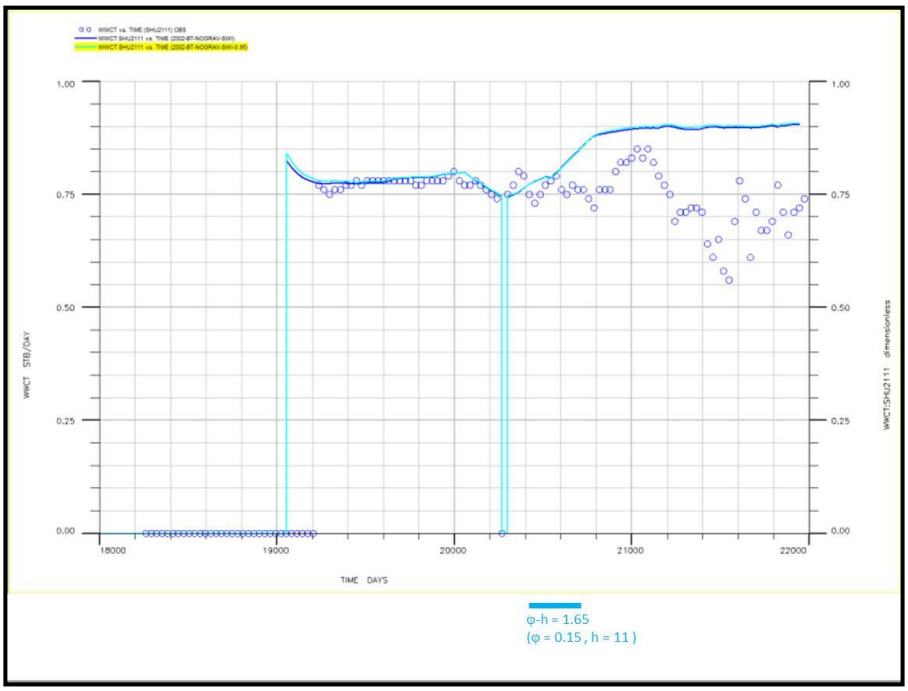

Figure 5.62: Sherrod 2111 water-cut match using wet model approach

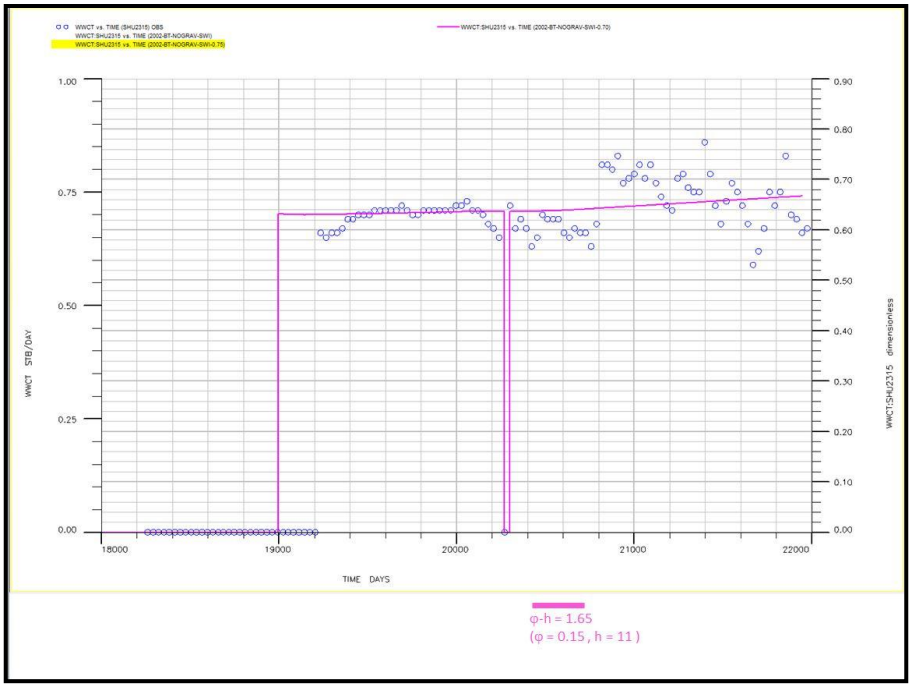

Figure 5.63: 'Sherrod 2315' water-cut match using wet model approach

5.6 Full Field Simulation Model

5.6.1 Objectives

A Full field simulation model was built in order to model simultaneously the 13 tracers injected as well as performances of all producers and injectors in Sherrod Area. The selection of full field boundary was done with precaution as tracer results showed interaction and ultra-high velocity gradients between patterns injection area and its surrounding. A selection of full field area should enclose all nearby water injection activities to capture history of early water movement in the field. The boundary of the full field model chosen for this study is shown in Figure 5.64 below and it includes 23

injectors and 195 producers. Eclipse input file for full field simulation model is included in Appendix G. The overall objectives of full field simulation model include:

1. Assess average reservoir properties capable of explaining wells' performance.
2. Investigate modeling 13 different tracers simultaneously using a full field simulation model.
3. Investigate well interference through fracture system and its effect on tracer solution.

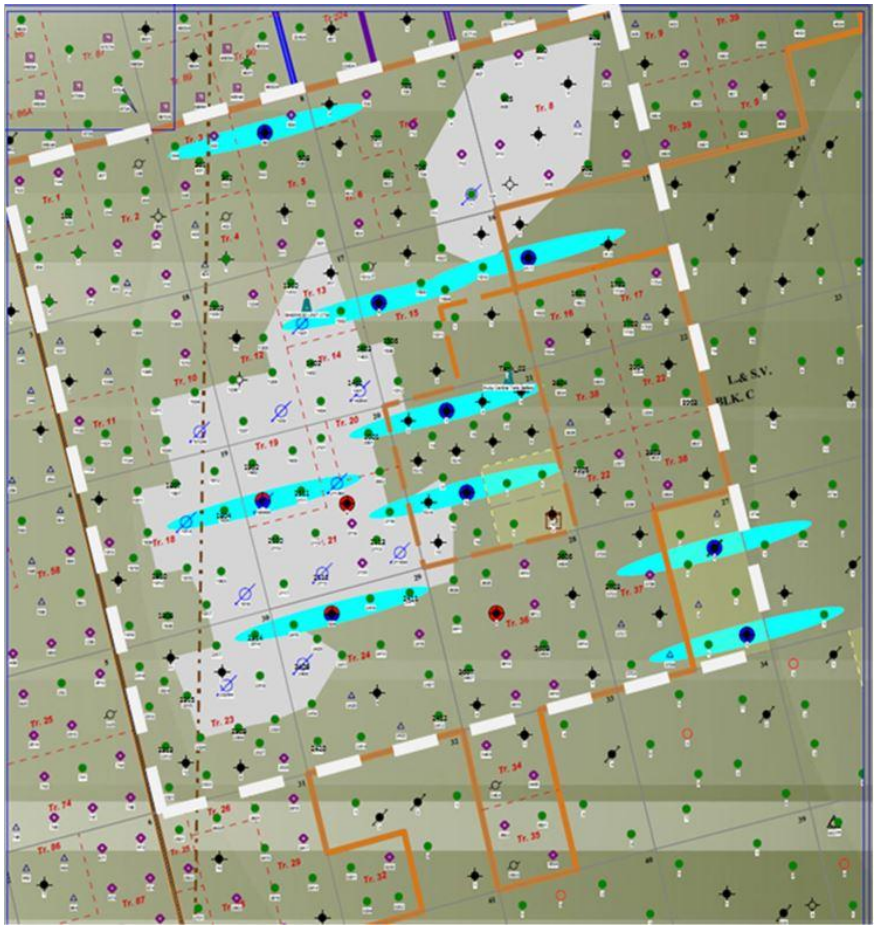

Figure 5.64: Boundary of full field model selected for the study

5.6.2 Model Limitations

The full field simulation model has the following limitations:

1. Heterogeneity and layering is not properly modeled due to absence of core studies and petro-physical data
2. Large grid cells effect quality of tracer solution

5.6.3 Matching Field Performance

The history matching process of the full field model has two parts: First part is to match high and moderate tracer shows for the 13 tracers used in the test. Second part is to match water-cuts of wells covering large area of the field.

Attempts to study tracer responses using full field simulation model has not been successful. The main reason behind such un-success is the extreme sensitivity of tracer solution to small convergence problems encountered by simulator. To achieve a simulation run free of convergence problems, a minimum time step of 0.1 days has to be used. Figure 5.65 show the effect of convergence problems on tracer solution: green tracer response is a tracer solution with no convergence problems while blue tracer curve is a tracer solution affected by one convergence problem. Due to this extreme sensitivity of tracer solution and the excessive CPU time required to run a full field model free of any convergence problem, a decision was made to use the full field model only to match water-cuts.

Sensitivity study on water-cut response presented earlier in section 5.2 of this study indicated that water-cut response is driven dominantly by three parameters: initial water

saturation of matrix-fracture system, thickness, and matrix porosity. While initial saturation could be inferred from initial water-cut wells, average matrix porosity and thickness of the field is estimated by trial and error. A matrix porosity-thickness product of 1.65 was found to match performance of several wells covering large area of the field. Figures 5.66 through 5.71 show water-cut matches for wells located in North-East, North, North-West, South, South-East, and South-West of the field using (φ h) product of 1.65 and variable initial water saturation.

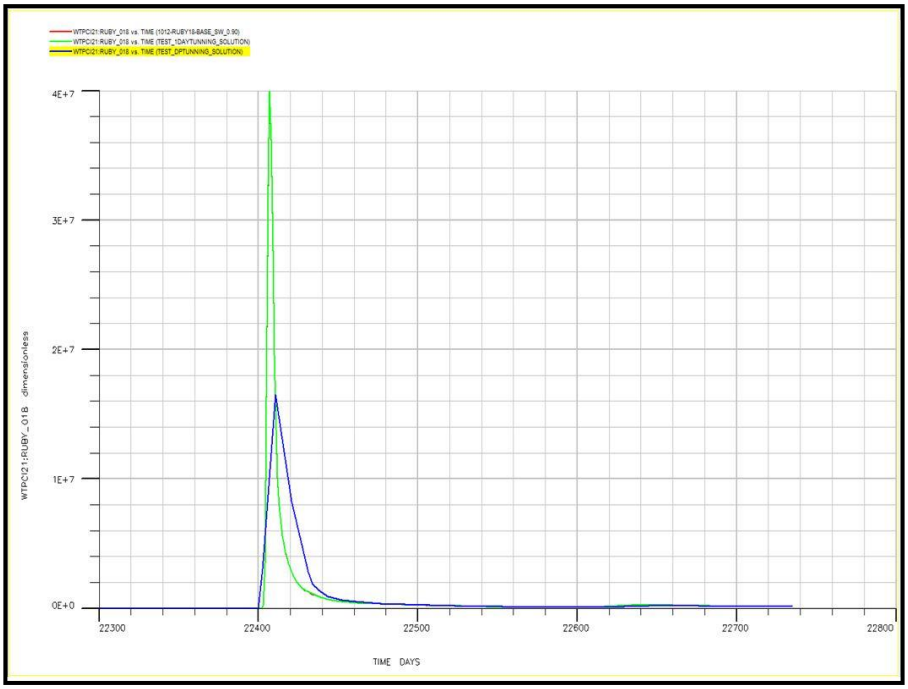

Figure 5.65: Effect of one convergence problem on tracer solution

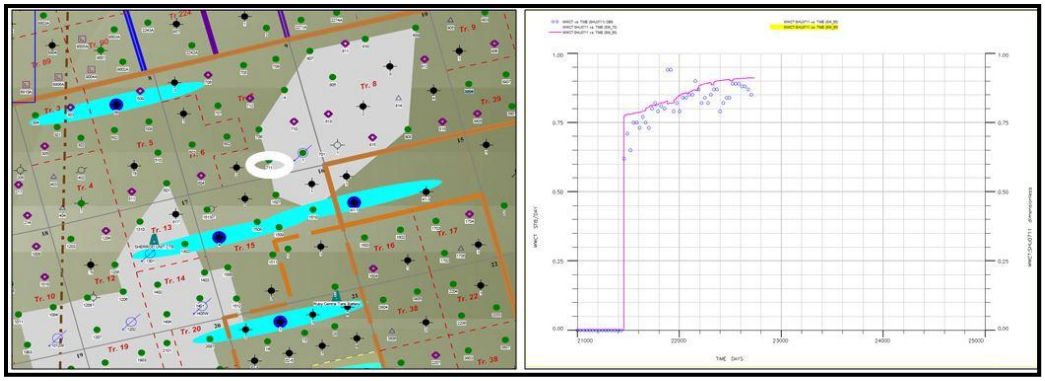

Figure 5.66: ‘Sherrod 711’ water-cut match North-East of field (full field model, Swi=0.60)

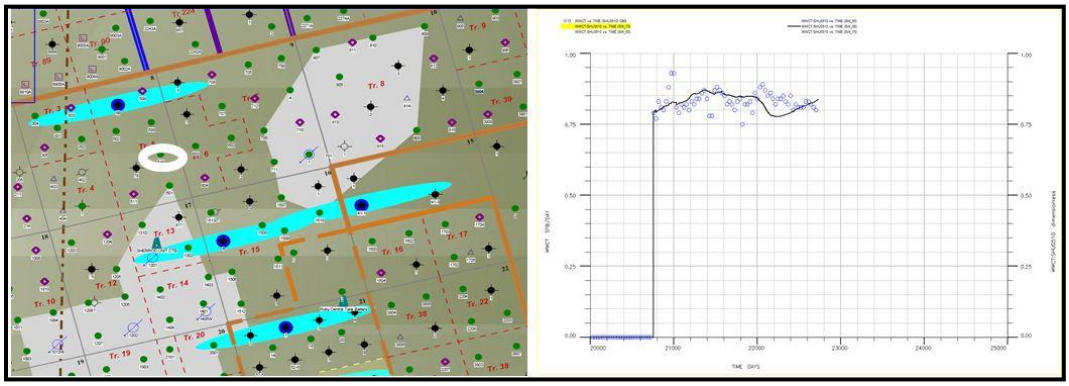

Figure 5.67: ‘Sherrod 510’ water-cut match North of field (full field model, Swi=0.95)

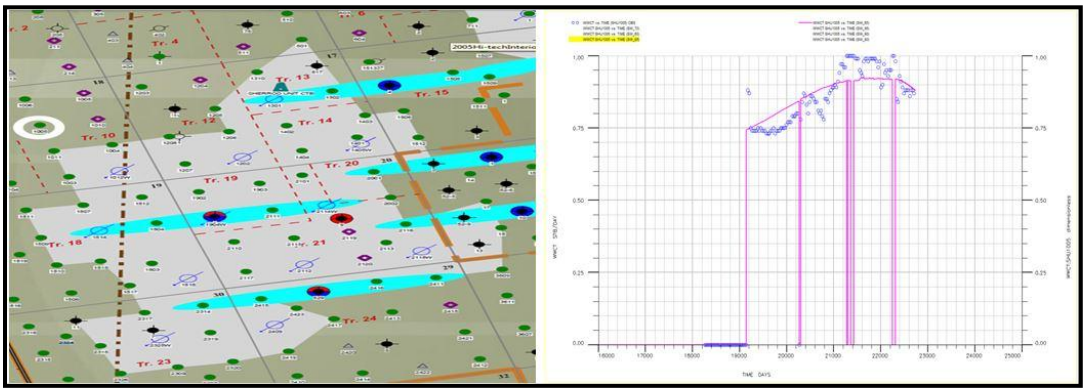

Figure 5.68: ‘Sherrod 1005’ water-cut match North-West of field (full field model, Swi=0.65)

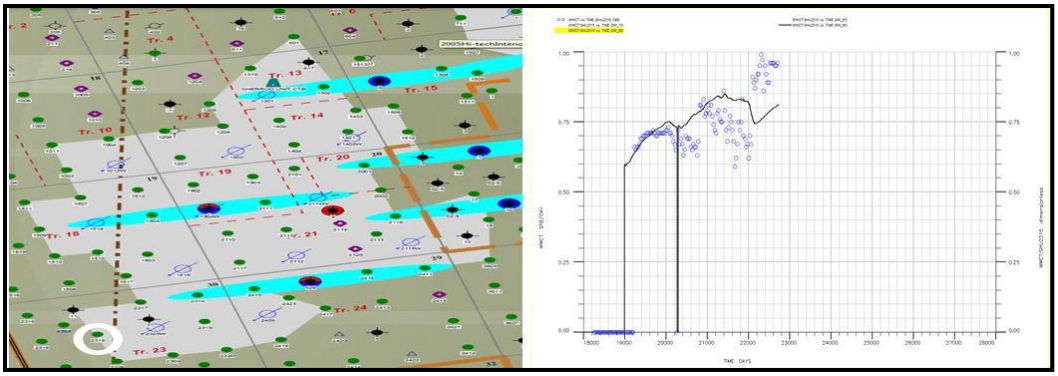

Figure 5.69: ‘Sherrod 2315’ water-cut match South-West of field (full field model, Swi=0.95)

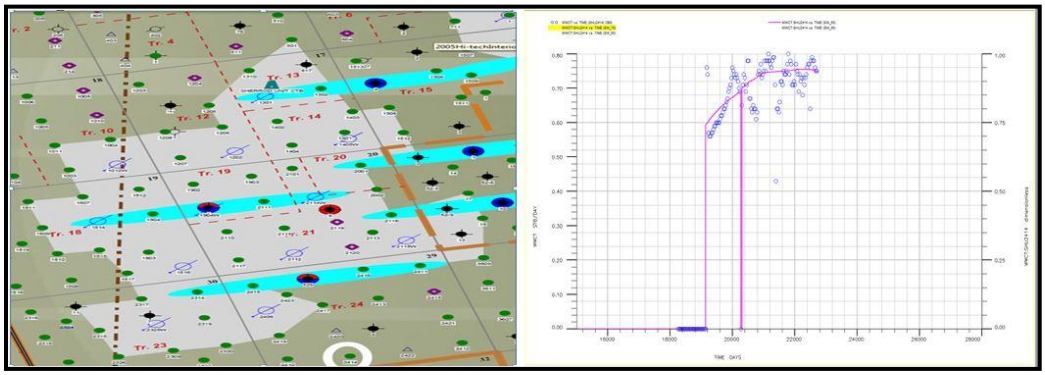

Figure 5.70: ‘Sherrod 2414’ water-cut match South of field (full field model, Swi=0.65)

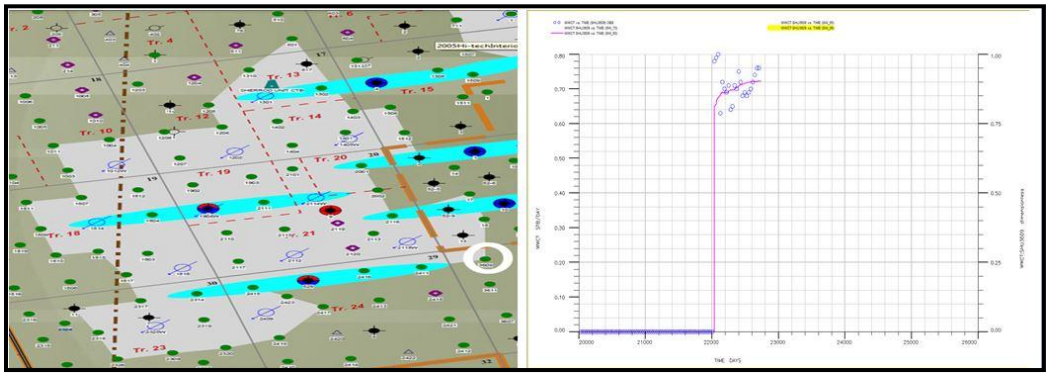

Figure 5.71: ‘Sherrod 3609’ water-cut match South-East of field (full field model, Swi=0.60)

5.7 Summary of Results

Sector and full field simulation models used to study tracer and water-cut responses highlight the following:

1- Tracer responses are primarily driven by fracture properties providing minimum information about properties of the matrix system

2- Tracer solution is highly uncertain because it is strongly affected by non-reservoir parameters like grid resolution, drainage area surrounding wells, water dilution from nearby injectors, and loss of injected water.

3- Tracer breakthrough time is primarily driven by (φ_f h) product. Different combinations of fracture porosity and thickness with the same product yield identical tracer responses.

4- The ultra-high tracer velocity of 8,900 ft /day between 'Sherrod 1012' and 'Ruby 18' located outside tracer area support the presence of an external water source flowing to Sherrod Area. This is because there is no mathematical solution to generate such ultra-high tracer velocities using fracture properties alone.

5- Overall tracers' response matches reflect tracer movement in highly stratified and fractured thin layers with low vertical communication. Assuming fracture porosity of 0.5%, layers thicknesses are in the range of 0.1 to 1.5 ft.

6- Matches of tracer responses with higher than 0.5% recovery reflect tracer movement in limited extension fracture system oriented dominantly in E-W and NE-SW directions.

7- Matches of tracer responses with 0.1-0.5% recovery reflect a more complex fracture network with extensions outside tracer study area. Two types of fracture exist: limited extent fractures in N-S & NW-SE directions, and regional extent fractures in E-W, and NE-SW directions.

8- Water-cut matches for both full field and sector models reflect a fracture system with high water saturation, and a matrix system with moderate pore volume of (φ h) product of 1.65.

9- Full field model is not practical to model tracers due to extreme sensitivity of tracer solution which requires infinitesimal & impractical time steps.

6. INVERSION MODELING APPROACHES

6.1 Introduction

The process of history matching where parameters controlling reservoir performance is modified until an acceptable match is achieved between simulated and observed response is a process that has been performed traditionally by trial and error. With the advancement of computational capabilities and optimization approaches, new tools were developed to assist the reservoir engineer in such a process [((45))]. These tools define an objective function based on the difference between observed data and simulated responses and uses gradient-based optimization techniques to minimize the objective function [((46))].

Whether the history match process is performed manually or with the aid of a gradient-based technique, two major difficulties is commonly encountered in any history matching study: First, which parameter(s) should be selected in order to achieve a history match. Second, how to ensure the consistency of changes applied to a simulation model with geological concepts and other fundamental data used to construct the model initially.

Bissell [((47))] proposed a "Gradzone Analysis" method which uses gradient information to guide reservoir engineer in choosing reservoir parameters to modify. This method is based on spectral analysis of the second derivative of the objective function (Hessian Matrix). Hessian Matrix is constructed using a quadratic approximation of the objective function near a minimum. To preserve relations between reservoir parameters or to

preserve the initial geological model from unreasonable deviation during the assisted history matching process, a prior term can be added to the objective function. The prior term in its simplest form contain estimation of standard deviations of the parameters to be adjusted. The prior term in general contains more geological concepts like correlation lengths, anisotropy, and permeability-porosity relationships. Any knowledge used in the initial construction of the simulation or geological model should be preserved as much as possible during the history matching process. The prior term is often neglected in the widely used traditional history matching approach although it forms a fundamental concept in the Bayesian approach to generate multiple geo-statistical models constrained to production data [(48)].

6.2 Inversion through Gradzone Analysis: Process Overview

One major advantage of gradient-based history matching approaches is their ability to provide useful information on which parameter to choose to start the history match. In general, Gradzone Analysis is a procedure for selecting zones in a reservoir model to apply a common multiplier to a particular reservoir property for all grid cells within a zone. Typically, the reservoir property is pore volume (e.g. porosity) or transmissibility (e.g. permeability). The overall flowchart of Gradzone Analysis study as described by Brun et. al.[(48)] is shown in Figure 6.1 below. The first step is to propose an objective function to be minimized. The second step involves selecting sample cells from the reservoir simulation model and performing simulation runs to construct the sensitivity matrix (first derivative of the objective function). Then, from the sensitivity matrix and

knowledge of standard deviation of parameters, an approximation of the Hesssian matrix (second derivative of objective function) can be constructed and normalized. Then, by decomposing the normalized Hessian matrix into eigenvectors and their corresponding eigenvalues, the reservoir engineer can determine the number and boundary of Gradzones needs to be constructed. Finally, one multiplier per Gradzone per reservoir property is calculated and the regression starts and iterate on all multipliers until no improvement in solution is observed. Each step of the study is discussed in more detail in the next subsections.

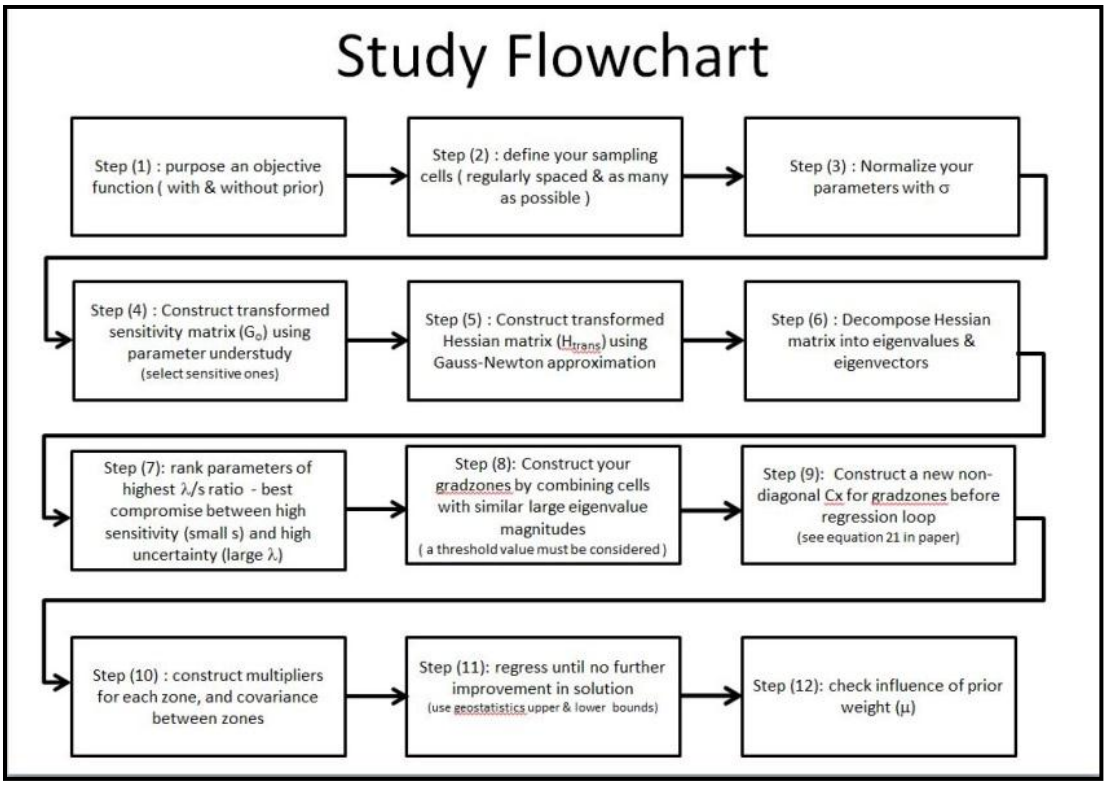

Figure 6.1: Flowchart summarizing steps in Gradzone Analysis as presented in SPE # 87680

6.2.1 Step # 1: The Objective Function

As mentioned earlier, the first step in Gradzone Analysis study is to select an objective function to be minimized. This function could be in the usual least-square form:

$$f(x) = \sum_{l=1}^{p} \left\{ \omega_l \frac{[y_l^c(x) - y_l^{obs}]}{\sigma_l} \right\}^2 \quad \text{.....(18)}$$

where f(x) is the objective function to be minimized, y_l^c is *l*th calculated point from a vector of a simulation response like water-cut, water rate, or bottom-hole pressure, y_l^{obs} is the corresponding observed value from data. The symbol "x" represents the reservoir parameter to be adjusted during the history match (e.g. thickness, porosity or permeability). σ_l is the standard deviation of the measurement error in the *l*th data point, and ω_l is the weight assigned to the *l*th data point.

If a prior term to be added to the objective function, the modified objective function, Q(x), will be:

$$Q(x) = f(x) + \frac{1}{2}\mu^2 \left(x - x^{prior}\right)^T C_0^{-1} \left(x - x^{prior}\right) \quad \text{.....(19)}$$

where C_o is the prior covariance matrix of the parameter to be adjusted "x", x^{prior} is the mean of the parameter "x", and μ^2 is used to adjust the relative weight between the response mismatch and prior information. The superscript "T" indicates the transpose of the vector. The objective function that has the prior term, Q(x), could be re-written as follows:

$$Q(x) = \frac{1}{2}.r(x)^T.C_{obs}^{-1}.r(x) + \frac{1}{2}.\mu^2.m(x)^T.C_o^{-1}.m(x) \quad \text{.....(20)}$$

where r, m, C_{obs} are defined by:

$$x = \begin{bmatrix} x_1 \\ \vdots \\ x_n \end{bmatrix}, r(x) = \begin{bmatrix} y_l^c(x) - y_l^{obs} \\ \vdots \\ y_p^c(x) - y_p^{obs} \end{bmatrix} \quad \text{.....(21)}$$

$$m = \begin{bmatrix} x_1 - x_1^{prior} \\ \vdots \\ x_n - x_n^{prior} \end{bmatrix}, C_{obs}^{-1} = \begin{bmatrix} 1/\sigma_l^2 & & 0 \\ & \ddots & \\ 0 & & 1/\sigma_l^2 \end{bmatrix} \quad \text{.....(22)}$$

$$C_o^{-1} = \begin{bmatrix} 1/\lambda_1^2 & & 0 \\ & \ddots & \\ 0 & & 1/\lambda_n^2 \end{bmatrix} \quad \text{.....(23)}$$

6.2.2 Steps # 2-5: Defining Sampling Cells, Sensitivity & Hessian Matrix Construction

If a history match problem is to be approached from an inversion point of view, then the potential parameter space is all the properties of all the grid cells. However, this will make the inversion approach impractical due the computational time required to handle such large simulation models and the large number of parameters. To make the inversion easier and more efficient, only the most sensitive parameters are selected and the number of simulation runs is reduced by effective sampling of simulation grids from the simulation model.

In Gradzone Analysis, reservoir simulation cells have to be sampled in such a way to maximize simulation model coverage. Thus, sample cells are expected be regularly spaced and as many as possible given the capability of available computational resources. Figure 6.2 below shows an example of sample cells selected for a 9x9 simulation model. The purpose of selecting sampling cells from the simulation model is to construct the sensitivity matrix, G_o. Sensitivity matrix is constructed by performing one base simulation run plus one complete history-match simulation run per sample cell

per adjustable parameter. This is in order to calculate the derivative of the response vector with respect to a change in the cell's parameter of interest. The sensitivity matrix, G_o is given by:

$$G_o = \begin{bmatrix} \frac{\partial y_1^{calc}}{\partial x_1} & \cdots & \frac{\partial y_1^{calc}}{\partial x_n} \\ \vdots & & \\ \frac{\partial y_p^{calc}}{\partial x_1} & \cdots & \frac{\partial y_p^{calc}}{\partial X_n} \end{bmatrix} \quad \text{.....(24)}$$

where "p" is number of observed data points and "n" is the total number of sampling cells. Sensitivity Matrix along with prior information provide a key guide to parameter selection for history match based on a compromise between high sensitivity and high uncertainty parameters. The Hessian Matrix, H_o, is given by:

$$H_o = G_o^T . C_{obs}^{-1} . G_o \quad \text{.....(25)}$$

where C_{obs} is the measurement error covariance matrix and superscript "T" indicate transpose of matrix or vector. The normalized Hessian Matrix, H, is given by:

$$H = H_o + \mu^2 C_o^{-1} = G_o^T . C_{obs}^{-1} . G_o + \mu^2 . C_o^{-1} \quad \text{.....(26)}$$

It must be noted that the Hessian Matrix, H_o, or the normalized Hessian Matrix, H has a dimension of n x n where "n", as mentioned earlier, is the total number of sampling cells:

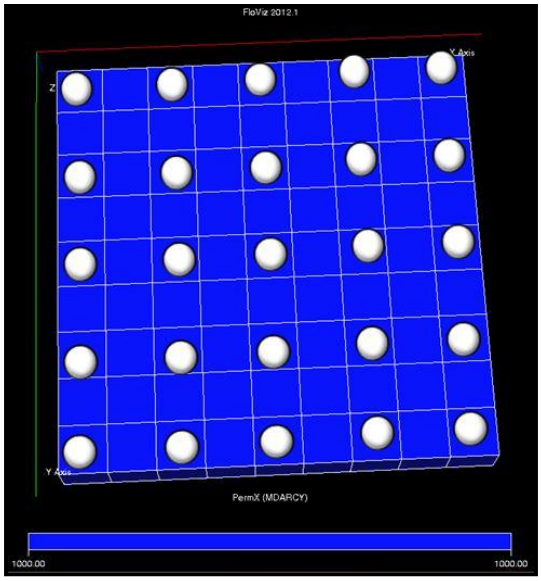

Figure 6.2: Sample cells locations for a 9x9 model

6.2.3 Steps # 6-8: Hessian Matrix Decomposition & Gradzones Construction

A Singular Value Decomposition (SVD) must be performed on the normalized Hessian matrix in order to extract its eigenvalues and their corresponding eigenvectors. The most important information is contained within the large magnitude eigenvalues which are usually the first few ones. Each eigenvalues can be treated as a Gradzone with the magnitudes of its corresponding eigenvectors determining the boundary of influence for each Gradzone. Thus, a threshold is applied on elements of each eigenvalue to remove cells with low eigenvector value which correspond to cells that have insignificant impact on the objective function (the history match). An eigenvalue with both positive and negative eigenvectors can be treated as two Gradzones. When two Gradzones intersect, the Gradzone corresponding to the higher eigenvector is chosen.

6.2.4 Steps # 9-12: Multipliers Construction, Regression, and Prior Weight

Once Gradzones have been defined, a prior covariance matrix for each Gradzone has to be constructed before performing the regression loop. Construction of multipliers can be illustrated by using a simulation model with two gradzones v_1 and v_2 as shown in the figure 6.3 below.

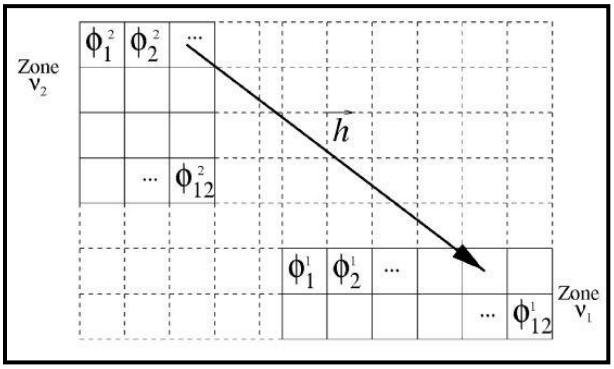

Figure 6.3: Example of multipliers construction for two Gradzones

The porosity of a given Gradzone can be calculated by averaging porosities of all grid cells within that zone. Thus for Gradzones v_1 and v_2 :

$$\phi_1 = \frac{\sum_{i \in v_1} V_i \phi_i}{\sum_{i \in v_i} V_i} \quad \text{.....(27)}$$

$$\phi_2 = \frac{\sum_{i \in v_2} V_i \phi_i}{\sum_{i \in v_i} V_i} \quad \text{.....(28)}$$

where V_i and ϕ_i is volume and porosity of grid cell "i", respectively. Based on this, the initial porosity multiplier for a given Gradzone could be expressed as follows:

$$\beta_1 = \frac{\phi_1}{\phi_i^{init}} = \frac{\sum_{i\epsilon v_1} V_i \phi_i}{\sum_{i\epsilon v_i} V_i \phi_i^{init}} \quad \text{.....(29)}$$

$$\beta_2 = \frac{\phi_2}{\phi_i^{init}} = \frac{\sum_{i\epsilon v_2} V_i \phi_i}{\sum_{i\epsilon v_i} V_i \phi_i^{init}} \quad \text{.....(30)}$$

Similarly for permeability, with the exception of using the logarithm of the multiplier rather than the multiplier itself, the permeability multiplier, α, for a given Gradzone can be expressed as follows:

$$ln\ \alpha_1 = \frac{\sum_{i\epsilon v_i} V_i \phi_i \ln(k_i / k_i^{init})}{\sum_{i\epsilon v_i} V_i} \quad \text{.....(31)}$$

$$ln\ \alpha_2 = \frac{\sum_{i\epsilon v_i} V_i \phi_i \ln(k_i / k_i^{init})}{\sum_{i\epsilon v_i} V_i} \quad \text{.....(32)}$$

Iterations performed on multipliers can be performed using Gauss-Newton approximation of the Hessian around a minimum using the following equations:

For permeability:

$$\alpha_{Gradzone,new} = \alpha_{Gradzone,old} + \Delta\alpha_{gradzone} \quad \text{.....(33)}$$

$$\Delta\alpha_{gradzone} = \Delta K_{Gradzone} / K_{Gradzone} \quad \text{.....(34)}$$

$$\Delta K_{Gradzone} = (\mu_{Gradzone} - k_{old}) + C_x . G_o^T [C_n + G_o . C_x . G_o^T]^{-1} [G_o . (k_{old} - \mu_{gradzone}) - (g(k_{old}) - d)] \quad \text{.....(35)}$$

For porosity:

$$\beta_{Gradzone,new} = \beta_{Gradzone,old} + \Delta\beta_{gradzone} \quad \text{.....(36)}$$

$$\Delta\beta_{gradzone} = \Delta\phi_{Gradzone} / \phi_{Gradzone} \quad \text{.....(37)}$$

$$\Delta\phi_{Gradzone} = (\mu_{Gradzone} - \phi_{old}) + C_x . G_o^T [C_n + G_o . C_x . G_o^T]^{-1} [G_o . (\phi_{old} - \mu_{gradzone}) - (g(\phi_{old}) - d)] \quad \text{.....(38)}$$

where $\mu_{gradzone}$ is the mean of the property being adjusted over the gradzone, g (ϕ_{old}) or g(k_{old}) is the simulation response vector generated by using a vector of the reservoir parameter being adjusted from the previous time step. Vector “d” is the observed data vector being matched ”C_x” is the variance matrix of the property, and the superscript “T” indicate the transpose of the vector/matrix.

6.3 Gradzone Analysis on Sherrod Area

6.3.1 Inversion Objectives

1. Invert water-cut responses to predict fracture properties governing flow in reservoir.
2. Create multi-layer models through simultaneous or sequential inversion of water-cut responses.
3. Investigate applications of inversion modeling in naturally fractured reservoirs.

6.3.2 Inversion Design

Inversion through Gradzone analysis requires the following elements:

1. Definition of surface response(s) to invert and property to be inverted.
2. Assigning weights to observed data.
3. Allocation of standard deviation of measurement error in observed data.
4. Design of areal and vertical sampling of simulation model grid cells.
5. Selection of number of eigenvalues to be used.
6. Selection of a threshold to be applied on eigenvectors of each eigenvalue.

6.3.3 Case Studies

The complex inter-connectivity of producers and injectors in Sherrod Area makes it difficult to select a small case study for inversion. Earlier in this study, the simultaneous water breakthrough of 44 wells in 2002 was studied both analytically and by constructing simulation models. This case could also be investigated by the use of inversion modeling as linking produced water with only three active injectors simplifies the problem.

Second case study to investigate is the limited number of inverted 9-spot patterns that exhibited weak communication with their surroundings. These patterns serve as the simplest case studies in Sherrod Area to test inversion. The pattern of injector Sherrod 1814 where significant tracer shows were only in a small area enclosed around the injector was chosen as a case study.

6.3.4 Case Study I: Simultaneous Water Breakthrough in 2002

6.3.4.1 Starting Point

The simulation model presented earlier in section 5.4 of this study was used for inversion. Initial properties of the simulation model and initial inversion design are shown in Tables 6.1 and 6.2 below. Observed water-cut data from the 44 wells were given equal weights and the property chosen to be inverted was the pore volume of the fracture/matrix system. Figure 6.4 below show locations of sampling cells used to run sensitivities. The presence of both negative and positive eigenvector elements in the first eigenvalue suggest that two Gradzones could be constructed from it as shown in

Figure 6.5 below. Performing regression on the two Gradzones did not show significant improvement in solution as root mean square value of the error was reduced by only 2.3%. Figures 6.6 and 6.7 show the model heterogeneity and pre and post inversion performance, respectively. The next subsections will investigate effect of changing inversion design on error reduction.

Property	Matrix	Fracture
Model dimention	82x91	
No. of layers	1	
Grid Cell Size	250'x250'	
Initial Saturation	0.22 (irreducable)	
Porosity	0.15	0.005
Permeability	1	200
Ky / Kx	1.0	1.0
Thickness	11	
Sigma	.01	

Table 6.1: Initial simulation model for inversion (Case Study I)

Property	Value
Property to invert	Pore Volume
Data weight, ω	1.0
Std. deviation of measurment error, σ_l	10%
Sampling Design	15x15
Number of Eigenvalues to use	1
Eigenvector thershold, λ	0.01

Table 6.2: Initial inversion design (Case Study I)

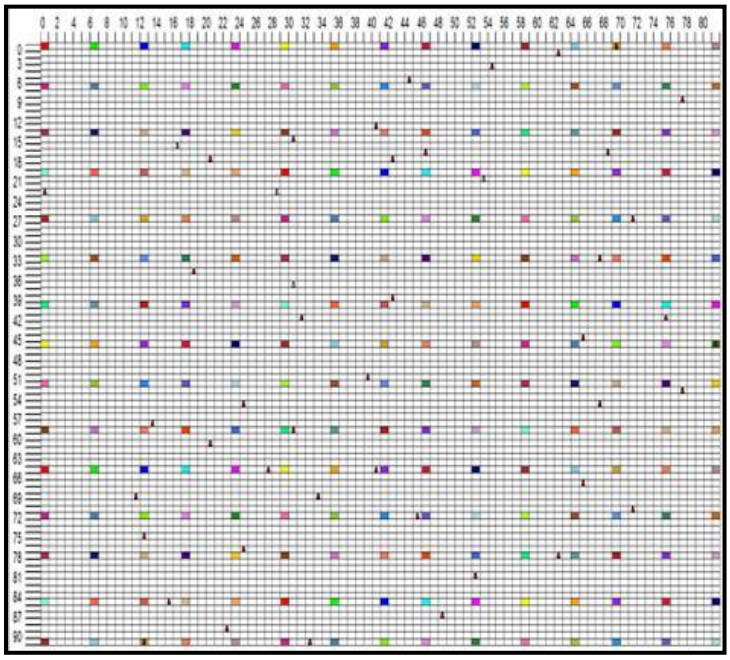

Figure 6.4: Sampling cells locations to run sensitivities (Case Study I)

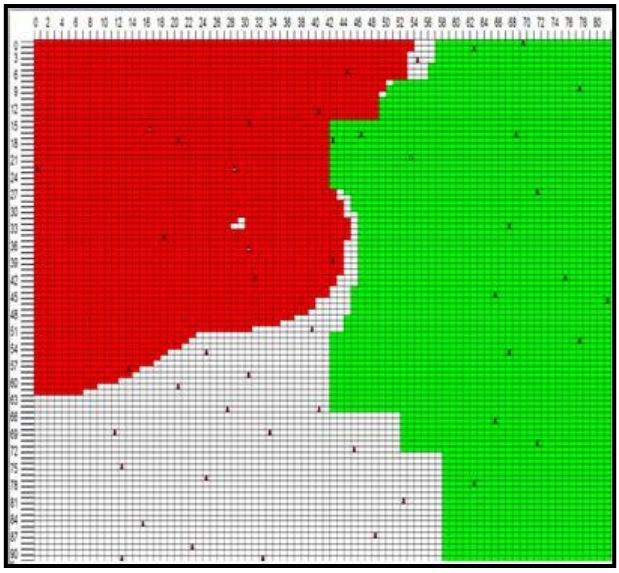

Figure 6.5: Gradzones using first eigenvalue to invert pore volume (Case Study I)

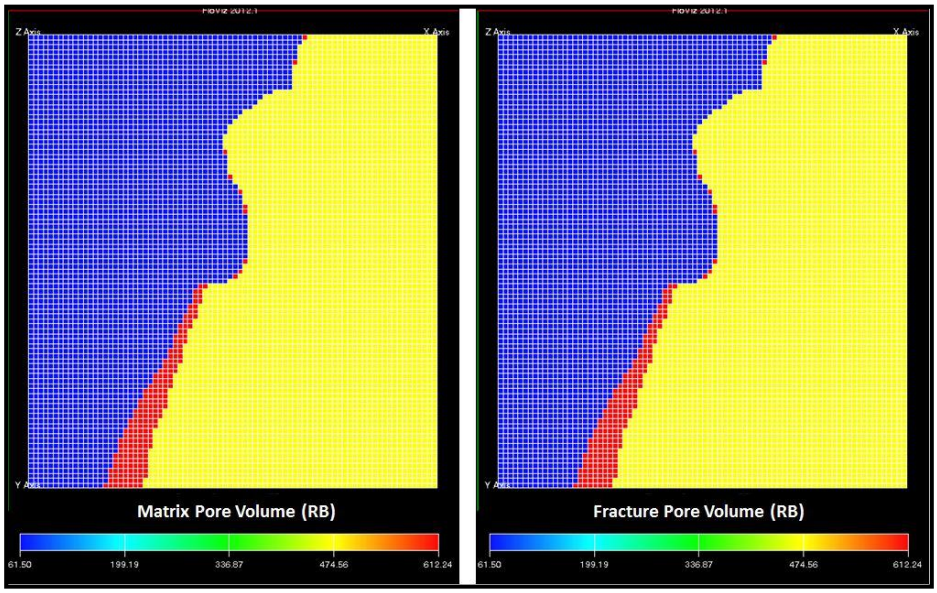

Figure 6.6: Pore volume of matrix/fracture system (Case Study I:1 layer inversion)

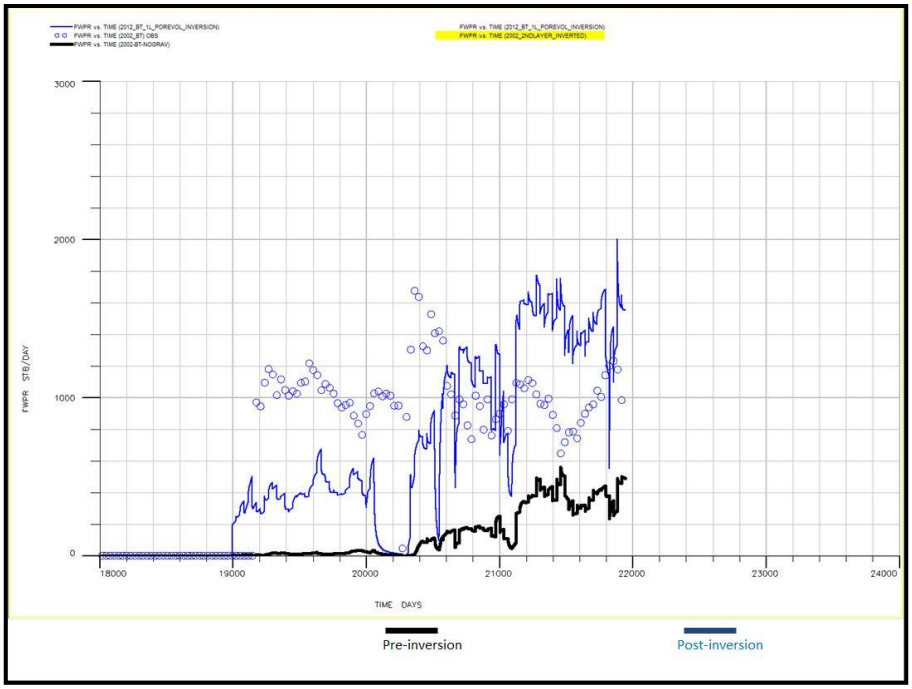

Figure 6.7: Pre and post inversion field water performance (Case Study I)

6.3.4.2 Choice of Property to be Inverted

Although reservoir parameters effecting water-cut response were investigated in the previous chapter, they were tested again in this sub-section. The same inversion design was tested but by using sigma and transmissibility in 'xy' direction as properties to be inverted. While using Sigma as the property to be inverted showed no improvement in solution, Transmissibility showed slight reduction in root mean square value of error by 0.4%. This shows that pore volume has the largest influence on water-cut performance. From this point forward, only pore volume will be used as an inversion property

6.3.4.3 Sampling Design

Sampling design to compute sensitivities was chosen initially to by 15 by 15 grid cells per simulation layer. A sampling design with lower number of grid cells significantly reduces the CPU time required to compute gradients and sensitivities. Thus, the inversion design was changed to use 10 x 10 grid cells per simulation layer. Figure 6.8 below show the effect of choosing a lower number of sampling cells on boundary of Gradzones. In term of error reduction, no change was observed

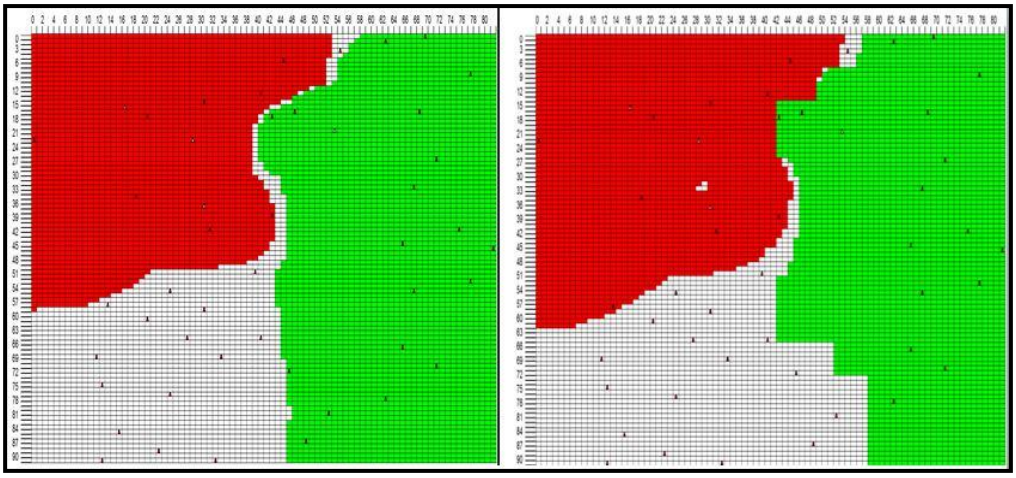

Figure 6.8: Gradzones using 10x10 (on left) and 15x15 sampling cells (on right)

6.3.4.4 Inverting a Multi-Layered Simulation Model

Inverting a multi-layered simulation model could be done using two different approaches: simultaneous inversion and sequential inversion. In the simultaneous inversion approach, the inversion is performed on all layers at the same time. While in

the sequential inversion approach, inversion is performed one layer at a time. Figures 6.9 and 6.10 show Gradzones and convergence behavior of solution for each case. While simultaneous inversion showed error reduction of 0.9%, sequential inversion showed error reduction of 17%. Figures 6.11 through 6.13 show the model heterogeneity and performance before and after inversion.

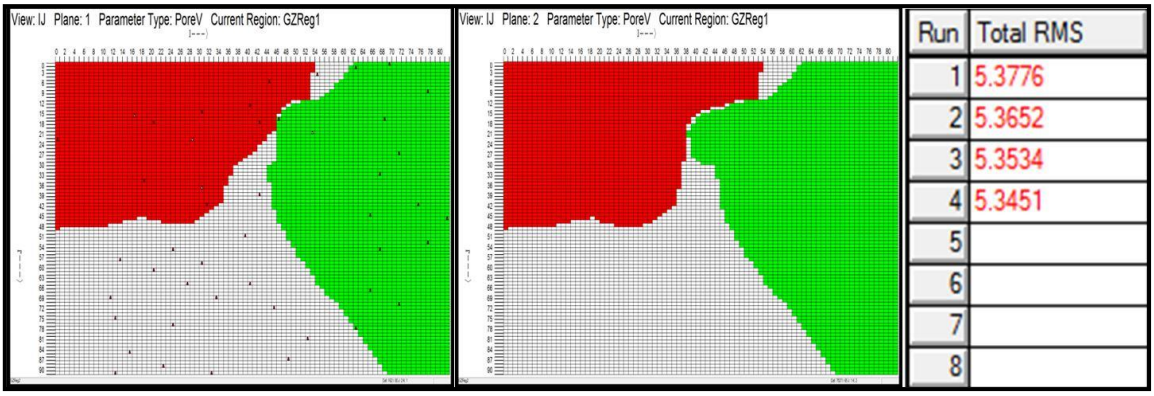

Run	Total RMS
1	5.3776
2	5.3652
3	5.3534
4	5.3451
5	
6	
7	
8	

Figure 6.9: Gradzones and solution convergence from simultaneous 2-layer inversion (Case Study I)

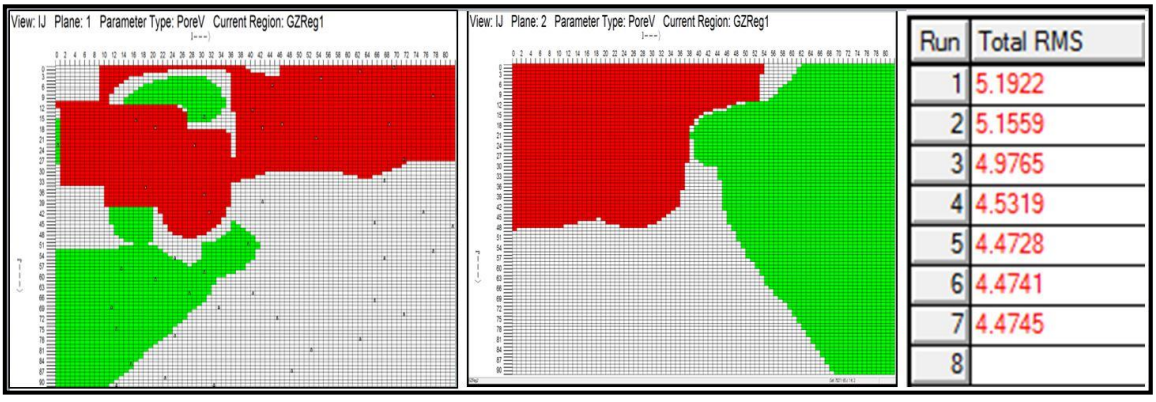

Run	Total RMS
1	5.1922
2	5.1559
3	4.9765
4	4.5319
5	4.4728
6	4.4741
7	4.4745
8	

Figure 6.10: Gradzones and solution convergence from sequential 2-layer inversion (Case Study I)

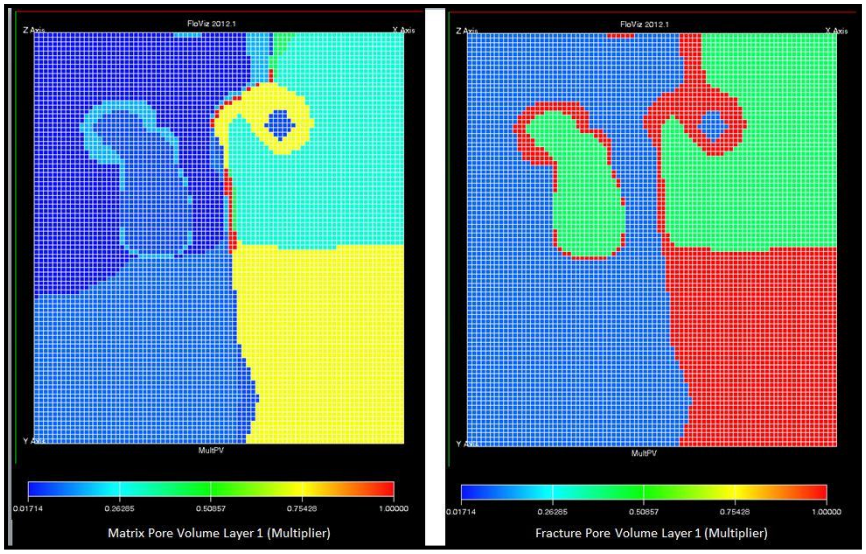

Figure 6.11: Inverted model of Case Study I using 2-layer sequential inversion: matrix & fracture layer # 1

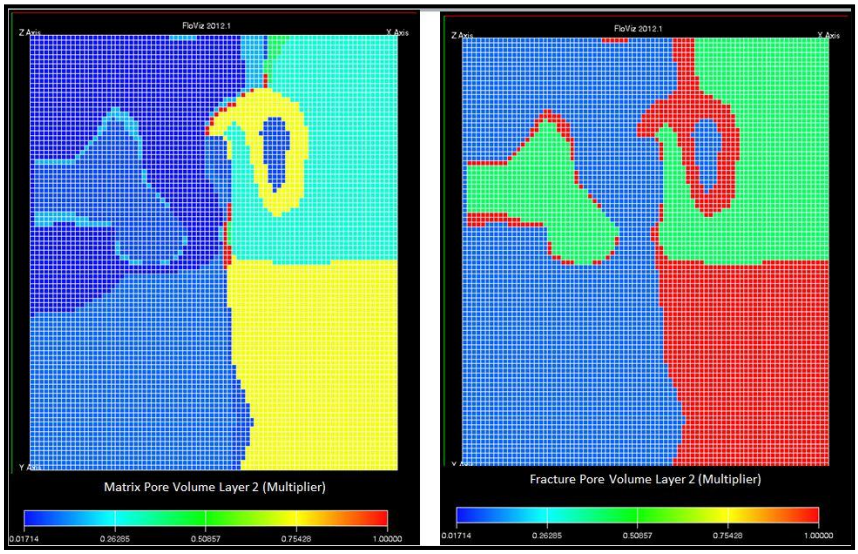

Figure 6.12: Inverted model of Case Study I using 2-layer sequential inversion: matrix & fracture layer # 2

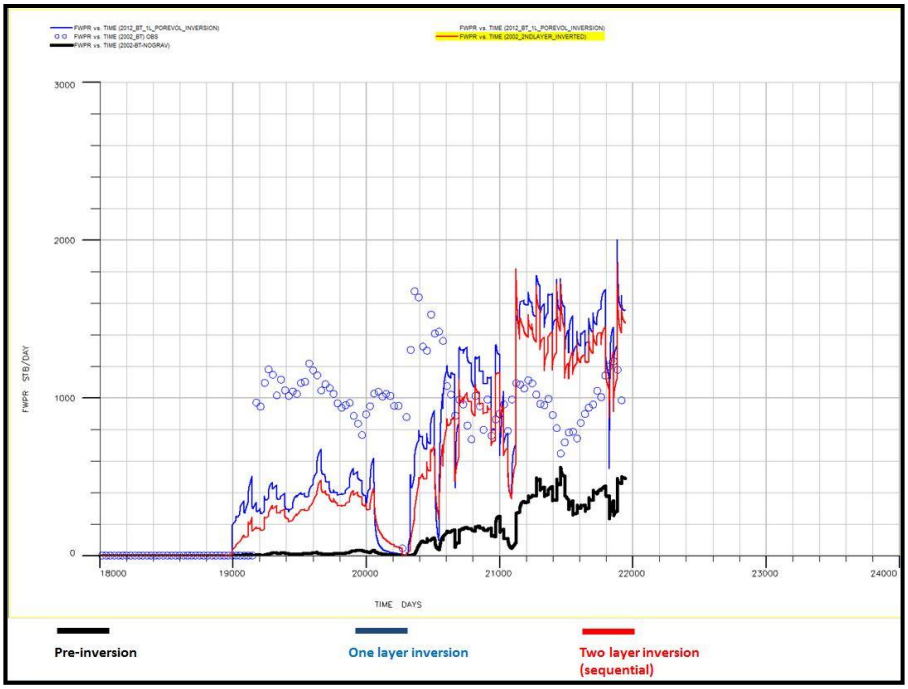

Figure 6.13: Comparison of field water performance from all inversion cases.

6.3.5 Case Study II: Pattern of Injector Sherrod 1814

A 5,200 by 5,300 feet sector model was built incorporating injector Sherrod 1814 and the 8 producers with moderate tracer shows around it. Initial properties of the simulation model and initial inversion design are shown in Tables 6.3 and 6.4 below. For the objective function, observed water-cut data from three key wells were given equal weights and the property chosen to be inverted was the pore volume of the system. Figure 6.14 below show the locations of the three key wells used in the objective function. The presence of only positive eigenvector elements in the first eigenvalue suggest that only one Gradzone could be constructed from it. Figure 6.15 below show the boundary of the first Gradzone. Performing regression on the Gradzone showed

significant improvement in solution as root mean square value of the error was reduced by 23.6%. Figures 6.16 through 6.19 show the model heterogeneity and performance before and after inversion. The next subsections will investigate effect of changing inversion design on error reduction.

Property	Matrix	Fracture
Model dimention	52x53	
No. of layers	1	
Grid Cell Size	100'x100'	
Initial Saturation	75%	
Porosity	0.15	0.005
Permeability	1	200
Ky / Kx	1.0	1.0
Thickness	4	
Sigma	.01	

Table 6.3: Initial simulation model for inversion (Case Study II)

Property	Value
Property to invert	Pore Volume
Data weight, ω	1.0
Std. Deviation of measurment error, σ_I	10%
Sampling Design	10x10
Number of Eigenvalues to use	1
Eigenvector thershold, λ	0.05

Table 6.4: Initial inversion design (Case Study II)

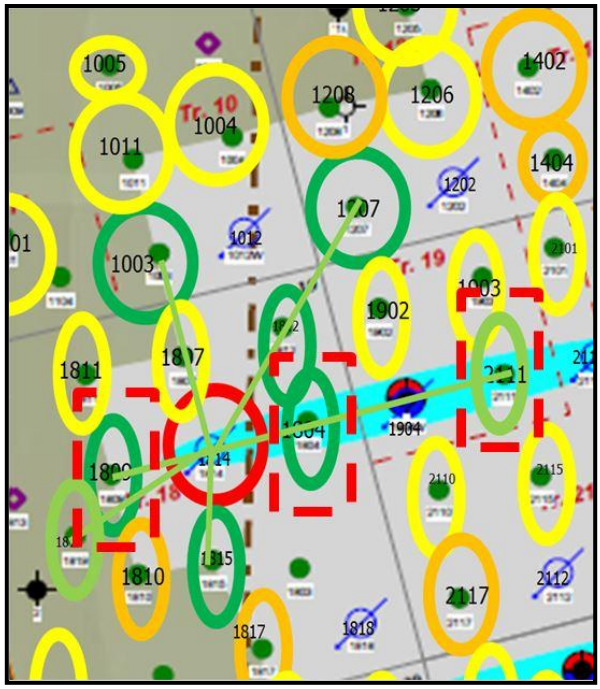

Figure 6.14: Three key wells used in objective function of pattern of 'Sherrod 1814' simulation model

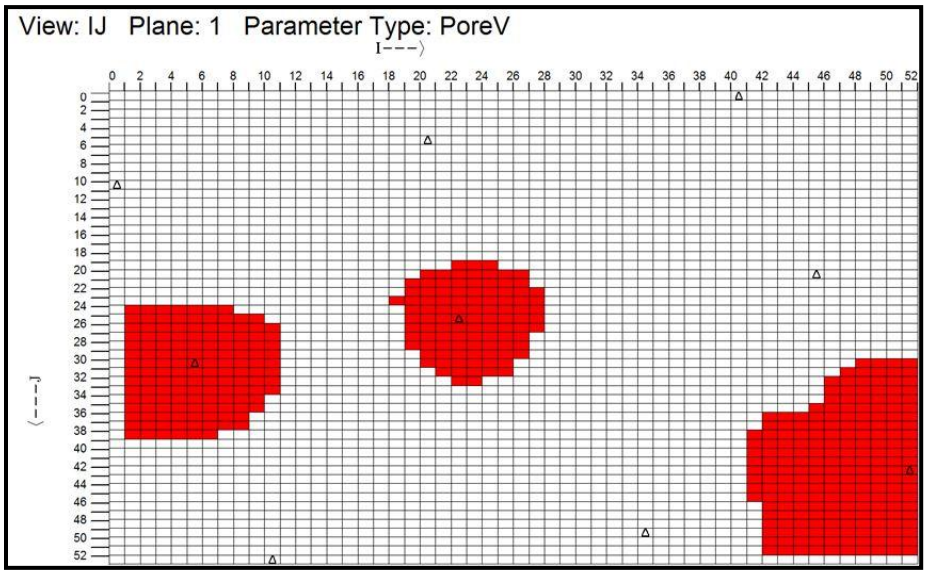

Figure 6.15: Boundary of first Gradzone used to invert one layer simulation model of pattern of 'Sherrod 1814'

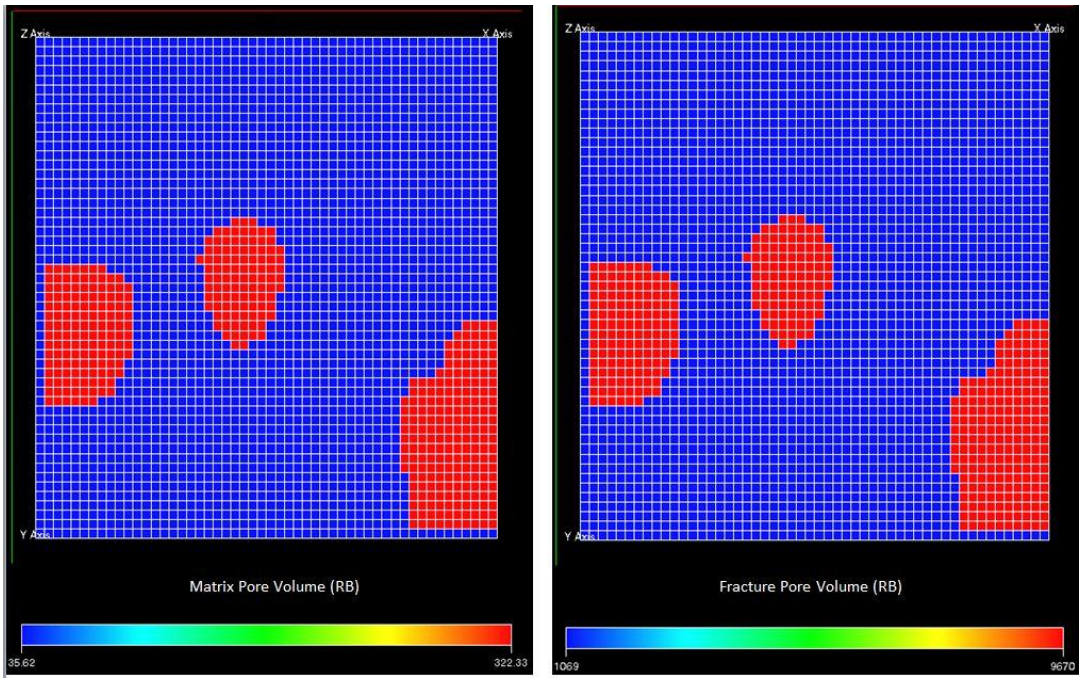

Figure 6.16: Matrix & fracture pore volume for pattern of 'Sherrod 1814' (1-layer inversion)

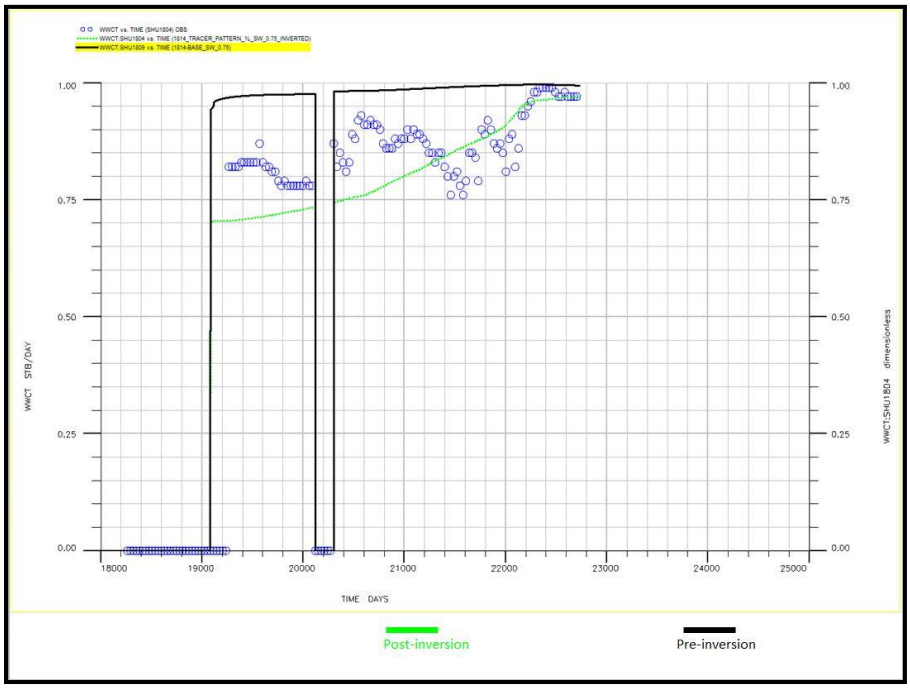

Figure 6.17: Pre and post inversion performance of 'Sherrod 1804'.

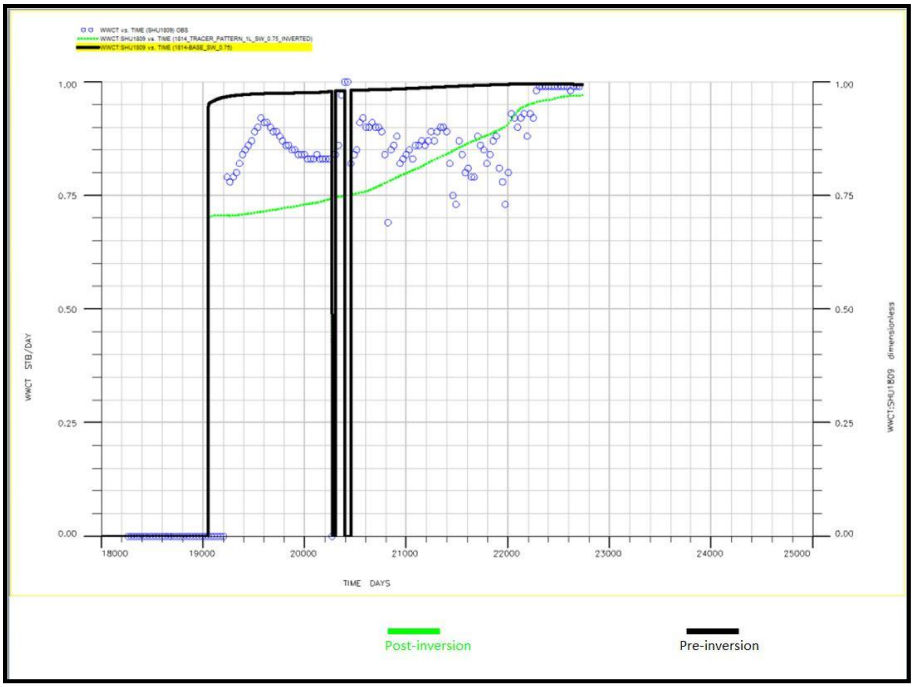

Figure 6.18: Pre and post inversion performance of ‘Sherrod 1809’

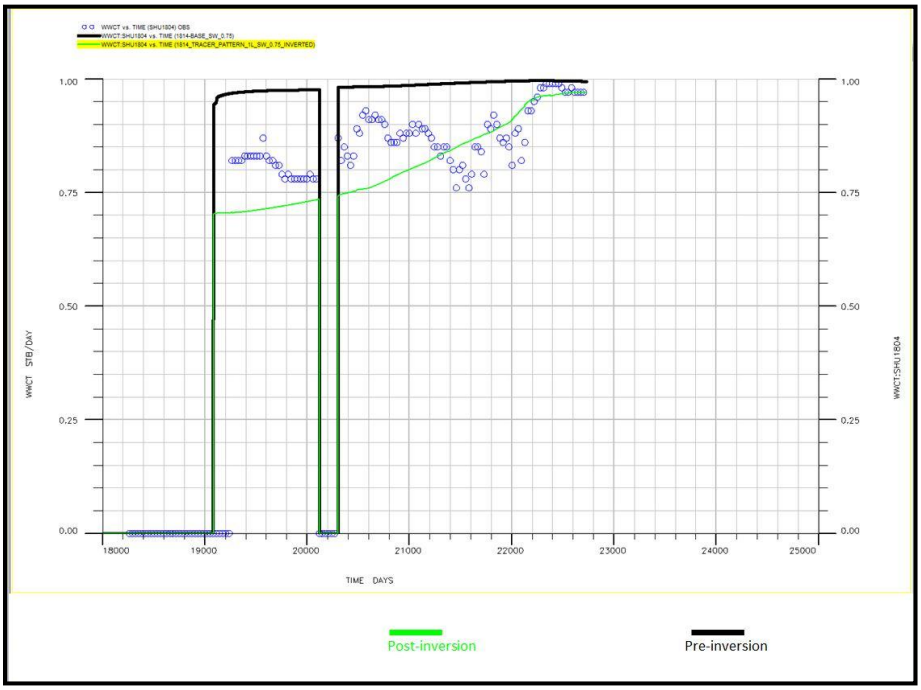

Figure 6.19: pre and post inversion performance of ‘Sherrod 2111’

6.3.5.1 Effect of Initial Water Saturation

Two cases with the same inversion design but different initial water saturation were studied. The objective of this case is to compare which initial water saturation shows lower error after inversion. Figures 6.20 and 6.21 show a comparison of the Gradzone shapes and solution convergence behavior for cases with initial water saturation of 65% and 75%, respectively. For the case of 65% initial water saturation, it shows less initial error compared to the case of 75% initial water saturation. However, by the end of regression, 75% initial water saturation case showed slightly lower error with a difference of 1.1%.

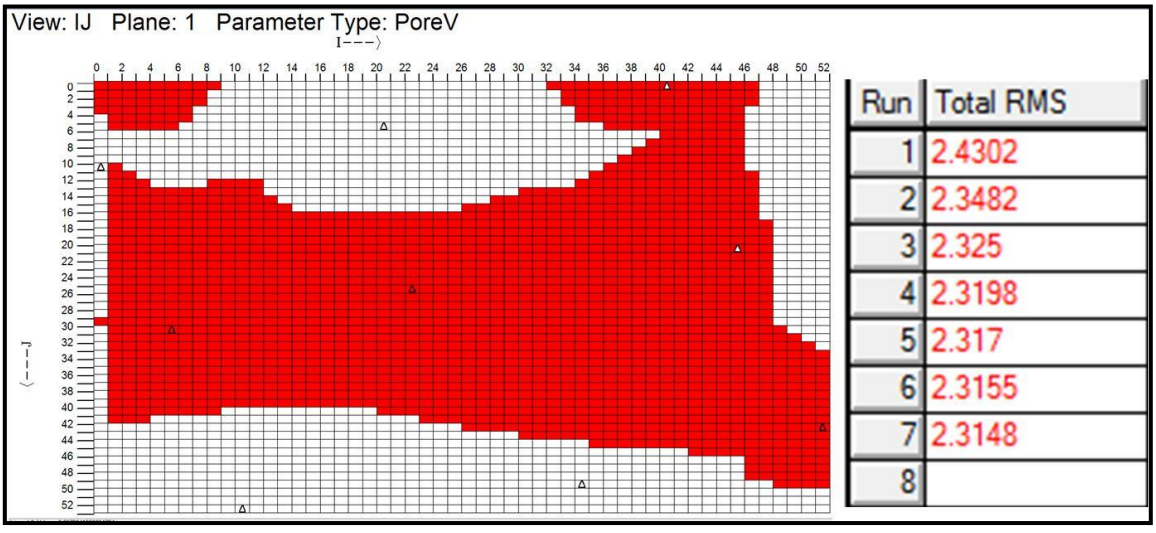

Figure 6.20: Gradzone & solution convergence for 65% initial water saturation case.

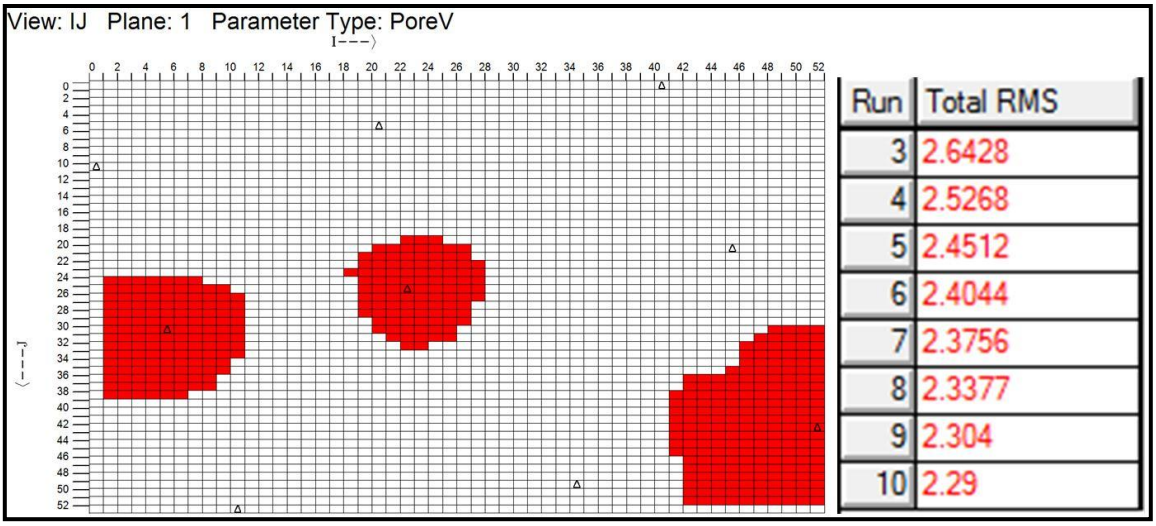

Figure 6.21: Gradzone & solution convergence for 75% initial water saturation case

6.3.5.2 Effect of Number of Gradzones & Eigenvector Threshold

For the case understudy, creating more Gradzone to cover larger area of the model did not show significant reduction in ultimate error. Similarly, using a lower eigenvector threshold value imposed on the first gradzone did not improve ultimate solution. Comparisons of Gradzones created for each case are shown in Figures 6.22 and 6.23 below.

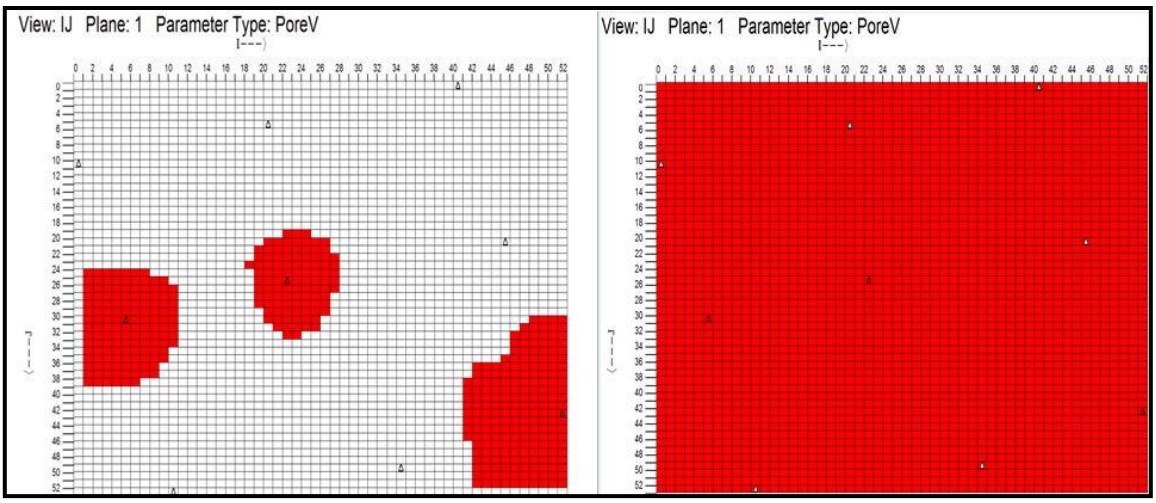

Figure 6.22: Gradzones using eigenvector threshold of 0.05 (left) and 0.01 (right)

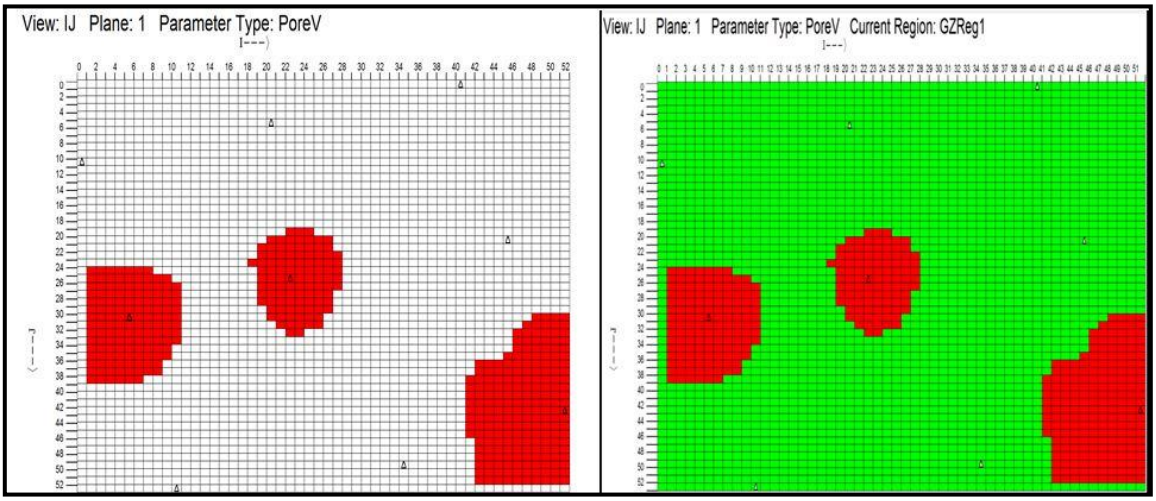

Figure 6.23: Gradzones using first eigenvalue (left) and second eigenvalue (right)

6.4 Limitations of Gradzone Analysis

Several limitations were observed while using Gradzone analysis package in Eclipse SimOpt:

1. Gradzone boundaries do not look realistic. This is due to the absence of any geological information that could be preserved during history matching
2. Convergence problems encountered while performing regression prevent improvement in solution by terminating the regression.
3. Inversion modeling by Gradzone Analysis showed limitations in stability of inversion when dealing with models with greater than 2 layers.

6.5 Summary of Results

1. Inversion modeling by Gradzone Analysis shows significant error reduction by 17% for the case study of 2002 field-wide simultaneous water breakthrough. Inversion results show that north-east and west side of the field have very low pore volumes compared to the south-east. North-east and west side of field have 2% and 35% of the pore volume existing in the north-east, respectively.

2. Inversion modeling by Gradzone Analysis shows significant error reduction by 23.3% for a case study of inverted 9-spot pattern showing weak communication with its surroundings. Inversion results show that pore volume of the matrix-fracture system should be much higher than what is initially assumed.

3. Sequential inversion approach showed to be the most effective approach for the case studies tested. It showed error reduction of 17% compared to 2.3% for single layer inversion and 0.9% for simultaneous two layer inversion.

4. Inversion modeling could be used to assess initial water saturation of matrix-fracture system by performing multiple inversions using identical models with different initial water saturation. Our case study showed initial water saturation of matrix-fracture system around pattern of Sherrod 1814 is more likely to be 75% based on water-cut responses.

5. Inversion modeling by Gradzone Analysis showed limitation when dealing with models with more than 2 layers.

7. ANALYSIS OF SHERROD INTER-WELL TRACER TEST DESIGN

7.1 Introduction

Inter-well tracer test of Sherrod Area in Spraberry Field presents a key case study to highlight best practices in the design of inter-well tracer tests in naturally fractured reservoirs. This is due to the large number of tracers injected and producers sampled, and the high complexity of fracture network encountered.

7.2 Objectives

The objective of this chapter is to utilize Sherrod inter-well tracer test as a case study to highlight best practices and lessons learned in the design and execution of inter-well tracer tests in naturally fractured reservoirs. History matched tracer responses will be utilized to analyze different design considerations, and to optimize cost and efficiency of these tests.

7.3 Elements of Tracer Tests Design

After selecting which type of tracers to use, design of inter-well tracer tests have four main elements to consider:

1. tracers injection locations
2. tracer injection design
3. operating conditions
4. sampling locations & schedules

7.3.1 Tracers Injection Locations

Tracers' injection locations presented earlier and shown in Figure 7.1 highlight that majority of tracers were injected through pattern injectors. Only one out of the two active non-pattern injectors, Sherrod 701, was tagged with a tracer.

From the performance of pattern injectors, poor tracer recovery was expected. This is because activation of injectors showed either no effect or a slight increase in the water performance of already high producing water-cut wells in the range of 80-90%. If pattern injectors and pattern producers were in good communication, they would have caused producers to die from excessively high water-cut. Two examples for impact of pattern injectors on performance of pattern producers few months before introducing tracers are shown in Figures 7.2 and 7.3. In the first example in Figure 7.2, the well shows no change in performance after injector activation. In the second example in Figure 7.3, the performance of the producer is adversely affected by the increase in water cut to above 99%. The value of tracers injected in this case is to highlight the direction of water movement outside the pattern. Results presented in previous sections showed how 6 out of the 11 pattern injectors are connected with producers 'Ruby 18' and 'Ruby 19' outside patterns injection area.

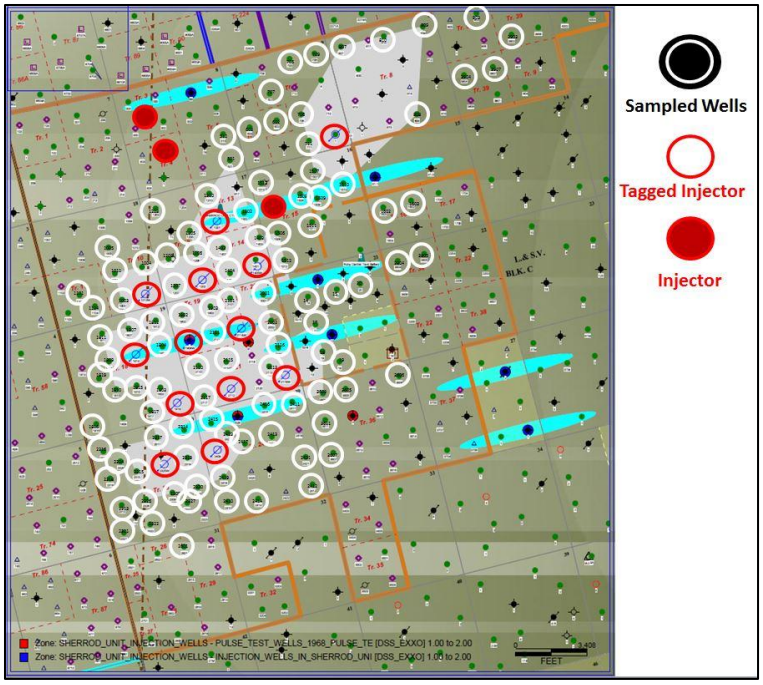

Figure 7.1: Sherrod inter-well tracer test injection & sampling locations

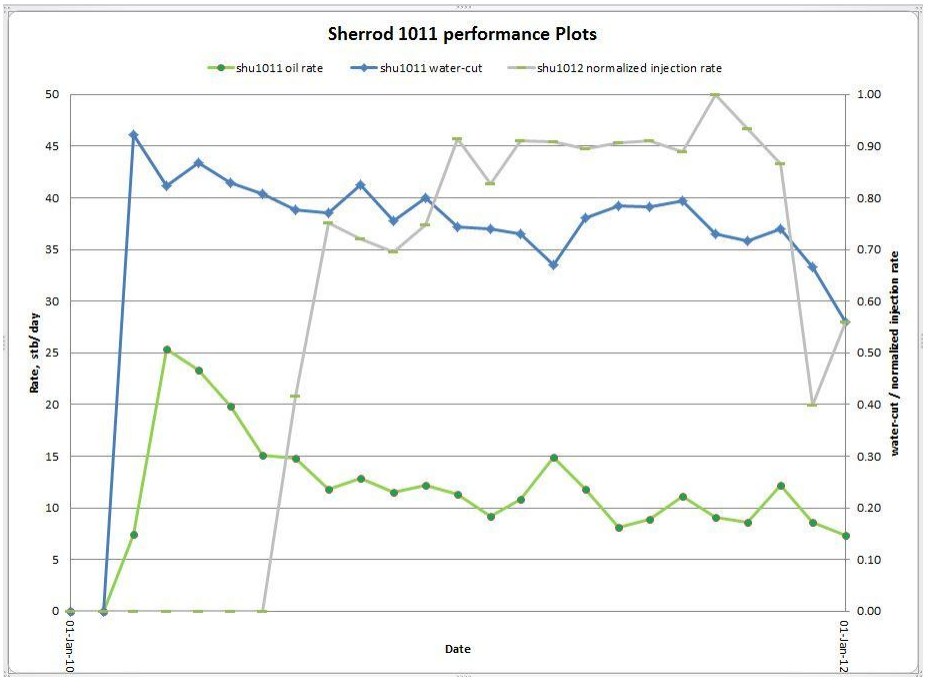

Figure 7.2: Example of well unaffected by activation of pattern injector

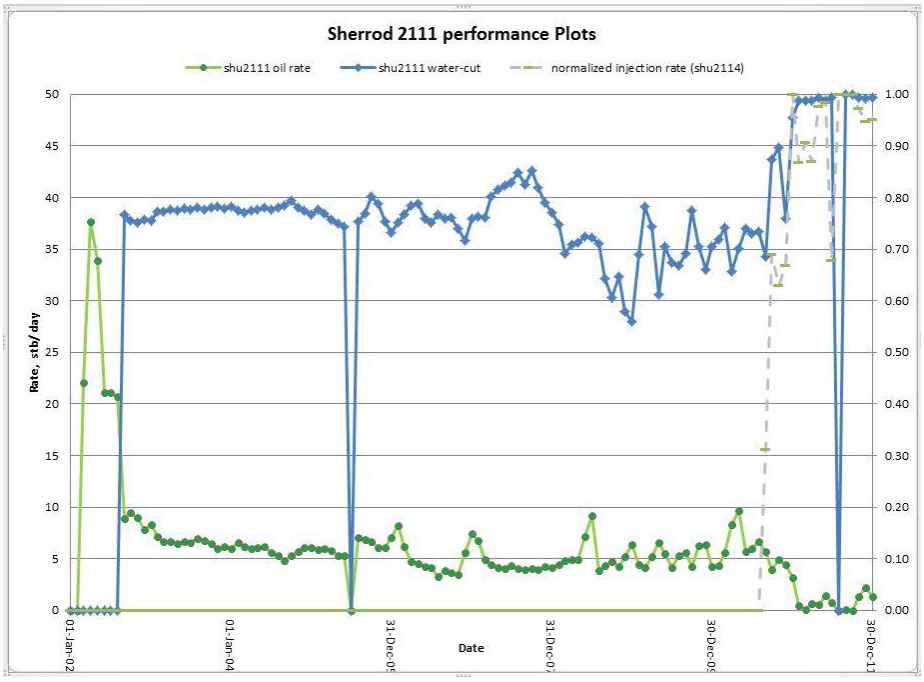

Figure 7.3: Example of well adversely effected by activation of pattern injector

7.3.2 Tracer Injection Design

Tracers' masses and volumes, tracers' injection schedules, and water injection rates used for mixing of the 13 tracers used in Sherrod inter-well tracer are shown in Table 7.1 below. The effect of tracer injection design such as volume of tracer to inject, mixing duration and injection rates are studied by utilizing a history matched tracer response between 'Sherrod 1809-Sherrod 2114'. Figure 7.4 show the tracer response match and the pair location.

The effect of all three parameters translates on concentration injected. A higher volume of tracer, a lower mixing rate, or lower mixing duration results in a more concentrated slug and vice versa. The effect of each parameter on injected

concentrations is shown in Figures 7.5 through 7.7. Figure 7.8 show the relation between concentration injected and peak concentration produced. Considering the low detection limit of 50 part per trillion used in Sherrod tracer test, a much lower tracer volume could have been used. From Figures 7.6 and 7.8, volume of tracer used in the test could have been reduced by 82% and still produce a high peak concentration of 10,000 ppt. Using less tracer volume not only reduce cost of running the tracer test, but also minimize the large number of excessively diluted tracer responses generated mostly by water recycling. In summary, tracer volumes used were much higher than what was actually needed even with the excessive dilution that affected all tracers' responses.

Injection Well ID	Tracer Type	Tracer Amount (L)	Tracer Amount (g)	Date of Injection	Start Time	End Time	Injection Time (hours)	Well Injection Rate (BPD)	Tracer Slug Volume (ml)	Injected Tracer Concentration (W/V) , ppt
Sherrod U 1814W	IWT 1900	200	20000	25-Apr-11	12:00 PM	4:00 PM	4	365	9,871,892	2,025,954,161
Sherrod U 1202W	IWT 2400	118	11800	25-Apr-11	5:00 PM	8:00 PM	3	321	6,497,474	1,816,090,446
Sherrod U 1818W	IWT 1100	212	21200	26-Apr-11	7:00 AM	11:30 AM	4.5	260	7,962,763	2,662,392,606
Sherrod U 2112W	IWT 1700	193	19300	26-Apr-11	12:00 PM	4:30 PM	4.5	345	10,477,666	1,842,013,354
Sherrod U 2409W	IWT 1200	231	23100	26-Apr-11	5:00 PM	10:00 PM	5	355	11,989,635	1,926,664,089
Sherrod U 1301W	IWT 1500	88	8800	27-Apr-11	6:00 AM	9:00 AM	3	390	7,838,763	1,122,626,180
Sherrod U 1904W	IWT 2200	159	15900	27-Apr-11	9:30 AM	2:30 PM	5	275	9,267,802	1,715,617,129
Sherrod U 1405W	IWT 1500	92	9200	27-Apr-11	3:00 PM	6:00 PM	3	310	6,252,863	1,471,326,133
Sherrod U 2114W	IWT 2500	128	12800	27-Apr-11	6:30 PM	11:00 PM	4.5	340	10,263,613	1,247,124,246
Sherrod U 2325W	IWT 1000	273	27300	28-Apr-11	6:00 AM	10:30 AM	4.5	190	5,937,019	4,598,267,439
Sherrod U 2118W	IWT 1600	148	14800	28-Apr-11	11:00 AM	2:30 PM	3.5	330	7,799,394	1,897,583,386
Sherrod U 1012W	IWT 2100	154	15400	28-Apr-11	3:00 PM	6:30 PM	3.5	325	7,689,464	2,002,740,492
Sherrod U 701W	IWT 2000	168	16800	28-Apr-11	7:00 PM	10:00 PM	3	145	3,049,694	5,508,749,854

Table 7.1: Tracer injection schedule & design for all tracers

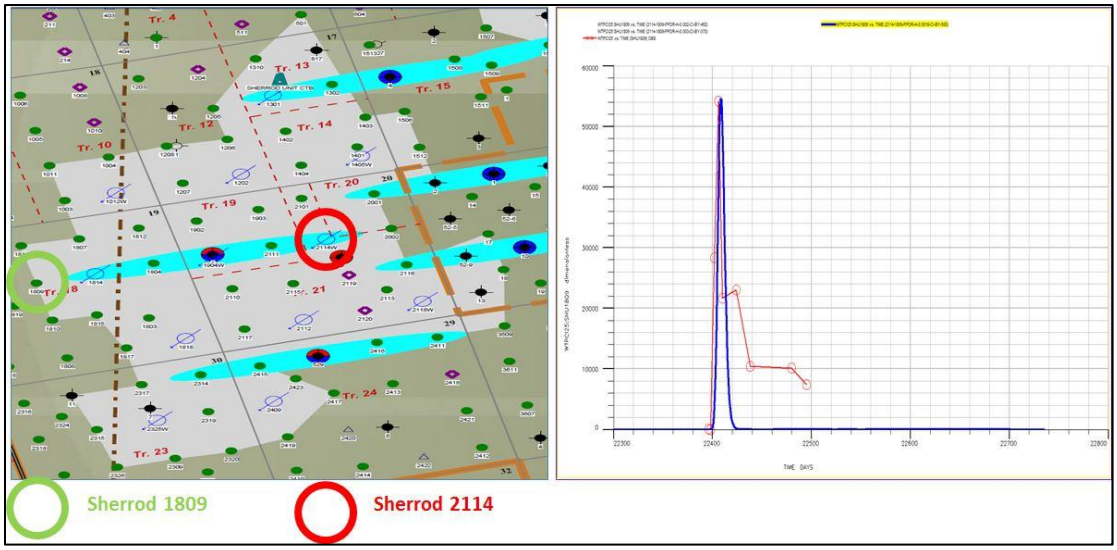

Figure 7.4: Tracer response used for analysis of test design

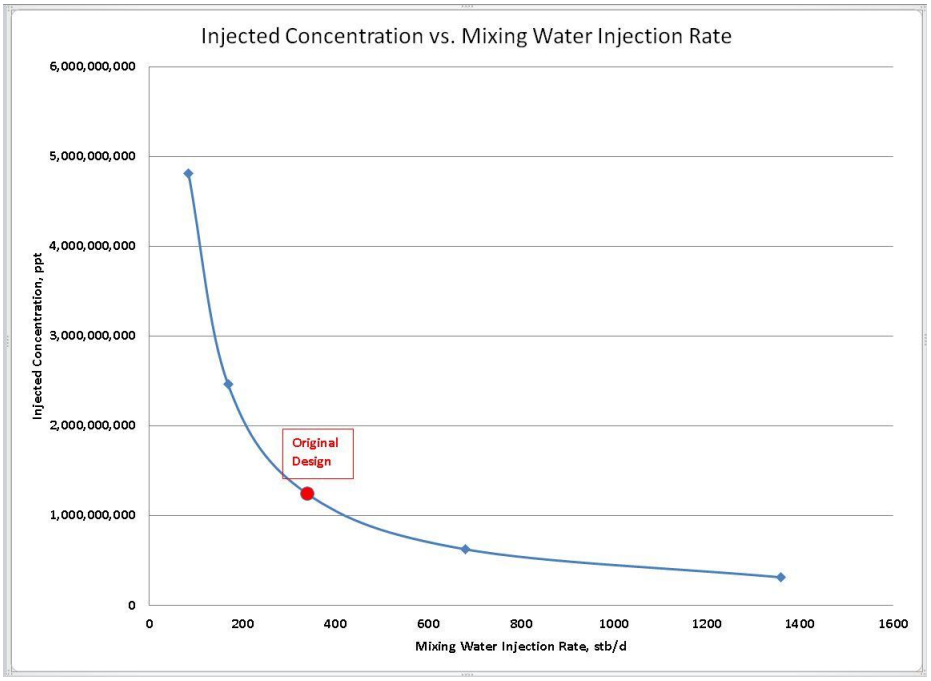

Figure 7.5: Effect of mixing injection rate on concentration injected

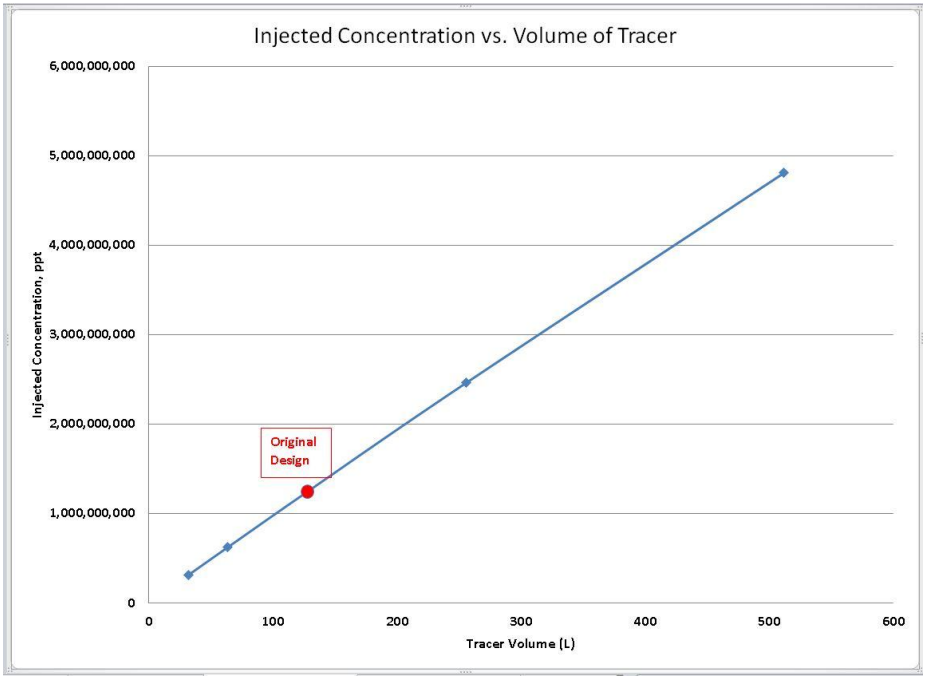

Figure 7.6: Effect of tracer volume on concentration injected

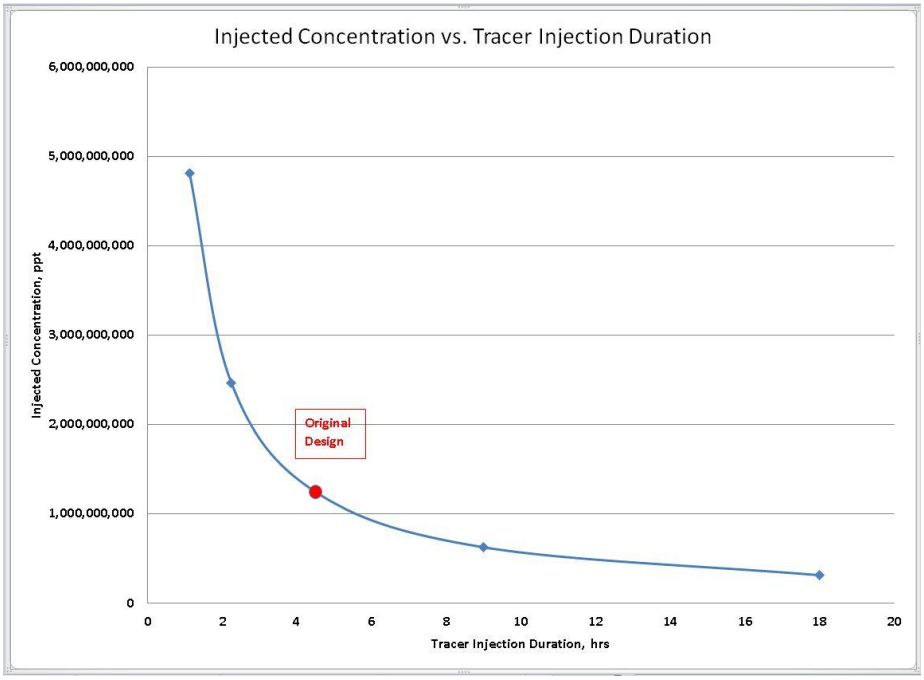

Figure 7.7: Effect of tracer mixing duration on concentration injected

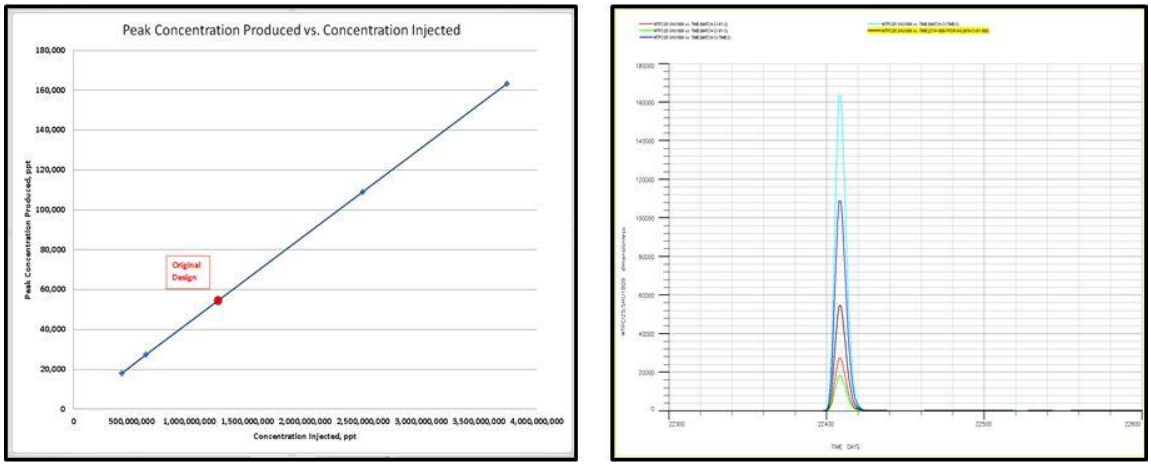

Figure 7.8: Effect of concentration injected on peak concentration produced

7.3.3 Operating Conditions Considerations

Effect of operating conditions, particularly injection rate, on tracer response was discussed partially in section 5.3 earlier. Injection rate for the pair under study was varied by a factor of 0.5 and 0.75. The impact of varying average injection rate on tracer response is shown in Figure 7.9 below and indicates that a lower average injection rate of a well will cause a lower peak concentration produced, a more diluted response and a further delay in tracer breakthrough for the same concentration injected. This highlight that wells' average injection rate should be considered in designing injected concentrations and duration of sampling schedule. This was already considered in the design of Sherrod tracer test by using a much higher concentration injected for the low injection rates wells as shown in Table 7.1 earlier.

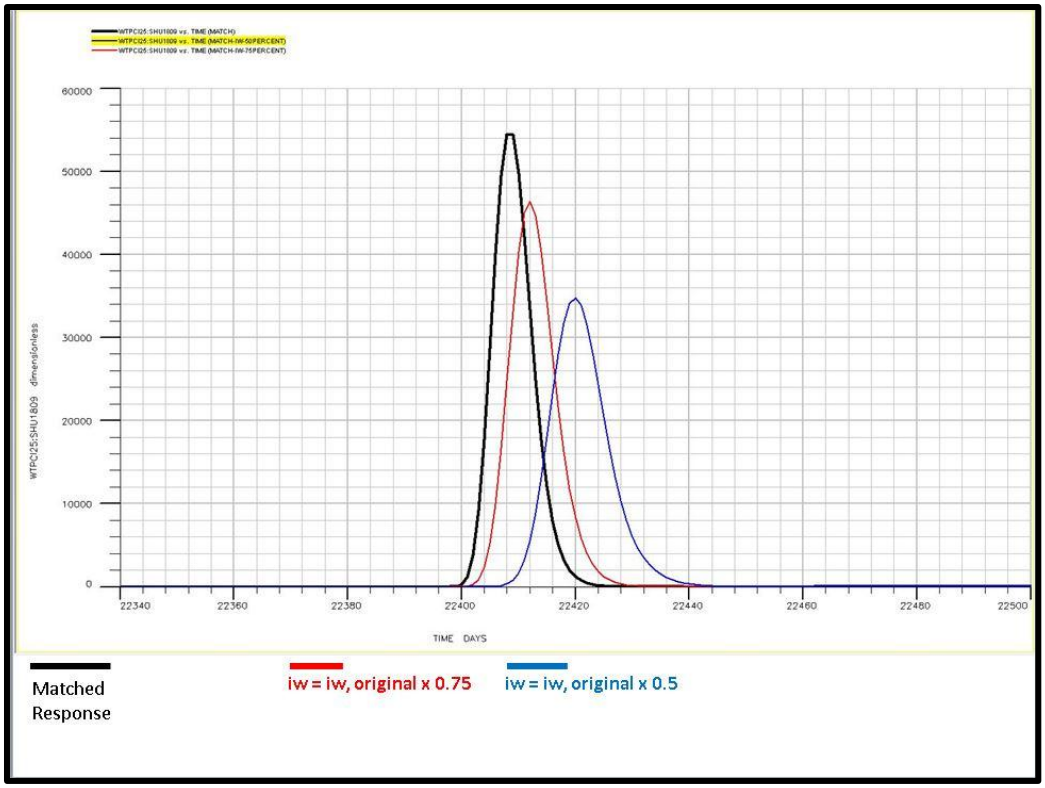

Figure 7.9: Effect of operating conditions on tracer response

7.3.4 Sampling Locations & Schedules

One important design consideration highlighted in Sherrod inter-well tracer test is the importance of early start of water sampling of producers. Figure 7.10 and Figure 7.11 below shows tracers' responses with same day and one day breakthrough, respectively. Figure 7.12 show examples of tracer responses with breakthrough time missed. Breakthroughs of these tracers were missed because of late sampling. This highlights the importance of sampling produced water from the same day of tracer injection.

A second important factor to consider is the length of the sampling schedule. This study showed earlier in section 4.7 that tracer responses obtained after the second week of the test were not adequate for fracture characterization because those were either excessively diluted or largely effected by water recycling. Thus, Sherrod inter-well tracer test could have been terminated by the end of the second week. This could have saved 100 days or 87.7% of operation time.

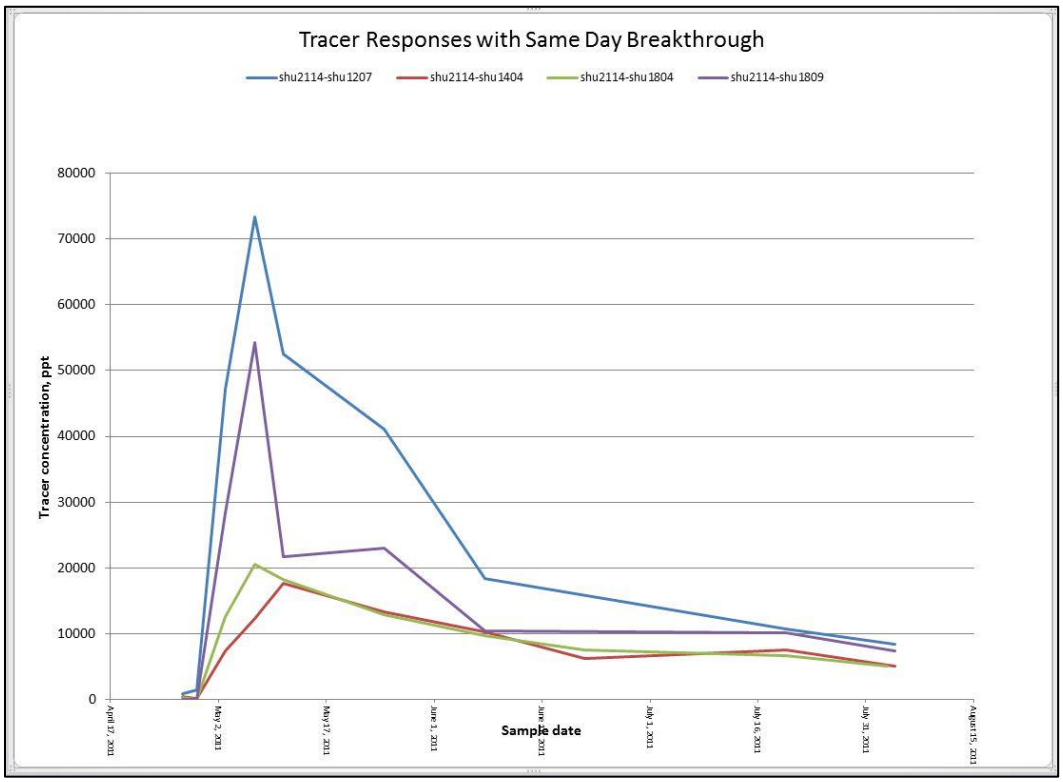

Figure 7.10: Tracer responses with same day breakthrough

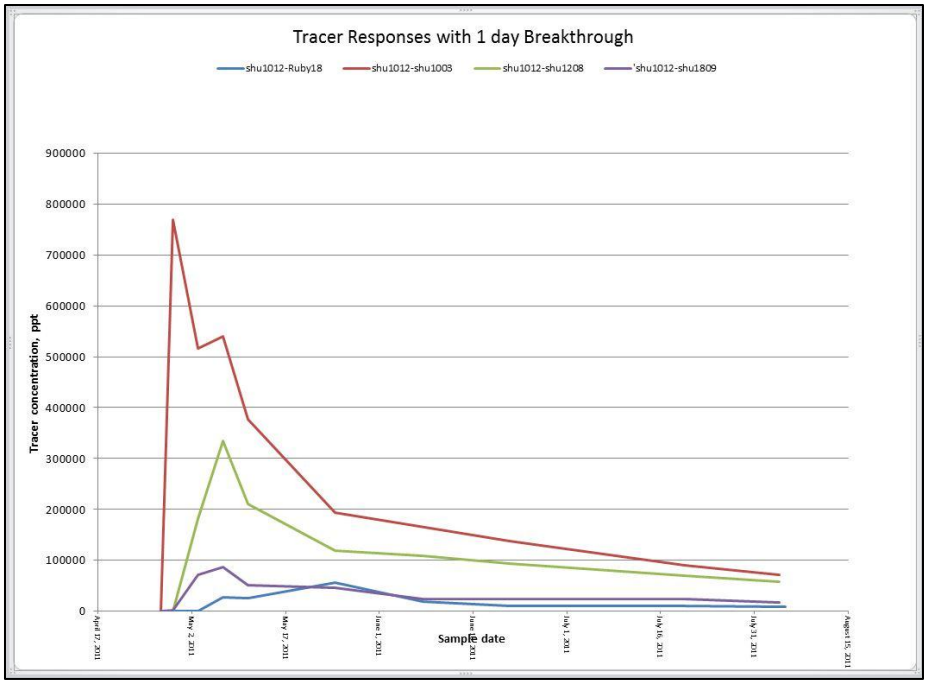

Figure 7.11: Tracer responses with one day breakthrough

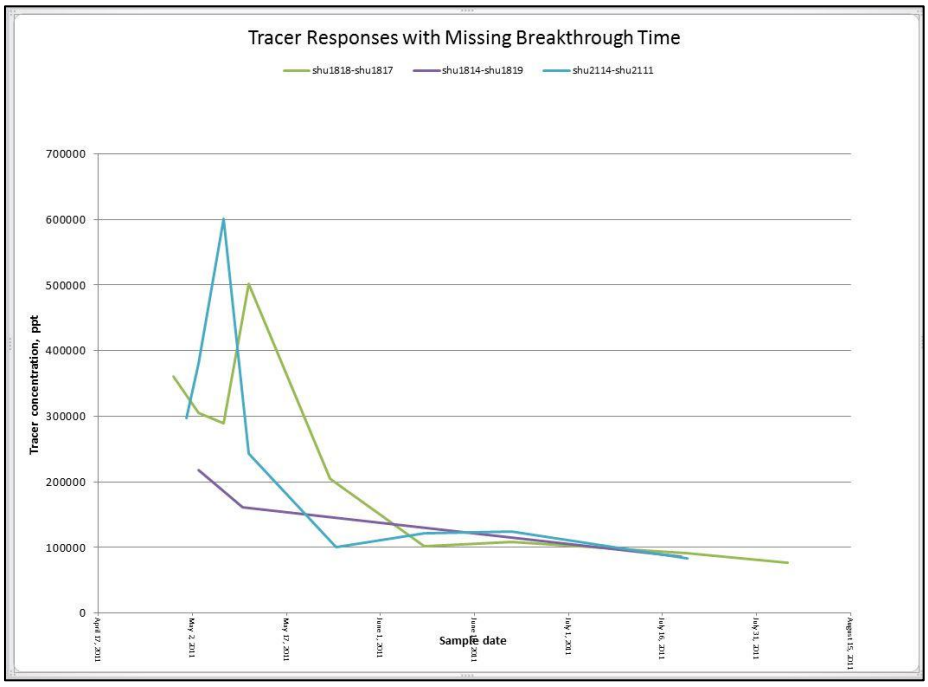

Figure 7.12: Tracer responses with breakthrough time missed

7.4 Summary of Design Considerations

Inter-well tracer test design in naturally fractured reservoirs through lessons learned from Sherrod Area could be summarized as follows:

1. Volume of tracers used was excessively large. Only 18% of the volumes used were required to capture and characterize the complex fracture network in the field. Using a combination of very low detection limit and excessive tracer volume was the main reason of creating high number of excessively diluted responses that added no value to characterization process.
2. Sampling of water produced should start from same day of tracer injection in order to avoid missing breakthrough time of ultra-high velocity tracers.
3. Test duration of Sherrod test should have been terminated by the second week when majority of responses turned to be intermittent and excessively diluted. This could have saved 87.7% of operating time without effecting test interpretation.
4. Tracers injected through low water injection rate wells are expected to exhibit delays in breakthrough time and to have lower peak concentration produced. Thus, relatively larger injected concentration should be used wells with relatively lower injection rates.

8. CONCLUSIONS AND RECOMMENDATIONS

8.1 Conclusions

In our study, water-cut and tracer responses of Sherrod Area in Spraberry field were analyzed using analytical, numerical simulation, and inversion modeling approaches. The objectives of the analytical approach were to effectively categorize tracer responses in order to quantify their significance in explaining water movement in the field, to map observations in order to understand water and tracer movement in the field, and to identify patterns and anomalies in water-cut and tracer responses in order to explain reservoir behavior. The objectives of numerical simulation study are to match tracers' responses, to explain the ultra-high tracer velocities observed in the field, and to explain water-cut behavior in the field. The objective of inversion modeling approach is to invert water-cut responses into multi-layer heterogeneous dual porosity models. Conclusions based on the research findings could be summarized as follows:

1. Maximum sweep directions obtained from Methods of Moments indicate the presence of four major inter-connected flow features oriented N76^{o}E governing water movement in the field.
2. Sherrod Area of Spraberry Field exhibit very poor waterflood performance. This is evidenced by field water production which follows precisely the field water injection rate.
3. Poor overall tracer recovery with none of the 13 injected tracer recovered by more than 9%.

4. Tracer responses could be categorized into four groups based on the distribution of tracer recovery for all tracers' responses.
5. Studying characteristics of tracer responses based on tracer recovery highlight several aspects of tracer responses:
    a. No correlation between tracer velocity and tracer recovery.
    b. Tracer responses with less than 0.01% recovery is highly effected by water recycling. As tracer recovery of the tracer response increase, the water recycling effect decrease.
    c. Number of peaks in a tracer response correlates strongly with tracer recovery. This indicates that a higher recovery tracer response captures more the layering between a pair of injector and producer.
6. For a field where wells injection rates are in the range of 100-400 stb/d, tracer responses with less than 0.1% recovery explains water movement of less than 1 bbl / day and thus should be ignored.
7. Sherrod Area of Spraberry Field receives water influx from an external water source. This is supported by the following observations:
    a. The abnormal increase in water-cut for a number of wells during field water injection shut-in between December 2004 and July 2005.
    b. The declining water cut trend for a number of wells that did not show any tracer. water-cuts declines from as high as 85% to as low as 40%.
    c. The abnormal higher than 99% water-cut appearing for a short period for a number of wells surrounding tracer study area.

d. The high fluctuation of water-cut values between as high as 90% to as low as 50% for a number of wells without changes in active injection rates that justify such behavior.
e. The extensive instantaneous dilution and the abnormal tracer velocity of 8900 ft/day for a tracer travelled across the field from Sherrod 1012 on west side to Ruby 18 which exist east side outside tracer study area.
f. The absence of a mathematical solution using dual porosity formulation to describe a tracer velocity of 8900 ft/day based on fracture properties alone.
g. Simultaneous water breakthrough of a group of 6 wells in 1973 without data showing an active injection system in the area.

8. Tracers recovered explains no more than 10% by average of patterns' water production
9. Tracer responses are highly affected by non-reservoir parameters like grid resolution, dilution, drainage area surrounding wells, and loss of injected water outside study area. These factors make fracture properties from tracers matches highly uncertain.
10. Breakthrough time of tracer responses provide a solution for ($\varphi_f h$) of the fracture layer. Peak of tracer responses are highly affected by dilution and are not a reliable measure of any fracture property.

11. Simultaneous breakthrough of 44 wells in 2002 is dominated by water flow in fracture system. This indicates very weak communication with matrix system which is most likely caused by high degree of fracture mineralization. This is supported by:
    a. Comparison between group water production rate and different combinations of injection rates of active injectors.
    b. A history match of field water performance using a dual porosity model with matrix-fracture water saturation of 80%.
12. Majority of pattern injectors, 6 out of 11, show that part of the injected water flow outside Sherrod Area toward east. Although tracers indicate small volumes, these volumes could be underestimated by excessive tracer dilution.
13. Inversion modeling results show that north-east and west side of the field have very low pore volume compared to the south-east. North-east and west side of field have 2% and 35% of the pore volume existing in the north-east, respectively.

8.2 Recommendations on Reservoir Management Practices

1. Injectors introduced in 2010 have either adverse or no effect on wells' oil rates and water-cuts. Thus, these wells add no value and should be shut-in
2. If a decision was made to keep 2010 injectors active, evaluation of cyclic production / cyclic water-injection strategy should be made in an attempt to improve water injection efficiency while maintaining reservoir pressure.

8.3 Recommendations for Future Work

1. Detailed inversion modeling studies to invert water-cuts of the 11 inverted 9-spot patterns under initial saturation uncertainty.
2. Assess of multiple fracture realizations obtained from Method of Moments and moderate and high tracer recoveries maps
3. Extending the work on the full field model by increasing vertical resolution.
4. Investigate in depth grid orientation, different types of grids, and longitudinal and transverse dispersion on tracer solution.

REFERENCES

1. Allison, Steven Bradley (1988). Analysis and design of field tracers for reservoir description. Master's thesis, The University of Texas at Austin.
2. Oyerinde, Adedayo Stephen (2004). A composite tracer analysis approach to reservoir characterization. Master's thesis, Texas A&M University.
3. Determination of Residual Oil Saturation. Interstate Oil Compact Commission. Oklahoma City, OK (1978).
4. Wagner, O.R. 1977. The Use of Tracers in Diagnosing Interwell Reservoir Heterogeneities - Field Results. Journal of Petroleum Technology 29 (11): 1410-1416. DOI: 10.2118/6046-pa
5. Alkouh, A.B. and Chen, H.-Y. 2008. Flow Anisotropy Analysis from Multiwell-Testing of Sabiriyah Field, North Kuwait. Paper presented at the Abu Dhabi International Petroleum Exhibition and Conference, Abu Dhabi, UAE. Society of Petroleum Engineers SPE-117002-MS. DOI: 10.2118/117002-ms.
6. Davis, J.A., Blair, R.K., and Wagner, O.R. 1976. Monitoring and Control Program for a Large Scale Miscible Flood. Paper presented at the SPE Annual Fall Technical Conference and Exhibition, New Orleans, Louisiana. 1976 Copyright 1976 00006097. DOI: 10.2118/6097-ms.
7. Ferrell, H.H., King, D.W., and Sheely, J., C.Q. 1988. Analysis of the Low-Tension Pilot at Big Muddy Field, Wyoming. SPE Formation Evaluation 3 (2): 315-321. DOI: 10.2118/12683-pa

8. Wagner, O.R., Baker, L.E., and Scott, G.R. 1974. The Design and Implementation of Multiple Tracer Program for Multifluid, Multiwell Injection Projects. Paper presented at the Fall Meeting of the Society of Petroleum Engineers of AIME, Houston, Texas. 1974 Copyright 1974 00005125. DOI: 10.2118/5125-ms.

9. Ohno, K., Nanba, T., and Horne, R.N. 1987. Analysis of an Interwell Tracer Test in a Depleted Heavy-Oil Reservoir. SPE Formation Evaluation 2 (4): 487-494. DOI: 10.2118/13672-pa

10. Abbaszadeh-Dehghani, M. and Brigham, W.E., "Analysis of Unit Mobility Ratio Well-to-Well Tracer Flow to Determine Reservoir Heterogeneity," U.S. DOE Report SF/11564-1, Feb. 1983.

11. Abbaszadeh-Dehghani, M. and Brigham, W.E. 1984. Analysis of Well-to-Well Tracer Flow to Determine Reservoir Layering. Journal of Petroleum Technology 36 (10): 1753-1762. DOI: 10.2118/10760-pa

12. Agca, C., Pope, G.A., and Sepehrnoori, K., "Modelling and Analysis of Tracer Flow in Oil Reservoirs" presented at the International Conference on Impact of Physico-Chemistry on the Study, Design, and Optimization of Processes in Natural Porous Media, Nancy, France, June 10-12, 1987; accepted for publication by Geoderma Journal, 1987.

13. Saad, N. and Sepehrnoori, K. 1989. Simulation of Big Muddy Surfactant Pilot. SPE Reservoir Engineering 4 (1): 24-34. DOI: 10.2118/17549-pa

14. Streamline Simulation: Theory and Practice. Akhil Datta-Gupta, Michael J. King. Society of Petroleum Engineers. Richardson, TX (2007)

15. Tracers in the Oil Field. Bernard Zemel. Elsevier Science B.V. Amsterdam, The Netherlands (1995)

16. McIntyre, F.J., Polkowski, G.A., Bron, J. et al. 1988. Radioactive Tracers Monitor Solvent Spreading in Rainbow Vertical Hydrocarbon Miscible Flood. SPE Reservoir Engineering 3 (1): 273-280. DOI: 10.2118/14440-pa

17. Brigham, W.E. and Abbaszadeh-Dehghani, M. 1987. Tracer Testing for Reservoir Description. Journal of Petroleum Technology 39 (5): 519-527. DOI: 10.2118/14102-pa

18. Cooke, C.E. Jr.: "Method of Determining Fluid Saturations in Reservoirs," U.S. Patent No. 3590923 (1971).

19. Tang, J.S. 1995. Partitioning Tracers and in-Situ Fluid-Saturation Measurements. SPE Formation Evaluation 10 (1): 33-39. DOI: 10.2118/22344-pa

20. Deans, H.A. and Carlisle, C.T. 1986. Single-Well Tracer Test in Complex Pore Systems. Paper presented at the SPE Enhanced Oil Recovery Symposium, Tulsa, Oklahoma. 1986 Copyright 1986, Society of Petroleum Engineers, Inc. 00014886. DOI: 10.2118/14886-ms.

21. James, A.I., Graham, W.D., Hatfield, K., Rao, P.S.C., Annable, M.D.: "Optimal Estimation of Residual Non-aqueous Phase Liquid Saturations Using Partitioning Tracer Concentration Data," Water Resources Research (1997), 33, No.12, 2621-2636.

22. James, A.I., Graham, W.D., Hatfield, K., Rao, P.S.C., Annable, M.D.: "Estimation of Spatially Variable Residual Nonaquous Phase Liquid Saturations in Nonuniform Flow Fields Using Partioning Tracer Data," Water Resources Research (2000), 36, No.4, 999-1012.

23. Vasco, D.W., Yoon, S., and Datta-Gupta, A. 1999. Integrating Dynamic Data into High-Resolution Reservoir Models Using Streamline-Based Analytic Sensitivity Coefficients. SPE Journal 4 (4): 389-399. DOI: 10.2118/59253-pa

24. Yoon, S., Barman, I., Datta-Gupta, A. et al. 1999. In-Situ Characterization of Residual Napl Distribution Using Streamline-Based Inversion of Partitioning Tracer Tests. Paper presented at the SPE/EPA Exploration and Production Environmental Conference, Austin, Texas. Copyright 1999,Society of Petroleum Engineers, Inc. 00052729. DOI: 10.2118/52729-ms.

25. Illiasov, P.: "Inversion of Field-Scale Partitioning Tracer Response for Characterizing Oil Saturation Distribution: A Streamline Approach," MS thesis, Texas A&M University, College Station, TX (2000).

26. Brigham, W.E. and Smith Jr., D.H. 1965. Prediction of Tracer Behavior in Five-Spot Flow, SPE # 1130. ISBN 978-1-55563-862-7.

27. Heisler, R.P. 1988. Interpretation of Radioactive Tracer Results in a Steamdrive Project. SPE Reservoir Engineering 3 (1): 281-287. DOI: 10.2118/15092-pa

28. Nelson, R.A.: Geological Analysis of Naturally Fractured Reservoirs, second edition, Gulf Professional Publishing, St. Louis (2001).

29. Jaeger, J.S. and Cook, N.G.W.: Fundamentals of Rock Mechanics, third edition, Chapman and Hall Ltd., New York City (1979).

30. Rock Fractures and Fluid Flow: Contemporary Understanding and Applications, Committee on Fracture Characterization and Fluid Flow, National Academy Press, Washington, D.C. (1996).

31. Chowdhury, Tanvir (2002). Improving dual-porosity simulation of waterfood performance in the naturally fractured spraberry trend. Master's thesis, Texas A&M University.

32. Guo, B., Schechter, D.S., and Baker, R.O. 1998. An Integrated Study of Imbibition Waterflooding in the Naturally Fractured Spraberry Trend Area Reservoirs. Paper presented at the SPE Permian Basin Oil and Gas Recovery Conference, Midland, Texas. Society of Petroleum Engineers 00039801. DOI: 10.2118/39801-ms

33. Putra, E. and Schechter, D.S. 1999. Reservoir Simulation of Waterflood Pilot in Naturally Fractured Spraberry Trend. Paper presented at the SPE Asia Pacific Oil and Gas Conference and Exhibition, Jakarta, Indonesia. Society of Petroleum Engineers 00054336. DOI: 10.2118/54336-ms.

34. Baker, R.O., Bora, R., Schechter, D.S. et al. 2001. Development of a Fracture Model for Spraberry Field, Texas USA. Paper presented at the SPE Annual Technical Conference and Exhibition, New Orleans, Louisiana. Copyright 2001, Society of Petroleum Engineers Inc. 00071635. DOI: 10.2118/71635-ms.

35. Schechter, D.S,, McDonald, P., Sheffield, T., and Baker, R.: “Reservoir Characterization and CO2 Pilot Design in the Naturally Fractured Spraerry Trend Area,” paper SPE 35469, presented at the SPE Pemian Basin Oil & Gas Recovery Conference held in Midland, Texas, 27-29, March 1996.

36. Guo, B. and Schechter, D.S: “Use of a Simple Mathematical Model for Estimating Formation Damage in Wells Intersecting Long Fractures,” paper SPE 38178 presented at the 1997 SPE European Formation Damage Conference held in The Hague, The Netherlands, 2-3 June 1997.

37. Guidroz, G.M.: ”E.T. O’Daniel Project – A Successful Spraberry Flood,” JPT, September 1967, pp. 1137-40.

38. McDonald, P., Lorenz, J.C., Sizemore, C. et al. 1997. Fracture Characterization Based on Oriented Horizontal Core from the Spraberry Trend Reservoir: A Case Study. Paper presented at the SPE Annual Technical Conference and Exhibition, San Antonio, Texas. 1997 Copyright 1997, Society of Petroleum Engineers, Inc. 00038664. DOI: 10.2118/38664-ms.

39. Lorenz John, and Copper Scott: “Natural Fractures in Horizontal Spraberry Core from the XBC Griddings 3049H well, Upton Co., Texas”, Augest 2012, FractureStudies LLC.

40. Dyes, A.B. and Johnston, O.C.: “Spraberry Permeability from Build up Curve Analyses,” AIME Vol. 198, 1953.

41. Baker, R.O. et al.: “Characterization of the Dynamic Fracture Transport Properties in a Naturally Fractured Reservoir,” paper SPE 59690 presented at the

2000 SPE Permian Basin Oil and Gas Recovery Conference held in Midland, Texas, 21-23 March.

42. Baker, R.O. et al.: "Using An Analytical Decline Model to Characterize Naturally Fractured Reservoirs," paper SPE 39623 presented at the 1998 SPE/DOE Improved Oil Recovery Symposium held in Tulsa, OK, 19-22April.

43. Honarpour, M,M., Huang, D.D., and Al-Hussainy, R: "Simultaneous Measurements of Relative Permeability,Capillary Pressure, and Electrical Resistivity with Microwave System for Saturation Monitoring," paper SPE 30540, presented at the SPE Annual technical Conference and Exhibition held in Dalas, Texas, 22-25 October, 1995.

44. Deans, H.A. and Mut, A.D.: "Chemical Tracer Studies to Determine Water Saturation at Prudhoe Bay," SPE Reservoir Engineering (February 1997) 52-57.

45. SimOpt User Guide 2003a, Schlumberger-GeoQuest Simulation Software Documentation (2003).

46. Hiriart-Urruty, J.B. and Lemarechal, C.: Convex Analysis and Minimization Algorithms I, Springer-Verlag, London (1993).

47. Bissell, R.: "Calculating Optimal Parameters For History-Matching" paper presented at the 1994 European Conference on the Mathematics of Oil Recovery, Roros, Norway, 7-10 June.

48. Brun, B., Gosselin, O., and Barker, J.W. 2004. Use of Prior Information in Gradient-Based History Matching. SPE Journal 9 (1): 67-78. DOI: 10.2118/87680-pa

APPENDIX A

WELL BY WELL PRODUCTION AND INJECTION DATA

Well by well production and injection data from July 1951 to March 2012 described in section 3.1 is included as a separate Microsoft Excel file.

APPENDIX B

TRACER RESPONSE DATA (WITHOUT CORRECTION)

Tracer concentration measurements described in section 3.3 is included as a separate Microsoft Excel file.

APPENDIX C

TRACER RESPONSE DATA (WITH CORRECTION)

Tracer concentration measurements after water recycling corrections described in section 3.3 is included as a separate Microsoft Excel File.

APPENDIX D

REPORTS OF AVAILABLE PRESSURE MEASURMENTS

Available limited pressure measurements described in section 3.4 is included as a separate PDF file.

APPENDIX E

METHOD OF MOMENT ANALYSIS CALCUATIONS

Method of Moments calculations described in section 4.3 is included as a separate Microsoft Excel file

APPENDIX F

WATER RATE DECOMPOSITION OF A PATTERN

Method of Moments calculations described in section is included as a separate Microsoft Excel file

APPENDIX G

FULL FIELD ECLIPSE SIMULATION MODEL

Full field simulation model described in section 5.6 is included as a separate Microsoft Excel file